AMERICAN UNIVERSITY OF BEIRUT

CYCLIC AXIAL BEHAVIOR OF CONCRETE COLUMNS
CONFINED WITH FRP SHEETS OR WITH A
COMBINATION FRP SHEETS AND ANCHORS

by
NAJWA FARHAN HANY

A dissertation
submitted in partial fulfillment of the requirements
for the degree of Doctor of Philosophy
to the Department of Civil and Environmental Engineering
of the Faculty of Engineering and Architecture
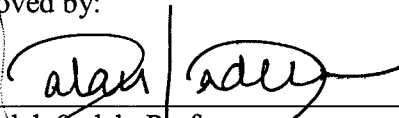at the American University of Beirut

Beirut, Lebanon
May 2017

AMERICAN UNIVERSITY OF BEIRUT

CYCLIC AXIAL BEHAVIOR OF CONCRETE COLUMNS CONFINED WITH FRP SHEETS OR WITH A COMBINATION FRP SHEETS AND ANCHORS
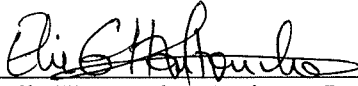
by
NAJWA FARHAN HANY

Approved by:

_____   Committee Chairperson
Dr. Salah Sadek, Professor
Department of Civil and Environmental Engineering, AUB
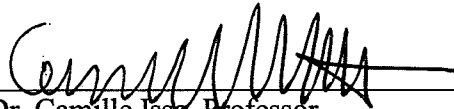

_____   Advisor
Dr. Mohamed Harajli, Professor
Department of Civil and Environmental Engineering, AUB

_____   Co-Advisor
Dr. Elie Hantouche, Assistant Professor
Department of Civil and Environmental Engineering, AUB

_____   Member of Committee
Dr. George Saad, Assistant Professor
Department of Civil and Environmental Engineering, AUB

_____   Member of Committee
Dr. Camille Issa, Professor
Department of Civil Engineering, Lebanese American University (LAU)

_____   Member of Committee
Dr. Hisham Basha, Professor
Department of Civil and Environmental Engineering, Rafik Hariri University (RHU)

Date of dissertation defense: May 12, 2017

AMERICAN UNIVERSITY OF BEIRUT

THESIS, DISSERTATION, PROJECT RELEASE FORM

Student Name:

_____
Last   First   Middle

◯ Master's Thesis   ◯ Master's Project   ◯ Doctoral Dissertation

☐   I authorize the American University of Beirut to: (a) reproduce hard or electronic copies of my thesis, dissertation, or project; (b) include such copies in the archives and digital repositories of the University; and (c) make freely available such copies to third parties for research or educational purposes.

☐   I authorize the American University of Beirut, to: (a) reproduce hard or electronic copies of it; (b) include such copies in the archives and digital repositories of the University; and (c) make freely available such copies to third parties for research or educational purposes
after:
        One ---- year from the date of submission of my thesis, dissertation, or project.
        Two ---- years from the date of submission of my thesis, dissertation, or project.
        Three ---- years from the date of submission of my thesis, dissertation, or project.

_____
Signature   Date

ACKNOWLEDGMENTS

AN ABSTRACT OF THE DISSERTATION OF

Najwa Farhan Hany   for   <u>Doctor of Philosophy</u>
                                      <u>Major</u>: Civil Engineering

Title: <u>Cyclic Axial Behavior of Concrete Columns Confined with FRP Sheets or with a Combination FRP Sheets and Anchors</u>

Confining concrete columns with external fiber reinforced polymer (FRP) jackets is a well-known technique widely used in strengthening and repairing existing columns. This method relies on the fact that concrete is a pressure-sensitive material that has its axial load capacity and axial failure ductility improved when provided with a confining pressure.

In the last two decades, many experimental and analytical studies have been carried out to evaluate the efficiency of FRP in enhancing columns strength and ductility. Most of these studies have concentrated on FRP-confined concrete specimens subjected to monotonic loading. Also, many analytical and design-oriented models have been proposed to describe the axial stress-strain behavior of FRP-confined concrete. However, most of the available models considered the case where the confinement level provided by the FRP leads to improvement of the concrete's ultimate strength resulting in post peak ascending behavior, very few predicted a post peak descending behavior and none of them predicted the cyclic stress-strain response for FRP confined rectangular column sections. Accordingly, guided by the test results of an experimental program performed at AUB and other test data reported in the technical literature, an axial stress-strain material model of FRP-confined concrete under cyclic loading is developed and validated, which constitutes the first part of this investigation. The model covers all important parameters in a unified manner, and predicts both ascending and descending post peak responses.

Despite the high efficiency of external jacketing in enhancing the strength and ductility of columns of circular cross-sections, its efficiency gets reduced when used to confine specimens of non-circular cross-sections. This is attributed to the fact that an externally-wrapped circular cross-section is fully and uniformly confined, however only part of an externally-wrapped rectangular cross-section is effectively confined. For FRP confined concrete columns of rectangular cross-sections, similar to the effect of internal confinement by transverse steel ties, anchoring the long side of the FRP jacket using FRP anchors distributed in the column volume increases the effectively confined area by restraining the FRP jacket from bulging out at the flat sides of the rectangular section. Another advantage of using FRP anchors is increasing the total cross-sectional area of

FRP which generates additional confining pressure. To date, only few studies have investigated how adding FRP anchors to concrete columns externally wrapped with FRP sheets affects the stress-strain behavior of these columns. In the second part of the current investigation, an experimental program of the cyclic axial stress-strain response of rectangular concrete columns confined with a combination carbon-fiber-reinforced polymer (CFRP) jacket and CFRP anchors is performed and the results are presented and discussed. The test variables include aspect ratio of the column section, area of FRP wraps, and area and configuration of the FRP anchors. It was found that adding FRP anchors improves the confinement effectiveness of the FRP jackets, leading to substantially enhanced envelope stress-strain response and ductility of axial failure. Based on the results of this study, analytical expressions are derived for predicting the stress-strain curve, taking into account the effect of FRP anchors. The proposed model is similar to that developed in the first part of this study with slight differences.

Further to the experimental and analytical work, many attempts have been made to model FRP-confined concrete columns using the finite element (FE) method. Many constitutive models were suggested to define concrete properties in FE software, especially for concrete subjected to confinement pressure. The theory of plasticity has been widely used to model confined concrete. Concrete damaged plasticity model (CDPM) available in the FE software (ABAQUS), has been widely used to model reinforced concrete. However, the use of CDPM has limitations when applied to confined concrete. This dissertation addresses these limitations and presents a modified concrete damaged plasticity model. A new set of strain hardening/softening constitutive relationships for both actively confined concrete and FRP-confined concrete are generated and a concrete dilation model is developed. The dilation model is expressed as a function of the stiffness of the FRP-jacket. The modified CDPM is applicable to columns with different types of cross-sections, including circular, square and rectangular and large range of concrete strengths varying from normal to high strength. Finite element results obtained using the developed modified CDPM showed a very good agreement with test data for FRP confined concrete columns reported in the technical literature.

One important practical application of FRP confinement is in strengthening the plastic hinge region of reinforced concrete (RC) columns for these columns to sustain a higher lateral deformation when subject to lateral loading caused by earthquakes. Nonlinear flexural analysis allows generating the moment-curvature ($M - \phi$) curve of a section, knowing the section geometry and materials properties. Using this method, $M - \phi$ curves are generated for unconfined RC sections, sections confined with external FRP sheets only or sections confined with a combination of FRP sheets. The closed form expressions generated in the first parts of the work are used to define the properties of confined concrete. The influence of different parameters on the $M - \phi$ curve is studied and discussed. The moment-curvature response is used to estimate the lateral drift capacity of cantilever columns subject to a constant axial load and an increasing lateral load. The columns are either unconfined or confined in their plastic hinge region. The results clearly show that confining the plastic hinge region with FRP sheets or with a combination of FRP sheets and anchors leads to a substantially improved performance of the columns especially in terms of drift capacity and ductility.

CONTENTS

ILLUSTRATIONS

TABLES

To my parents, Farhan and Amira

To my brother Assaad and sisters Leyla, Samar, Sara and Wafaa

CHAPTER I

INTRODUCTION

The use of FRP sheets as externally bonded reinforcement has significantly increased in the past few years. These sheets are bonded to existing concrete structures in need of strengthening and/or retrofitting. The applications of this rehabilitation technique comprise: (i) flexural and shear strengthening of reinforced concrete (RC) beams, (ii) seismic and axial compression strengthening of RC columns, and (iii) strengthening of RC beam-columns joints for the structure to withstand large earthquakes and other lateral loads. Additional reasons that have contributed to the growing use of this technique are its cost-effectiveness and the reduced effort and time it requires compared to the traditional means.

One of the most encountered applications of this method is in strengthening existing concrete columns (Figure I-1) where applying external FRP reinforcement increases the axial load carrying capacity of the column which allows it meeting increased loads demands. For damaged columns (especially corrosion-damaged), the FRP sheets provide a barrier that protects concrete from the aggressive environment. For RC columns with insufficient transverse reinforcement and/or seismic detailing, wrapping by external FRP sheets increases the column shear capacity. It also enhances the flexural ductility of the plastic hinge region and prevents debonding of lap splices that could reduce the column flexural strength. These latter applications fall into the category of seismic strengthening of existing RC columns.

To date, many experimental and analytical investigations have been performed to evaluate the axial stress-strain response of concrete columns confined with external

FRP sheets. These studies clearly demonstrated that wrapping a concrete column with external FRP sheets increases its axial strength and ductility. This is interpreted by the fact that as concrete dilation increases under axial compression, the tensile stresses generated in the FRP sheets provide confining pressure to the concrete core which improves it strength and ductility. For that reason, confinement by FRP sheets is considered of passive type insofar as it is generated as a result of concrete dilation.

A.   Research background and related work

1.   *Experimental and analytical investigations on the compressive behavior of FRP-confined concrete columns*

In the past two decades, a large number of experimental and analytical studies have been carried out to examine the compressive behavior of FRP-confined concrete. A comprehensive summary is provided by (ACI-440.2R-08). Most of the available studies have concentrated on concrete columns of circular cross-sections (Mirmiran & Shahawy, 1997; Samaan, Mirmiran, & Shahawy, 1998; Spoelstra & Monti, 1999; Xiao & Wu, 2000; Lam & Teng, 2003a; Csuka & Kollar, 2010). Fewer, focused on concrete columns of non-circular (square and rectangular) cross-section (Lam & Teng, 2003b; Harajli, Hantouche, & Soudki, 2006; Rousakis, Karabinis, & Kiousis, 2007; Youssef, Feng, & Mosallam, 2007; Chaallal, Shahawy, & Hassan, 2003). As a result, several models have been proposed to predict the axial stress-strain response of FRP-confined concrete. Few models are analysis-oriented and a greater number are design-oriented in which closed-form expressions are calibrated based on experimental results. (Ozbakkaloglu, Lim, & Vincent, 2013) reviewed and assessed the eighty-eight existing design and analysis-oriented models for columns of circular cross-sections, while (Lim & Ozbakkaloglu, 2014a) assessed existing models for columns of square and

rectangular cross-sections. In addition, most of the available axial stress-strain models predicted the response of confined columns where the confinement level leads to a post-peak ascending behavior and very few considered the case of descending behavior.

The majority of experimental and analytical results reported in the technical literature concentrated on specimens subjected to monotonic axial compressive loading. Very few considered the case of concrete columns subject to cyclic loading (Lam L. , Teng, Cheung, & Xiao, 2006; Lam & Teng, 2009; Wang, Wang, Smith, & Lu, 2012a; Wang, Wang, Smith, & Lu, 2012b; Wang, Wang, Smith, & Lu, 2012c) (Abbasnia & Holakoo, 2012; Abbasnia, Hosseinpour, Rostamian, & Ziaadiny, 2012; 2013; Abbasnia, Ahmadi, & Ziaadiny, 2012; Ozbakkaloglu & Akin, 2012). Among these studies, (Lam L. , Teng, Cheung, & Xiao, 2006) conducted an experimental program on plain concrete specimens of circular cross-section, confined with CFRP and subjected to monotonic and cyclic compressive loading. The experimental results of the cyclically loaded specimens along with results from previously published studies were utilized by (Lam & Teng, 2009) for developing new algebraic expressions that describe the different aspects of the cyclic response of concrete cylinders. (Wang, Wang, Smith, & Lu, 2012b; 2012c) developed two cyclic axial stress-strain models for FRP confined reinforced concrete columns of large cross-section, one for square, and the other for circular cross-sections, based on their own experimental work. An experimental investigation of the influence of parameters such as confinement level, aspect ratio, unconfined concrete compressive strength and corner radius on the behavior of concrete prisms confined with FRP under cyclic loading was carried out by (Abbasnia, Hosseinpour, Rostamian, & Ziaadiny, 2012; Abbasnia, Ahmadi, & Ziaadiny, 2012). The study focused on evaluating the effect of these parameters on the plastic strain and

the stress degradation and concluded that the plastic strain decreases with an increase in unconfined concrete strength while the strength degradation is independent of these parameters. (Ozbakkaloglu & Akin, 2012) carried out an experimental program to evaluate the response of normal strength concrete (NSC) and high strength concrete (HSC) cylinders confined with AFRP and CFRP under monotonic and cyclic axial compression. For the same confinement level, the strength and strain enhancement were found more important for NSC than for HSC cylinders. Their study showed also that the plastic strain of confined columns is independent of the amount of confinement and the type of FRP. However, contrary to what was concluded by (Lam & Teng, 2009; Abbasnia, Ahmadi, & Ziaadiny, 2012), the effect of the unconfined concrete strength on the plastic strain was found negligible.

2. *Use of FRP anchors with externally bonded FRP sheets*

A recent technique used in strengthening existing structures involves anchoring the FRP sheets by means of FRP anchors. These anchors are formed using a strip of the jacket material, folded (Figure I-2), inserted into pre-prepared holes and fanned out over the jacket (Figure I-3).

One application of the anchoring technique is in repairing and strengthening reinforced concrete columns with deficient lap splices (Kim, Jirsa, & Bayrak, 2011; Harajli & Hantouche, 2014).

Anchors are also used to increase the flexural capacity of beams or slabs strengthened with FRP strips by preventing or limiting debonding of these strips (Lam & Teng, 2001; Orton, Jirsa, & Bayrak, 2008).

4

(Kim, Quinn, Ghannoum, & Jirsa, 2014) used FRP anchors to increase the shear resistance of FRP-strengthened T-beams.

For FRP-confined concrete columns of rectangular cross-sections, it is anticipated that anchoring the long side of the FRP jacket using FRP anchors will increase the effectively confined area by restraining the FRP jacket from bulging out at the flat sides. This effect is similar to that of internal confinement by transverse steel ties (Mander, Priestley, & Park, 1988). Another theoretical advantage of using FRP anchors is increasing the total cross-sectional area of FRP which generates additional confining pressure to the cross-section. To date, only few studies have investigated how adding FRP anchors to concrete columns externally wrapped with FRP sheets affects the stress-strain behavior of these columns.

Among these studies, (Tan, 2002) reported improvement of the load capacity for reinforced concrete columns with transverse fiber sheets anchored along the wider faces than for specimens with an unanchored jacket. The study proposed a simplified method to calculate upper and lower limits for the enhanced axial load capacity. The experimental investigation was limited to specimens of rectangular section of aspect ratio 3.65 and only three out of the fifty-two tested specimens were anchored. In evaluating the shear capacity of short square reinforced concrete columns jacketed by FRP with and without anchors, (Ghobarah & Galal, 2004; Galal, Arafa, & Ghobarah, 2005) quantified the improved compressive strength of the retrofitted columns at the ultimate stage using (Mander, Priestley, & Park, 1988) model. One out of seven tested specimens was anchored using FRP anchors. Similar to (Tan, 2002), the FRP anchors were assumed to contribute to the total confining pressure by increasing the effectively confined area. (Li, Lv, Zhang, Sha, & Zhou, 2013) who used FRP anchors to enhance

the flexural strength of RC columns assumed also that the presence of anchors increases the effectively confined area and consequently the compressive strength. (Ilki, Peker, Karamuk, Demir, & Kumbasar, 2008) also studied the ability of the CFRP anchors to overcome the low flexural stiffness of the CFRP jacket wrapping RC columns. Based on their experimental results, the improvement provided by the anchors to the stress-strain response was not significant. However, their experimental study was limited to only five anchored specimens with cross-section aspect ratios of 1 and 2, and the anchors cross-sectional area was not specified. (Karantzikis, Papanicolaou, Antonopoulos, & Triantafillou, 2005) investigated the effect of adding FRP anchors at the reentrant corner of L-shaped columns wrapped with FRP and found that this method allows mobilizing the confining stresses supplied by the FRP jacket.

3. *Finite element (FE) modeling of FRP-confined concrete columns*

Further to the experimental and analytical work, many attempts have been made to model FRP-confined concrete columns using the FE method. The main advantage of the FE method is its ability to deal with geometric non-linearity and the interactions of different materials. An additional advantage is that it can be utilized for performing extensive parametric studies without resorting to expensive and time-consuming experimental work. The main complexity encountered while modeling FRP-confined concrete columns using an FE software is to properly define the different materials properties (i.e. FRP sheets and concrete). FRP laminates are usually modeled as linear elastic materials (Yu, Teng, Wong, & Dong, 2010a; Yu, Teng, Wong, & Dong, 2010b; Jiang & Wu, 2012). When the fibers are in the hoop directions, only the hoop properties are crucial. On the other hand, many constitutive models have been

6

suggested to define concrete properties in FE software, especially for concrete subjected

to confinement pressure. The theory of plasticity has been widely used to model

confined concrete. The first types of concrete plasticity models were based on:

nonlinear elasticity, endo-chronic plasticity, classical plasticity, multi-laminate or

micro-plane plasticity, and bounding surface plasticity. However, as reported by

(Mirmiran, Zagers, & Yuan, 2000), these models are either of limited applicability or

require a large number of parameters to be calibrated.

More recently, Drucker-Prager (D-P) type was one of the most used types of

plasticity models for modeling confined concrete (Yu, Teng, Wong, & Dong, 2010a;

Jiang & Wu, 2012; 2014; Mirmiran, Zagers, & Yuan, 2000; Eid & Paultre, 2007)

(Karabinis, Rousakis, & Manolitsi, 2008; Issa, Chami, & Saad, 2009; Doran, Koksal, &

Turgay, 2009; Koksal, Doran, & Turgay, 2009; Wu, Wang, Yu, & Li, 2009)

(Hajsadeghi, Alaee, & Shahmohammadi, 2011; Rousakis T. C., Karabinis, Kiousis, &

Tepfers, 2008). Studies using the D-P type plasticity model reported good results when

predicting the monotonic behavior of FRP confined concrete.

Other researches modeled FRP-confined concrete using a Karagozian and Case

(K-C) type plasticity model (Youssf, ElGawady, Mills, & Ma, 2014).

In 2010, (Yu, Teng, Wong, & Dong, 2010a) assessed existing D-P type

plasticity models and proposed criteria for the yield function, hardening/softening rule

and flow rule that should be included in a D-P type plasticity model, to accurately

predict the behavior of both actively and passively confined concrete. D-P model

modified by (Yu, Teng, Wong, & Dong, 2010a) showed some limitations addressed in a

companion paper (Yu, Teng, Wong, & Dong, 2010b) using modified damaged plasticity

model available in (ABAQUS). This model was later improved by (Teng, Xiao, Yu, &

Lam, 2015) to capture the three dimensional behavior of FRP and steel confined concrete columns. (Kabir & Shafei, 2012) also used concrete damage plasticity combined with smooth cap plasticity to model FRP-confined circular RC columns subjected to eccentric axial loading. A recent study by (Ozbakkaloglu, Gholampour, & Lim, 2016), proposed a modified concrete damaged plasticity model for FRP-confined concrete of both normal and high strengths.

B.   Problem statement and motivation

As stated in the literature review part, many experimental and analytical studies have investigated the axial stress-strain response of FRP-confined concrete columns. Most of the available axial stress-strain models consider the case where the confinement level provided by the FRP leads to improvement of the concrete's ultimate strength resulting in post peak ascending behavior. However, only few models predict the responses of concrete at low confinement levels that could lead to post peak descending behavior. Also, no model was reported earlier for describing the cyclic stress-strain response for FRP-confined rectangular column sections. Therefore, a new model is needed to predict the cyclic response of FRP- confined concrete specimens to include different cross section shapes and confinement levels that could lead to descending post peak stress-strain behavior.

In addition, FRP anchors are widely used to anchor externally bonded FRP sheets. Nevertheless, the use of FRP anchors in concrete columns is limited. To the best of the writer's knowledge, all analytical and experimental studies performed to evaluate the stress-strain response of rectangular columns confined with FRP sheets and anchors were limited to a relatively small number of specimens and design variables.

That is, no comprehensive study or test data was reported earlier on the influence of the FRP anchor stiffness and distribution in the concrete volume on the monotonic as well cyclic axial stress-strain response of FRP-confined rectangular columns. Moreover, no model has been proposed to evaluate the complete cyclic axial stress-strain response of rectangular concrete columns confined with a combination of FRP sheets and anchors. The need for such experimental data and analytical modeling motivates the second part of the work. Furthermore, axial stress-strain models of confined concrete are needed to generate the moment-curvature ($M - \phi$) response of confined concrete sections and to analytically study the flexural deformations of concrete columns subject to simulated seismic loading.

Finite element programs are extensively used to model structural problems. Modeling FRP-confined concrete using an FE software has been the subject of many research studies. Different types of plasticity and damaged-plasticity models have been used to define the concrete properties. Concrete damaged plasticity model (CDPM) available in ABAQUS, has been extensively used to model reinforced concrete. However, it shows limitations when modeling either concrete confined with a constant confinement pressure or FRP-confined concrete. Therefore, modifications need to be introduced to CDPM for accurate modeling of concrete columns confined with external FRP sheets.

C.   Research goals and objectives

The objectives of the current research are as follows:

- To provide a design-oriented stress-strain model that predicts the

envelope and cyclic axial stress-strain responses of CFRP-confined columns taking into

9

account the effect of several design parameters. These include: the specimen cross-section shape (circular, square, rectangular), the cross-section aspect ratio of non-circular cross-sections, and the area of external CFRP reinforcement. The model should be able to predict the response of specimens in which the confinement level leads to an envelope curve with a post peak descending branch. Data generated by an experimental program performed at AUB in addition to experimental data reported in the technical literature will be used to develop the model.

- To carry out an experimental program that studies the cyclic axial stress-strain response of rectangular concrete columns confined with a combination CFRP jacket and CFRP anchors. The following design parameters will be explored: the aspect ratio of the column section, the area of the CFRP wraps, and the area and configuration of the CFRP anchors.

- To assess the ability of the stress-strain model proposed for specimens confined with external CFRP sheets only, to be extended to the case of anchored specimens. As a result of this assessment, the original model can be modified or refined to predict the stress-strain response for both anchored and unanchored specimens.

- To make use of the axial stress-strain model in getting the $M - \phi$ response of confined sections and study the effect of different parameters on this response. These $M - \phi$ curves can also be used to get analytically the lateral load-drift response of real-scale columns.

- To propose a modified Concrete Damaged Plasticity Model that defines accurately the inelastic behavior of concrete subject to axial compressive loading and confined with external FRP sheets. In this aim, the effect of the different input parameters of CDPM available in (ABAQUS) on the axial and lateral response of

confined columns will be studied. The results of this evaluation will be used to develop

a new expression of the dilation angle and new strain hardening/softening constitutive

relationships. The proposed model will be validated against results of an experimental

program performed at AUB and other results available in the technical literature.

D.   Dissertation organization

This dissertation is divided into 7 chapters. Chapter I reviews the relevant

literature about the three subtopics that will be covered in the dissertation: (i)

Experimental and analytical investigations on the compressive behavior of FRP-

confined concrete columns; (ii) Use of FRP anchors with externally bonded FRP sheets;

and (iii) Finite element (FE) modeling of FRP-confined concrete columns. After

observing available studies, the points that need further investigation and that motivate

the current work are identified. Chapter II presents the results of an experimental

program performed at AUB on CFRP-confined concrete specimens subjected to axial

cyclic loading. These results, in addition to other results available in the technical

literature, are used to develop a design-oriented stress-strain model that predicts the

envelope and cyclic axial stress-strain responses of CFRP-confined columns taking into

account the effect of several design parameters. Chapter III presents the details of the

experimental program performed to investigate the effect of adding CFRP anchors on

CFRP-confined concrete columns. Chapter IV shows the modifications introduced to

the model proposed in Chapter II in order to account for the effect of anchors on the

axial stress-strain response. Chapter V proposes a modified Concrete Damaged

Plasticity Model in (ABAQUS) that defines the inelastic behavior of concrete subject to

axial compressive loading and confined with external FRP sheets. The proposed model

is validated against available experimental results. Making use of the axial stress-strain model proposed in Chapter IV, the moment-curvature ($M - \phi$) responses of confined concrete sections are obtained in Chapter VI. A parametric study is performed to evaluate the effect of different parameters on the $M - \phi$ response. These $M - \phi$ curves are in turn used to generate the lateral load-drift response of cantilever columns subject to concentric axial load and a lateral load applied at its tip. Finally, a summary of all the results and conclusions and recommendation for future work is presented in Chapter VII. Additional Figures showing details of the experimental work are finally provided in Appendix A.

Figure I-1 - FRP-wrapped concrete column (Black, 2014)

Figure I-2 - FRP anchor prepared by folding a strip of the FRP sheet
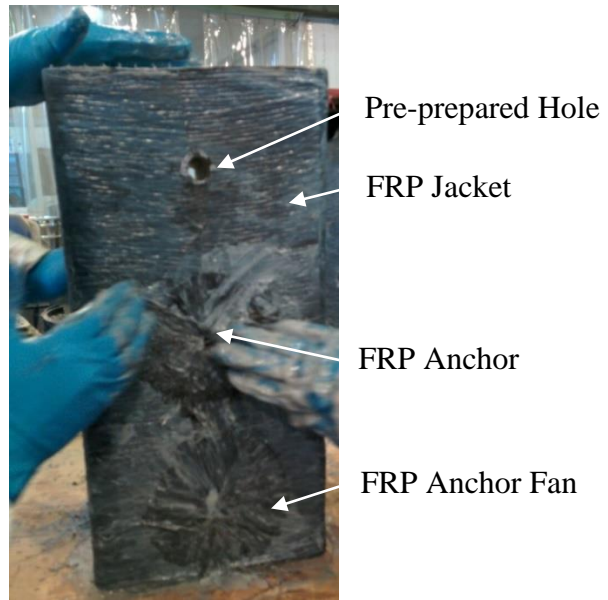
Figure I-3 - Insertion of FRP anchors in the pre-prepared holes

CHAPTER II

AXIAL STRESS-STRAIN MODEL OF CFRP-CONFINED CONCRETE UNDER MONOTONIC AND CYCLIC LOADING

A.   Introduction

As stated in the literature review part, many experimental and analytical investigations have been conducted to evaluate the stress-strain response of concrete columns confined with carbon-fiber-reinforced polymer (CFRP) laminates and several axial stress-strain models have been proposed. However, as mentioned earlier, few models predict the responses of concrete at low confinement levels that could lead to post-peak descending behavior, and no model was reported earlier for describing the cyclic stress-strain response of FRP confined rectangular column sections.

In this chapter, experimental results of the axial stress-strain response of eighteen carbon-fiber-reinforced polymer (CFRP) confined circular, square, and rectangular column specimens when subjected to cyclic axial compression are presented and discussed. This experimental program was performed at AUB at an earlier stage. Guided by these test results and other test data reported in the technical literature, a constitutive axial stress-strain material model of CFRP-confined concrete under axial cyclic loading is developed and validated.

B.   Experimental Program

1.   Test Parameters and Test Specimens

A total of 18 plain concrete specimens are tested under axial cyclic compression loading. The specimens are divided into four series (*C, S, R*1 and *R2*) depending on their cross-sectional shape. The terms *C* and *S* represent circular and square sections respectively, while *R*1 and *R2* represent rectangular sections of two different aspect ratios. Figure II-1 shows specimens' details while Table II-1 summarizes the specimens' designations, dimensions and CFRP confinement details. In Table II-1, the letter *U, P* or *F* indicate the wrapping mode, where *U* stands for unconfined, *P* for partially confined (using discrete strips) and *F* for fully confined specimens, respectively. The number following *P* and *F* corresponds to the number of applied CFRP layers. The terms $D =$ diameter of circular specimens; *b* and $h =$ the short and long sides of the rectangular section, respectively; $R =$ corner radius, and $t_{wrap} =$ total thickness of the CFRP wraps. All specimens were 500 *mm* in height. In each series, five specimens were tested: one unconfined (control) specimen, one specimen wrapped with one layer of discrete CFRP strips having a width of 50 *mm* and a clear spacing of 50 *mm*, and three specimens wrapped respectively with one, two and three layers of CFRP applied along the full specimen height. Unfortunately, because of limited capacity of the testing machine, the CFRP confinement of the circular specimens was limited to discrete strips similar to the remaining specimens, and one full wrap. For the square and rectangular specimens, the corners are rounded to a radius of 10 *mm*.

All specimens were cast using a single batch of Ready Mix concrete. The concrete mix consisted of coarse aggregate having 10 *mm* maximum size, natural sand, and Portland cement (Type I). The 28-day concrete compressive strength, obtained

using standard 15 *cm* x 30 *cm* concrete cylinders, was measured at 20 *MPa* for all specimens. The design properties of the CFRP sheets used are: thickness $t = 0.13$ *mm* per layer, modulus of elasticity $E_{frp} = 230,000$ *MPa*, ultimate or rupture strain $\varepsilon_{fu} = 0.015$ and ultimate strength $f_{fu} = 3500$ *MPa*. The surface of the specimens was treated and painted with epoxy resin, and the CFRP sheets were then applied in the transverse direction around the columns with 100 *mm* overlap. All specimens were capped using a 5 *mm* thick sulfur layer.

The specimens were tested in displacement control at a slow rate using 1,000 *KN* capacity 4-column universal MTS testing machine. The displacement level was increased in prescribed increments until failure of the specimens. Three full loading-unloading cycles were conducted at each strain level. The axial strain is measured using two linear variable differential transducers (LVDTs) supplied by Omega Engineering, USA. The LVDTs were attached diametrically opposite on the circular specimens, and on opposite sides of the square and rectangular specimens, over a 250 *mm* gage length at the middle region of the column as shown in Figure II-2. The average strain over the full height of the specimens (gage length = 500 *mm*) is also measured using two additional diametrically opposite LVDTs (Figure II-2). The lateral concrete strain is measured using two electric strain gages of 5 *mm* gage length (supplied by Omega Engineering) mounted on the CFRP wraps at mid-height of the specimens. The strain gages are placed 180° apart on circular specimens and on two consecutive sides of square and rectangular specimens. For the square specimens, the average lateral strain is also measured using two LVDTs attached on either side of the specimens over a gage length of 160 *mm*. For the rectangular specimens, the two lateral LVDTs are attached on two

consecutive sides of the specimens over gage lengths of 140 *mm* and 180 *mm* for the series *R*1 and 130 *mm* and 200 *mm* for the series *R*2.

2. *Test Results*

Figure II-3(a) and (b) show typical failure modes of the confined and the control unconfined specimens, respectively. For the unconfined specimens, failure occurred by complete crushing of concrete as expected. For the confined specimens, failure occurred due to rupture of the CFRP sheets which resulted in a sudden drop of load resistance. For the square and rectangular specimens, the CFRP wraps ruptured at the corners. Figure II-4(a) and (b) show the axial stress-strain response of all concrete specimens in test series *C* and *S*; while Figure II-5(a) and (b) show the same for the specimens in test series *R*1 and *R*2, respectively.

3. *Envelope response*

Figure II-6 shows idealization of the stress-strain response of the specimens. The test results related to the envelope curve are summarized in Table II-2. In this table, f'_t is the concrete stress corresponding to the peak of the first branch of the stress-strain response at a strain ε_c close to or slightly higher than 0.002; ε_{cu} is the ultimate concrete strain at which the specimens developed failure due to CFRP rupture; and f'_{cu} is the ultimate concrete strength corresponding to ε_{cu}.

The peak stress in all unconfined specimens developed at an axial strain very close to 0.002. The peak stress for the unconfined specimens was measured at 16.6 *MPa* for the circular specimen *CU*, 18.5 *MPa* for the square specimen *SU*, 17.6 *MPa* for the rectangular specimen *R*1*U*, and 20.2 *MPa* for the rectangular specimen *R*2*U*;

18

most of which are slighter lower than the cylindrical concrete compressive strength of 20.0 *MPa*.

For the CFRP confined specimens, the envelope stress-strain response is characterized by a three-stage behavior, which is typical of the response of CFRP confined concrete reported in the technical literature.

The first stage of the response coincides to a large extent with the ascending branch of the stress-strain curve of the unconfined specimens. Due to concrete dilatation, the FRP confinement is activated at an axial strain level close to 0.002; depending on the area of the FRP and the shape and dimensions of the specimen cross-section, the second branch of the curve is either *ascending* or *descending*. Specimen failure at an ultimate stress f'_{cu} and strain ε_{cu}, represents the third stage of the response when the FRP jacket ruptures and the axial load suddenly drops. Among the specimens which exhibited a post-peak ascending branch were the circular specimens partially and fully confined with one layer of CFRP (*CP*1 and *CF*1) and the square and rectangular specimens of series $R1$ confined with 3 layers of CFRP (*SF*3 and $R1F3$). For the remaining specimens, the confinement provided by the CFRP improved the peak axial strength but resulted in a post-peak descending behavior.

For the confined specimens, the improvement in the peak axial stress of the first stage, f'_t and the ultimate axial strength f'_{cu}, over the unconfined concrete compressive strength, f'_{co}, is evaluated using the ratios f'_t/f'_{co} and f'_{cu}/f'_{co} presented in Table II-2. As for the ultimate axial strain ε_{cu}, the results reported in Figure II-4 and Figure II-5 and in Table II-2 show that its value is greatly improved by the CFRP confinement. However, the influence of the cross-section shape on the ultimate axial strain is not as evident as its influence on the axial strength.

4. *Cyclic response*

The cyclic response is idealized as shown in Figure II-6. It can be seen from the results in Figure II-4 and Figure II-5 that the cyclic response for a full cycle is composed of two distinct and well defined paths: (i) a curvilinear unloading path characterized by a progressively diminishing slope, until it intersects the strain axis at a strain referred to in this study as the envelope plastic strain $\varepsilon_{pl,env}$, and (ii) an almost linear reloading path which intersects the envelope curve at (ε_{ret}, σ_{ret}).

The following observations can be drawn from the cyclic response in Figure II-4 and Figure II-5, which have implications on the axial stress-strain model proposed in this study (see also Figure II-6): (i) the intrinsic shape of the cyclic response at all envelope unloading strain levels $\varepsilon_{un,env}$ is independent of the shape of the cross section; (ii) as a result of concrete deterioration, the difference between the plastic strain $\varepsilon_{pl,env}$ and the envelope unloading strain $\varepsilon_{un,env}$ grows larger with increase in $\varepsilon_{un,env}$ leading to larger strain energy absorption and dissipation capacity; and (iii) the reloading path experiences slight degradation in strength with increase in number of cycles. The dependency of the cyclic response on the cross-section shape (corner radius and aspect ratio) was previously studied by (Abbasnia, Ahmadi, & Ziaadiny, 2012; Abbasnia, Hosseinpour, Rostamian, & Ziaadiny, 2012; 2013) and the intrinsic shape of the unloading/reloading curves was found unaffected by the cross-section shape. As for the variation of the plastic strain $\varepsilon_{pl,env}$ with the unloading strain $\varepsilon_{un,env}$, almost all earlier studies e.g. (Lam L., Teng, Cheung, & Xiao, 2006; Wang, Wang, Smith, & Lu, 2012a; 2012c; Abbasnia & Holakoo, 2012; Abbasnia, Ahmadi, & Ziaadiny, 2012) (Abbasnia, Hosseinpour, Rostamian, & Ziaadiny, 2012; Abbasnia, Hosseinpour, Rostamian, &

Ziaadiny, 2013; Ozbakkaloglu & Akin, 2012) reported a linearly increasing relationship

consistent with the second observation. Degradation of stress in the reloading cycle is

in complete agreement with the experimental results reported by (Lam L. , Teng,

Cheung, & Xiao, 2006; Abbasnia & Holakoo, 2012; Abbasnia, Ahmadi, & Ziaadiny,

2012; Abbasnia, Hosseinpour, Rostamian, & Ziaadiny, 2012). Note also that the plastic

strain $\varepsilon_{pl,env}$ increases slightly with increase in number of cycles for the same

unloading strain $\varepsilon_{un,env}$, which was also reported by other investigators (Lam & Teng,

2009; Abbasnia, Ahmadi, & Ziaadiny, 2012). Nonetheless, the corresponding increase

is deemed small and can be neglected when generating a theoretical model of the stress-

strain response under cyclic loading.

C.   Generalized Stress-Strain Model

A constitutive model is proposed to better predict the axial stress-strain

response of FRP confined concrete under generalized loading. Idealized in Figure II-6,

the corresponding model adopts existing prediction models, except that the

characteristic parameters are refined on the basis of the current test results and other test

data reported in the technical literature. The proposed model is applicable for common

types of sections including circular, square and rectangular, and is capable of predicting

the stress-strain response for low or moderate amount of FRP confinement which may

cause a post-peak softening or descending behavior.

1.   Envelope Monotonic Response

Previous studies have shown that the envelope of the stress-strain of a confined

specimen subjected to cyclic loading is almost identical to the stress-strain curve of the

same specimen subjected to monotonic loading e.g. (Lam L. , Teng, Cheung, & Xiao, 2006; Lam & Teng, 2009; Abbasnia & Holakoo, 2012).

The envelope stress-strain curve can be divided into the following two distinct stages as shown in Figure II-6. A first stage up to a transition point at which $\sigma_c = f'_t$ and $\varepsilon_c = \varepsilon_t$, and a second stage extending from the transition point to the ultimate point when the CFRP ruptures, which is referred to as $\sigma_c = f'_{cu}$ and $\varepsilon_c = \varepsilon_{cu}$. The second part of the envelope curve can be either ascending describing a hardening behavior or descending indicating a softening behavior.

The proposed envelope model consists of two branches: a parabolic first branch describing the first stage of the response and a linear second branch describing the second stage. The corresponding model is similar to the one developed by (Lam & Teng, 2003a; 2003b), which is currently adopted by (ACI-440.2R-08, 2008), with differences in computing f'_{cu}, ε_{cu} and the intercept of the second branch of the response with the stress axis. Note that in assessing different prediction models using a large set of database, (Ozbakkaloglu, Lim, & Vincent, 2013) found that the model proposed by (Lam & Teng, 2003a) is one of the best performing models for predicting the strength enhancement for circular column sections. It should be indicated that the model proposed by (Lam & Teng, 2003a) was later refined by (Teng, Jiang, Lam, & Luo, 2009) based on new experimental results developed by the same research group and results from a parametric study using an accurate analysis-oriented stress–strain model. The modified model is only applicable to circular specimens, and although it takes into account the enhancement in the ultimate axial stress and strain for specimens showing softening behavior, it neglects the improvement in the axial stress at first peak for these specimens.

The model proposed by (Lam & Teng, 2003a; 2003b) assumes that the intercept of the second part of the curve is equal to f'_{co}. However, the same study mentions that the actual value is close to $1.09 f'_{co}$. Lam and Teng's approach considered only the case where the confinement level is able to produce a hardening behavior (post-peak ascending branch). However, for specimens experiencing a softening behavior (post-peak descending branch), based on the current experimental results and on results available in the literature, the intercept of the second branch is found larger and reaches values close to $1.2 f'_{co}$. To be able to describe hardening and softening behaviors using a unified model, an average value of $1.15 f'_{co}$ is considered as the intercept of the second part. Therefore, introducing this modification on the model proposed by (Lam & Teng, 2003a; 2003b) leads to the following relationship between the concrete compressive stress σ_c and axial strain ε_c:

$$\sigma_c = E_c \varepsilon_c - \frac{(E_c - E_2)^2}{4.6 f'_{co}} (\varepsilon_c)^2 \qquad for \qquad 0 \leq \varepsilon_c \leq \varepsilon_t \qquad \text{(II-1)}$$

$$\sigma_c = 1.15 f'_{co} + E_2 \varepsilon_c \qquad for \qquad \varepsilon_t \leq \varepsilon_c \leq \varepsilon_{cu} \qquad \text{(II-2)}$$

Where ε_t is the transition strain defined as:

$$\varepsilon_t = \frac{2.3 f'_{co}}{E_c - E_2} \qquad \text{(II-3)}$$

in which E_c = elastic modulus of the unconfined concrete defined as per (ACI-318-11/318R-11, 2011), i.e., $E_c = 4,730 \sqrt{f'_{co}}$ and $E_2 = (f'_{cu} - 1.15 f'_{co})/\varepsilon_{cu}$ represents the slope of the second branch of the envelope curve.

To account for the softening behavior, the expressions developed by (Lam & Teng, 2003a; Lam & Teng, 2003b) for the ultimate stress f'_{cu} and ultimate strain ε_{cu}

need to be modified. Using regression analysis of the current results combined with the

results of (Abbasnia & Ziaadiny, 2013) and (Lam & Teng, 2003b), and with the help of

statistical software, new expressions f'_{cu} and ε_{cu} were developed. Table II-3 shows

the geometric and material properties of the specimens tested by (Abbasnia & Ziaadiny,

2013) and (Lam & Teng, 2003b). The specimens tested by (Abbasnia & Ziaadiny,

2013) were 300 *mm* in height, fully wrapped with 2 layers of CFRP having the

following properties: thickness $t = 0.176$ *mm* per layer, modulus of elasticity $E_{frp} =$

241,000 *MPa*, ultimate tensile strain $\varepsilon_{fu} = 0.0163$. As for the specimens tested by (Lam

& Teng, 2003b), they consisted of square and rectangular specimens of 300 *mm* in

height wrapped with various numbers of CFRP layers, of thickness $t = 0.165$ *mm* per

layer, modulus of elasticity $E_{frp} = 257,000$ *MPa* and ultimate tensile strain $\varepsilon_{fu} = 0.0198$.

The experimental results of (Abbasnia & Ziaadiny, 2013) and (Lam & Teng, 2003b) are

shown in Table II-4. The ultimate tensile strain for (Lam & Teng, 2003b) is estimated

using the reported rupture strain values and the reported percentage of rupture strain

over the ultimate strain.

For the data assembled in Table II-1 and Table II-3, the unconfined concrete

compressive strength varied between 16.6 *MPa* and 51.5 *MPa*, the cross-sectional areas

varied between 156 *cm²* and 336 *cm²*, and the aspect ratio of the rectangular specimens

ranged between 1.0 and 2.0. The modified expressions of the ultimate axial stress and

strain are formulated as follows:

$$\frac{f'_{cu}}{f'_{co}} = 0.7 + 4.62 \left(\frac{b}{h}\right)^{0.92} \left(\frac{A_e}{A_c}\right) \left(\frac{f_l}{f'_{co}}\right) \tag{II-4}$$

$$\frac{\varepsilon_{cu}}{\varepsilon_{co}} = 3.89 + 14.76 \left(\frac{h}{b}\right)^{0.94} \left(\frac{A_e}{A_c}\right) \left(\frac{f_l}{f'_{co}}\right) \tag{II-5}$$

In these equations, ε_{co} is the axial strain at maximum stress for unconfined concrete taken equal to 0.002; A_e/A_c is the confinement effectiveness coefficient representing the ratio of the effectively confined area to the cross section area (

Figure II-7). For fully confined plain rectangular columns, the parameter A_e/A_c is dependent on the cross section aspect ratio and corner radius:

$$\frac{A_e}{A_c} = 1 - \frac{(b/h)(h-2R)^2 + (h/b)(b-2R)^2}{3A_c} \tag{II-6}$$

For fully confined circular columns, $A_e/A_c = 1.0$. For partially confined circular or rectangular columns, the confinement effectiveness coefficient A_e/A_c should be multiplied by a coefficient k_v given by the following equations (Mander, Priestley, & Park, 1988):

$$k_v = \left(1 - \frac{s'}{2D}\right)^2 \qquad \text{for circular columns} \tag{II-7}$$

$$k_v = \left(1 - \frac{s'}{2b}\right)\left(1 - \frac{s'}{2h}\right) \qquad \text{for rectangular columns} \tag{II-8}$$

in which s' is the clear spacing of the transverse FRP strips (Figure II-1). The confining pressure f_l provided by the CFRP:

$$f_l = \left(\frac{\rho_f E_{frp}}{2}\right)\varepsilon_{h,rup} \tag{II-9}$$

where ρ_f = volumetric ratio of the FRP reinforcement, and $\varepsilon_{h,rup}$ = measured strain at which the FRP ruptured in tension.

For fully wrapped columns, the volumetric ratio is expressed as

$\rho_f = 4t_{wrap}/D$ where D is the diameter of circular column section, or the equivalent

diameter for non-circular section given as $D = \sqrt{b^2 + h^2}$ first introduced by (Lam &

Teng, 2003b) and adopted later by many researchers to develop their models. For columns confined with discrete FRP strips (partially wrapped) having a strip width W and center-to-center spacing s (Figure II-1), the volumetric ratio of FRP reinforcement is calculated as $\rho_f = \left(4Wt_{wrap}\right)/(sD)$.

Defining the stiffness of the FRP jacket as:

$$K_l = \left(\frac{\rho_f E_{frp}}{2}\right)\left(\frac{A_e}{A_c}\right)$$ (II-10)

Equations (II-4 and II-5) can be written as:

$$\frac{f'_{cu}}{f'_{co}} = 0.7 + 4.62\left(\frac{b}{h}\right)^{0.92}\left(\frac{K_l}{f'_{co}}\right)\varepsilon_{h,rup}$$ (II-11)

$$\frac{\varepsilon_{cu}}{\varepsilon_{co}} = 3.89 + 14.76\left(\frac{h}{b}\right)^{0.94}\left(\frac{K_l}{f'_{co}}\right)\varepsilon_{h,rup}$$ (II-12)

It is worth noting that, due to the curvature of the CFRP wraps and non-uniform stress distribution in the CFRP material, the rupture of the CFRP occurs at strain values significantly smaller than the ultimate rupture strain obtained from direct coupon tests (Lam & Teng, 2003a). (Pessiki, Harries, Kestner, Sause, & Ricles, 2001) attributed the reduction in the FRP rupture strain to the residuals strains resulting from geometric imperfection in the substrate concrete, the large size of FRP jackets compared to FRP specimens used for coupon test and the flaws in the application process where misalignment or damage of jacket fibers can occur during handling and lay-up. A recent study (Wu & Jiang, 2013) has shown that the discrepancies between nominal and experimental rupture strain values are rather arising from the difference in strain measurements systems used for the flat coupon test and for the FRP jacket. They suggested adopting a normalized FRP fabrication method and strain measurement system allowing the strain reduction factor to be taken equal 90%. In a recent study

conducted by (Lim & Ozbakkaloglu, 2014b), the material properties (concrete strength

and type of FRP) were revealed important in determining when the FRP jacket breaks.

The presence of an overlap region where measured strains are significantly lower than

the average strain, and the testing technique may also cause reduction in the measured

rupture strain. (Lim & Ozbakkaloglu, 2014b) reported that the brittle failure of concrete

with high unconfined strength results in localized macrocracks causing the FRP jacket

to fail at an early stage. The same study reports a decrease in the rupture strain with

increase in FRP modulus of elasticity. In this study, the average ratio of the rupture

strain measured using both strain gages and LVDTs as described earlier for the CFRP

confined specimens tested to the ultimate tensile strain of the CFRP material is

measured at 60% but unfortunately with a significantly high standard deviation,

indicating inaccurate measurement of the rupture strain. (Lam & Teng, 2003a)

suggested using a value of the rupture strain $\varepsilon_{h,rup}$ for carbon, glass, and aramid fiber

reinforcement (CFRP, GFRP, AFRP), equal respectively to 58.6%, 62.4% and 85.1% of

the ultimate tensile strain ε_{fu} of the material. Also, (Abbasnia & Ziaadiny, 2013)

reported an average rupture strain of the CFRP confinement of about 60% of the

ultimate tensile strain with a standard deviation as low as 15.0%, which is very close to

that suggested by (Lam & Teng, 2003a). For the purpose of the analytical modeling

carried out in this study, a value of the rupture strain $\varepsilon_{h,rup}$ equal to 60% of the ultimate

tensile strain of the CFRP material was used for all specimens tested in this

investigation. This same approach was also used for some specimens in Table II-4

tested by (Abbasnia & Ziaadiny, 2013) in which the rupture strain was not reported.

As shown in Figure II-8 and Figure II-9, the accuracy of the proposed

expressions of f'_{cu}/f'_{co} and $\varepsilon_{cu}/\varepsilon_{co}$ is validated against experimental results

available in the literature including data from the experiments carried out by (Abbasnia & Ziaadiny, 2013; Harajli, Hantouche, & Soudki, 2006; Lam & Teng, 2003b; Lam L. , Teng, Cheung, & Xiao, 2006; Rochette & Labossière, 2000; Rousakis, Karabinis, & Kiousis, 2007; Shehata, Carneinro, & Shehata, 2002), and (Wang, Wang, Smith, & Lu, 2012a; 2012c) as well as the current experimental data. The average absolute error *AAE* is used to assess the accuracy of the proposed model. The average absolute error is defined as: $AAE = \left(\sum_{i=1}^{n} \left| (\mathrm{mod}_i - \mathrm{exp}_i)/\mathrm{exp}_i \right| \right)/N$, where $\mathrm{mod}_i - \mathrm{exp}_i = $ difference between the value predicted by the model and the experimentally measured value for specimen i, and $N = $ number of specimens. These comparisons show that the proposed model is able to predict with reasonable accuracy the ultimate stress, but with less accuracy in predicting the ultimate strain. The large variability in the ultimate strain values was also reported by many researchers. The main advantage of this proposed model is its ability to predict the descending branch for low confinement levels. Note that the proposed expression in Eq. (II-4) predicts that when the confinement ratio f_l / f'_{co} for a circular section is lower than 0.065 leads to an ultimate stress f'_{cu} less than f'_{co}. This is to some extent consistent with the value of 0.07 pointed out by (Lam & Teng, 2003b). On the other hand, (Lim & Ozbakkaloglu, 2014b) suggested that, for NSC and HSC cylinders, a strain-hardening response is expected to occur after the first peak if the confinement stiffness K_l ($K_l = \rho_f E_{frp}/2$ for fully confined specimens of circular sections) is greater than a threshold value, K_{lo}. The threshold confinement stiffness was found dependent on the unconfined concrete compressive strength f'_{co} as $K_{lo} = f'_{co}{}^{1.65}$. The expression of K_{lo} was later modified by (Lim & Ozbakkaloglu, 2014a) to $K_{lo} = 73.7 e^{0.027 f'_{co}}$.

It should be mentioned that a more general model for predicting the stress f'_{cu} and strain ε_{cu} at ultimate was recently proposed by (Lim & Ozbakkaloglu, 2014a), which is applicable for hardening and softening responses. Detailed description of this model can be found in (Lim & Ozbakkaloglu, 2014a). Because of the limitations imposed on the range of ratios of corner radius to equivalent section diameter, and type of FRP wrapping (fully wrapped as opposed to partially wrapped), the model cannot be extended to the data generated or used in the current study. Nonetheless, despite these limitations the model predicted well the ultimate stress f'_{cu} of the data used in the current study with an absolute average error $AAE = 8.4\%$ (Figure II-10a), but with a little lower level of accuracy in predicting the ultimate strain ε_{cu} (Figure II-10b) ($AAE = 44.3\%$). Note that the model proposed in this study predicts the data in Figure II-10 (this same data is already included in Figure II-8 and Figure II-9) with an $AAE = 8.4\%$ for the ultimate stress and 24.6% for the ultimate strain.

2. *Cyclic Response*

Figure II-6 shows idealization of the cyclic response along with response characteristic parameters. The main characteristic parameters consist of the following: (i) the point on the envelope monotonic curve ($\varepsilon_{un,env}$, $\sigma_{un,env}$) from which unloading occurs, (ii) the strain, referred to as envelope plastic strain $\varepsilon_{pl,env}$, at which the unloading curve potentially intersects the strain axis, and (iii) the point $(\varepsilon_{ret}, \sigma_{ret})$ where the reloading curve intersects the monotonic envelope curve. Cycles in which reloading takes place before reaching $\varepsilon_{pl,env}$ or unloading takes place before reaching ε_{ret}, are referred to as internal or incomplete cycles.

a)	Unloading curve

Using regression analysis of test data, a new expression is developed to describe the unloading curve. In addition to the 14 confined specimens tested in the current experimental program, in order to account for a wider range of specimens' parameters (cross-section shape, aspect ratio, confinement level, unconfined concrete compressive strength), 10 specimens tested by other investigators are also considered in the analysis. These include 6 plain concrete specimens ($CI-SC1$, $CI-SC2$, $CI-RC$, $CII-SC1$, $CII-SC2$, $CII-RC$) tested by (Lam L. , Teng, Cheung, & Xiao, 2006), two circular plain concrete specimens ($C2H0L1C$ and $C2H0L2C$) tested by (Wang, Wang, Smith, & Lu, 2012c), and two square plain concrete specimens ($S2H0L1C$ and $S2H0L2C$) tested by (Wang, Wang, Smith, & Lu, 2012a).

(Wang, Wang, Smith, & Lu, 2012b; 2012c) suggested a non-linear expression of the unloading curve which describes well the intrinsic shape of the unloading response of the specimens tested in the current investigation. This expression takes the following form:

$$\frac{\sigma_c}{\sigma_{un,env}} = B_o \left(\frac{\varepsilon_c - \varepsilon_{pl,env}}{\varepsilon_{un,env} - \varepsilon_{pl,env}} \right)^{B_1} + \left(1 - B_o\right) \left(\frac{\varepsilon_c - \varepsilon_{pl,env}}{\varepsilon_{un,env} - \varepsilon_{pl,env}} \right) \qquad \text{(II-13)}$$

where $(\varepsilon_c, \sigma_c)$ are the coordinates of a given point on the unloading curve. Based on their own test results, (Wang, Wang, Smith, & Lu, 2012b; 2012c) proposed different expressions for B_o and B_1 for circular and square specimens. In order to account for other test data and other types of cross sections to include circular, rectangular and square sections, refined expressions of the coefficients B_o and B_1 were derived in the current study.

The expressions proposed by (Wang, Wang, Smith, & Lu, 2012b; 2012c) for

B_o were mainly as a function of the confinement coefficient f_l / f'_{co} provided by both

the CFRP wraps and the internal steel reinforcement. For plain concrete specimens, the

corresponding expressions predict variation of B_o with f_l / f'_{co} between a minimum of

0.7 and a maximum of 0.8 for circular specimens and between 0.6 and 0.9 for square

specimens. Analysis of the 24 specimens in the current investigation shows that a

constant value of $B_o = 0.8$ can be adopted for plain concrete specimens of circular,

square and rectangular cross-section. The modified expression of the unloading curve

can then be written as follows:

$$\frac{\sigma_c}{\sigma_{un,env}} = 0.8\left(\frac{\varepsilon_c - \varepsilon_{pl,env}}{\varepsilon_{un,env} - \varepsilon_{pl,env}}\right)^{B_1} + 0.2\left(\frac{\varepsilon_c - \varepsilon_{pl,env}}{\varepsilon_{un,env} - \varepsilon_{pl,env}}\right) \tag{II-14}$$

The coefficient B_1 represents the degree of non-linearity of the unloading

curve. Previous researches have shown that the non-linearity is mainly dependent on

the unloading strain $\varepsilon_{un,env}$. Once again, by means of a regression analysis of the 24

specimens shown in Figure II-11, the following expression for B_1 is proposed:

$$B_1 = 2.172\left(\frac{\varepsilon_{un,env}}{\varepsilon_{co}}\right)^{0.324} \tag{II-15}$$

b)   Plastic Strain

Earlier models (Lam & Teng, 2009) accounted for the slight increase in the

plastic strain $\varepsilon_{pl,env}$ with number of cycles for the same unloading point ($\varepsilon_{un,env}$,

$\sigma_{un,env}$) on the envelope curve. This was achieved by defining an internal plastic strain

(for internal or incomplete cycles) and proposing expressions to quantify it as a function

of the number of cycles. However, in this study, in order to simplify the model, the plastic strain $\varepsilon_{pl,env}$ is assumed constant irrespective of the number of cycles. This assumption is believed to have insignificant effect on the accuracy of constitutive concrete stress-strain material models of the type under investigation, as well as the outcomes of analytical studies when such models are incorporated in numerical analysis schemes for evaluating the behavior of FRP confined concrete members.

Figure II-12 shows typical variation of the envelope plastic strain $\varepsilon_{pl,env}$ with the confinement ratio f_l/f'_{co} (taken for the specimens in series *R2* of the current investigation) and Figure II-13 shows a plot of variation of the envelope plastic strain versus the envelope unloading strain for the four column sections tested in the current investigation. From Figure II-12, the confinement ratio is seen to have little effect on the magnitude of the plastic strain. Also, from Figure II-13, the value of the plastic strain is independent of the geometry (circular, square or rectangular) or aspect ratio of the section. These observations are consistent with earlier observations reported in other experimental studies (Lam L. , Teng, Cheung, & Xiao, 2006; Lam & Teng, 2009; Abbasnia, Hosseinpour, Rostamian, & Ziaadiny, 2012). As for the effect of the corner radius, it was previously studied by (Abbasnia, Ahmadi, & Ziaadiny, 2012) and found to be of minor importance. The influence of the unconfined concrete compressive strength, f'_{co}, on the envelope plastic strain is also examined by analyzing the data assembled from the current experiment (assuming an average value of f'_{co} of 18.0 *MPa*) with data collected from different experimental studies for covering a range of unconfined concrete compressive strength f'_{co} mostly used in practice ($f'_{co} \leq 50$ *MPa*). These include (Lam L. , Teng, Cheung, & Xiao, 2006) ($f'_{co} = 38.9$ *MPa* and

41.1 *MPa*), (Wang, Wang, Smith, & Lu, 2012a; 2012c) ($f'_{co} = 25.5$ *MPa*), (Abbasnia,

Hosseinpour, Rostamian, & Ziaadiny, 2013) ($f'_{co} = 30$ *MPa* and 33 *MPa*), (Abbasnia

& Holakoo, 2012) ($f'_{co} = 46.3$ MPa) and (Abbasnia, Hosseinpour, Rostamian, &

Ziaadiny, 2012) ($f'_{co} = 50$ MPa). Figure II-14 shows variation of the envelope plastic

strain against the envelope unloading strain for different unconfined concrete

compressive strength. It can be seen that for the same envelope unloading strain, the

envelope plastic strain is slightly larger for smaller f'_{co}. However, within the

considered range of unconfined concrete strengths (16.6 *MPa* $\leq f'_{co} \leq 50$ *MPa*), its

effect can be neglected. (Lam & Teng, 2009) and (Abbasnia, Hosseinpour, Rostamian,

& Ziaadiny, 2012) accounted for the influence of unconfined concrete compressive

strength when developing expressions of the plastic strain, however, (Ozbakkaloglu &

Akin, 2012) considered this effect negligible, even for high values of f'_{co} reaching 110

MPa.

Based on regression analysis of the previously mentioned test, refined

expressions of the envelope plastic strain are proposed (Figure II-15a and b). For small

values of the envelope unloading strain ($\varepsilon_{un,env} \leq 0.001$), the plastic strain is assumed to

be negligible consistent with previous research (Lam & Teng, 2009; Wang, Wang,

Smith, & Lu, 2012b; 2012c; Abbasnia, Hosseinpour, Rostamian, & Ziaadiny, 2012;

Abbasnia, Hosseinpour, Rostamian, & Ziaadiny, 2013). Accordingly, the proposed

expressions are:

$$\varepsilon_{pl,env} = 0 \qquad for \qquad \varepsilon_{un,env} \leq 0.001 \tag{II-16}$$

$$\varepsilon_{pl,env} = 0.4552\varepsilon_{un,env} - 0.0003 \qquad for\ 0.001 < \varepsilon_{un,env} \leq 0.0035 \tag{II-17}$$

$$\varepsilon_{pl,env} = 0.7827\varepsilon_{un,env} - 0.0014 \qquad for\ \varepsilon_{un,env} > 0.0035 \tag{II-18}$$

33

The proposed expression for the envelope plastic strain when $\varepsilon_{un,env} > 0.0035$ is in close agreement with expressions proposed for CFRP confined cylinders by other researchers (Lam L. , Teng, Cheung, & Xiao, 2006; Ozbakkaloglu & Akin, 2012).

c)   Reloading path

The reloading path is assumed to be linear with a slope which slightly decreases with increase in number of cycles as a result of concrete stress degradation (Figure II-4 and Figure II-5). This degrading stress can be simulated using a stress degradation ratio $\varphi_N = \sigma_N / \sigma_{un,env}$, in which σ_N is the stress during the reloading cycle at a strain level equal to the envelope unloading strain $\varepsilon_{un,env}$ corresponding to cycle no. N ($N = 0$, 1, 2, 3, …) (Figure II-6), where $\sigma_{N=0} = \sigma_{un,env}$. The experimental results show that for small unloading strains ($\varepsilon_{un,env} \leq 0.001$), the loss of stress is negligible and φ_N is almost equal to 1 irrespective of the number of cycles. However, for $\varepsilon_{un,env} > 0.001$, the stress degradation becomes more significant. Figure II-16 plots the variation of φ_N with cycle number $(N+1)$ for $\varepsilon_{un,env} > 0.001$. Using regression analysis, the following simple expression is derived to describe the stress degradation with number of cycles:

$$\varphi_N = \frac{\sigma_N}{\sigma_{un,env}} = 1 - 0.09 Ln(N+1) \qquad (\text{II-19})$$

Eq. (II-19) predicts stress reductions relative to the envelope unloading stress $\sigma_{un,env}$ of about 6%, 10%, and 12% for the 1st, 2nd, and 3rd reloading cycles. The reloading path is generated by joining linearly points ($\varepsilon_{pl,env}$, 0) and ($\varepsilon_{un,env}$, σ_N).

The corresponding line intersects the envelope curve at (ε_{ret}, σ_{ret}) as shown in Figure II-6. The equation of the reloading curve is expressed as:

$$\sigma = \varphi_N \sigma_{un,env} \left(\frac{\varepsilon_c - \varepsilon_{pl,env}}{\varepsilon_{un,env} - \varepsilon_{pl,env}} \right)$$

(II-20)

Note that, the coordinates (ε_{ret}, σ_{ret}) can be easily calculated from the intersection point between the envelope curve defined by Eqs. (II-1) and (II-2) and the reloading curve defined in Eq. (II-20).

It should be indicated that a further reasonable simplification of the model, with no significant loss of accuracy, would be to neglect the strength degradation beyond the first reloading cycle. If this simplification is adopted, which is highly recommended, it is suggested to use $\varphi_N = 0.92$, regardless of the number of cycles. In this case, the dotted reloading paths in the right cycle of Figure II-6 would all coincide with the same solid line joining points ($\varepsilon_{pl,env}$, 0) and ($\varepsilon_{un,env}$, 0.92 $\sigma_{un,env}$).

For internal or incomplete cycles, unloading from any point between ($\varepsilon_{pl,env}$, 0) and (ε_{ret}, σ_{ret}) can be traced using Eq. (II-14) in which $\varepsilon_{un,env}$ and $\sigma_{un,env}$ are replaced with ε_{un} and σ_{un} at which unloading occurs (Figure II-6). On the other hand, reloading from any point on the unloading curve before reaching ($\varepsilon_{pl,env}$, 0) is assumed to be linear with a slope equal to the initial slope of the unloading curve (Figure II-6) E_{un}, calculated using Eq. (II-14) as:

$$E_{un} = (0.8B_1 + 0.2) \left(\frac{\sigma_{un,env}}{\varepsilon_{un,env} - \varepsilon_{pl,env}} \right)$$

(II-21)

What follows is a step-by-step procedure for generating the cyclic stress-strain response: Given the geometric properties of the cross-section (diameter D for a circular

section or depth h, width b, and corner radius R of a square/rectangular section); the material properties of concrete (f'_{co}, E_c) and CFRP (E_{frp}, ε_{fu}) and the number and configuration of CFRP layers (n and s), the ultimate stress and strain are calculated using Eqs. (II-4) and (II-5) and the envelope stress-strain response is generated using Eqs. (II-1), (II-2) and (II-3). Generating any unloading/reloading cycle requires specifying the envelope unloading strain $\varepsilon_{un,env}$. Subsequently, the envelope unloading stress $\sigma_{un,env}$, the envelope plastic strain $\varepsilon_{pl,env}$ and the degree of non-linearity B_1 are calculated respectively using Eqs. (II-1, II-2), (II-16, II-17, II-18), and (II-15). These parameters are used in Eq. (II-14) to generate the unloading response. If unloading drops to zero stress, reloading follows the curve defined by Eq. (II-20) (with φ_N = 0.92). If unloading is terminated before reaching zero stress at a strain $\varepsilon_{pl,env} < \varepsilon < \varepsilon_{un,env}$, reloading is assumed linear with a slope defined by Eq. (II-21) in a first stage and follows the envelope reloading curve defined by Eq. (II-20) (with φ_N = 0.92) in a second stage.

A new unloading strain (ε_{un}) is specified. If its value is such that $\varepsilon_{pl,env} < \varepsilon_{un} < \varepsilon_{ret}$ (where ε_{ret} is calculated from the intersection point between the envelope curve defined by Eqs. (II-1) and (II-2) and the reloading curve of the previous cycle defined in Eq. (II-20), an internal unloading curve is generated using Eq. (II-14) with ($\varepsilon_{un,env}$, $\sigma_{un,env}$) substituted by (ε_{un}, σ_{un}); and if its value is greater than ε_{ret} ($\varepsilon_{un} > \varepsilon_{ret}$), then the reloading curve meets the envelope curve at (ε_{ret}, σ_{ret}) and a new envelope unloading cycle starts.

D.   Proposed Model versus Experimental Results

Figure II-17 and Figure II-20 show comparisons of the model predictions with the test results generated in the experimental part of this investigation. The envelope response of the proposed model is also validated against the experimental results of few specimens tested by (Lam & Teng, 2003b) and (Abbasnia & Ziaadiny, 2013) as shown in Figure II-21 and Figure II-22, respectively. Details of these specimens are given in Table II-3 and Table II-4. Furthermore, the cyclic response of the proposed model is compared with selected experimental results corresponding to square specimens having section dimensions $b = h = 204 mm$ of (Wang, Wang, Smith, & Lu, 2012a) (Figure II-23); circular specimens having diameter $D = 204 mm$ of (Wang, Wang, Smith, & Lu, 2012c) (Figure II-24); circular specimens having diameter $D = 152 mm$ of (Lam L. , Teng, Cheung, & Xiao, 2006) (Figure II-25); and specimens tested by (Abbasnia, Hosseinpour, Rostamian, & Ziaadiny, 2012) consisting of square specimens $C2SJ2L3$ and $C1SJ1L2b$ ($b = h = 152 mm$), and rectangular specimen $C1R1JL3a$ and $C1R1JL3b$ ($b = 90\ mm,\ h = 152\ mm$), as shown in Figure II-26.

It can be seen from the comparisons shown in Figure II-17 through Figure II-26 that, despite some discrepancy, the model is able to reproduce the experimental results of the current investigation and other test data with good accuracy. The proposed model presents a simple approach that accounts for all types of sections and confinement parameters in unified expressions. Also, it is capable of predicting with good accuracy the monotonic and cyclic stress-strain behavior of FRP confined concrete with ascending or descending branches in the post peak response.

Table II-1 – Specimens' geometry and material properties

Specimen	D (mm)	b (mm)	h (mm)	$\frac{h}{b}$	$\frac{A_e}{A_c}$	Wrapping mode	t_{wrap} (mm)	f'_{co} (MPa)
CU					-	-	0.00	
CP1	200	-	-	1.00	0.765	Partial	0.13	16.60
CF1					1.000	Full	0.13	
SU					-	-	0.00	
SP1					0.347	Partial	0.13	
SF1	-	160	160	1.00	0.488	Full	0.13	18.50
SF2					0.488	Full	0.26	
SF3					0.488	Full	0.39	
R1U					-	-	0.00	
R1P1					0.346	Partial	0.13	
R1F1	-	140	180	1.29	0.490	Full	0.13	17.60
R1F2					0.490	Full	0.26	
R1F3					0.490	Full	0.39	
R2U					-	-	0.00	
R2P1					0.346	Partial	0.13	
R2F1	-	130	200	1.54	0.490	Full	0.13	20.20
R2F2					0.490	Full	0.26	
R2F3					0.490	Full	0.39	

* $r = 10$ mm for all non-circular specimens

Table II-2 – Specimens' test results

Specimen	$\dfrac{f_l}{f'_{co}}$ *	$\dfrac{\varepsilon_{cu}}{\varepsilon_{co}}$	$\dfrac{f'_t}{f'_{co}}$	$\dfrac{f'_{cu}}{f'_{co}}$
CU	-	1.75	1.00	-
CP1	0.081	3.90	1.15	1.21
CF1	0.162	9.30	1.22	1.45
SU	-	2.00	1.00	-
SP1	0.064	3.05	1.09	0.80
SF1	0.129	5.30	1.18	1.07
SF2	0.258	6.25	1.28	1.24
SF3	0.386	8.60	1.24	1.33
R1U	-	2.00	1.00	-
R1P1	0.067	3.10	1.02	0.68
R1F1	0.134	3.75	1.15	1.02
R1F2	0.268	3.75	1.33	1.22
R1F3	0.402	11.30	1.33	1.41
R2U	-	2.75	1.00	-
R2P1	0.056	3.05	0.98	0.79
R2F1	0.111	5.00	1.04	0.79
R2F2	0.223	10.75	1.11	0.89
R2F3	0.335	8.90	1.14	0.98

* f_l is calculated using Eq. (II-9) assuming $\varepsilon_{h,rup} = 0.6\,\varepsilon_{fu}$

Table II-3 - Geometry and material properties of the specimens tested by (Abbasnia & Ziaadiny, 2013) and (Lam & Teng, 2003b)

Specimen	D (mm)	b (mm)	h (mm)	$\dfrac{h}{b}$	$\dfrac{A_e}{A_c}$	R (mm)	f'_{co} (MPa)	t_{wrap} (mm)
(Abbasnia & Ziaadiny, 2013)								
A1	-	150	150	1.00	0.550	13.6	32.0	0.352
A2	-	150	150	1.00	0.668	22.6	32.0	0.352
A3	-	150	150	1.00	0.796	34.5	34.0	0.352
A4	-	150	150	1.00	0.862	42.0	34.0	0.352
A5	-	120	180	1.50	0.620	18.1	35.0	0.352
A6	-	120	180	1.50	0.734	27.6	32.0	0.352
A7	`	120 c	180	1.50	0.804	34.5	32.0	0.352
A8	-	90	180	2.00	0.593	13.6	34.0	0.352
A9	-	90	180	2.00	0.723	22.6	32.0	0.352
A10	-	90	180	2.00	0.772	26.8	32.0	0.352
A11	150	-	-	1.00	1.000	75.0	32.0	0.352
B1	-	150	150	1.00	0.550	13.6	49.0	0.352
B2	-	150	150	1.00	0.668	22.6	51.5	0.352
B3	-	150	150	1.00	0.796	34.5	51.5	0.352
B4	-	150	150	1.00	0.862	42.0	50.0	0.352
B5		120	180	1.50	0.620	18.1	50.0	0.352
B6	-	120	180	1.50	0.734	27.6	51.5	0.352
B7		120	180	1.50	0.804	34.5	50.0	0.352
B8	-	90	180	2.00	0.593	13.6	49.0	0.352
B9		90	180	2.00	0.723	22.6	49.0	0.352
B10	-	90	180	2.00	0.772	26.8	49.0	0.352
B11	150	-	-	1.00	1.000	75.0	47.0	0.352
(Lam & Teng, 2003b)								
S1R15	-	150	150	1.00	0.570	15.0	33.7	0.165
S1R25	-	150	150	1.00	0.696	25.0	33.7	0.165
S2R15	-	150	150	1.00	0.570	15.0	33.7	0.330
S2R25	-	150	150	1.00	0.696	25.0	33.7	0.330
S3R15	-	150	150	1.00	0.570	15.0	24.0	0.495
S3R25	-	150	150	1.00	0.696	25.0	24.0	0.495
S4R15	-	150	150	1.00	0.570	15.0	24.0	0.660
S5R25	-	150	150	1.00	0.696	25.0	41.5	0.825
R4R15	-	150	225	1.50	0.534	15.0	41.5	0.660
R4R25	-	150	225	1.50	0.644	25.0	41.5	0.660

*All the specimens are fully wrapped

Table II-4 – Experimental results of the specimens tested by (Abbasnia & Ziaadiny, 2013) and (Lam & Teng, 2003b)

Specimen	$\varepsilon_{h,rup}$ (mm/mm)	$\dfrac{f_l}{f'_{co}}$	$\dfrac{\varepsilon_{cu}}{\varepsilon_{co}}$	$\dfrac{f'_t}{f'_{co}}$	$\dfrac{f'_{cu}}{f'_{co}}$
(Abbasnia & Ziaadiny, 2013)					
A1	0.0099	0.2474	10.25	1.119	1.224
A2	0.0091	0.2274	9.25	1.063	1.424
A3	0.0109	0.2564	8.55	1.060	1.512
A4	0.0111	0.2611	6.80	1.118	1.536
A5	0.0100	0.2241	8.60	1.143	1.162
A6	0.0102	0.2500	7.65	1.031	1.334
A7	0.0099	0.2426	7.15	1.094	1.466
A8	0.0111	0.2752	9.35	1.118	0.941
A9	0.0102	0.2687	8.90	1.125	1.218
A10	0.0087	0.2292	8.50	1.063	1.327
A11	0.0109	0.3853	11.45	1.188	2.087
B1	0.0104	0.1697	3.93	1.020	0.939
B2	0.0109	0.1693	6.85	1.068	1.089
B3	0.0108	0.1677	5.60	1.049	1.208
B4	-	0.1564*	5.05	1.100	1.300
B5	-	0.1534*	5.25	1.060	1.000
B6	0.0095	0.1447	4.20	1.058	1.094
B7	-	0.1534*	5.75	1.060	1.210
B8	0.0050	0.0860	5.20	1.061	0.735
B9	-	0.1649*	6.25	1.061	0.816
B10	0.0080	0.1376	8.35	1.112	0.908
B11	0.0095	0.2286	7.55	1.149	1.749
(Lam & Teng, 2003b)					
S1R15	0.0103	0.1222	3.75	1.018	0.979
S1R25	0.0105	0.1246	4.60	1.039	1.157
S2R15	0.0097	0.2302	4.35	1.083	1.507
S2R25	0.0108	0.2563	4.25	1.157	1.780
S3R15	0.0087	0.4348	9.00	1.333	2.542
S3R25	0.0116	0.5797	7.50	1.167	2.708
S4R15	0.0091	0.6064	7.50	1.333	2.500
S5R25	0.0115	0.5540	6.75	1.084	2.289
R4R15	0.0107	0.3235	6.15	1.205	1.084
R4R25	0.0074	0.2237	5.25	1.253	1.373
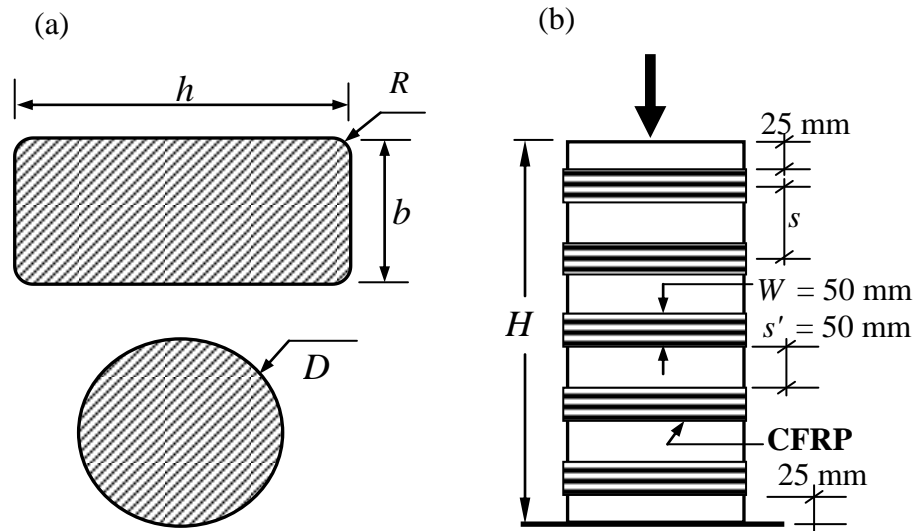
Figure II-1 - Specimens details: (a) Cross-sectional properties of rectangular and circular specimens, (b) Configuration of partially wrapped specimens
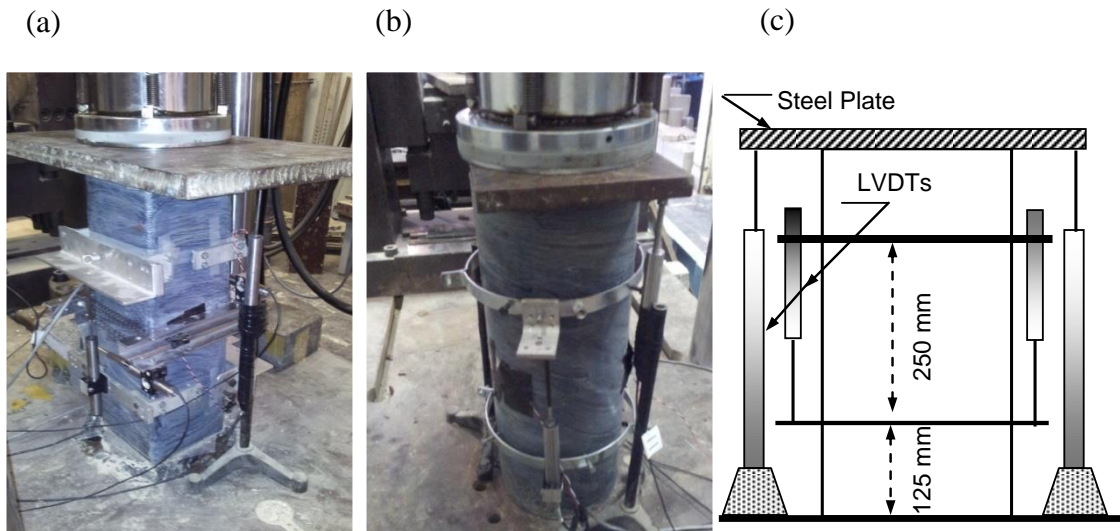
Figure II-2 - Instrumentation and test set-up: (a) Specimen *SF1*, (b) Specimen *CF1*, (c) LVDTs on square specimens

(a)   (b)

Figure II-3 - Typical failure modes of specimens: (a) Confined – (b) Unconfined
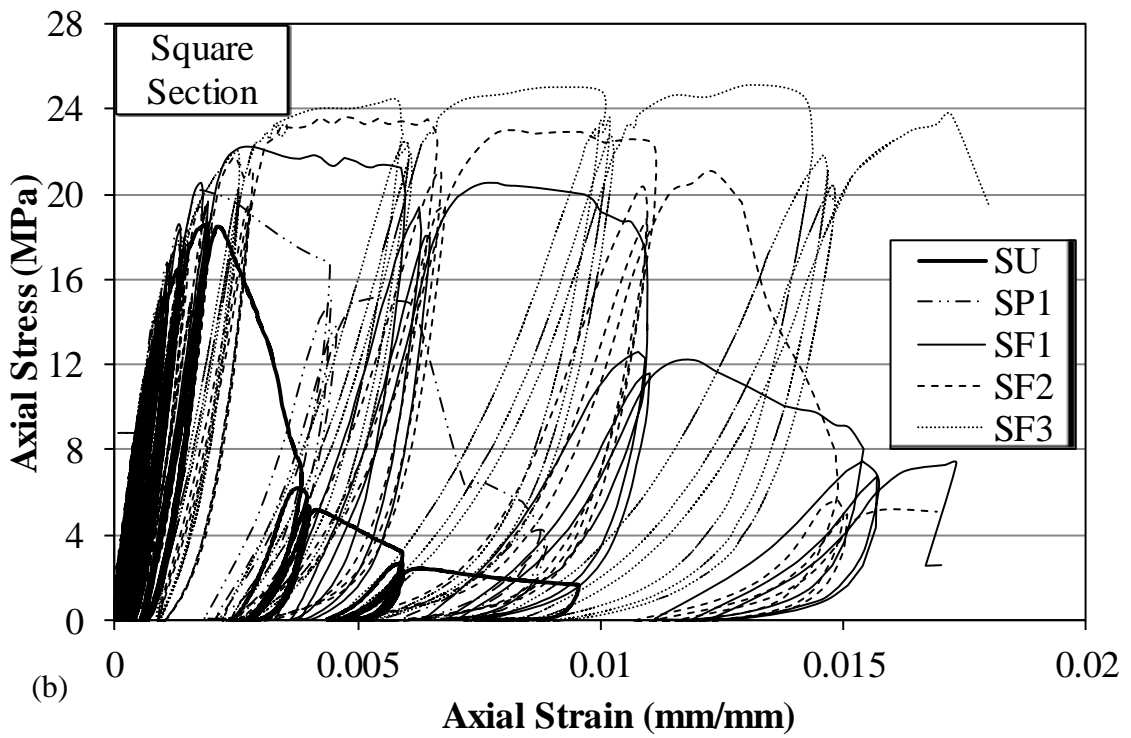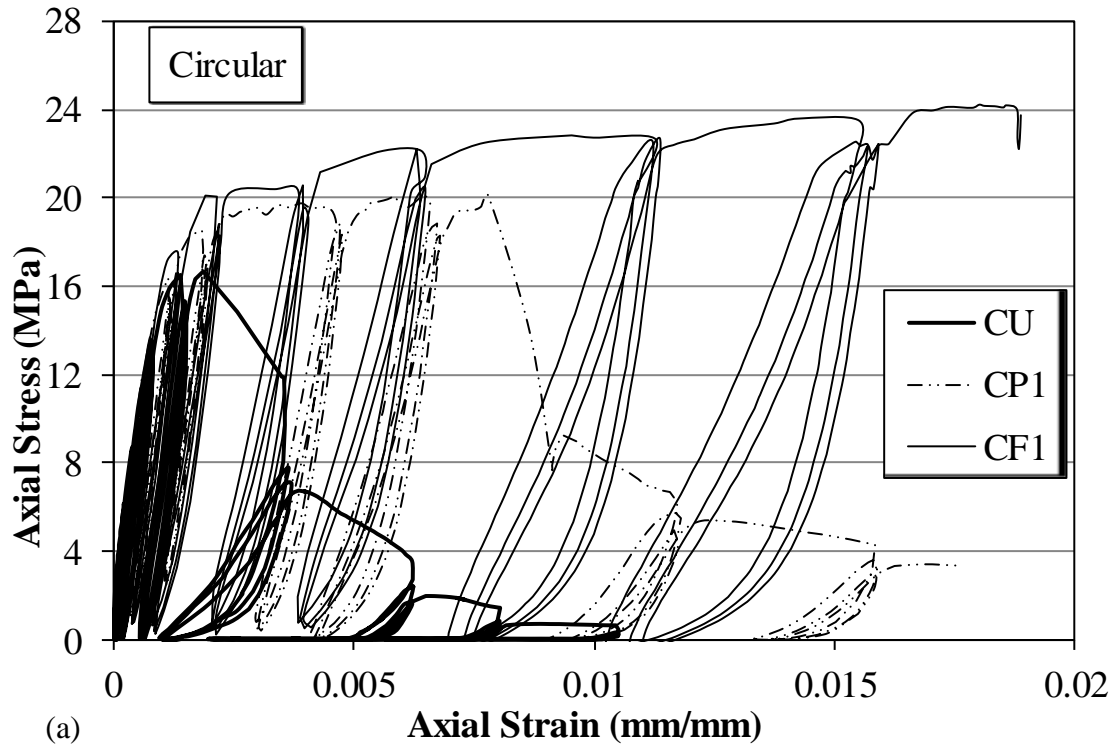
Figure II-4 - Stress-strain response of the tested specimens: (a) Series *C*, (b) Series *S*
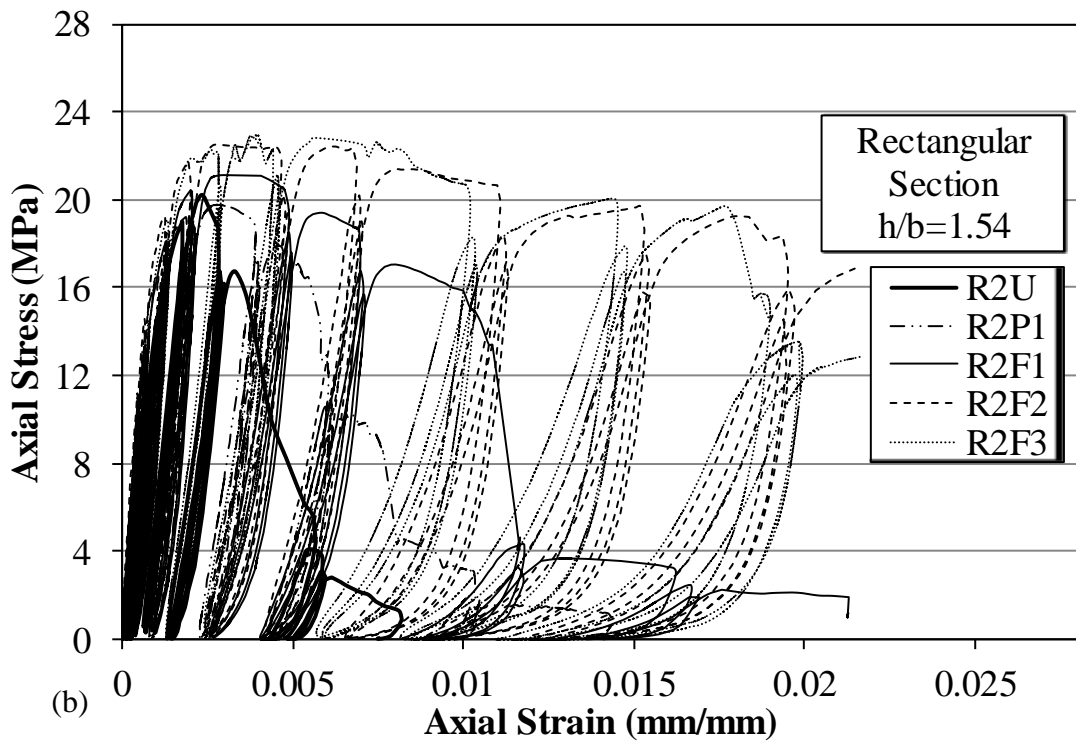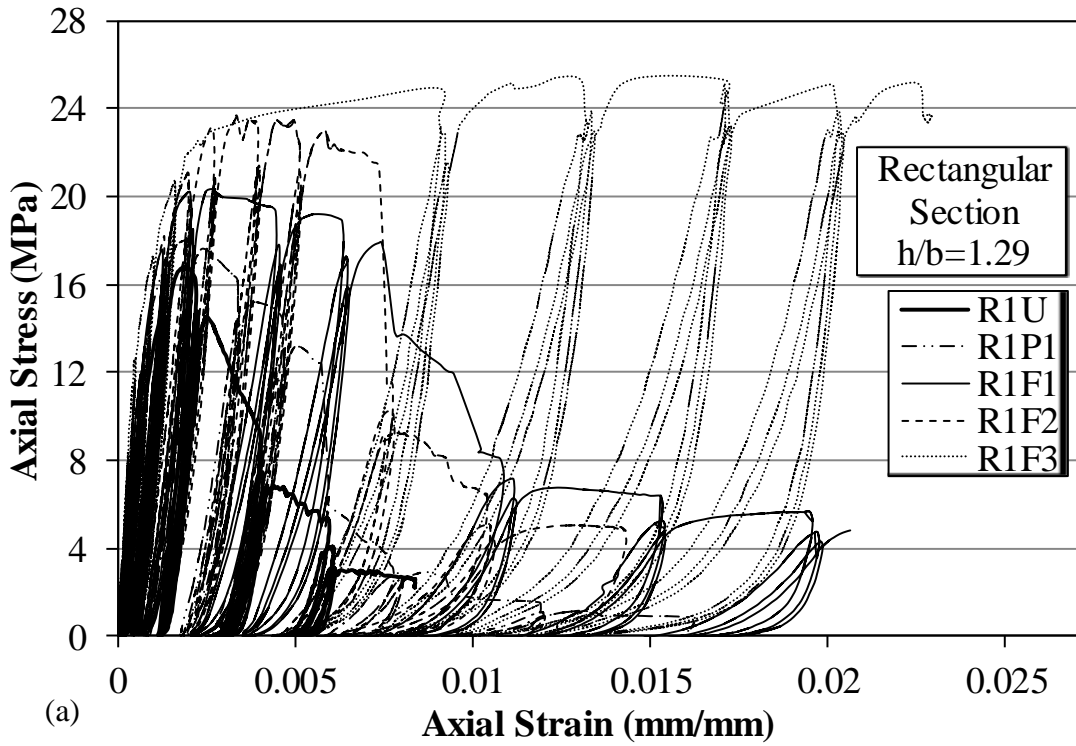
Figure II-5 - Stress-strain response of the tested specimens: (a) Series *R*1, (b) Series *R2*
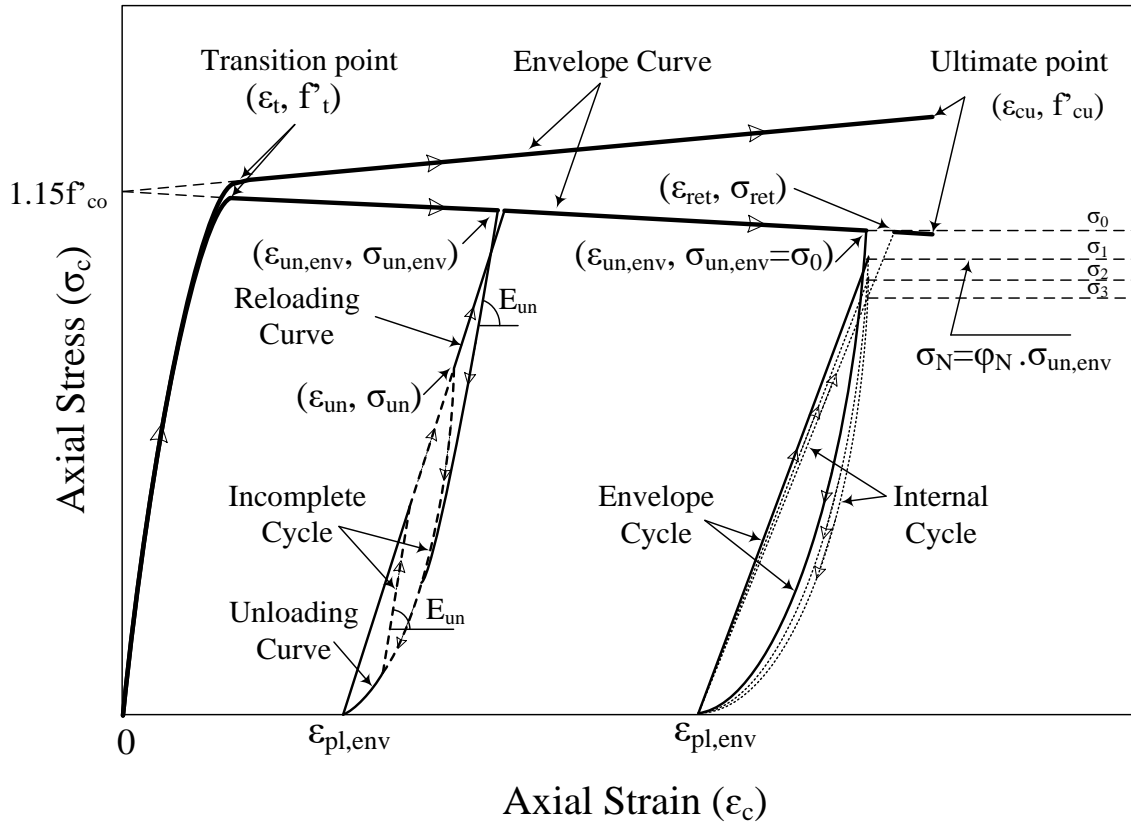
Figure II-6 - Idealization of the envelope and cyclic stress-strain responses
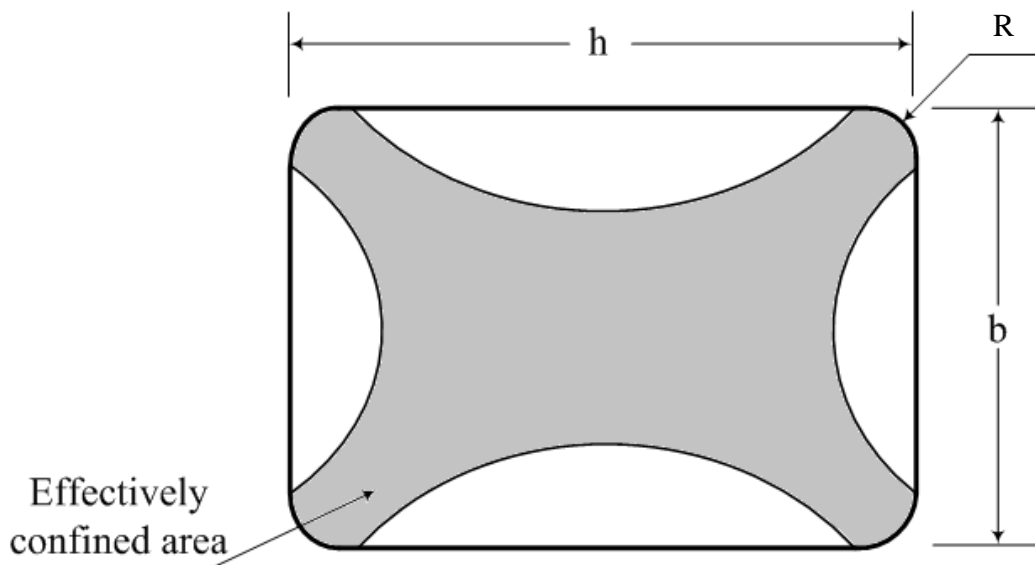
Figure II-7 - Effectively confined area of a rectangular cross-section
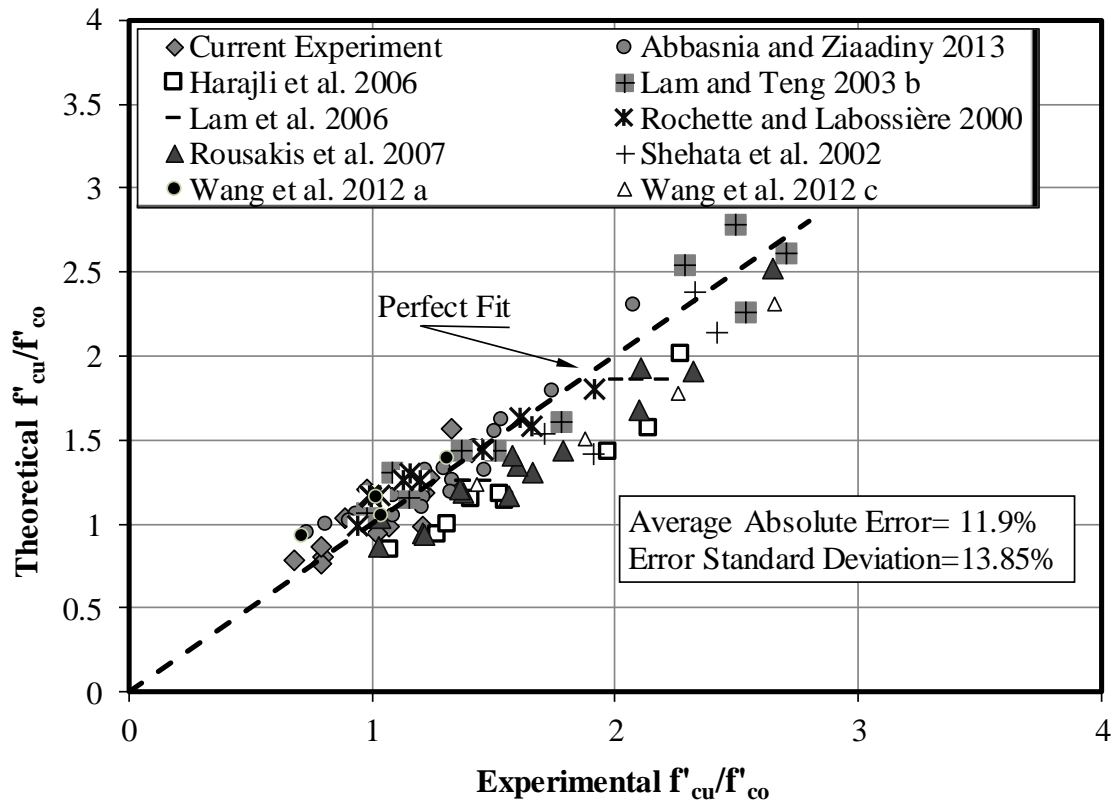
Figure II-8 - Comparison of the proposed model of f'_{cu}/f'_{co} with experimental results
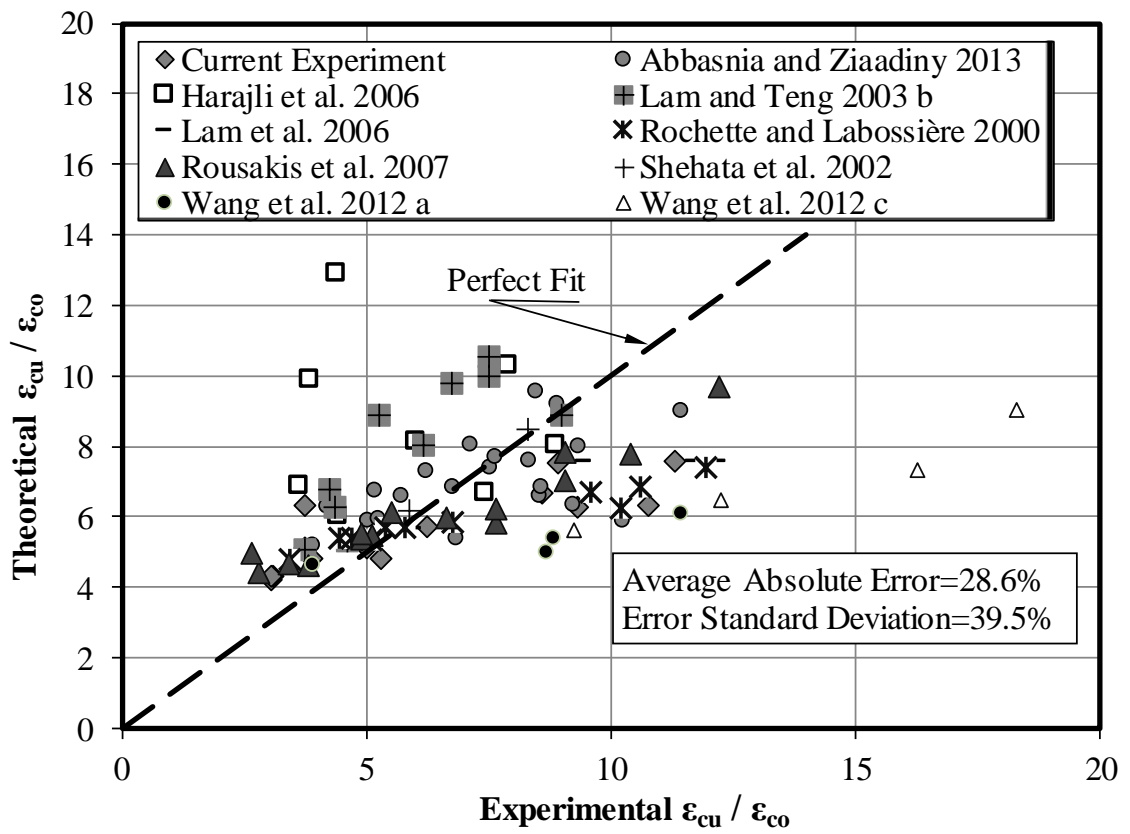
Figure II-9 - Comparison of the proposed model of $\varepsilon_{cu}/\varepsilon_{co}$ with experimental results
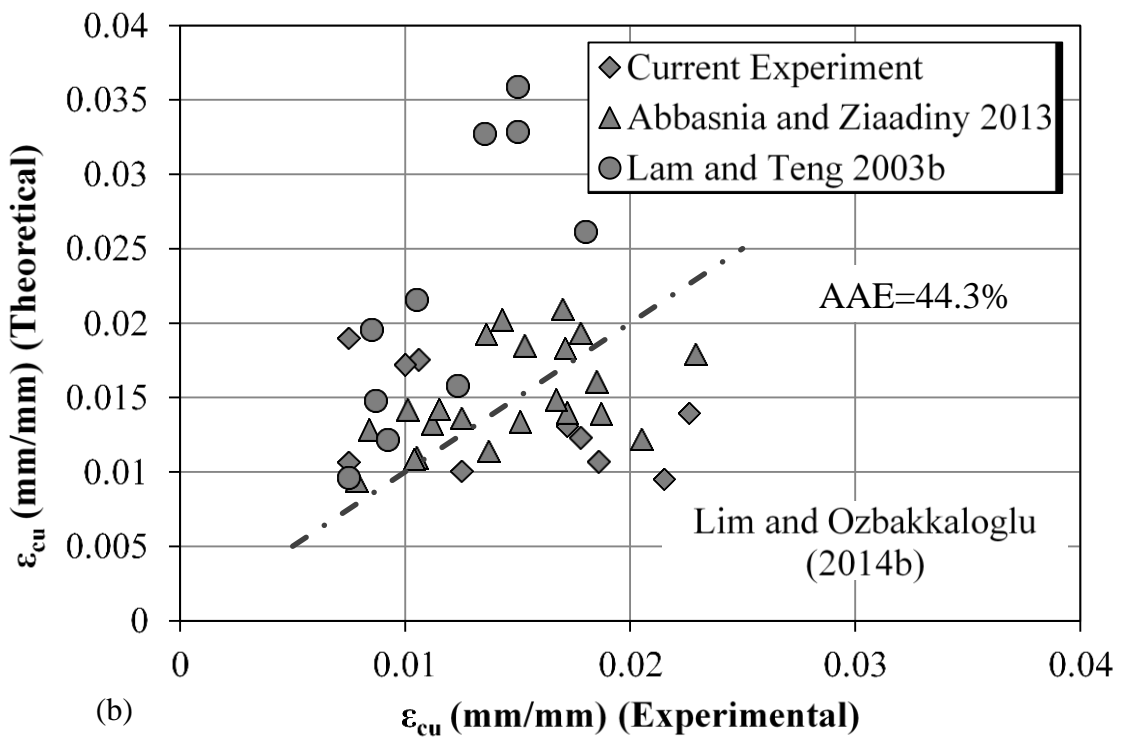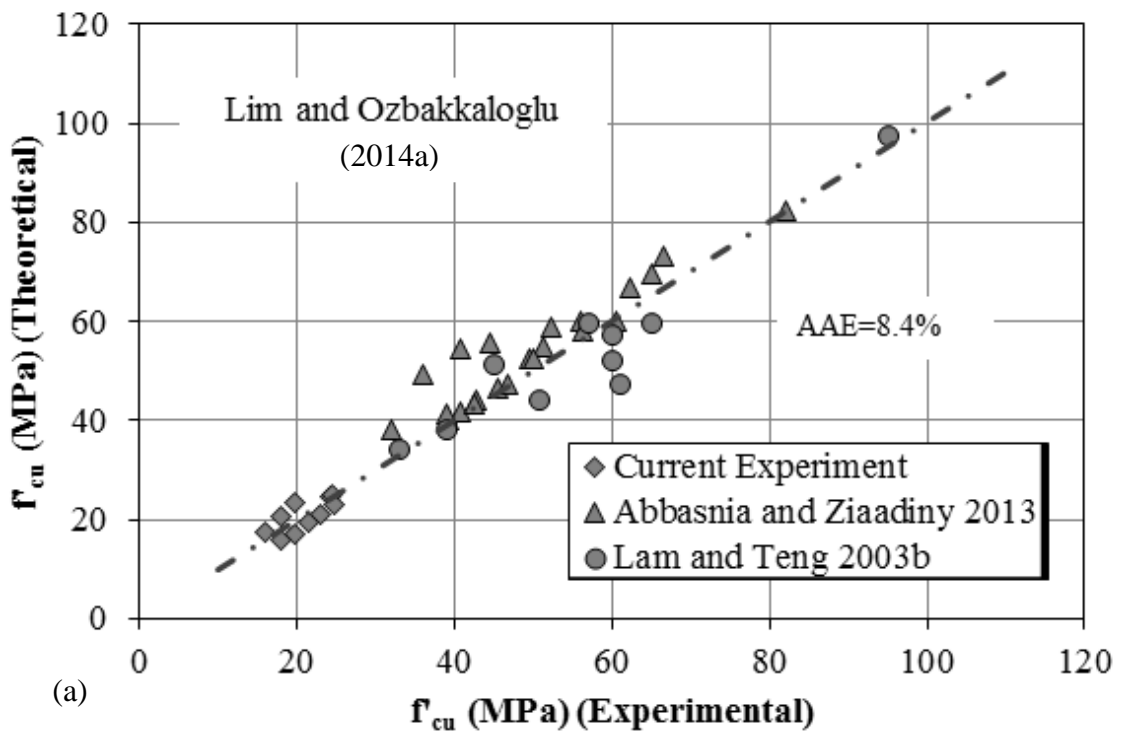
Figure II-10 - Performance of the (Lim & Ozbakkaloglu, 2014a) model in predicting:
(a) the ultimate stress f'_{cu}; (b) the ultimate strain ε_{cu}
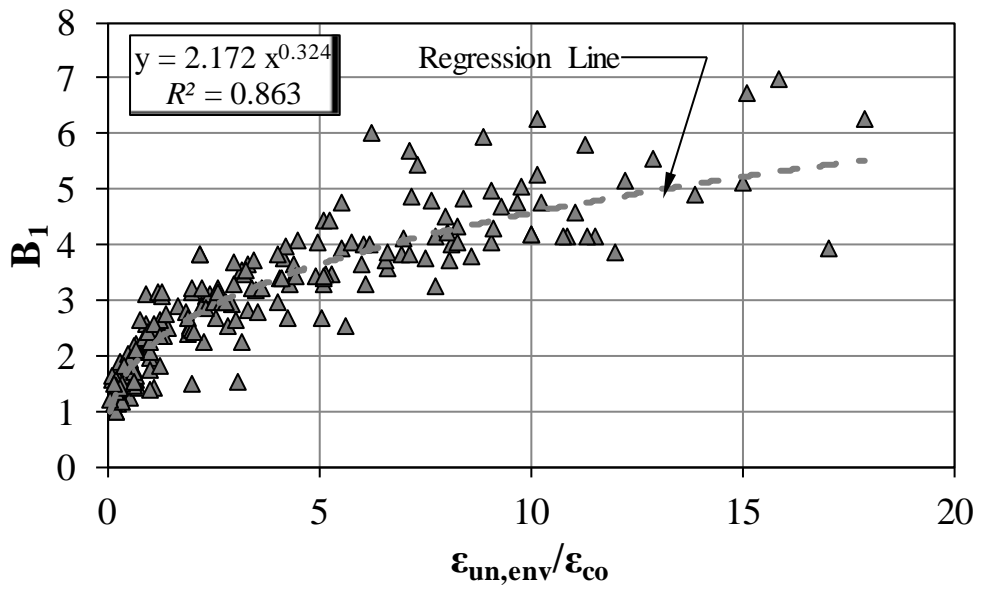
Figure II-11 - Variation of B_1 with $\varepsilon_{un,env}\big/\varepsilon_{co}$
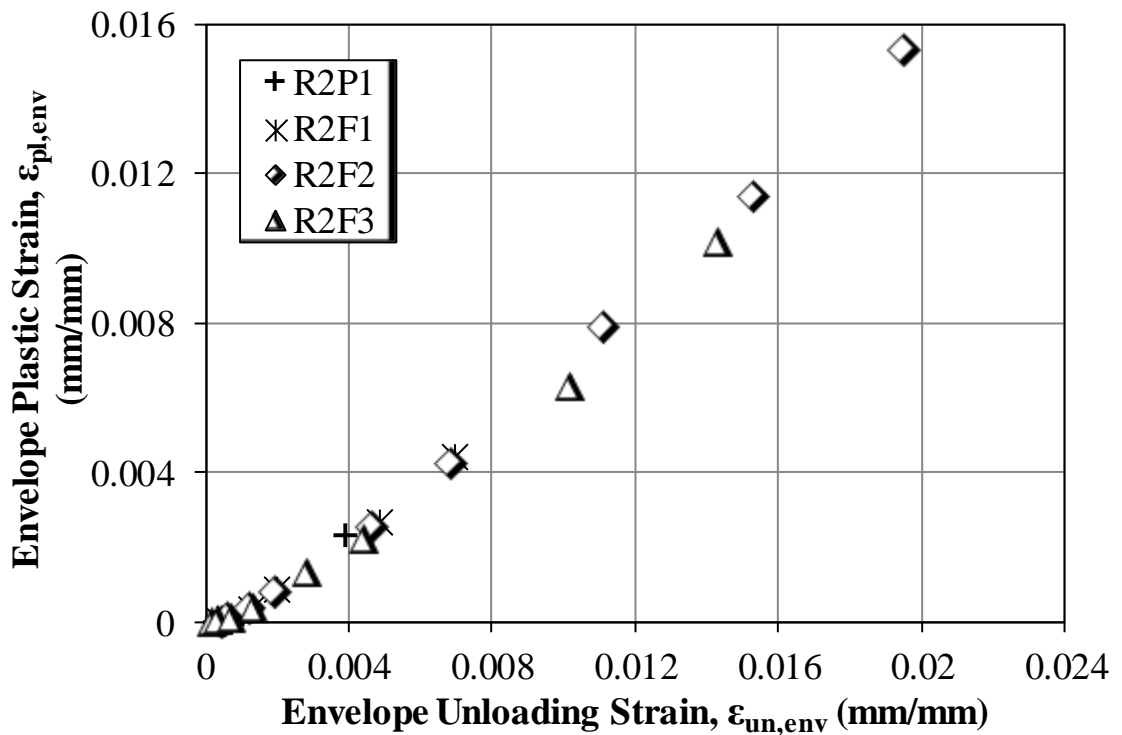
Figure II-12 - Envelope plastic strain $\varepsilon_{pl,env}$ versus envelope unloading strain $\varepsilon_{un,env}$ for different confinement levels
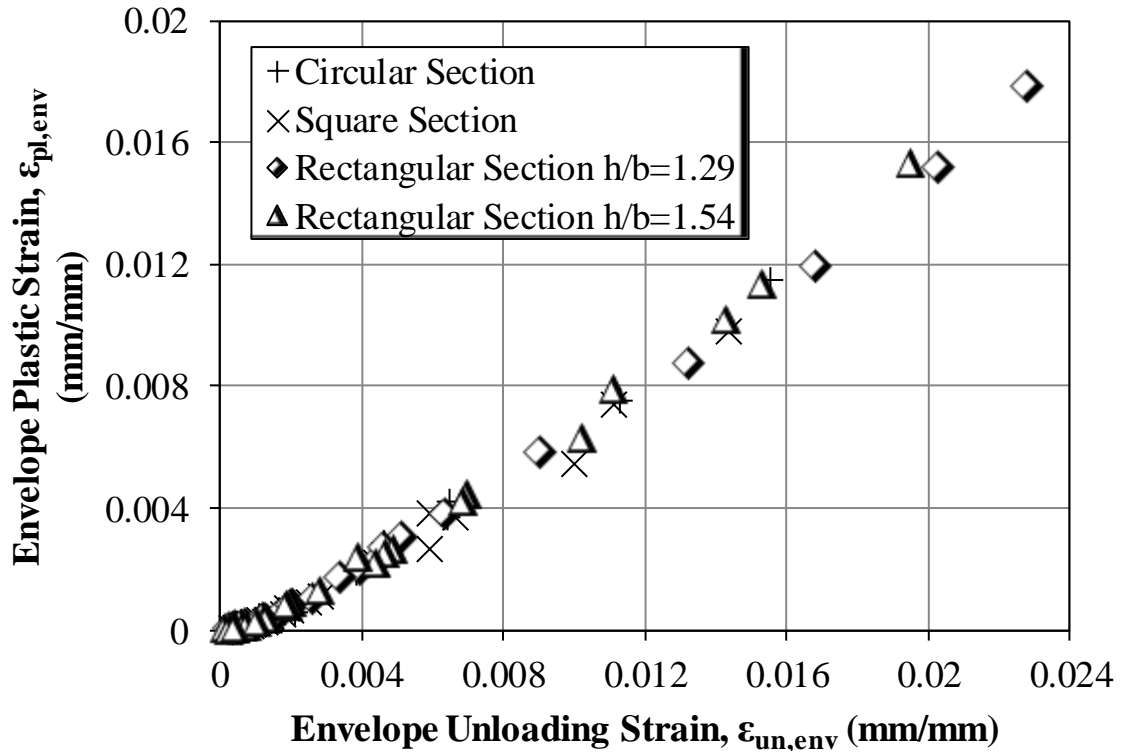
Figure II-13 - Envelope plastic strain $\varepsilon_{pl,env}$ versus envelope unloading strain $\varepsilon_{un,env}$ for different cross section aspect ratios
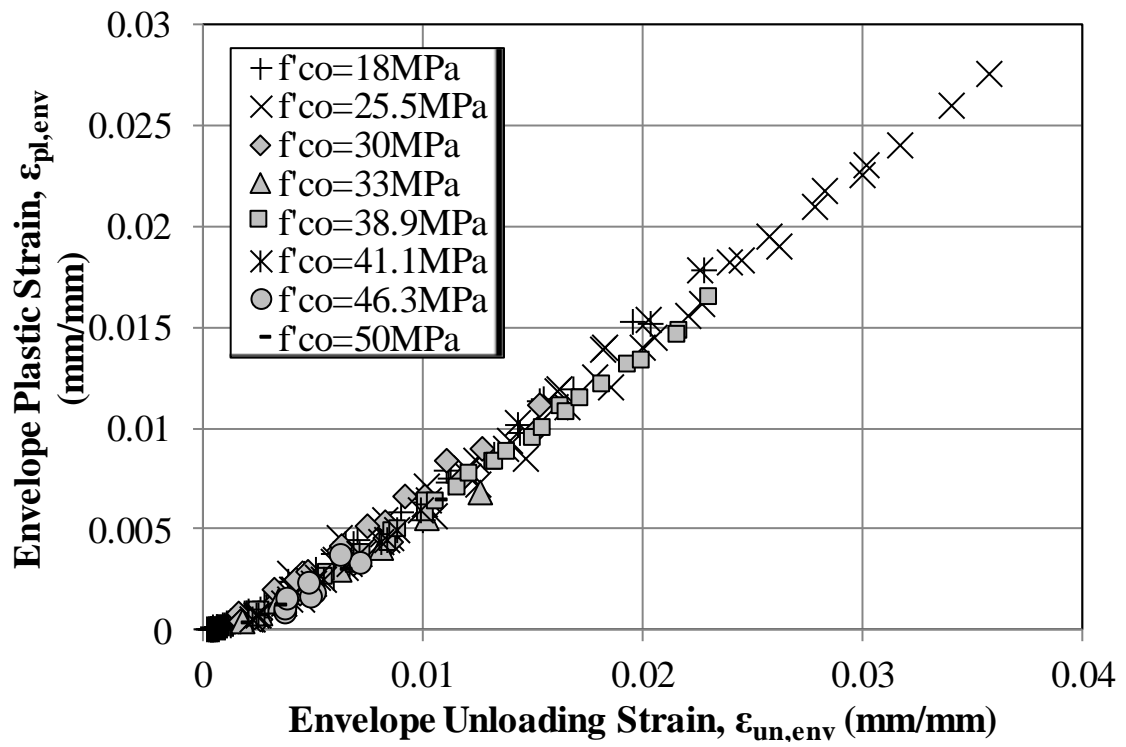
Figure II-14 - Envelope plastic strain $\varepsilon_{pl,env}$ versus envelope unloading strain $\varepsilon_{un,env}$ for different unconfined concrete strengths
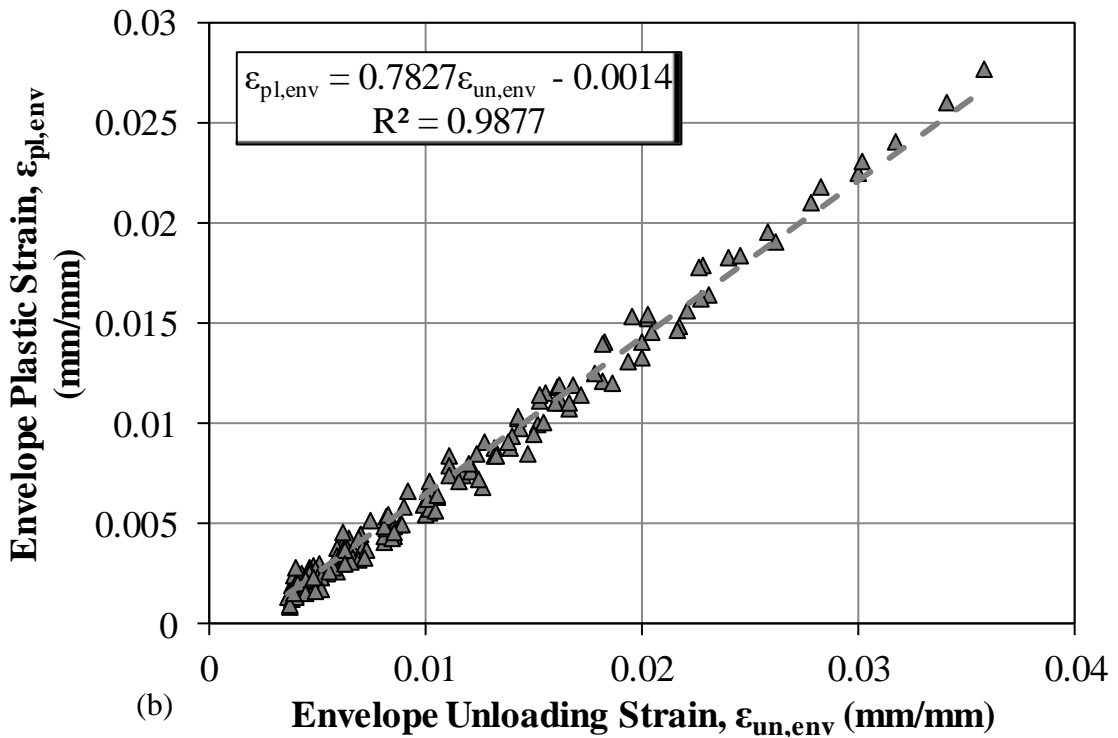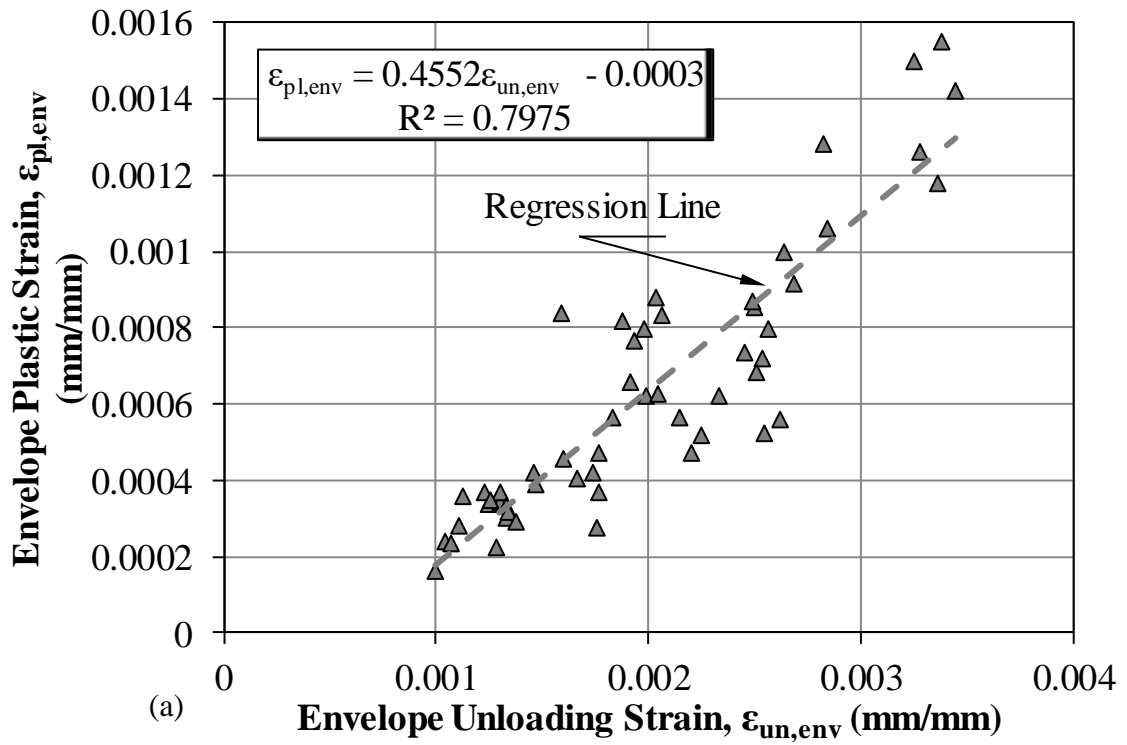
Figure II-15 - Envelope plastic strain $\varepsilon_{pl,env}$ versus envelope unloading strain $\varepsilon_{un,env}$:
(a) $0.001 \le \varepsilon_{un,env} \le 0.0035$; (b) $\varepsilon_{un,env} > 0.0035$
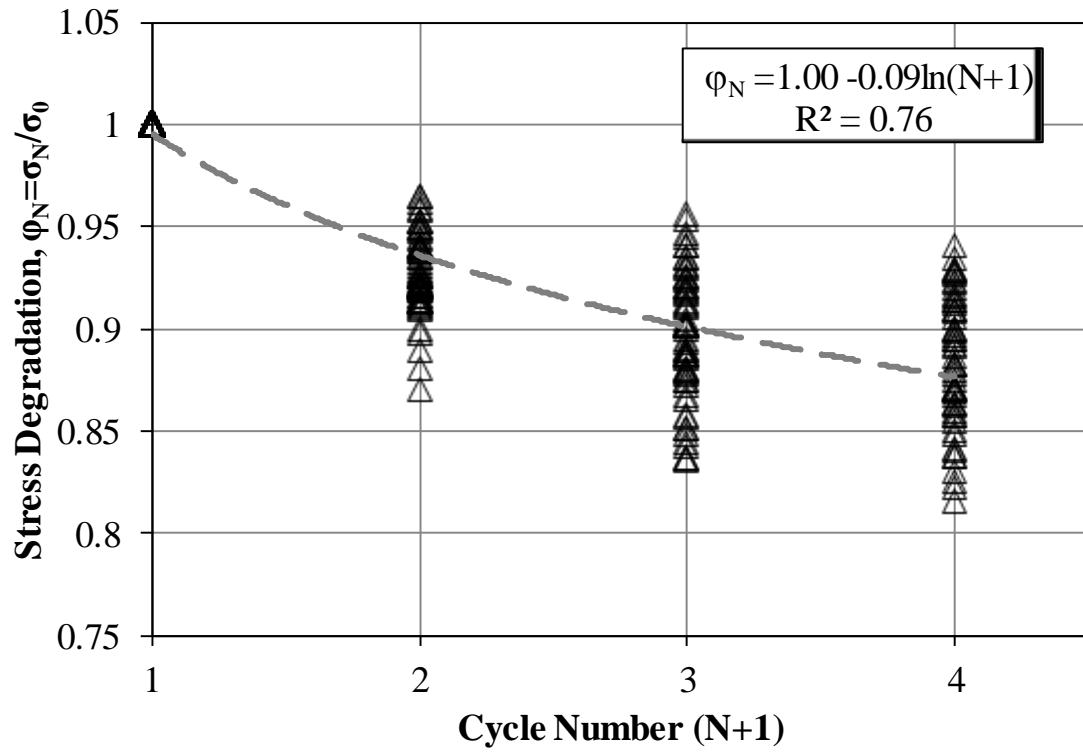
Figure II-16 - Stress degradation parameter φ_N versus unloading/reloading cycle number $N+1$

The chart shows:
- Y-axis: Stress Degradation, $\varphi_N = \sigma_N/\sigma_0$
- X-axis: Cycle Number (N+1)
- Equation box: $\varphi_N = 1.00 - 0.09\ln(N+1)$, $R^2 = 0.76$
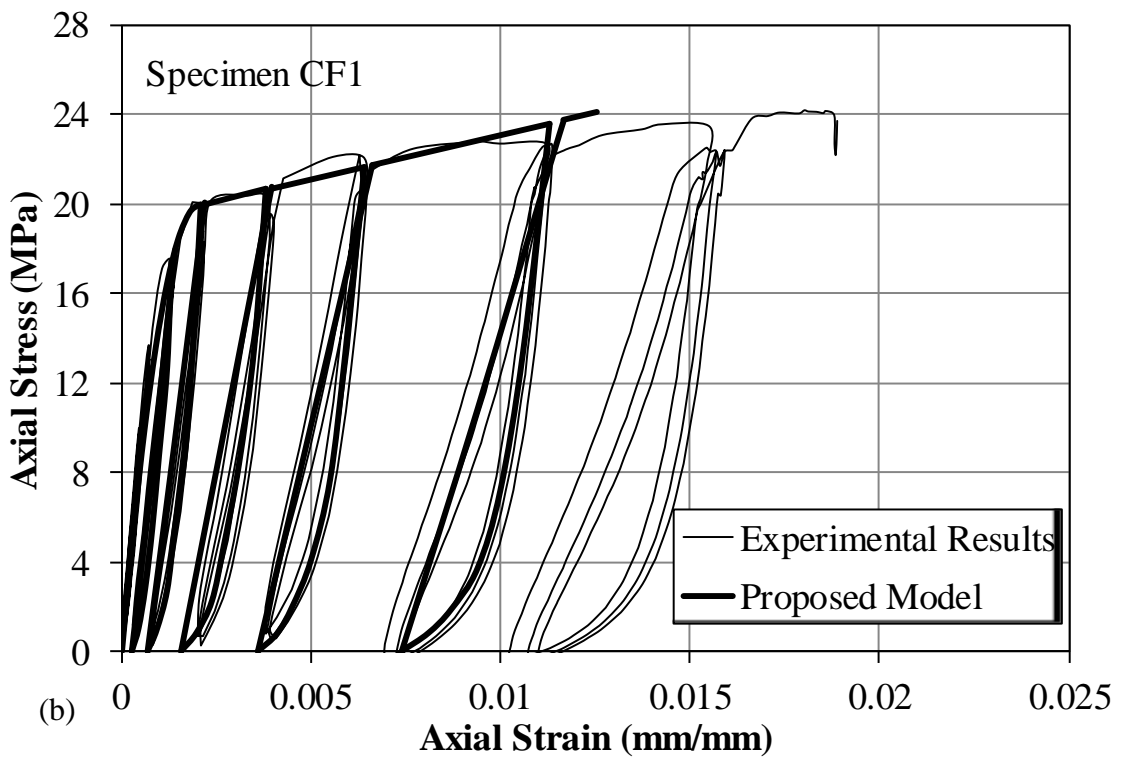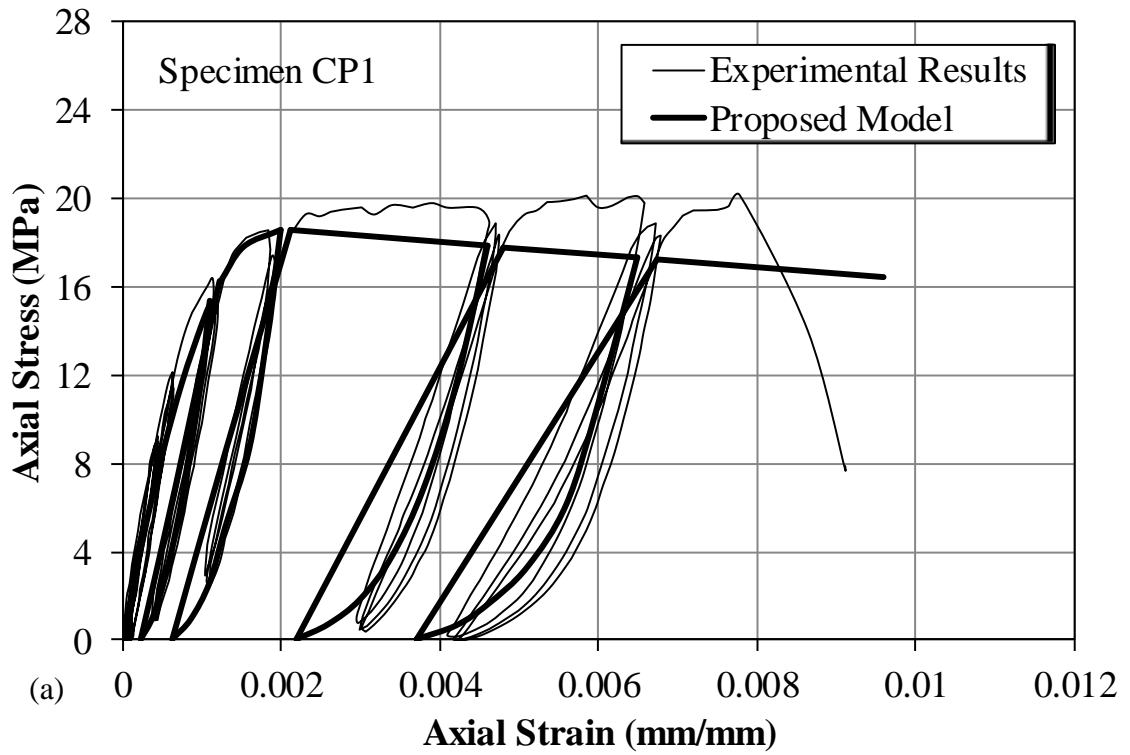
Figure II-17 - Proposed cyclic model versus the experimental results for the circular specimens

(a)

(b)
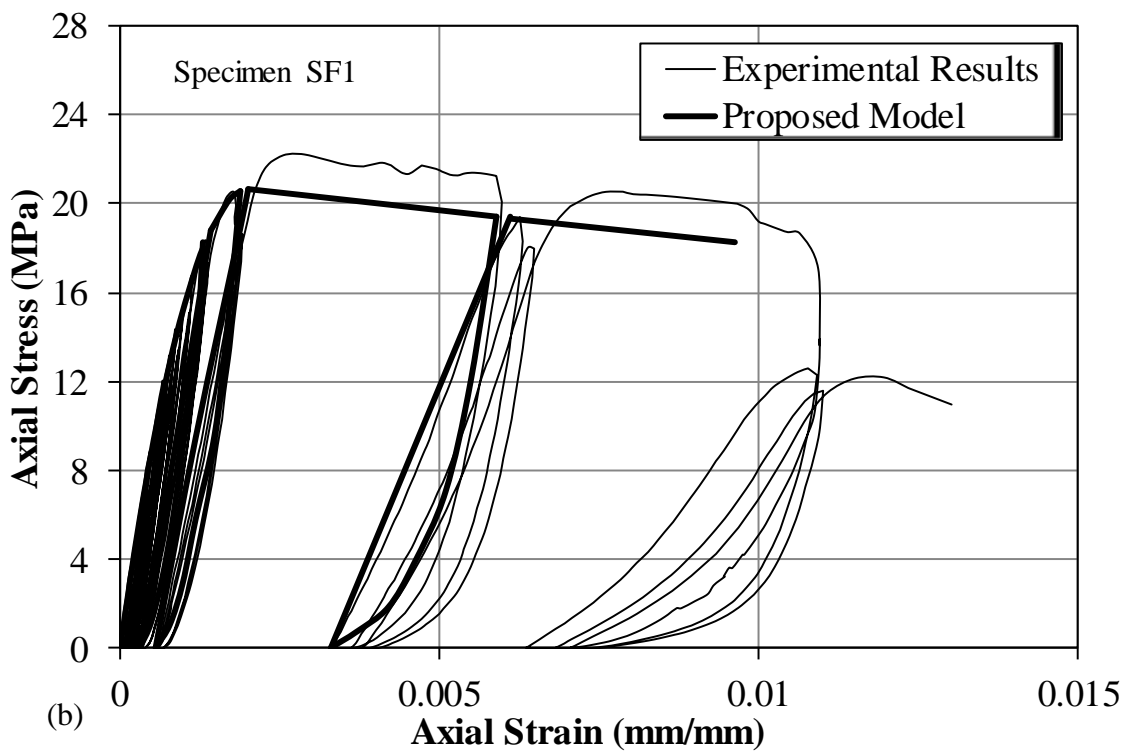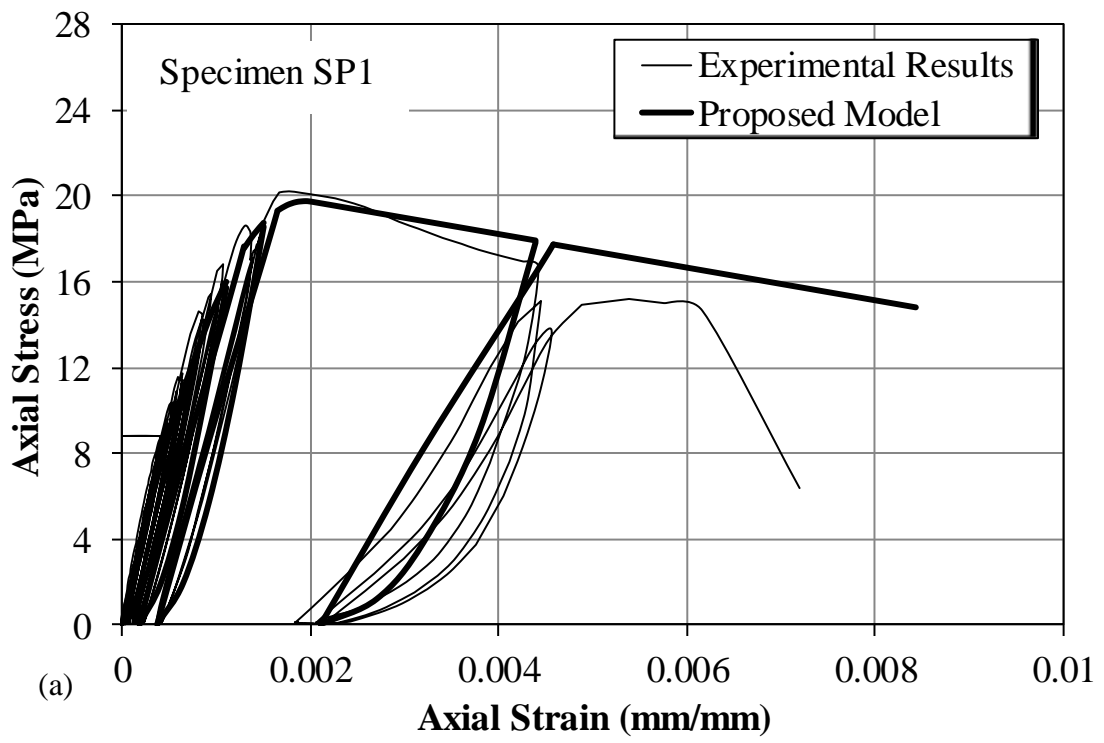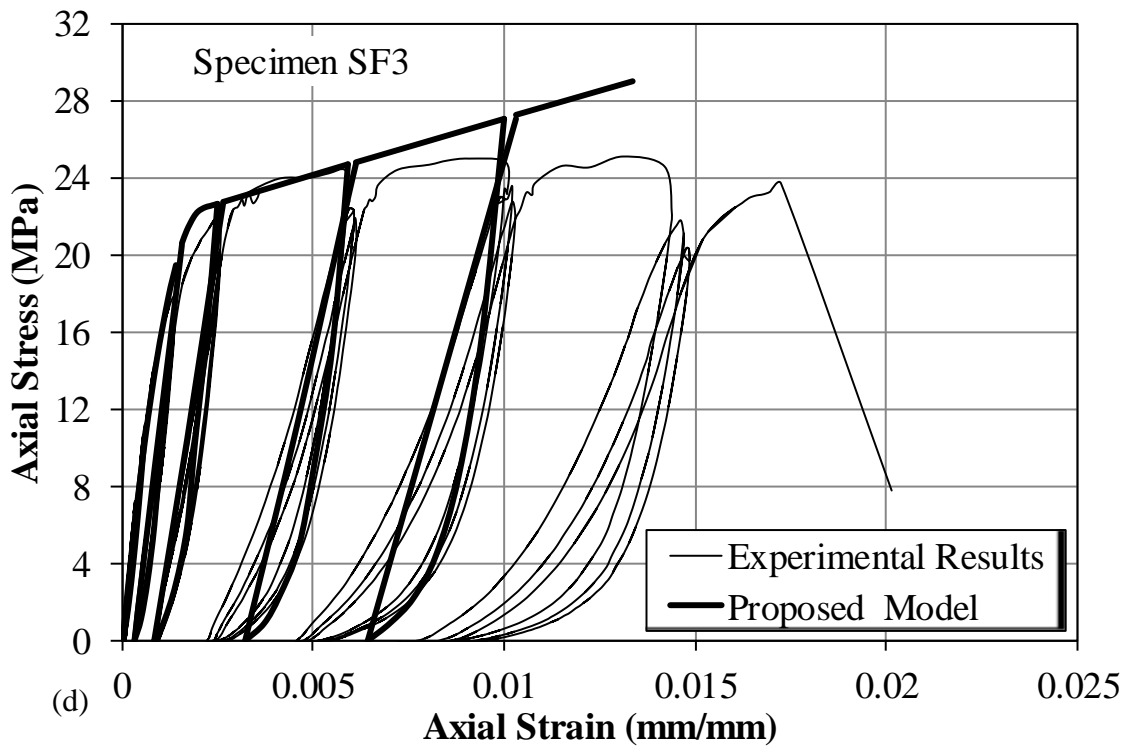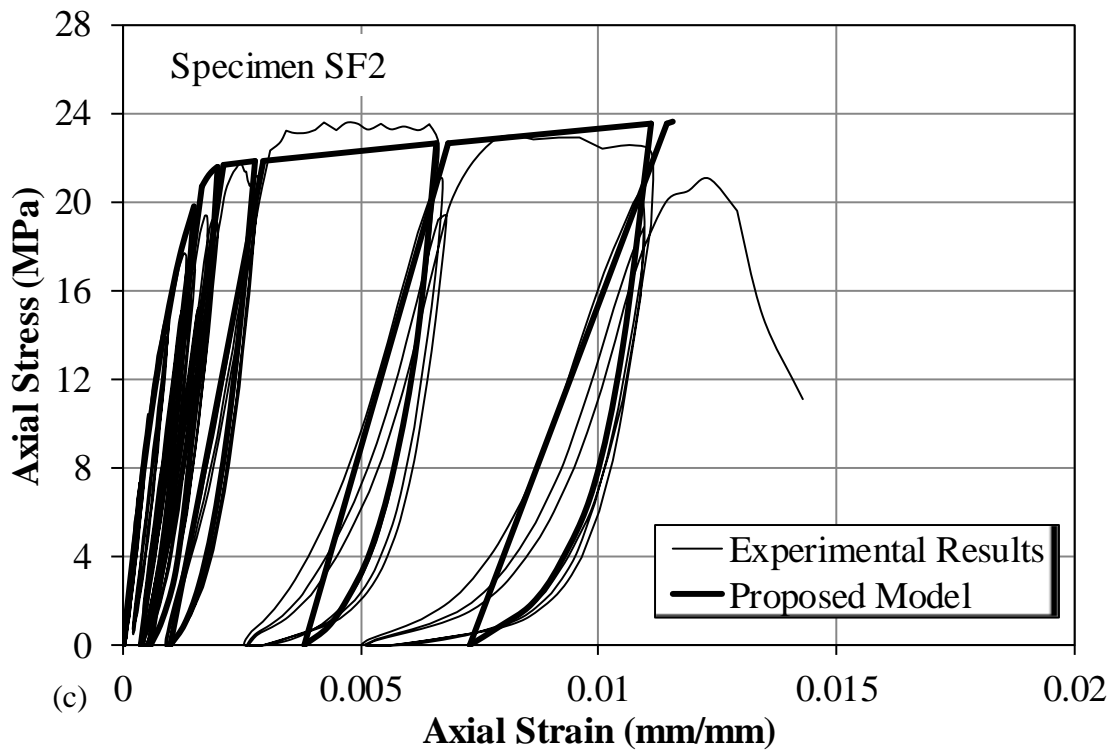
Figure II-18 - Proposed cyclic model versus the experimental results for the square specimens

(a)

(b)
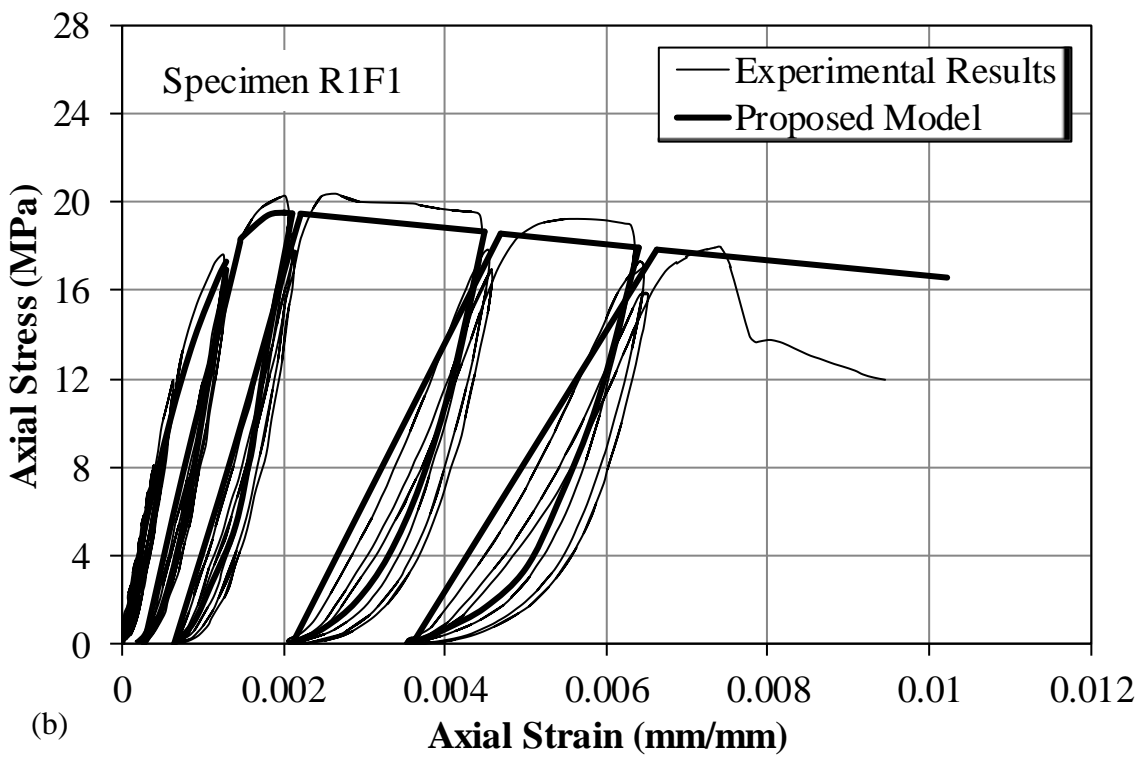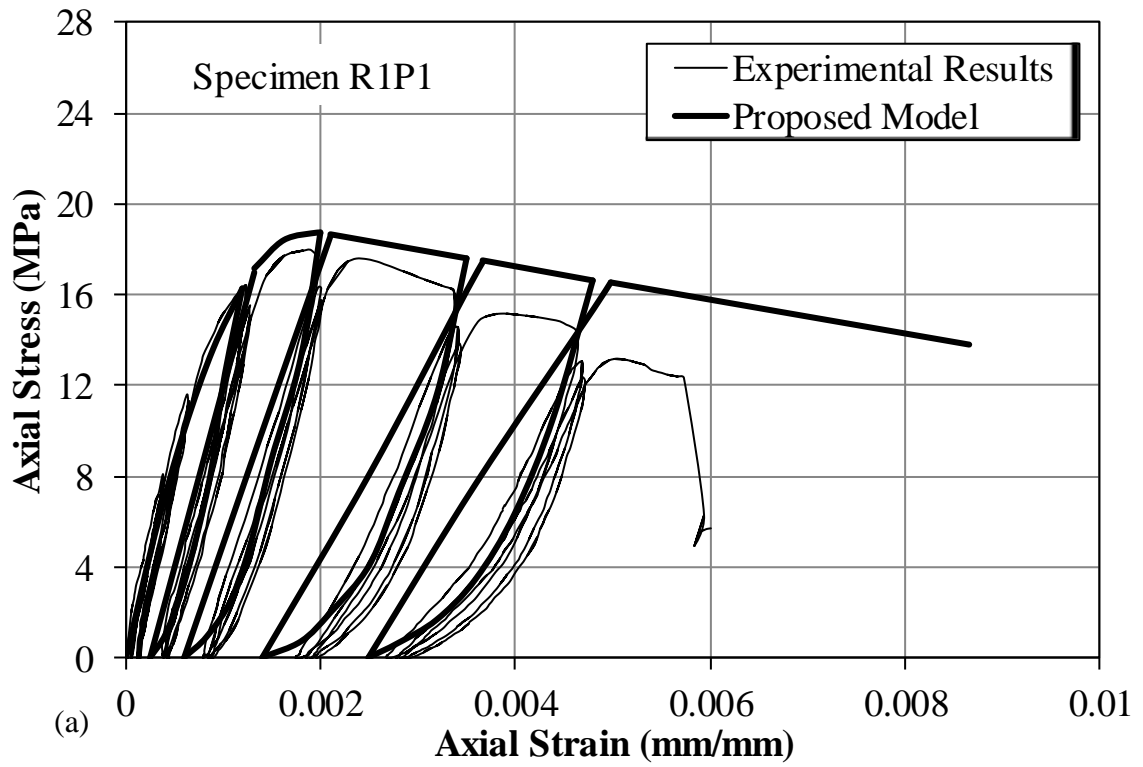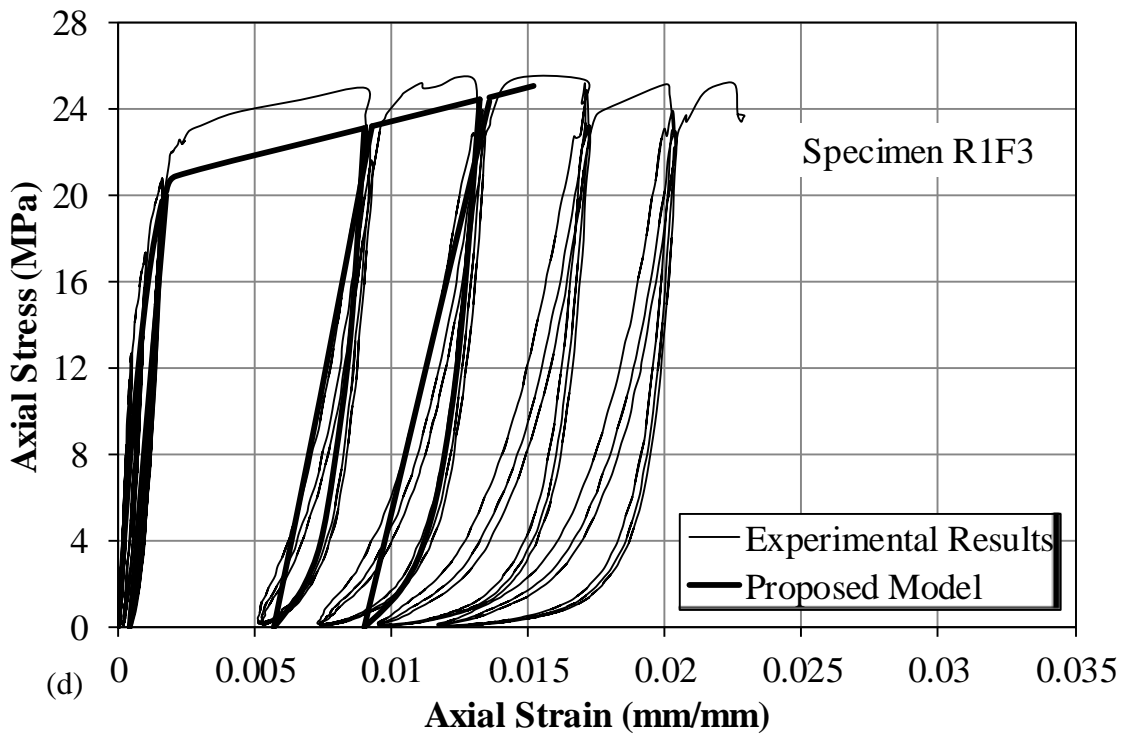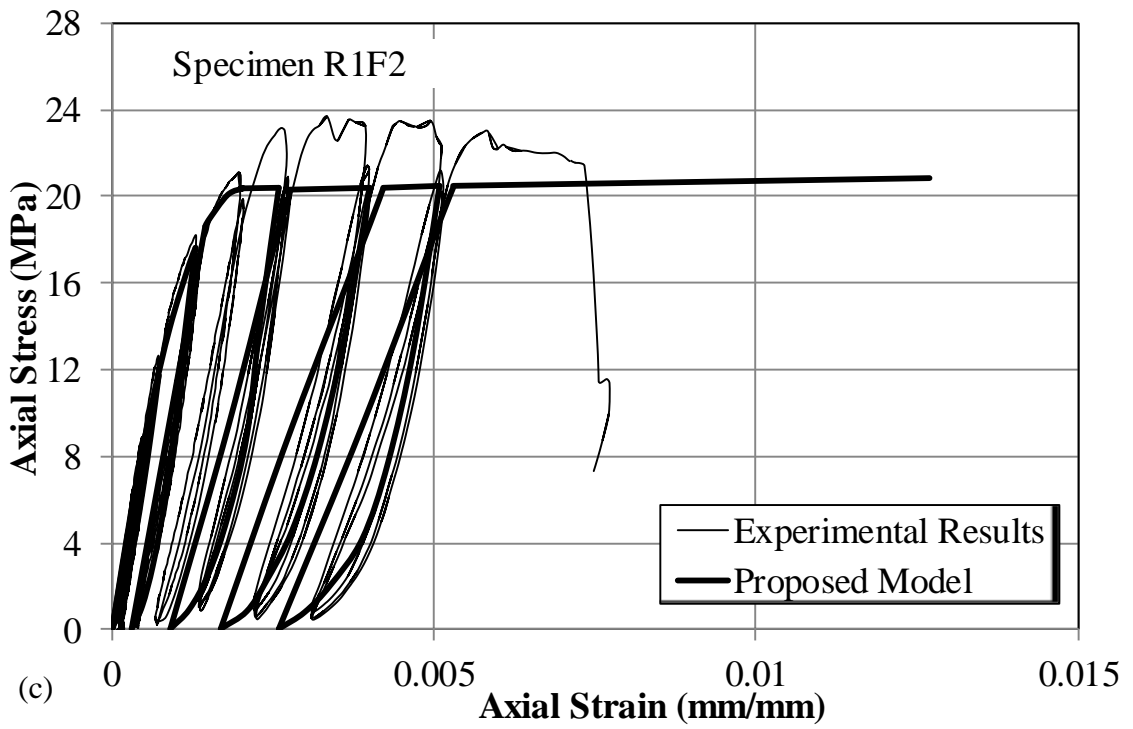
Figure II-19 - Proposed cyclic model versus the experimental results for rectangular specimens of series *R*1

(a)

(b)

60

(c)

(d)
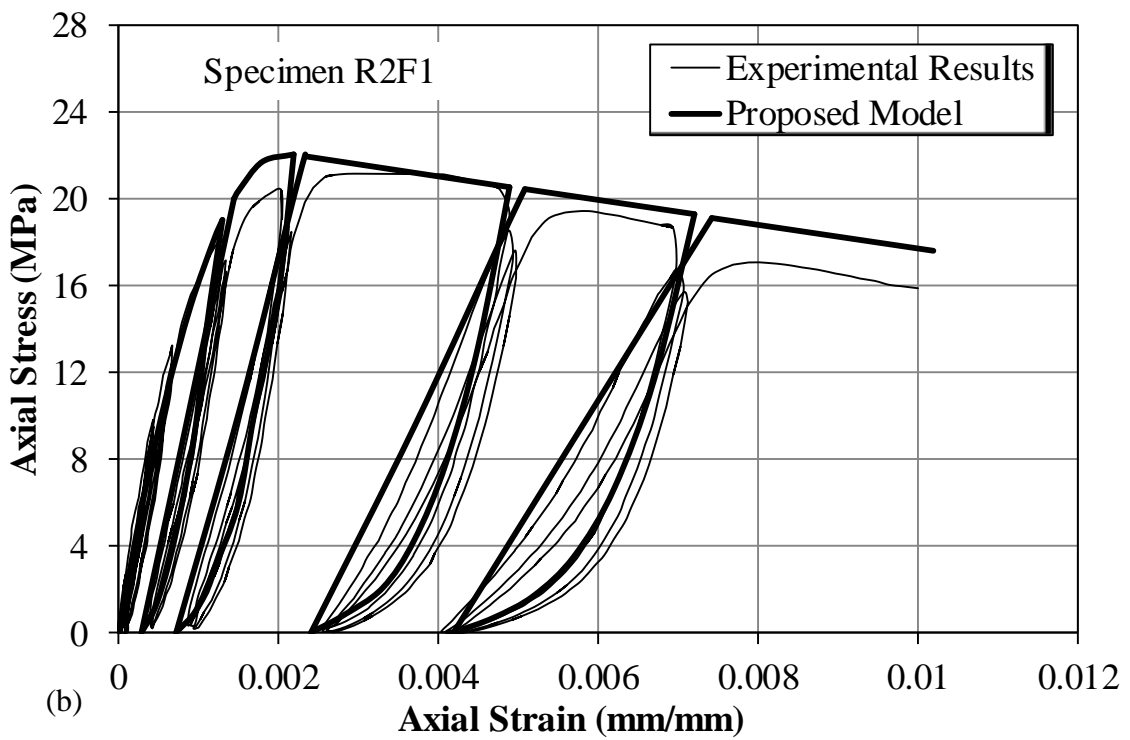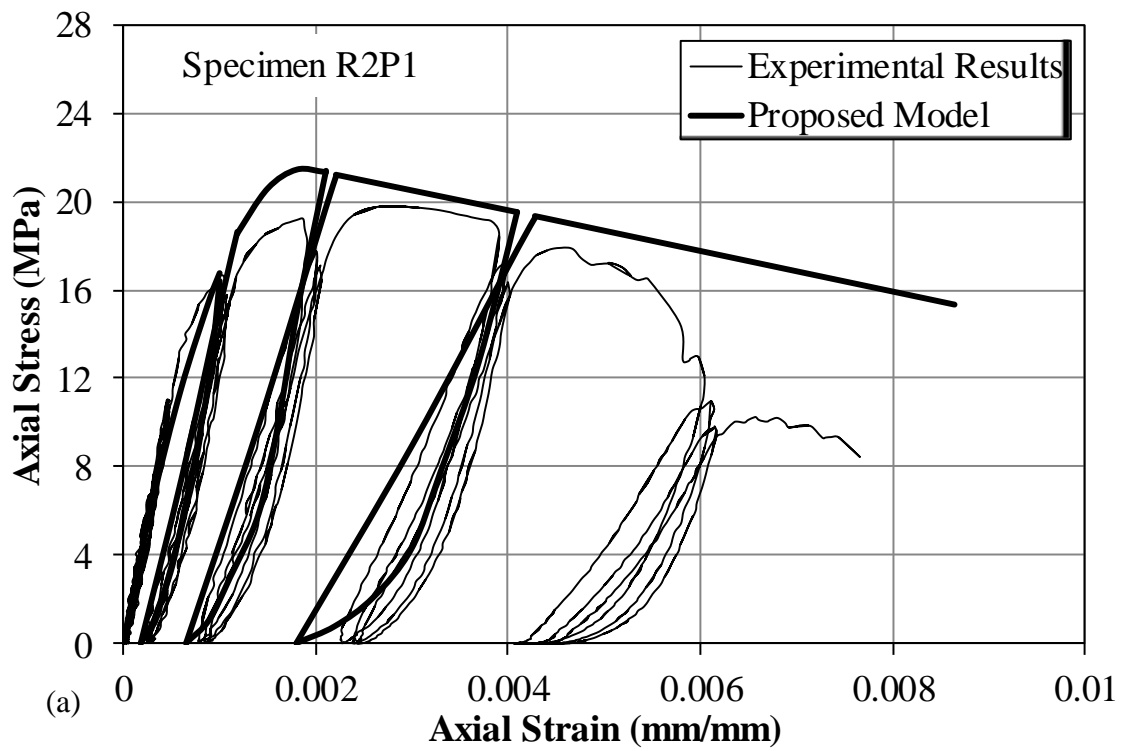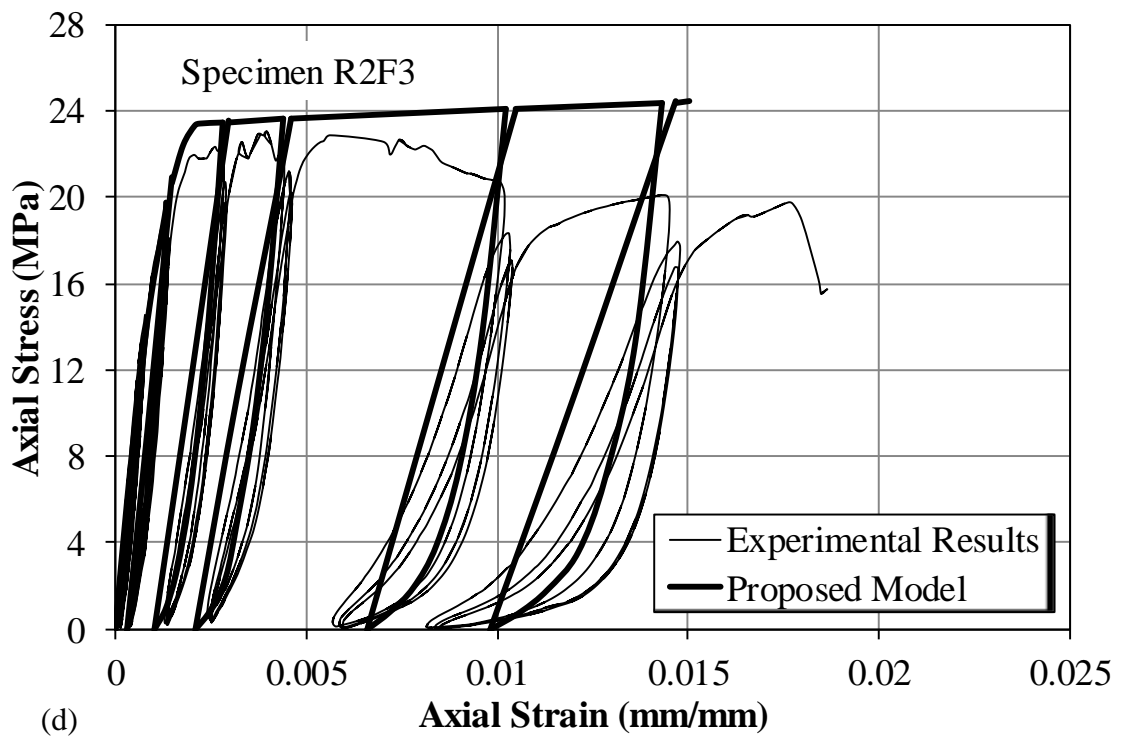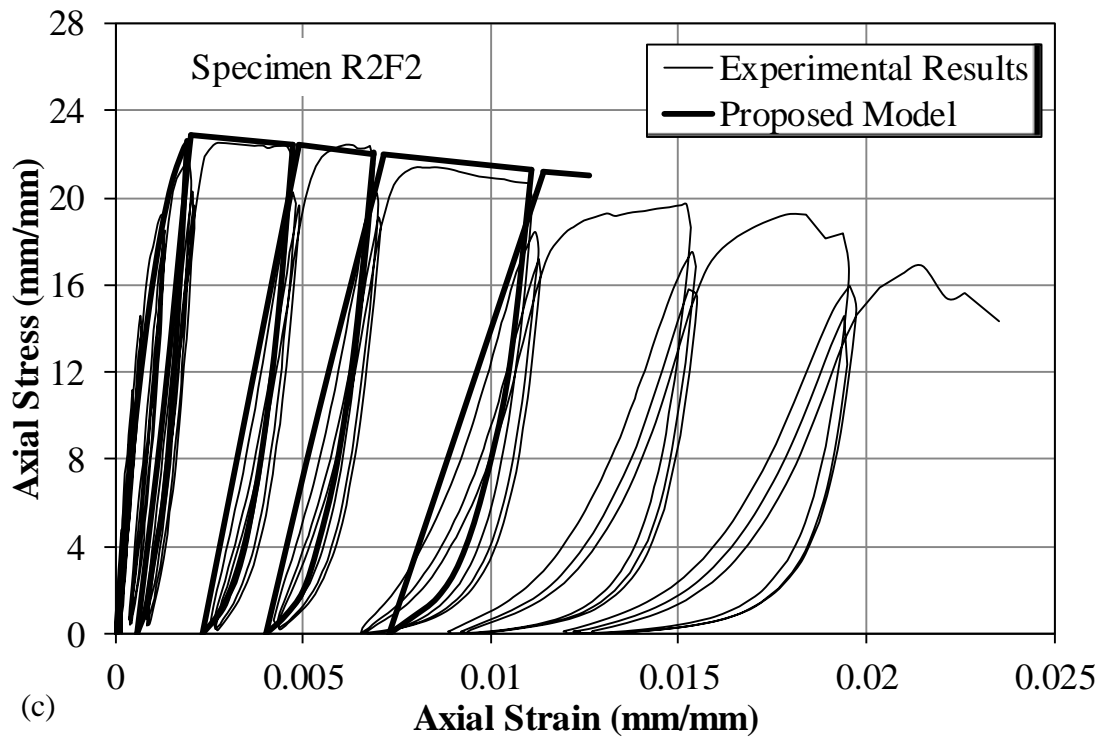
Figure II-20 - Proposed cyclic model versus the experimental results for rectangular specimens of series *R*2

61
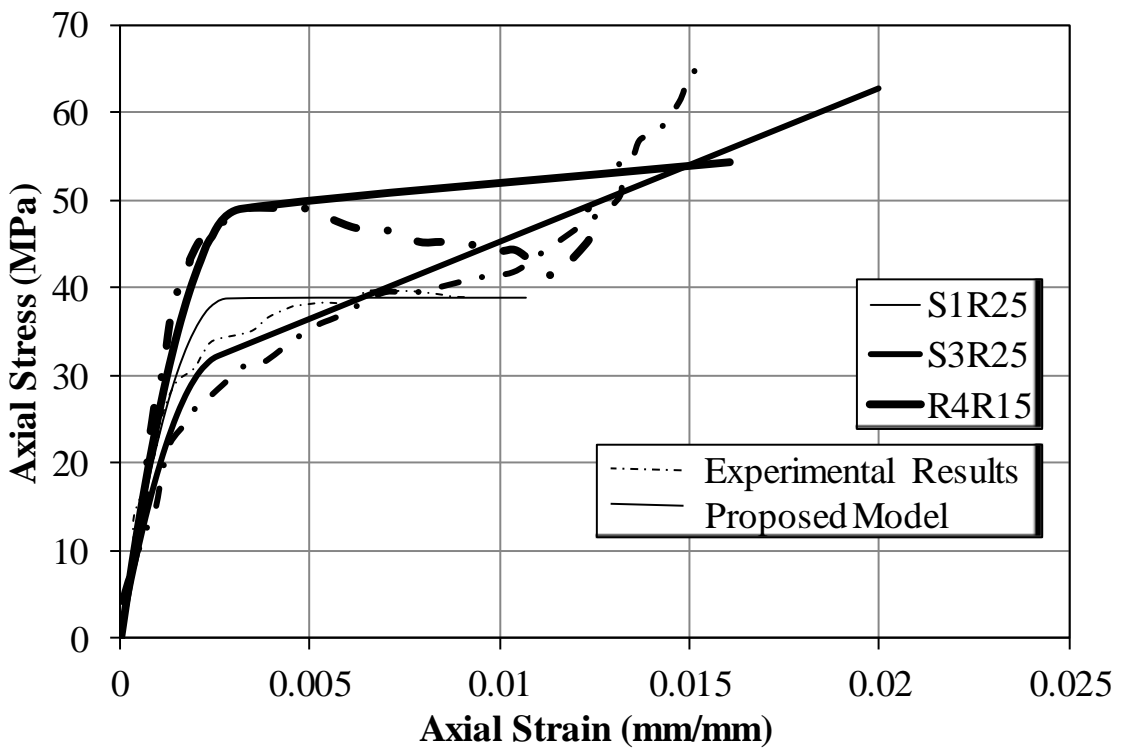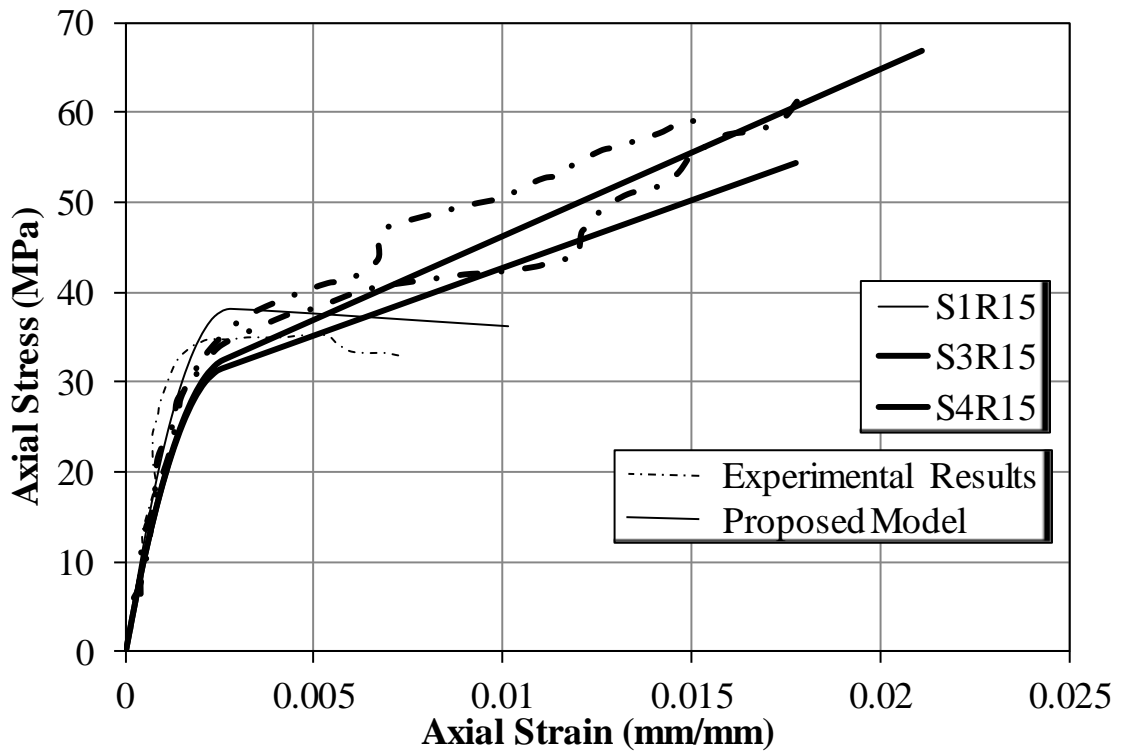
Figure II-21 - Comparison of the proposed envelope model with experimental results of (Lam & Teng, 2003b)

(a)

(b)
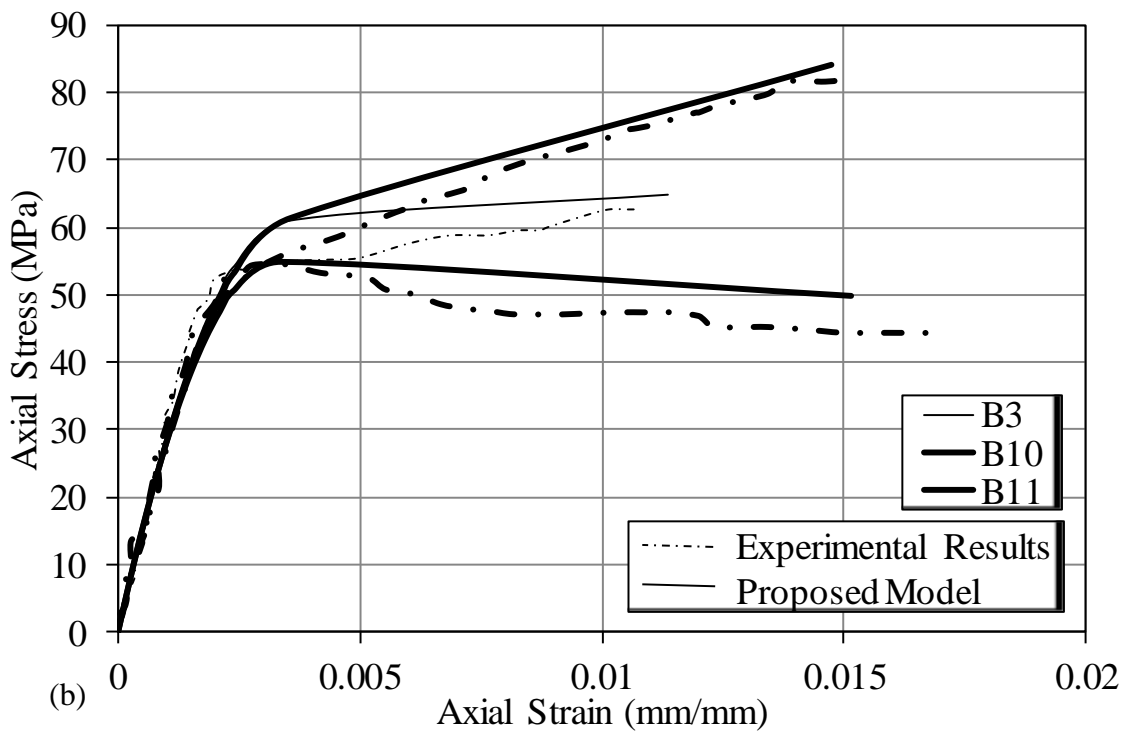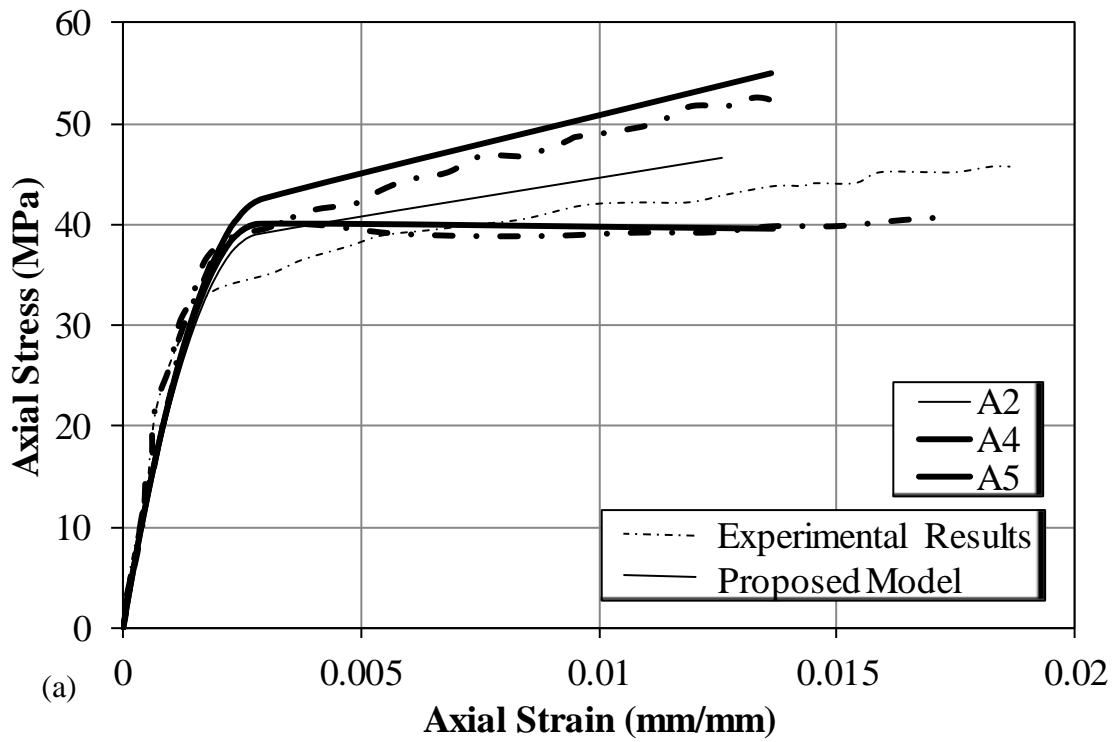
Figure II-22 - Comparison of the proposed envelope model with experimental
results of (Abbasnia & Ziaadiny, 2013)
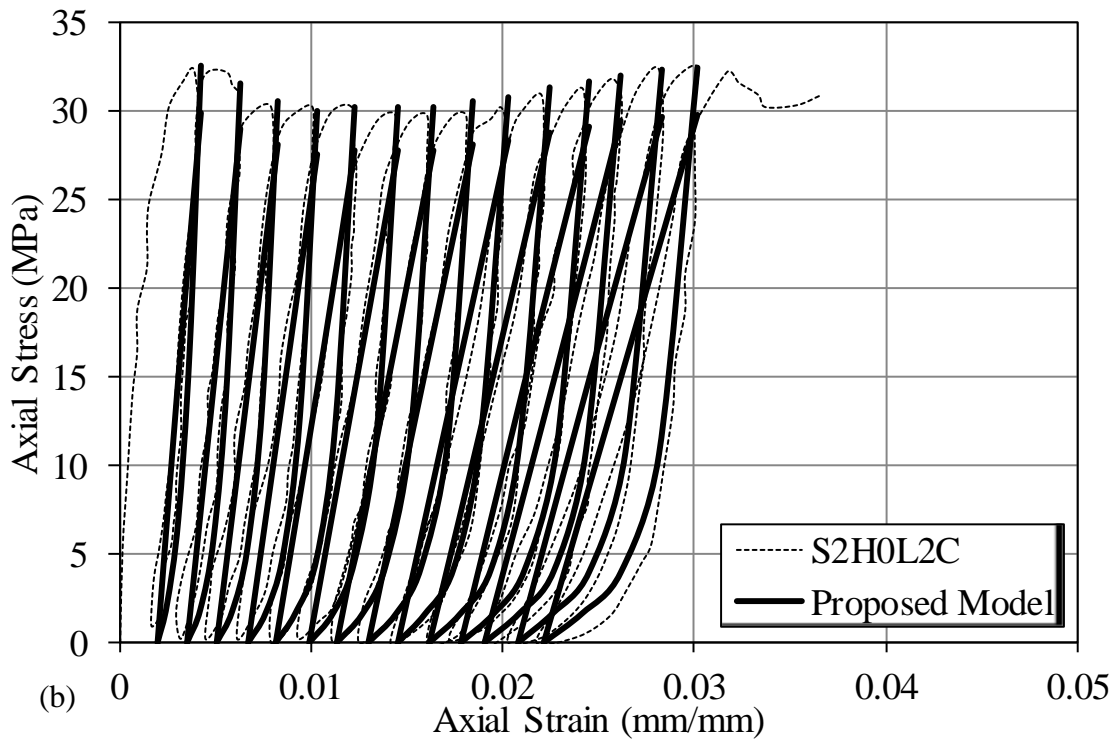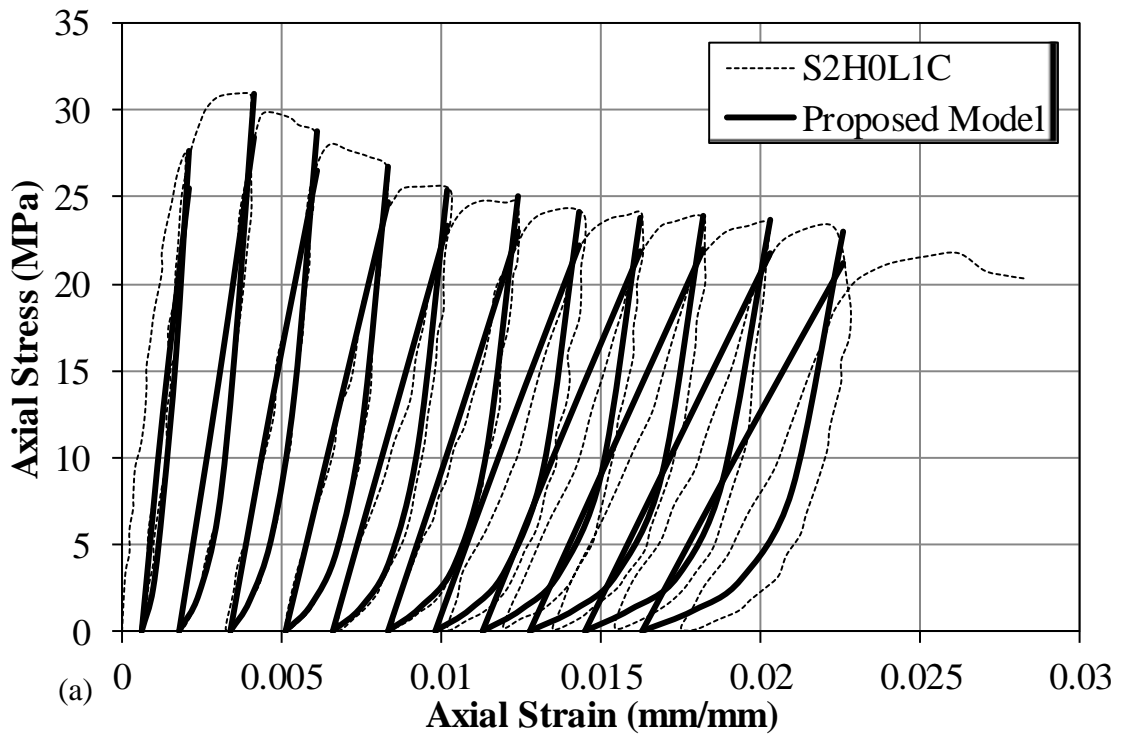
Figure II-23 - Proposed cyclic model versus experimental results of (Wang, Wang, Smith, & Lu, 2012a)

(a)

(b)
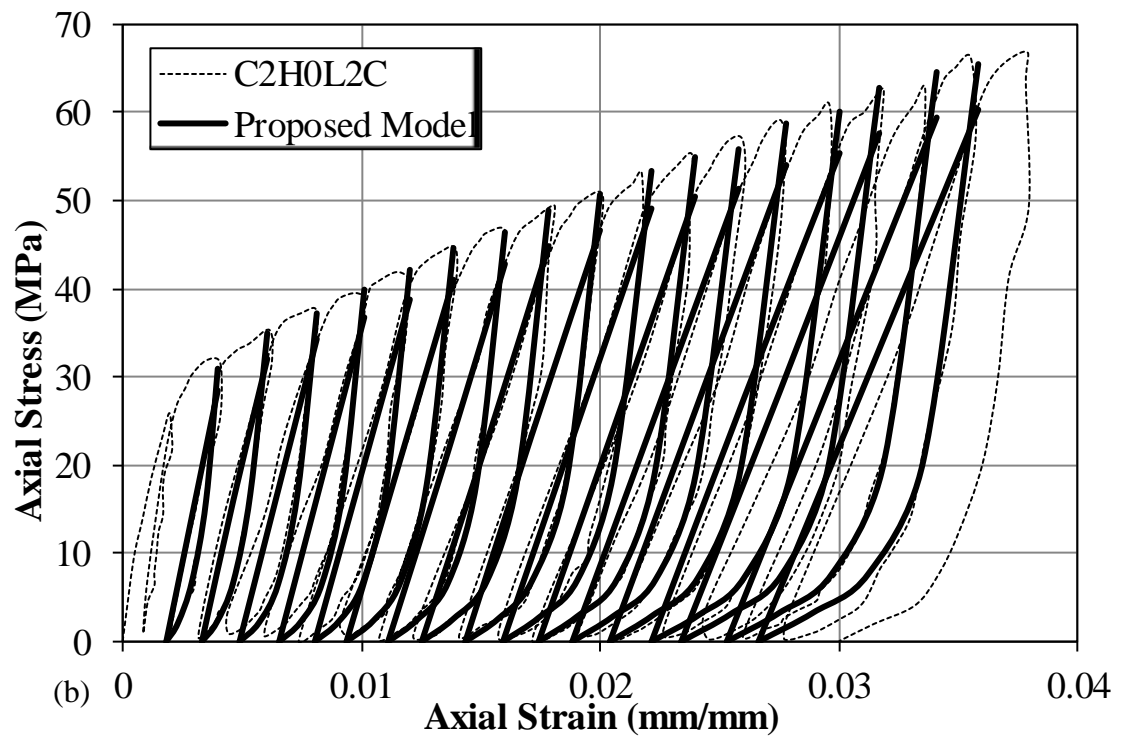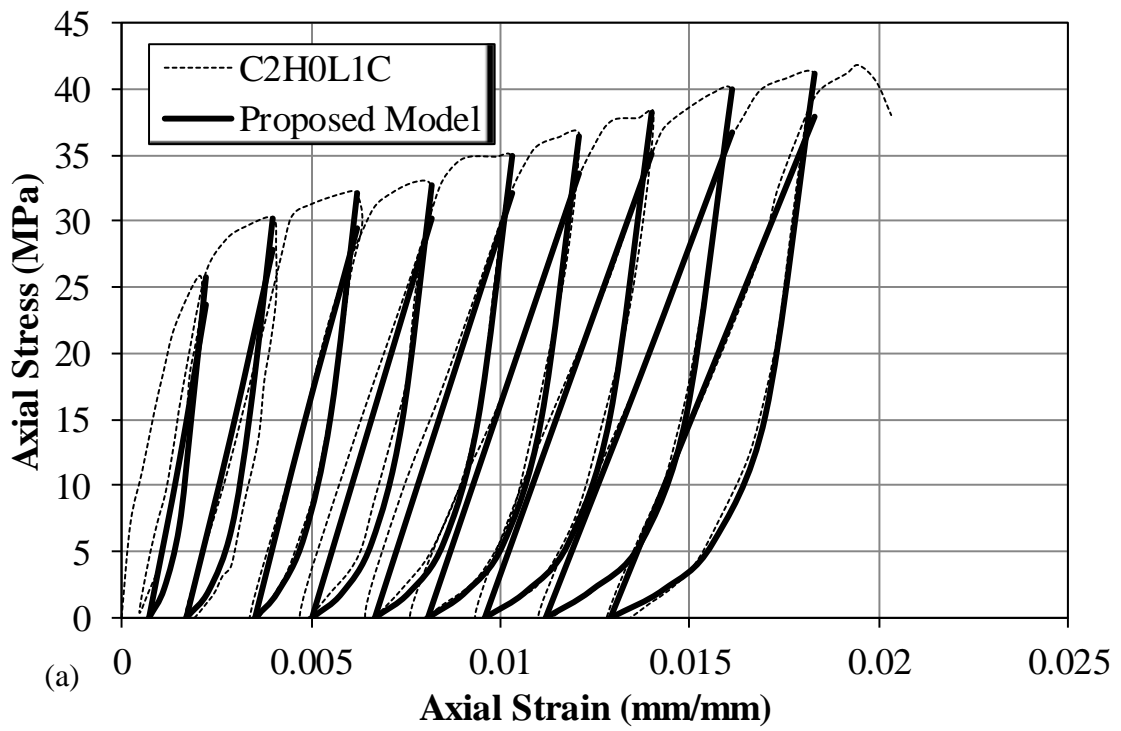
Figure II-24 - Proposed cyclic model versus experimental results of (Wang, Wang, Smith, & Lu, 2012c)

(a)

(b)
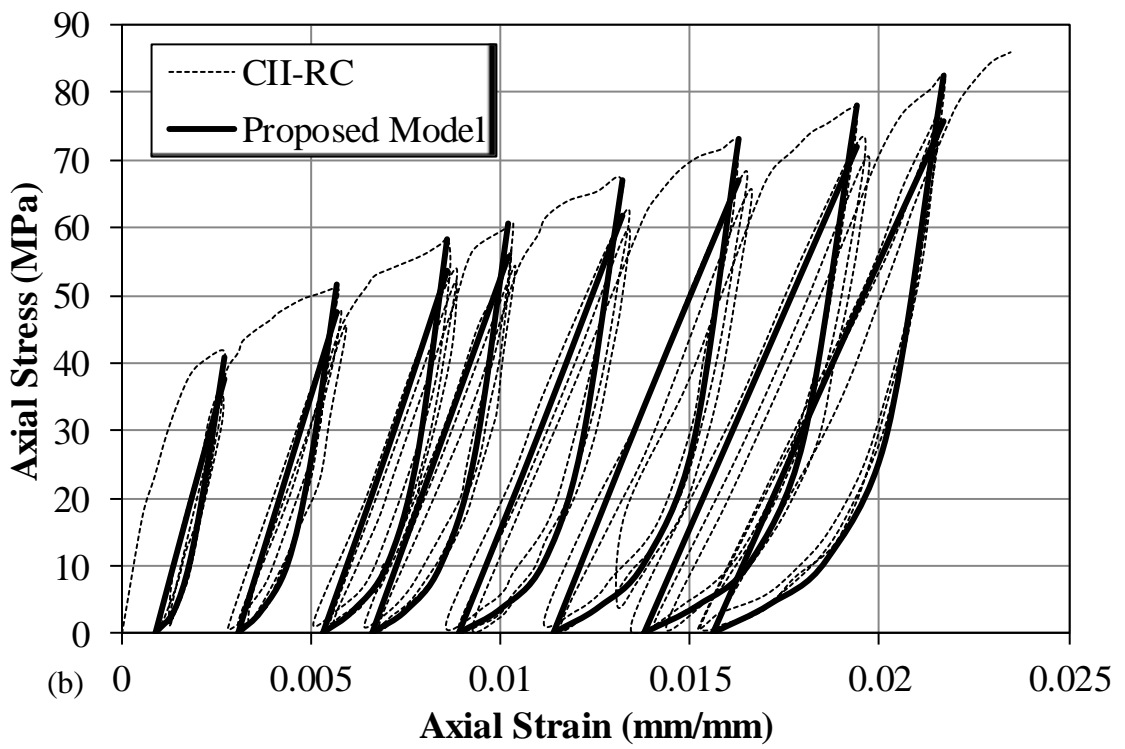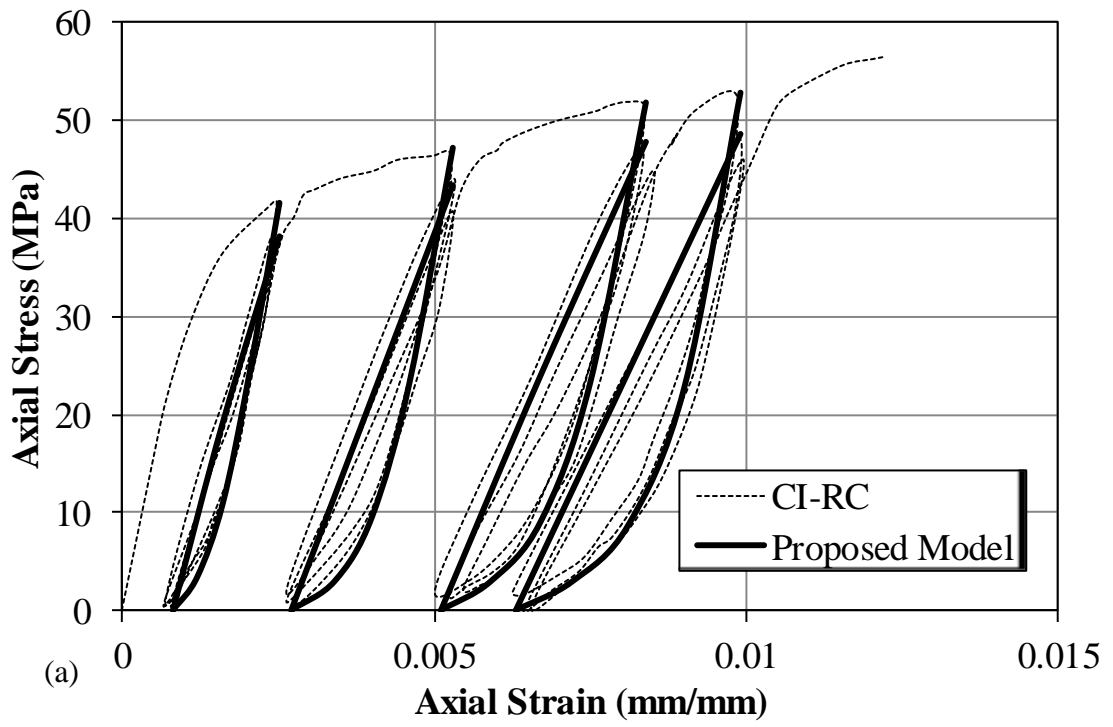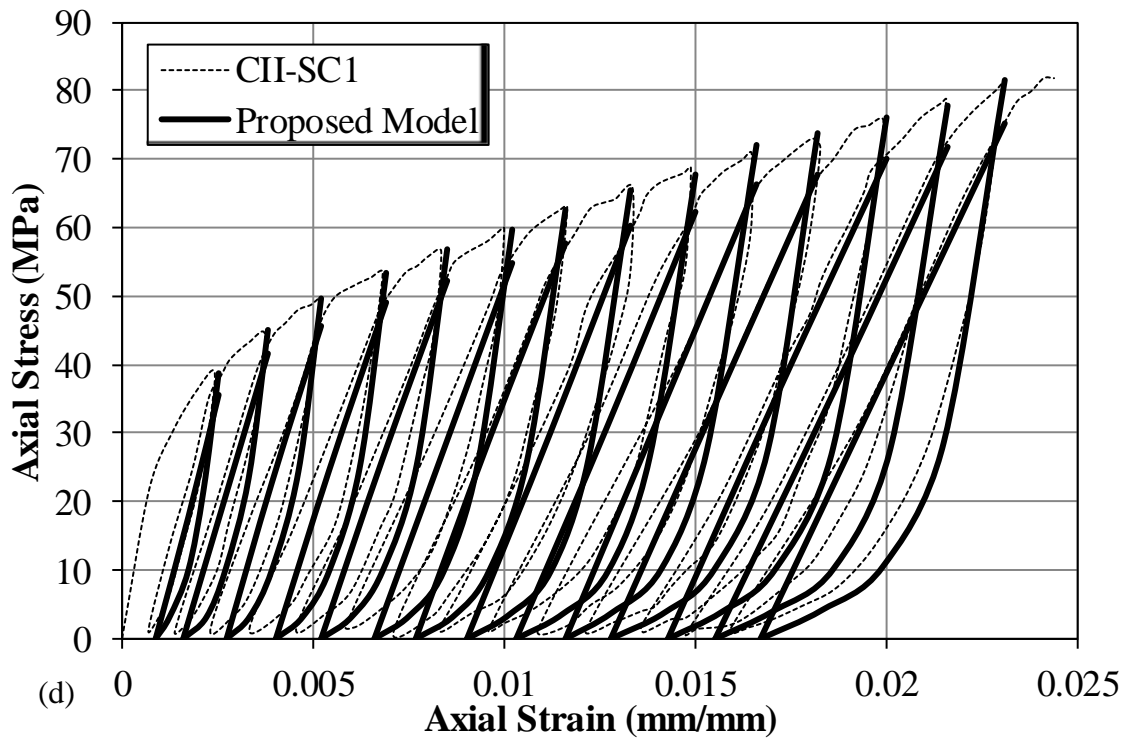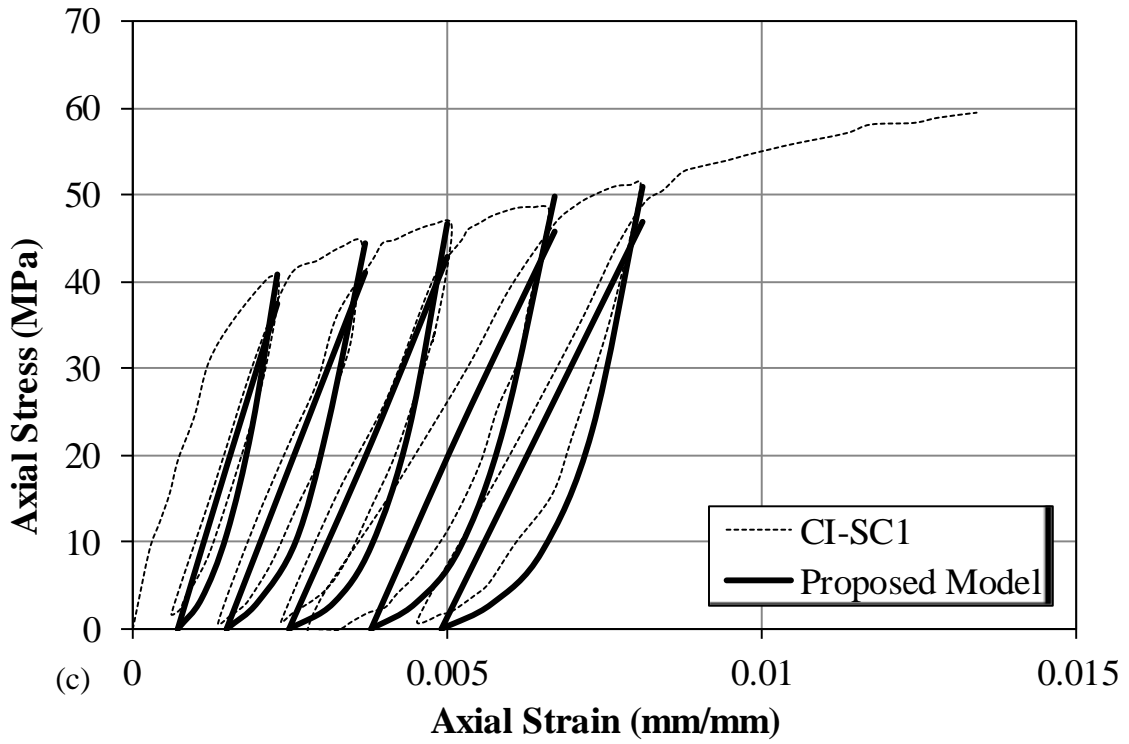
Figure II-25 - Proposed cyclic model versus experimental results of (Lam L. , Teng, Cheung, & Xiao, 2006)

(a)

(b)

68

(c)

(d)
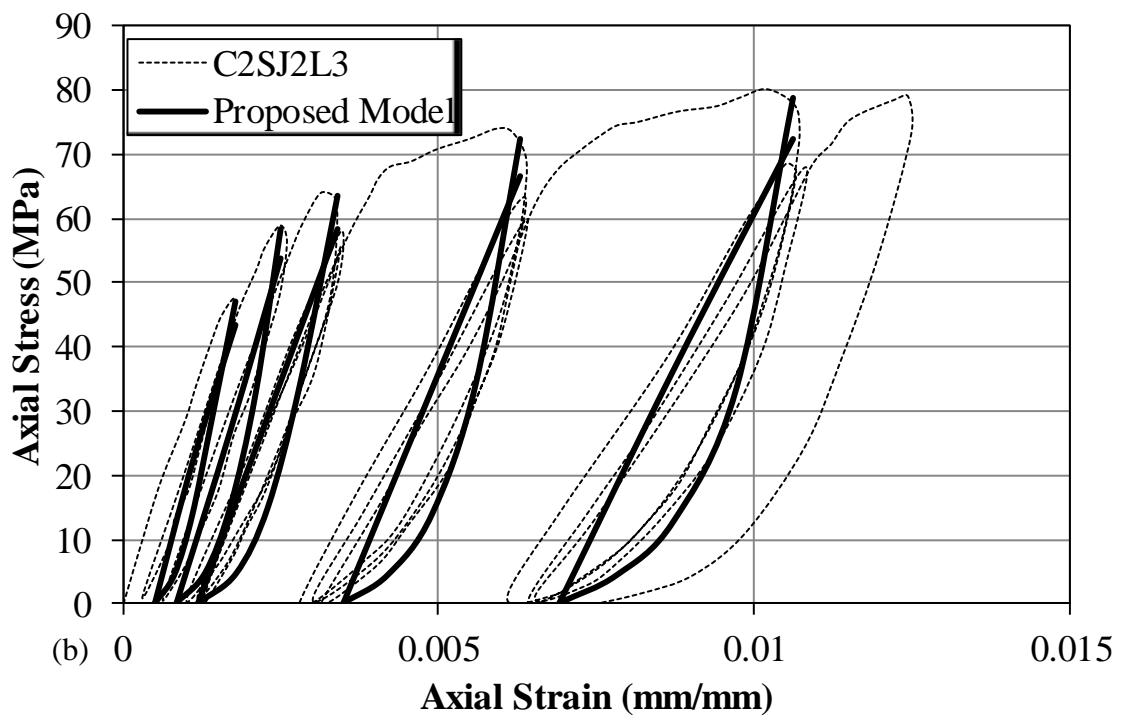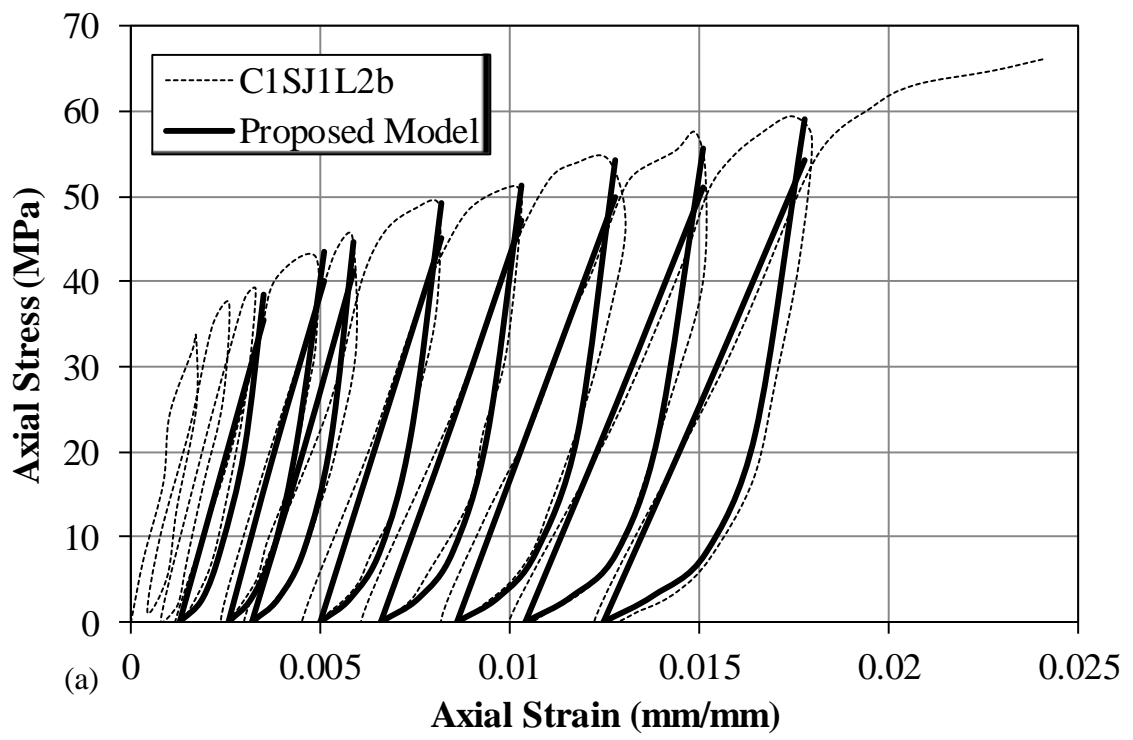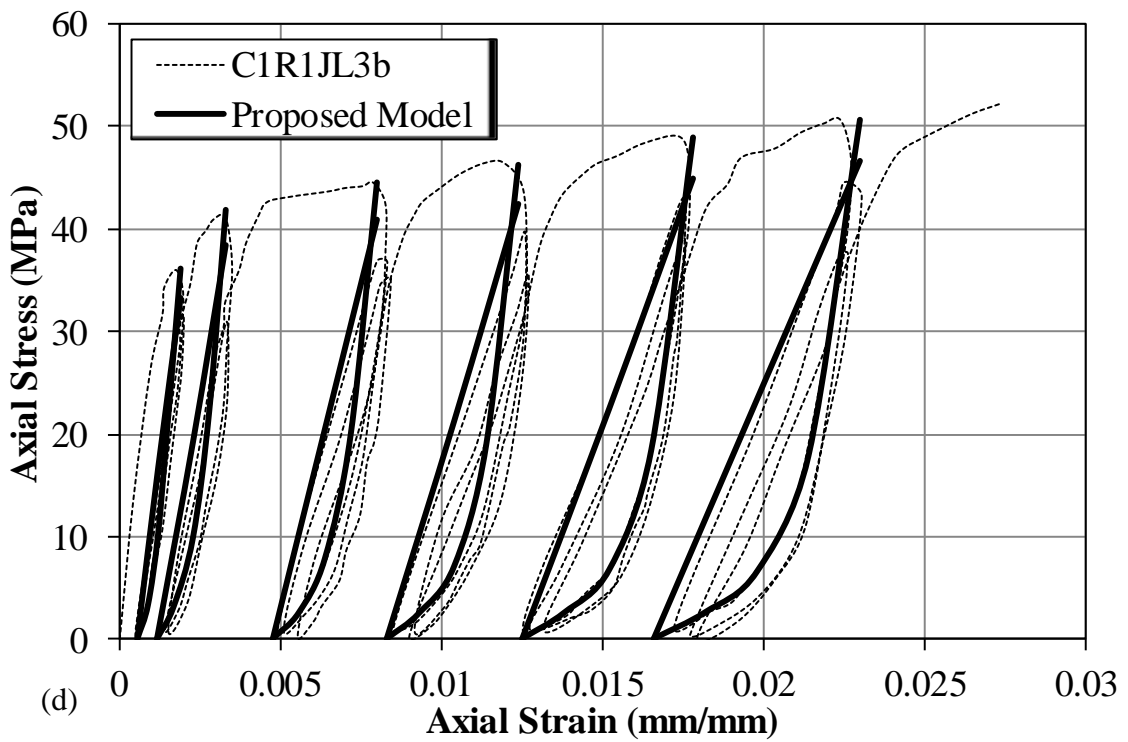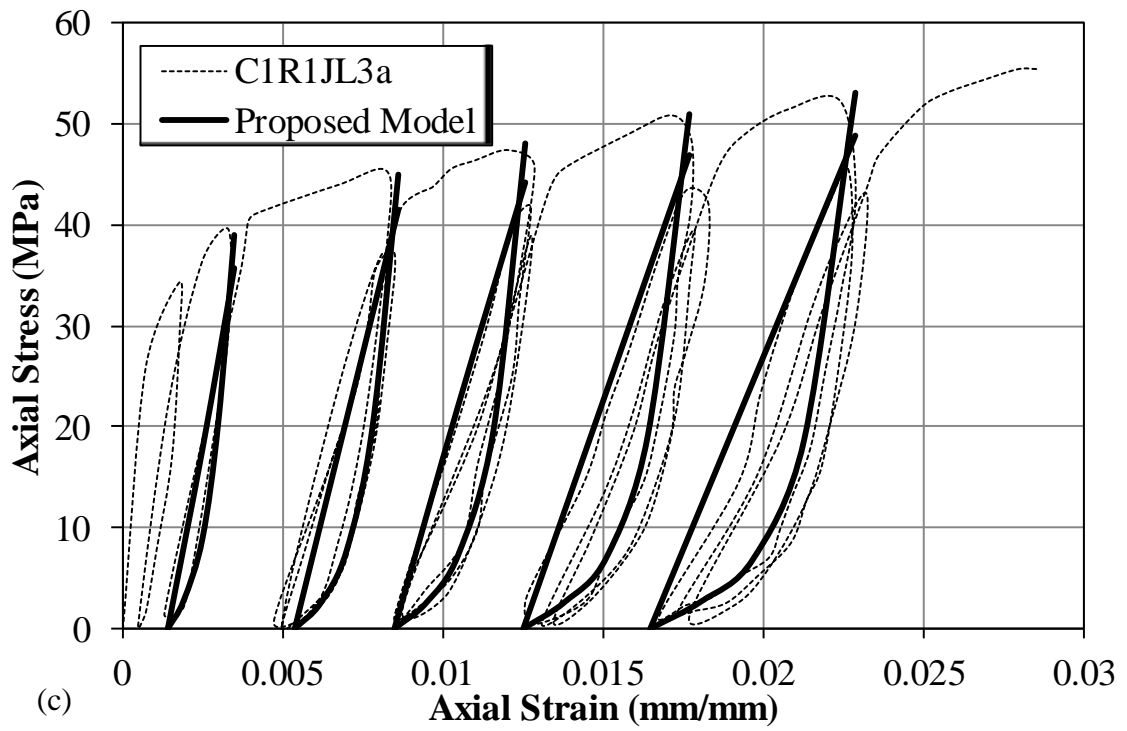
Figure II-26 - Proposed cyclic model versus the experimental results of (Abbasnia, Ahmadi, & Ziaadiny, 2012)

CHAPTER III

EXPERIMENTAL INVESTIGATION OF THE AXIAL STRESS-STRAIN RESPONSE OF RECTANGULAR COLUMNS CONFINED USING CFRP JACKETS AND ANCHORS

A. Introduction

As stated in the literature review part, only few studies have investigated the effect of adding FRP anchors to concrete columns externally wrapped with FRP sheets and how it affects the column stress-strain response. As a result, it was decided to perform an experimental program that investigates this effect.

In this chapter, the results of the experimental program of the cyclic axial stress-strain response of rectangular concrete columns confined with a combination carbon-fiber-reinforced polymer (CFRP) jacket and CFRP anchors are presented and discussed.

B. Experimental program

A total of 27 plain concrete rectangular specimens are fabricated and tested under cyclic axial compressive loading. Each specimen represents a unique set of values of test variables. The specimens are divided into three series (denoted S, M, and L) depending on their cross section aspect ratio (depth-to-width ratio); where S, M, and L correspond respectively to specimens of aspect ratios 1.5, 1.92, and 3.0. The cross section dimensions b x h for the specimens in series S, M, and L are respectively 140 mm x 210 mm, 125 mm x 240 mm, and 100 mm x 300 mm. The corresponding heights

70

are respectively 420, 480, and 600 *mm*. All specimens have approximately the same cross-sectional area of 30,000 *mm*^{2}. Each series comprises one unconfined (control) prismatic specimen, specimens wrapped with CFRP jacket, and specimens wrapped with a carbon-fiber-reinforced polymer (CFRP) jacket in which CFRP anchors are provided (referred to as anchored specimens). All wrapped columns have their corners rounded to a radius *R* = 10 *mm*. All anchored specimens had 25 *mm*- diameter holes (Figure I-3) secured before pouring concrete using polyvinylchloride (PVC) tubes. Before CFRP application, the concrete surface was treated and painted with epoxy resin, and the CFRP sheets were then wrapped in the transverse direction around the columns with 150 *mm* overlap. The CFRP anchors were fabricated by folding a CFRP sheet with the fibers oriented parallel to the axis of the anchors (Figure I-2). The sheet width was determined according to the required anchor cross-sectional area as explained later. After the CFRP jacket has hardened, the CFRP anchors were soaked with epoxy resin and inserted in the preprepared holes (Figure I-3) (after removing the PVC tubes) from one side of the column with the help of thin steel wires tied to the anchor (Figure I-2), and pulled out from the other side. The lengths of the anchors were designed such that each anchor is allowed to extend some 60 *mm* beyond the face of the column on either side, and then spread out in a fan-shape against the hardened CFRP jacket (Figure I-3). A pilot test using one specimen showed that the anchors tend to develop premature bond failure, leading to a partially effective confinement of the underlying CFRP jacket. Consequently, in order to improve the bond strength between the CFRP anchors and underlying CFRP jacket, it was decided early in the test program to wrap all anchored specimens (except one in Series *S*, which was used for a pilot test) with one additional CFRP layer over their full height. The last CFRP layer is applied separately after the

underlying layers and anchors have hardened. This layer is also applied in the transverse direction around the columns with a 150 *mm* overlap. Additional figures showing specimens preparation are provided in Appendix A.

Table III-1 presents a summary of the specimens' details. Specimens belonging to Series S, M, and L are respectively designated as *Slcr*, *Mlcr*, and *Llcr* where l indicates total number of CFRP layers, c is number of anchor columns, and r is number of anchor rows.

Figure III-1(a) shows a typical cross section and elevation of a specimen belonging to Series *M* provided with two columns of anchors ($c = 2$) and three rows ($r = 3$).

Figure III-1(b) shows cross sections of specimens of Series *S*, Series *M* with $c = 1$, and Series *L* with $c = 2$ and $c = 3$. Any tested anchored specimen belongs to one of the five cross sections shown in

Figure III-1. The anchors in all anchored specimens were equally spaced in the vertical as well as in the horizontal directions. In Table III-1, *H* indicates a specimen's height (Figure III-1); *e* indicates cross-sectional area of an individual anchor; *W* denotes the width of the CFRP sheet folded to form an anchor such that $e = W \times t$ ($t = 0.13$ *mm*) is the nominal thickness of one CFRP layer; T_e stands for total cross-sectional area of the CFRP anchors throughout the specimen height ($T_e = c \times r \times e$). Specimen $S113$ (used for the pilot test) is the only anchored specimen to which no CFRP layer is added to cover the fans. In each specimen, T_e is selected equal to the total cross-sectional area of the underlying CFRP jacket (i.e., excluding the last top layer) crossing the vertical plane of the specimen.

As can be seen in Table III-1, for Specimens in Series *M* and *L*, for each number of CFRP layers *l*, two different anchor configurations (number of anchor

columns c) are tested while maintaining the same total cross-sectional area T_e of the CFRP anchors throughout the specimen height. For test Series M, c takes values of 1 and 2, and for series L, c takes values of 2 and 3. The purpose of this variation is to evaluate the influence of the transverse distribution of the anchors on the behavior of anchored specimens.

All specimens are cast using a single batch of ready-mix concrete. The 28-day concrete compressive strength, obtained using standard 15 cm x 30 cm concrete cylinders, was measured at 35 MPa. The design properties of the CFRP sheets are those specified in Chapter II. The specimens were tested in displacement control at a slow rate of approximately 0.06 mm/s using a 2,000 KN - capacity Tinius Olsen (Horsham, Pennsylvania) universal testing machine.

The displacement level is increased in prescribed increments until failure of the specimens. Three full loading-unloading cycles were conducted at each strain level. Figure III-2 shows the front and side views of typical experimental set up of a tested specimen. As seen in these figures, the axial strain is measured using four linear variable differential transducers (LVDTs) (supplied by Omega Engineering, Stamford, Connecticut). Two LVDTs are attached on opposite sides of the rectangular specimens over a gage length of $H/2$ at the middle region of the column. Two other LVDTs, mounted near two diagonally opposite corners, are used to measure the average strain over the full height of the specimens (gauge length $H/2$). The lateral strain is measured using four electric strain gauges (supplied by Omega Engineering) mounted on the CFRP wraps at midheight of the specimen (Figure III-3) and using also two lateral LVDTs for measuring the overall lateral displacement of two opposite sides of the specimen (Figure III-2). In order to avoid placing a strain gauge on an anchor or anchor

fan where the accuracy of the strain measurement may potentially decrease, two strain-gauge configurations were used, one for the anchored specimens and the other for the remaining CFRP-confined specimens (Figure III-2).

C.   Test results

1.   *Failure mode*

Figure III-4(a and b) show the failure modes of a specimen confined with CFRP jacket without anchors and the Pilot Specimen S113 and Figure III-4(c) shows the failure mode of Specimen S313, which represents the typical failure mode of anchored specimens. For specimens confined with CFRP jackets with no anchors, failure occurred by rupture of the CFRP sheets at the corners. As pointed out earlier, Specimen S113 experienced premature bond failure between the anchor fans and the underlying CFRP jacket associated with the large tensile stresses in the anchors (Figure III-4b) which caused an inferior stress-strain response of this specimen.

In the following, the typical progressive failure of the anchored specimens (except S113, L224 and L424) is described. As concrete dilation increases, the tensile stresses developed in the anchors at the specimens' midheight tried to separate the anchor fan from the underlying jacket. The last layer covering the fans provided a pressure that improves the bond resistance between the fan and the underlying jacket. However, close to the fan edge, excessive dilation was observed resulting in local rupture of the CFRP sheet with further increase in concrete dilation. In a final stage, complete failure of the specimens occurred by rupture of the CFRP sheets at the corners. Figures showing typical failure mode of anchored specimens are provided in Appendix A.

Non-typical failures were observed for specimens *L*224 and *L*424 which led to inferior stress-strain response of these specimens. This may be due to imperfect alignment of the specimens with the applied load.

2.   *Envelope response*

Figure III-5,Figure III-6 and Figure III-7 show the axial stress-strain responses of all tested specimens, with the aim of studying the improvement provided by the two types of confinement (with anchors and without anchors) to the axial response, and comparing the efficiency of these two types. The stress-strain responses of the pilot specimen *S*113 and specimens *L*224 and *L*424 that experienced unusual failure modes are not reported. Figure III-8 shows idealization of the stress-strain response of the specimens confined with CFRP sheets with anchors and without anchors. For the specimens confined with no anchors, the idealization is the same as that shown in Figure II-6. Figure III-9 plots the axial stress-lateral strain curves of three specimens (*M* 400*, M* 413 and *M* 423). The axial stress-lateral strain curves of the remaining specimens are not plotted for brevity. Instead, the values of the lateral strain at ultimate (the hoop rupture strain, $\varepsilon_{h,rup}$) are shown in Table III-2. The average hoop rupture strain of all the tested specimens reported in Table III-2 is close to 45% ε_{fu} corresponding to an efficiency factor of 0.45. For the tested specimens, the hoop rupture strain tends to decrease with increase in the cross section aspect ratio. For specimens confined with external CFRP sheets only, the effect of the number of FRP layers on $\varepsilon_{h,rup}$ is not noticeable. For specimens confined with a combination of FRP sheets and anchors, $\varepsilon_{h,rup}$ tends to increase with increase in the number of layers.

A summary of the test results of the envelope axial stress-strain response for all specimens, is provided in Table III-2 and Table III-3. Table III-2 summarizes all the results related to strains where Table III-3 shows the results related to stresses. In these tables, f'_t = concrete stress corresponding to the peak of the first branch of the stress-strain response at a strain $\varepsilon_c = \varepsilon_t$; ε_{cu} = ultimate concrete strain at which the specimens developed failure; f'_{cu} = ultimate concrete strength corresponding to ε_{cu}; $\varepsilon_{t,2}$ and $f'_{t,2}$ = axial strain and corresponding axial stress, respectively, at which the second branch terminates without complete rupture of the FRP sheet at the corner for some of the anchored specimens (Figure III-8). Note that test measurements which were deemed unreliable were specified in Table III-2.

a)   Unconfined specimens

As shown in Figure III-5, Figure III-6 and Figure III-7, the peak stress in all unconfined specimens (*S* 000, *M* 000 and *L* 000) developed at an axial strain close to 0.002. This peak was measured at 31.53 *MPa* for specimen *S* 000, 28.79 *MPa* for specimen *M* 000 and 28.5 *MPa* for specimen *L* 000, all of which are lower than the cylindrical concrete compressive strength of 35.0 *MPa*. This is mainly due to the higher slenderness ratio of these specimens compared to the 15 *cm* x 30 *cm* cylinder. In addition, slenderer specimens (*M* 000 and *L* 000) tend to have lower compressive strength than the least slender (*S* 000).

b)   CFRP confined specimens (without anchors)

Figure III-5, Figure III-6 and Figure III-7 show that, for purely CFRP wrapped specimens ($l \neq 0, c = 0$ and $r = 0$), as has been widely reported in the technical literature,

the first stage of the envelope response coincides to a large extent with that of the unconfined specimens ($l = 0$, $c = 0$ and $r = 0$). The second stage of the response starts at an axial strain close to ε_t due to concrete dilation and could be either ascending or descending (Figure III-8). This second stage terminates by rupture of the CFRP jacket and sudden drop of the axial load at an ultimate stress f'_{cu} and strain ε_{cu}. For all the tested specimens (Figure III-5, Figure III-6 and Figure III-7), the confinement provided by the CFRP jacket improved the peak axial strength and the corresponding strain but resulted in a post-peak descending behavior. Figure III-10 compares the axial stress-strain response of the unconfined specimen and the specimens confined with CFRP sheets without anchors in test series *S*. This comparison, typical to all series, shows that for a given specimen geometry, increasing the number of CFRP layers, increases the peak stress and reduces the steepness of the post-peak descending branch. Also, as commonly reported in the literature, for the same area of CFRP jacket, the improvement in the post-peak branch becomes more pronounced as the aspect ratio of the rectangular section decreases.

c)   CFRP anchored specimens

For CFRP anchored specimens ($l \neq 0$, $c \neq 0$ and $r \neq 0$) (Figure III-5, Figure III-6 and Figure III-7), as a result of improved confinement provided by the anchors, the first stage of the response extends to a greater strain ε_t than that of the companion specimens without anchors. Beyond a strain ε_t, the second stage of the response is either descending, or constant stress, or slightly ascending (Figure III-8). The axial strain at which the constant or slightly ascending branch terminates is referred to in

Table III-2 respectively as $\varepsilon_{t,2}$, while the axial stress is denoted as $f'_{t,2}$ and presented in Table III-3. The constant or slightly ascending branch is followed by a descending branch (Figure III-8) that continues until failure of the specimen. Among all the anchored specimens, only specimen $S413$ (Figure III-5c) of aspect ratio 1.5 (least aspect ratio studied) experienced an ascending second branch in which the axial stress increased from $f'_t = 40.69\ MPa$ at $\varepsilon_t = 0.0051$ to $f'_{t,2} = 44.25\ MPa$ at $\varepsilon_{t,2} = 0.011$. For this specimen, the reduction in stress beyond $\varepsilon_{t,2} = 0.011$ occurred as a result of a localized rupture of the CFRP jacket at the fan edge due to excessive concrete dilation. This reduction in stress progressed until complete failure of the specimen at $\varepsilon_{cu} = 0.0195$ and $f'_{cu} = 35.38\ MPa$, accompanied with brittle CFRP rupture at the corners of the specimen close to midheight. As for specimens $S313$ (Figure III-5b), $M413$, $M423$ (Figure III-6c) and $L423$ (Figure III-7c), an almost constant second branch is observed before drop in stress. All the remaining anchored specimens exhibited a descending branch accompanied by excessive bulging and localized ruptures near the anchor fan before complete failure by rupture of the CFRP jacket at the corner-midheight region.

d)   Comparison between anchored and unanchored specimens

As shown in Figure III-5, Figure III-6 and Figure III-7, the presence of anchor holes reduced the cross sectional area in the horizontal plane at the anchors location causing a slight reduction in the peak axial stress during the first stage of the response of anchored specimens when compared with their companion specimens wrapped with the same number of CFRP layers but without anchors.

Figure III-5(c) compares the axial stress-strain response of unanchored specimen $S400$ against its companion anchored specimens $S413$. Despite reduction in peak stress due to the presence of holes, the post-peak response (in the second stage) was improved due to the presence of anchors. However, this improvement was considerably larger for the specimens wrapped with four CFRP layers (S 413 versus $S400$) than the specimens wrapped with three layers (S 313 versus S 300) (Figure III-5b).

Similar to specimens in series S, Figure III-6 and Figure III-7 show that adding CFRP anchors to specimens in series M and L resulted also in sizable increases in the stresses mobilized during the second stage of the response, leading to a more ductile compression failure. Note that while the presence of anchors improved the stress-strain behavior in the second stage of the response, it did not have a noticeable effect on the strain ε_{cu} at ultimate.

Figure III-6 and Figure III-7 show that varying the anchor configuration does not lead to noticeable variations in the stress-strain response, except for a slight reduction in the peak stress for higher number anchor holes. This conclusion holds for all anchored specimens of series M and L, except specimen M 423 wrapped with four layers and provided with 2 columns of anchors that exhibited higher strength in the second branch of the stress-strain curve when compared to specimen having the same geometry and the same number of layers but provided with one column of anchors (M 413) (Figure III-6c).

The influence of the specimen cross-section aspect ratio and the area of the CFRP anchors on the improvement of the second branch of the envelope curve was evaluated in this study using the slope β of the stress-strain curve during the second

stage of the response. Defining $\beta_{anchored}$ and $\beta_{unanchored}$ as the corresponding slopes of the anchored and their companion unanchored specimens, respectively, the percent change in slope $k = \left| \dfrac{\beta_{anchored} - \beta_{unanchored}}{\beta_{unanchored}} \right| \times 100\%$ was calculated for the various specimen (except for $L224$ and $L424$). The results are presented in Table III-4.

It can be observed in Table III-4 that for the same test parameters, the slope β of the second stage of the stress-strain response decreases (becomes steeper) with increasing aspect ratio of the cross section. This observation was common for the anchored and the unanchored specimens. However, the percent improvement in the corresponding slope due to the addition of anchors, as reflected in the values of k, was independent of the aspect ratio of the cross section.

As for the influence of the cross-sectional area of the CFRP anchors, it can be seen from Table III-4 that as the number of CFRP layers increases, which is accompanied by increase in the cross-sectional area of the CFRP anchors, the increase in the value of k, which indicates improvement in the slope of stress-strain response, becomes more significant. For instance, for the specimens in series M provided with one column of anchors, $k = 30.86\%$ for the specimen wrapped by 2 layers and increases to 51.46% and 71.60% when the number of CFRP layers increases to 3 and 4, respectively.

3.   *Cyclic response*

The cyclic response for anchored and unanchored confined specimens (Figure III-5,Figure III-6 and Figure III-7) is composed of an unloading cycle followed by a reloading cycle. As was noted in Chapter II for specimens confined with external FRP sheets only, the unloading path is curvilinear while the reloading cycle is almost linear.

The same parameters used to define the cyclic response of specimens confined with external FRP sheet only (Chapter II) are used to define the cyclic response in Figure III-8.

As observed in Figure III-5, Figure III-6 and Figure III-7, the intrinsic shape of the unloading and reloading curves at all envelope unloading strain levels $\varepsilon_{un,env}$ is independent of the shape of the cross section, confinement level, and presence or absence of anchors. In addition, as the envelope unloading strain increases, the difference between the plastic strain and the envelope unloading strain increases. Also, due to repeated unloading/reloading cycles at a given strain level, the strength in the reloading paths decreases slightly as the number of cycles of increases. These conclusions were previously made in Chapter II for specimens confined with external FRP sheets only. Figure III-8 schematizes the fact that the strength degradation grows larger with increase in the number of cycles as $\sigma_o = \sigma_{un,env} > \sigma_1 > \sigma_2 > \sigma_3$, where σ_1 σ_2, and σ_3 are the stress values at $\varepsilon_{un,env}$ measured at the first, second, and third reloading paths respectively. Also, similarly to what was reported in Chapter II for unanchored specimens, the plastic strain $\varepsilon_{pl,env}$ increases by a small amount with increase in number of cycles for the same unloading strain $\varepsilon_{un,env}$.

Table III-1 - Summary of the specimens' details

Specimen	h (mm)	b (mm)	H/b	H (mm)	l	c	r	e (mm²)	T_e (mm²)
S000	210	140	1.50	420	0	0	0	0	0
S100					1	0	0	0	0
S113						1	3	36.4	109.2
S300					3	0	0	0	0
S313						1	3	72.8	218.4
S400					4	0	0	0	0
S413						1	3	109.2	327.6
M000	240	125	1.92	480	0	0	0	0	0
M200					2	0	0	0	0
M213						1	3	41.6	124.8
M223						2	3	20.8	124.8
M300					3	0	0	0	0
M313						1	3	83.2	249.6
M323						2	3	41.6	249.6
M400					4	0	0	0	0
M413						1	3	124.8	374.4
M423						2	3	62.4	374.4
L000	300	100	3.00	600	0	0	0	0	0
L200					2	0	0	0	0
L224						2	4	19.5	156
L234						3	4	13	156
L300					3	0	0	0	0
L324						2	4	39	312
L334						3	4	26	312
L400					4	0	0	0	0
L424						2	4	58.5	468
L434						3	4	39	468

Table III-2 - Summary of test results related to strains

Specimen	ε_t (mm/mm)	$\varepsilon_{t,2}$ (mm/mm)	ε_{cu} (mm/mm)	$\dfrac{\varepsilon_{cu}}{\varepsilon_{co}}$	$\varepsilon_{h,rup}$ (mm/mm)
$S000$	0.0025	-	-	-	-
$S100$	0.0039	-	0.0074	2.96	0.0090
$S300$	0.0042	-	0.0168	6.73	0.0083
$S313$	0.0048	0.0078	0.0150	6.02	0.0067
$S400$	0.0042	-	0.0153	6.12	0.0070
$S413$	0.0051	0.0110	0.0195	7.80	NA
$M000$	0.0019	-	-	-	-
$M200$	0.0021	-	0.0096	5.00	0.0067
$M213$	0.0035	-	0.0102	5.34	0.0096
$M223$	0.0040	-	0.0073	3.81	0.0067
$M300$	0.0036	-	0.0194	10.08	0.0072
$M313$	0.0052	-	0.0165	8.60	0.0129
$M323$	0.0050	-	0.0148	7.71	0.0107
$M400$	0.0034	-	0.0126	6.56	0.0057
$M413$	0.0045	0.0074	0.0171	8.92	0.0137
$M423$	0.0055	0.0075	0.0134	7.00	0.0069
$L000$	0.0019	-	-	-	-
$L200$	0.0030	-	0.0041	2.19	0.0013
$L224$	0.0038	-	0.0058	3.11	0.0018
$L234$	0.0037	-	0.0084	4.52	0.0030
$L300$	0.0036	-	0.0127	6.83	0.0044
$L324$	0.0046	-	0.0108	5.81	0.0047
$L334$	0.0051	-	0.0093	5.00	0.0059
$L400$	0.0032	-	0.0086	4.65	0.0019
$L424$	0.0050	0.0064	0.0144	7.74	0.0081
$L434$	0.0066	-	0.0144	7.76	NA

Table III-3 - Summary of test results related to stresses

Specimen	f'_t (MPa)	$\dfrac{f'_t}{f'_{co}}$	$f'_{t,2}$ (MPa)	$\dfrac{f'_{t,2}}{f'_{co}}$	f'_{cu} (MPa)
S000	31.53	1.00	-	-	-
S100	36.50	1.16	-	-	27.53
S300	38.48	1.22	-	-	24.96
S313	35.77	1.13	36.25	1.15	27.37
S400	41.28	1.31	-	-	27.97
S413	40.69	1.29	44.25	1.40	35.38
M000	28.79	1.00	-	-	-
M200	33.77	1.17	-	-	15.68
M213	34.59	1.20	-	-	23.02
M223	33.92	1.18	-	-	24.49
M300	38.16	1.33	-	-	17.27
M313	40.45	1.41	-	-	24.03
M323	37.81	1.31		-	28.07
M400	38.72	1.35	-	-	23.23
M413	39.98	1.39	40.88	1.42	28.20
M423	41.43	1.44	41.80	1.45	38.89
L000	28.50	1.00	-	-	-
L200	35.54	1.25	-	-	29.90
L224	33.97	1.19	-	-	23.15
L234	33.15	1.16	-	-	23.24
L300	39.55	1.39	-	-	17.53
L324	40.20	1.41	-	-	22.26
L334	40.03	1.40	-	-	25.04
L400	39.47	1.39	-	-	23.32
L424	40.09	1.41	38.50	1.35	24.13
L434	40.37	1.42	-	-	32.96

Table III-4 - Slopes of the second branch of the stress-strain response

Specimen	$\beta_{anchored}\left(\dfrac{MPa}{mm/mm}\right)$	$\beta_{unanchored}\left(\dfrac{MPa}{mm/mm}\right)$	k (%)
$S313$	−830	−1,080	23.15
$S413$	0	−1,070	100.00
$M213$	−2,240	−3,240	30.86
$M223$	−2,300	−3,240	29.01
$M313$	−1,000	−2,060	51.46
$M323$	−1,000	−2,060	51.46
$M413$	−480	−1,690	71.60
$M423$	−320	−1,690	81.07
$L234$	−1,710	−5,090	66.40
$L324$	−2,860	−4,530	36.87
$L334$	−2,150	−4,530	52.54
$L434$	−960	−3,780	74.60

(a) **Series M with c=2**

(b)
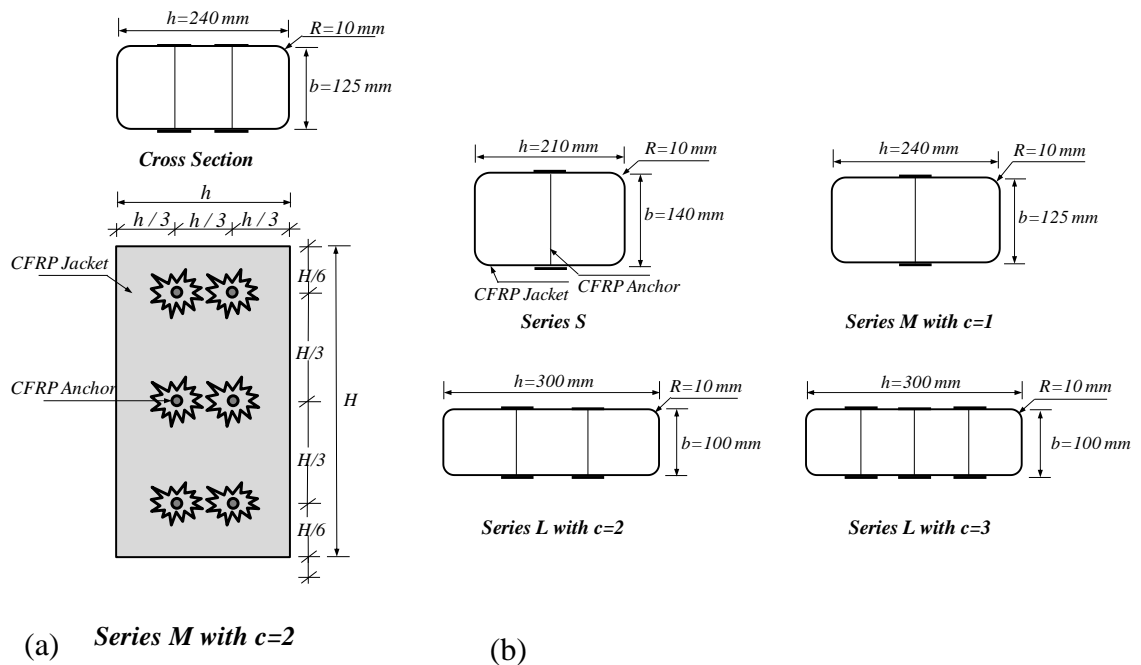
Figure III-1 - Schematic of (a) typical cross section and elevation of specimens of series M with $c = 2$, (b) cross sections of specimens of series S, series M with $c = 1$, and series L with $c = 2$ and $c = 3$
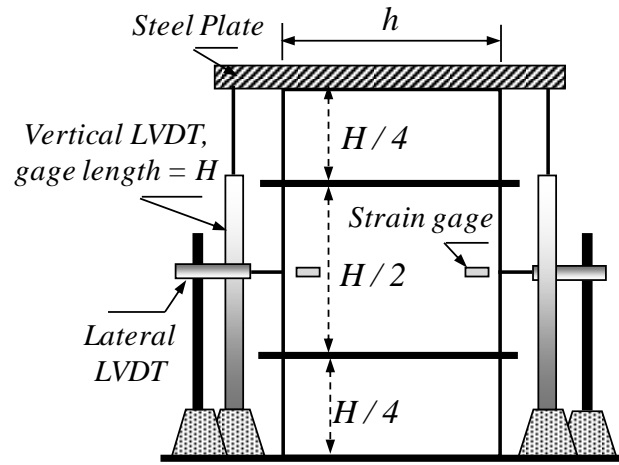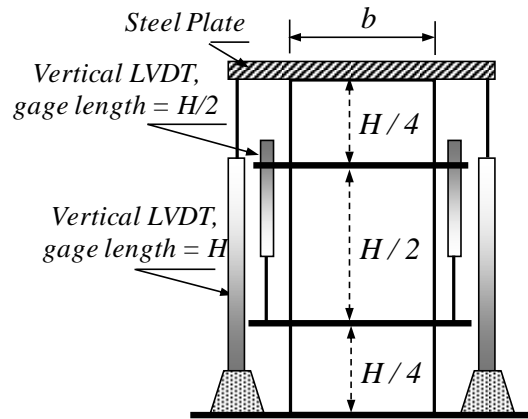
Figure III-2 - Typical experimental set up of a tested specimen: (a) front view; (b) side view
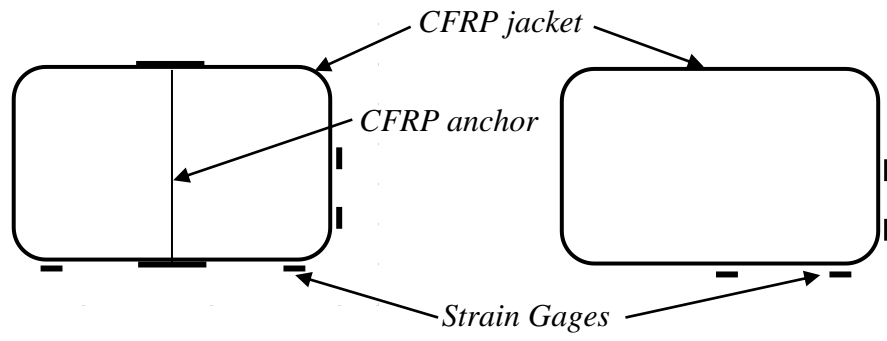
Figure III-3 - Strain gauge configurations on cross section at specimen midheight
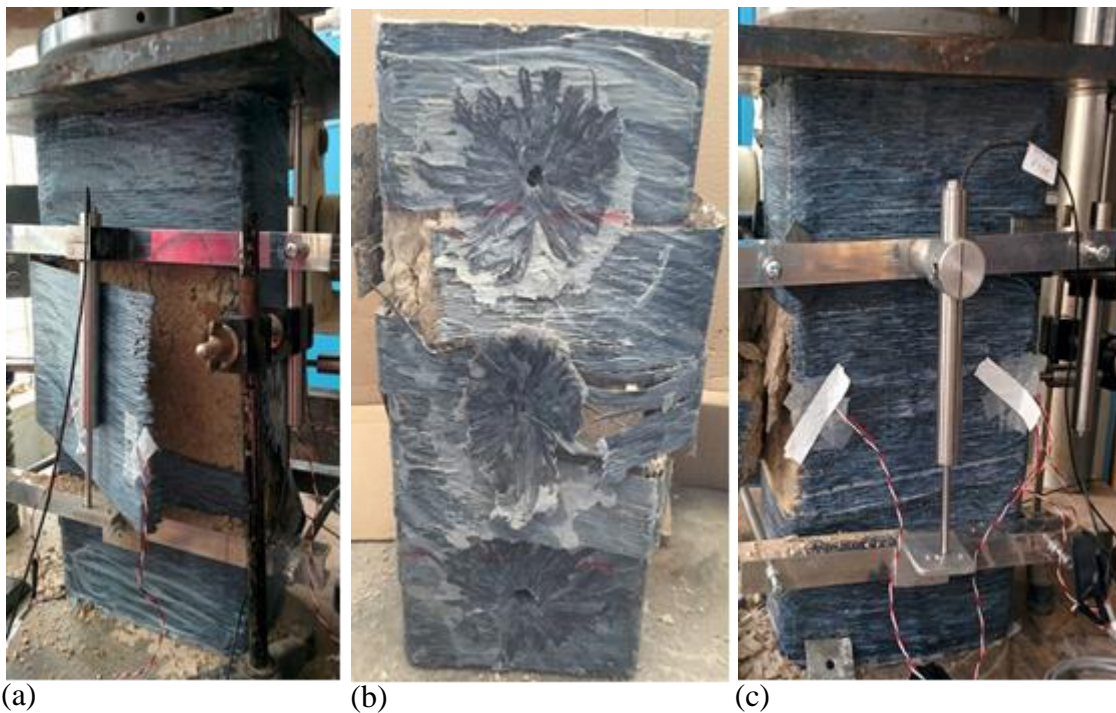
Figure III-4 - Failure mode of (a) Specimens confined with CFRP jacket without anchors; (b) Pilot Specimen $S113$; (c) Specimen $S313$

(a)

(b)
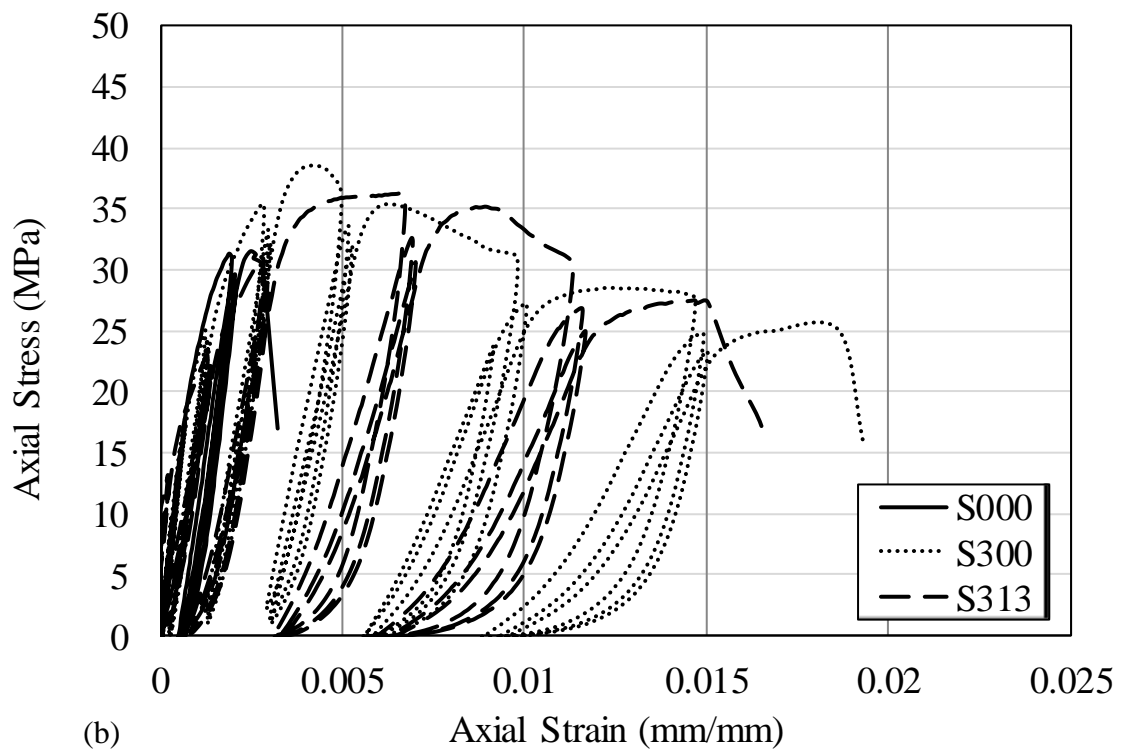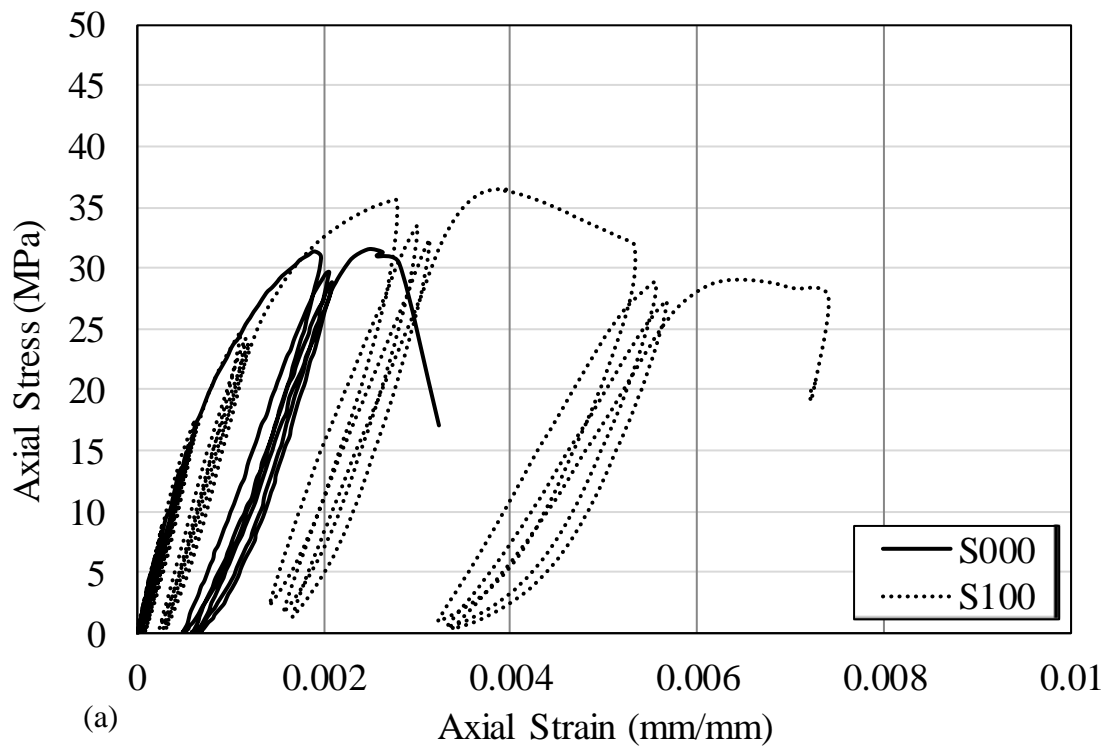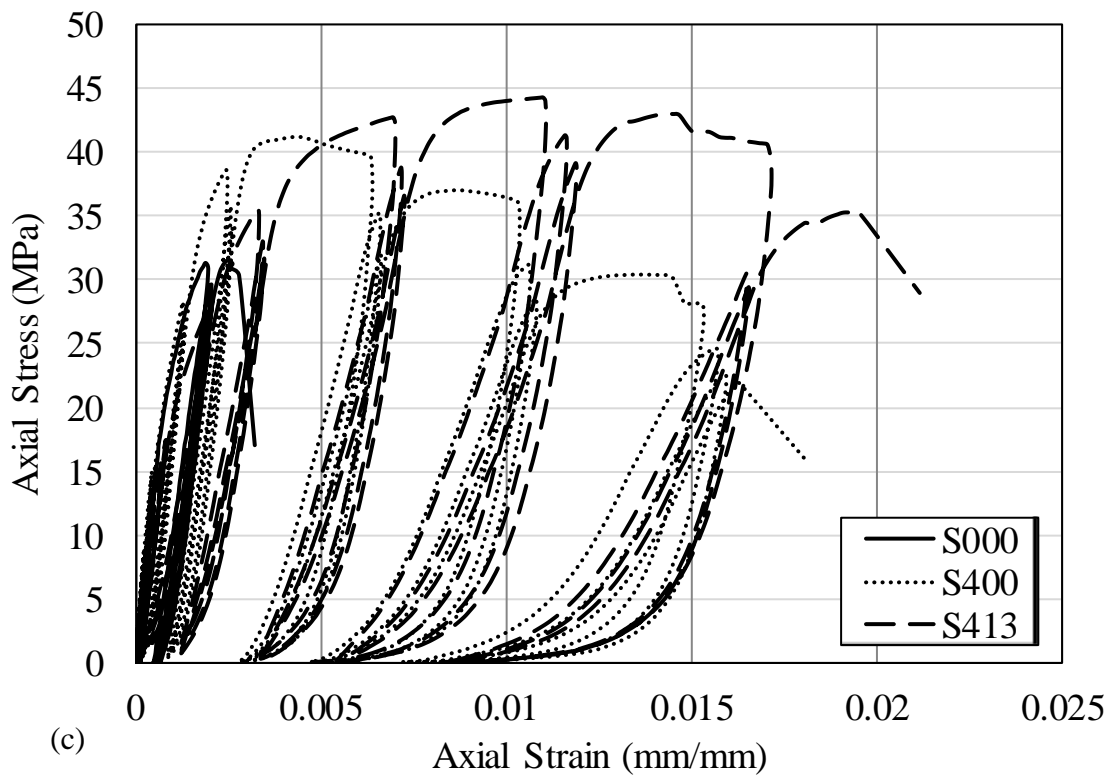
Figure III-5 - Experimental axial stress-strain curves of selected specimens of series *S*

(a)

(b)
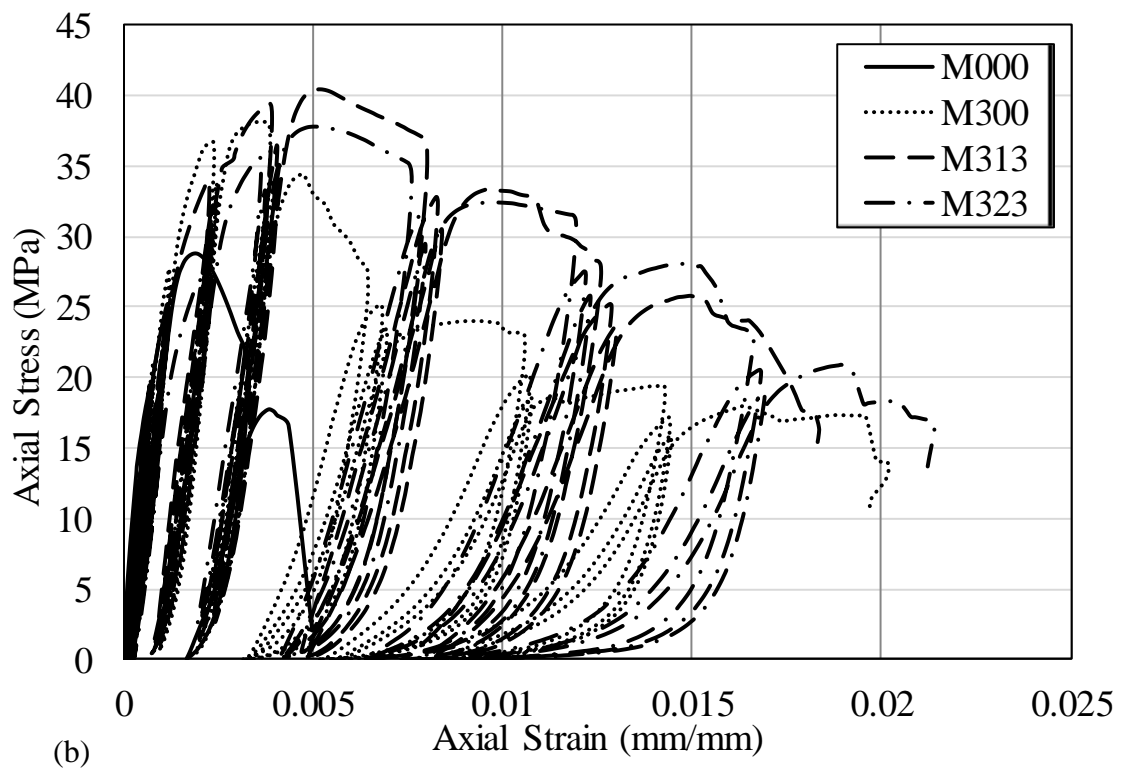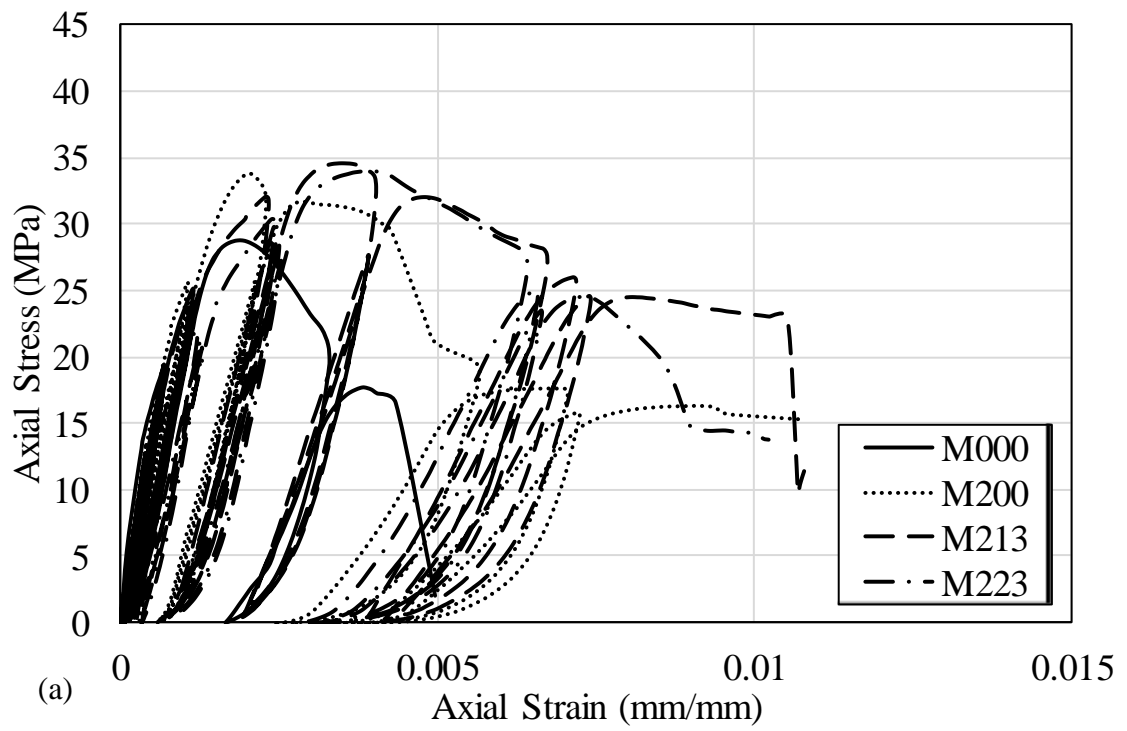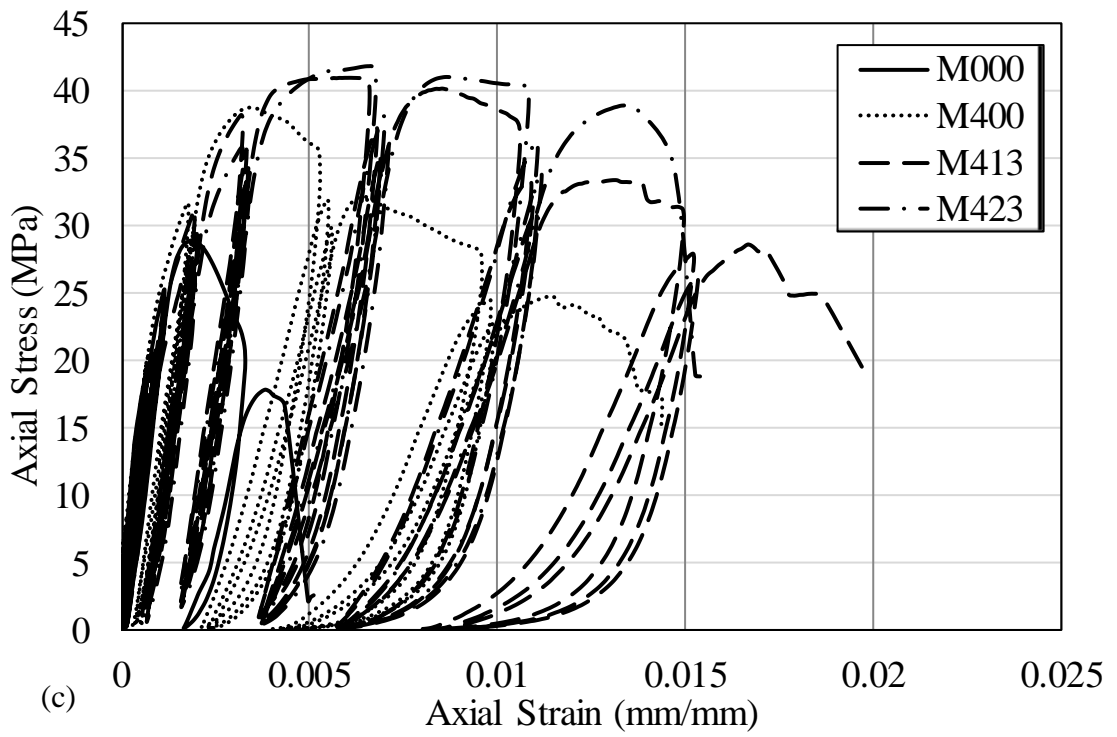
Figure III-6 - Experimental axial stress-strain curves of selected specimens of series *M*

(a)

(b)

94
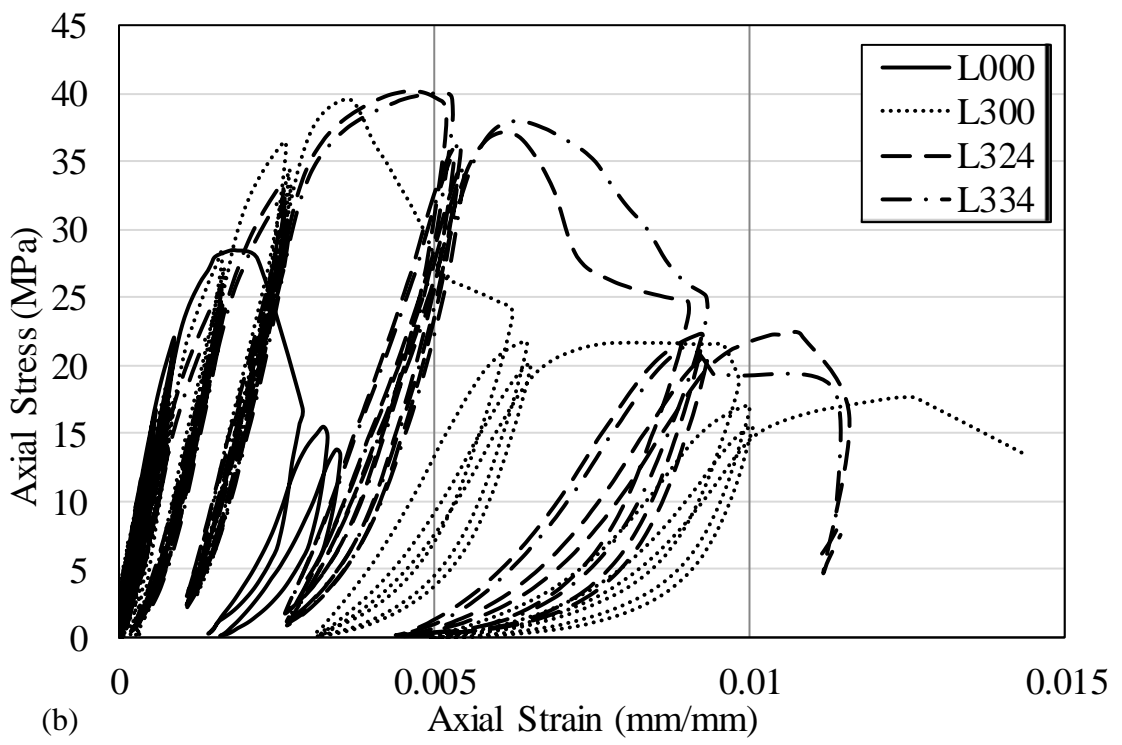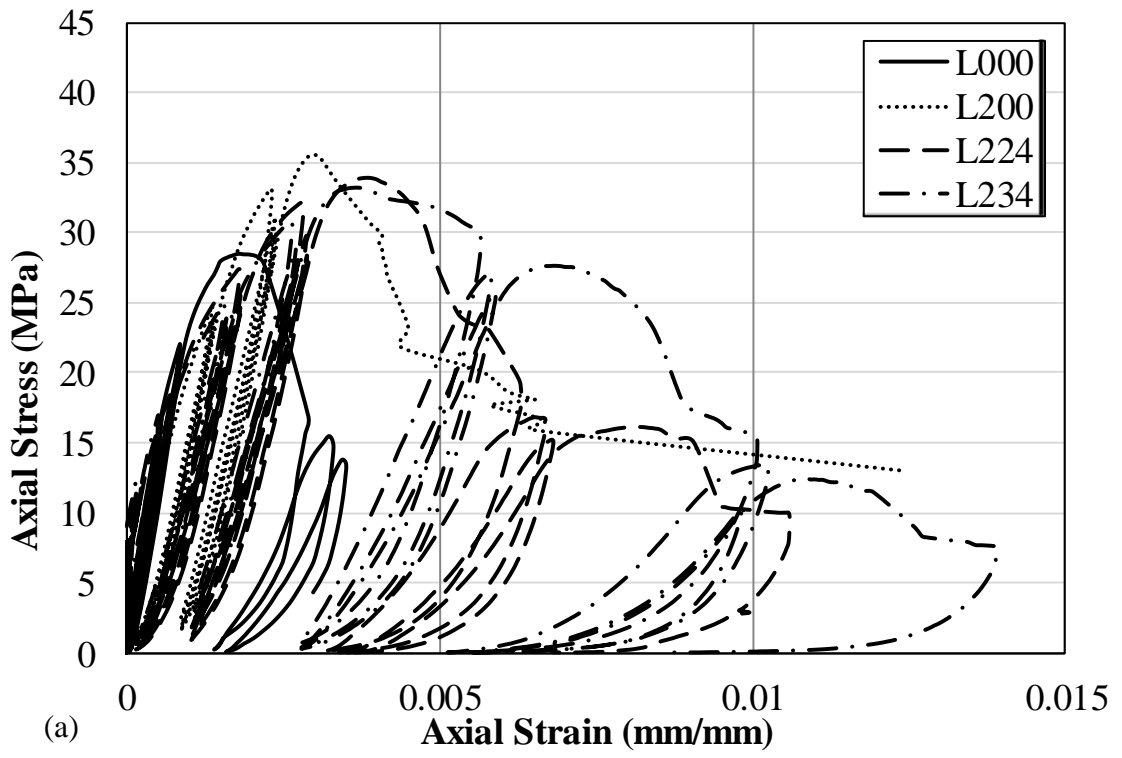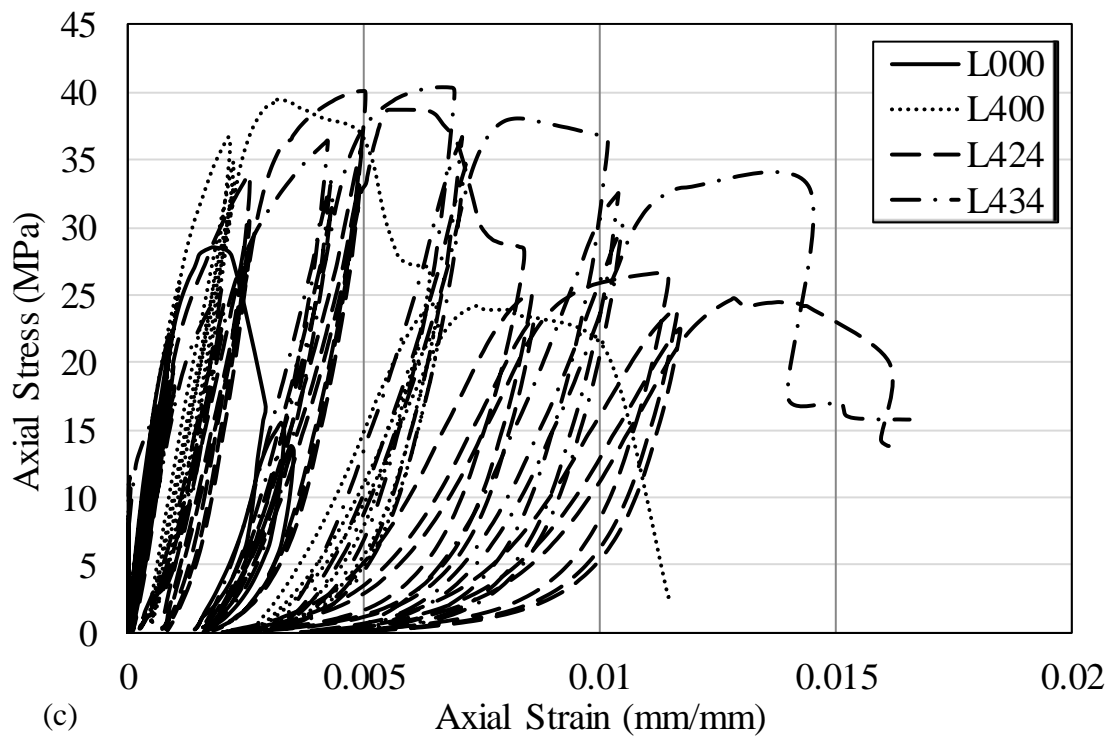
Figure III-7 - Experimental axial stress-strain curves of selected specimens of series *L*
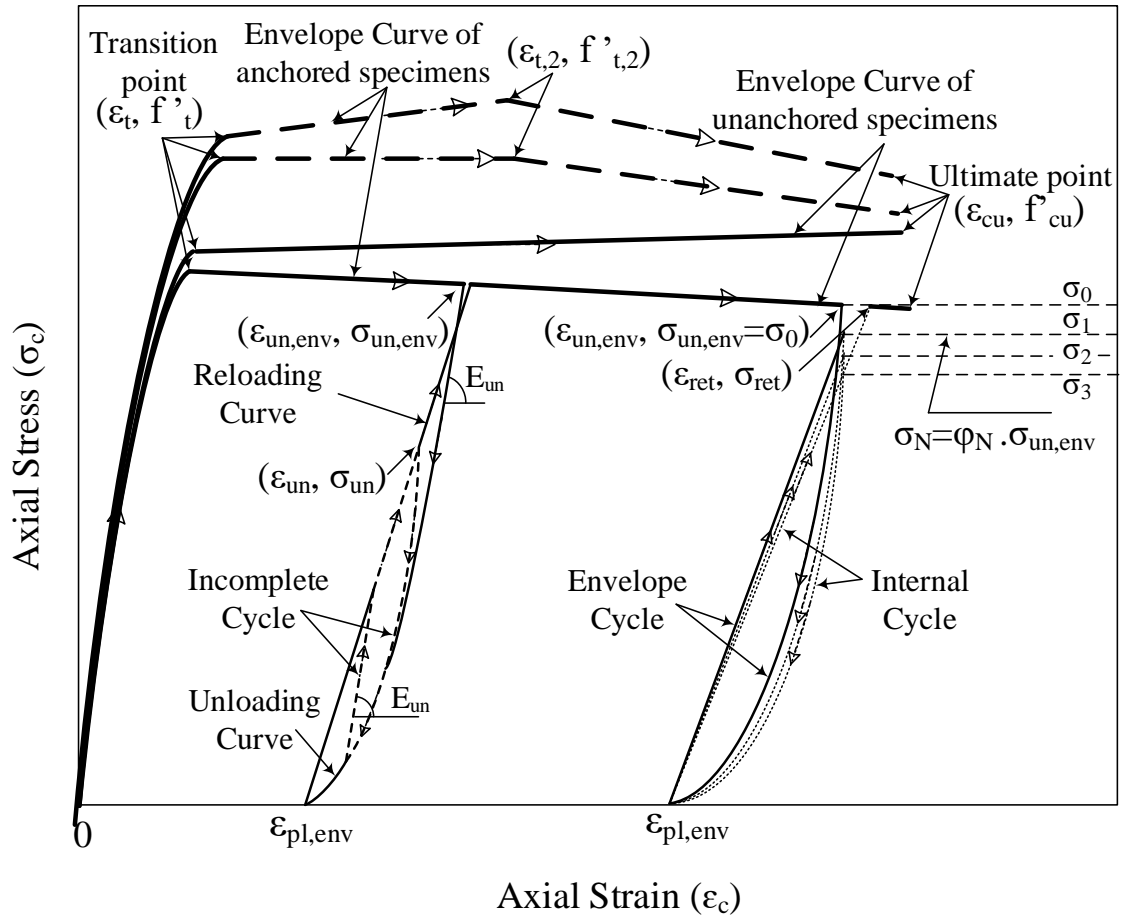
Figure III-8 - Idealization of the envelope and cyclic stress-strain responses of confined anchored and unanchored specimens
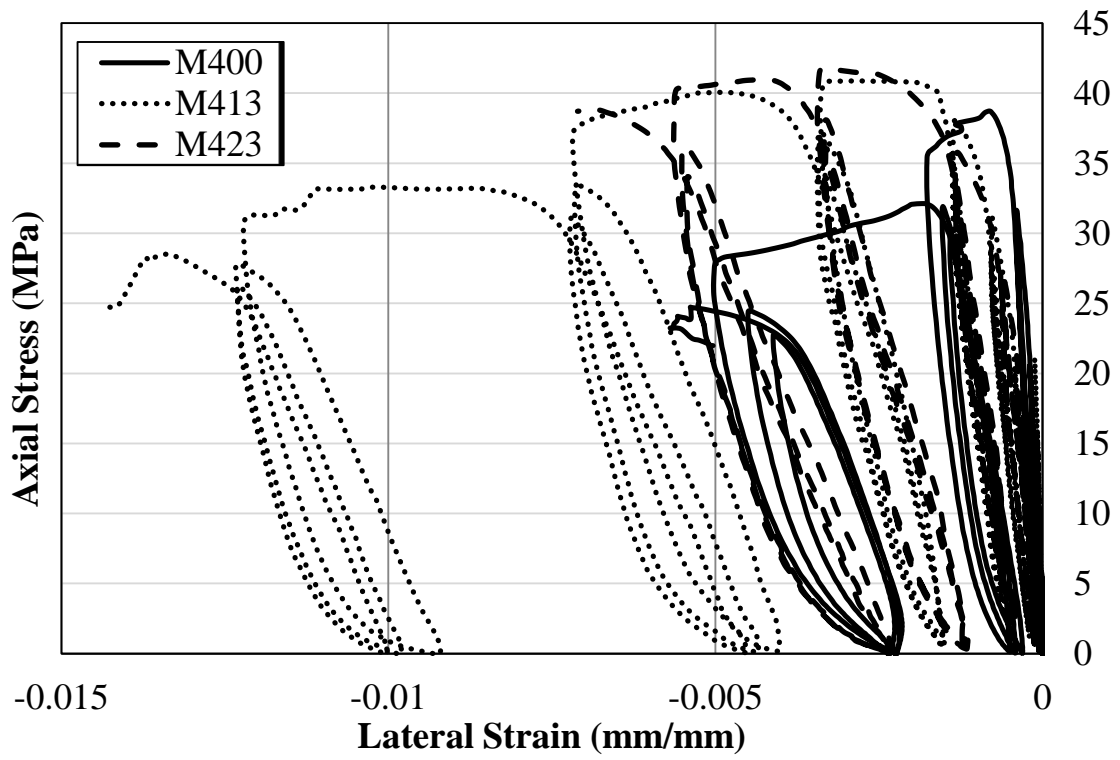
Figure III-9 - Axial stress-lateral strain curves of specimens $M400$, $M413$ and $M423$
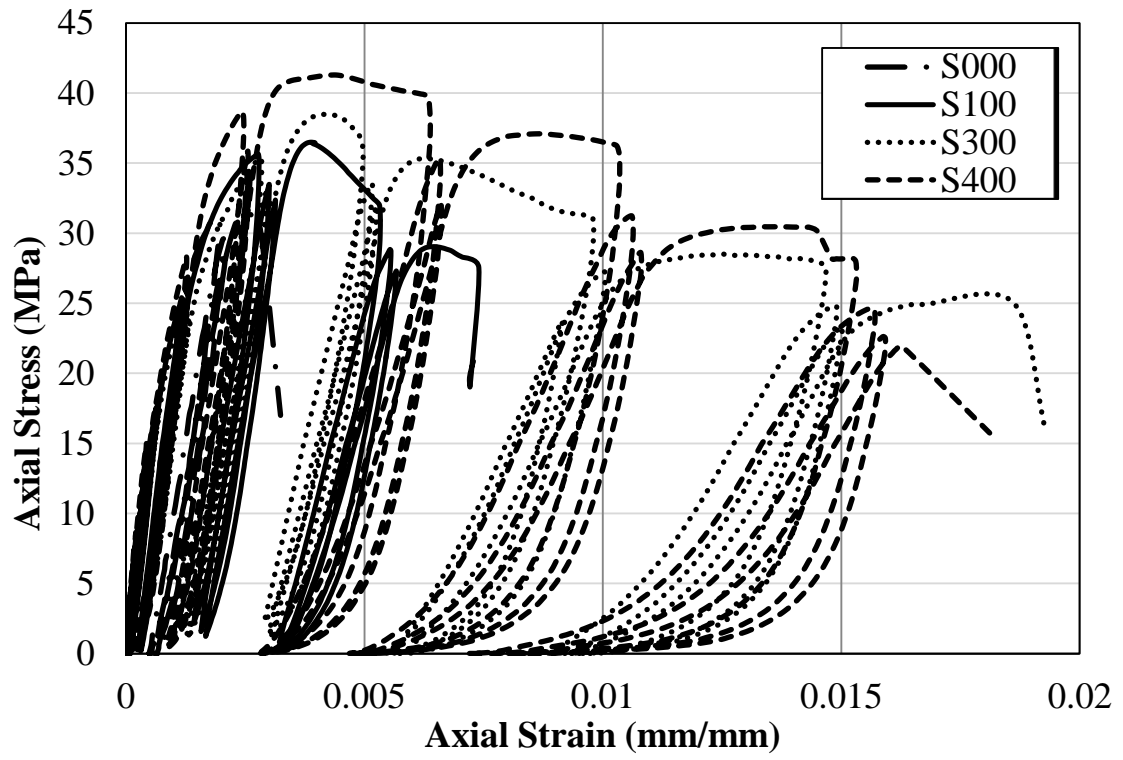
Figure III-10 - Axial stress-strain curves of specimens unconfined and confined unanchored specimens of series *S*

CHAPTER IV

ANALYTICAL MODELING OF THE AXIAL STRESS-STRAIN RESPONSE OF RECTANGULAR COLUMNS CONFINED USING CFRP JACKETS AND ANCHORS

A.   Introduction

Based on the results reported in Chapter III, analytical expressions are derived in this Chapter for predicting the stress-strain curve, taking into account the effect of CFRP anchors. This model presents a modification of the model proposed in Chapter II given that the latter underestimated the value of the first peak stress and slightly overestimates the ultimate stress and strain. when compared to the new experimental results. The accuracy of the new proposed expressions is assessed through comparison with the experimental results.

B.   Generalized Stress-Strain Model

A constitutive model, idealized in Figure III-8, is proposed to predict the axial stress-strain response of concrete specimens wrapped with external CFRP sheets only or with a combination of CFRP sheets and anchors and subjected to cyclic loading, in a unified manner. The proposed model is composed of an envelope part and a cyclic part.

1.   Envelope Response

The proposed envelope model consists of two branches: a parabolic branch followed by a linear branch to describe the first and second stages of the response, respectively. Using a straight line to draw the second branch of the curve disregards the

improvement of stress observed in some anchored specimens at the axial strain $\varepsilon_{t,2}$ after the peak of the first branch and before reaching the ultimate point. This improvement was pointed out while describing the experimental results and is shown in Figure III-8, as $f'_{t,2} \geq f'_t$. However, as will be shown when comparing the experimental results to the proposed model, this simplification does not cause any significant loss of accuracy of the model. The model presented in the following paragraphs represents a slight modification of the model proposed in Chapter II for concrete columns confined with external CFRP only. The first stage of the response (σ_c - ε_c) is defined using the expression proposed by (Mander, Priestley, & Park, 1988) for steel confined concrete:

$$\sigma_c = \frac{f'_t\ x\ r}{r - 1 + x^r} \hspace{5cm} \text{(IV-1)}$$

Where $x = \dfrac{\varepsilon_c}{\varepsilon_t}$, $r = \dfrac{E_c}{E_c - E_{\sec}}$, $E_{\sec} = \dfrac{f'_t}{\varepsilon_t}$.

This stage extends to the point of coordinates (ε_t, f'_t). The second stage is a line joining the peak point of the first branch (ε_t, f'_t) to the ultimate point (ε_{cu}, f'_{cu}). Expressions of (ε_t, f'_t) and (ε_{cu}, f'_{cu}) are proposed in the following.

a)   Volumetric ratio of FRP reinforcement

As reported in Chapter II, for circular concrete specimens of diameter D fully wrapped with external FRP jackets, the volumetric ratio of FRP reinforcement is $\rho_f = 4t_{wrap}/D$. For columns confined with discrete FRP strips (partially wrapped) having a strip width W and center-to-center spacing $_s$ (Figure II-1b), this ratio is

$\rho_f = (4Wt_{wrap})/(sD)$. For specimens of rectangular cross sections, these same two

expressions are used to compute ρ_f with D being the diameter of the equivalent

circular cross-section defined as $D = \sqrt{b^2 + h^2}$.

However, for rectangular specimens, confined using external FRP sheets or a

combination of FRP sheets and anchors, the geometric volumetric ratio of FRP is

defined as:

$$\rho'_f = \frac{A_x h + A_y b}{A_c H} \tag{IV-2}$$

Where A_x and A_y are the total area of FRP crossing respectively a vertical plane parallel

to the short side of the transversal section and another parallel to the long side. This

definition accounts for the cross-sectional area of both external FRP sheet and the

composite inserted into the hole.

For small corner radii, typical to specimen strengthened with external FRP

sheets, the cross-sectional area A_c is very close to bh therefore Eq. (IV-2) reduces to

$$\rho'_f = \frac{A_x}{bH} + \frac{A_y}{hH} \tag{IV-3}$$

The diameter of the equivalent circular section that conserves this volumetric

ratio for specimens externally wrapped with FRP is $D' = 2bh/(b+h)$.

As stated in Chapter II, the volumetric ratio of FRP in rectangular cross section

externally confined with FRP sheets is computed as $\rho_f = 4t_{wrap}/D$ or

$\rho_f = (4Wt_{wrap})/(sD)$ with $D = \sqrt{b^2 + h^2}$. This is equivalent to defining the ratio as:

$$\rho_f = \rho'_f \times \frac{D'}{D} = \left(\frac{A_x}{bH} + \frac{A_y}{hH} \right) \times \frac{D'}{D} \tag{IV-4}$$

Equation (IV-4) is also used to define the volumetric ratio in specimens confined with a combination of FRP jacket and anchors in the aim of having the same definition of the volumetric FRP ratio in sections confined using FRP jacket only or a combination of FRP jacket and FRP anchors.

The values of ρ_f, computed using Eq (IV-4) for all the tested specimens, are reported in Table IV-1.

b)   Effectively Confined Area

As noted in Chapter II, for specimens of rectangular cross-section wrapped with FRP over their entire height, only part of the cross-section is effectively confined (Figure II-7 and Figure IV-1b). Accordingly, many researchers defined the effectively confined area as per Eq. (II-6) which assumes that the initial slope of the parabola is parallel to the diagonal of the rectangular cross-section. Also, as mentioned previously, for partially confined circular or rectangular columns, the confinement effectiveness coefficient A_e/A_c should be multiplied by a coefficient k_v given by Eqs. (II-7) and (II-8).

For the anchored confined specimens, the specimen height is divided into two regions shown in (Figure IV-1a). *Region I* is located at the mid-distance between two anchor rows and spreads over one-third the distance between these two rows ($d/3$). In this region, the anchors effect is assumed negligible and the effectively confined area is shown in (Figure IV-1b) and quantified using Eq. (II-6). *Region II* is located at the anchors level and extends above and below the anchor to one-third the distance between two adjacent anchors. In this region, the presence of anchors increases the effectively confined area, as shown in (Figure IV-1b). In this case, for edge parabolas, the arching action is assumed to originate at the end of the corner radius from one side and at one-

third the distance between the edge anchor and the end of the corner radius from the other side; for an internal parabola, it originates at one-third the distance between two consecutive anchors from both sides. The initial slope of each parabola is parallel to the diagonal of the rectangle delimited by the section edges and the FRP anchors. The corresponding effectively confined area is defined as:

$$\frac{A_e}{A_c} = 1 - \frac{1}{3A_c}\left[\frac{(c+1)b}{h}\sum_{i=1}^{c+1}w_{x,i}^2 - \frac{h}{(c+1)b}(b-2R)^2\right] \tag{IV-5}$$

where $w_{x,i}$ is the length of the base of the parabola i as shown in (Figure IV-1b). For an internal parabola, $w_{x,i} = h/[3(c+1)]$, while for an edge parabola

$$w_{x,i} = 2h/[3(c+1)] - R.$$

The weighted average between the two effectively confined areas defined in Eqs. (II-6) and (IV-5) is used to define the effectively confined area of the anchored specimen such that:

$$\frac{A_e}{A_c} = \frac{1}{3}\left(\frac{A_e}{A_c}\right)_1 + \frac{2}{3}\left(\frac{A_e}{A_c}\right)_2 \tag{IV-6}$$

where $(A_e/A_c)_1$ and $(A_e/A_c)_2$ are the effectively confined areas defined respectively in Eqs. (II-6) and (IV-5).

c)   <u>Proposed Expressions for f'_t and ε_t</u>

The values of f'_t/f'_{co} generated in the current experimental program (Table III-3) were combined with f'_t/f'_{co} data obtained from the experimental program performed at AUB reported in Chapter II (Table II-2)which included unanchored confined specimens of circular, square and rectangular cross-sections, partially wrapped and fully wrapped with various numbers of FRP layers. Analysis of the combined

103

results shows that f'_t / f'_{co} increases with increase in K_l / f'_{co}, as well as with increase in the aspect ratio h / b. K_l is the stiffness of the FRP confinement defined using Eq. (II-10).

Similar observations are noted when analyzing the values of $\varepsilon_t / \varepsilon_{co}$. Regression analysis of the data using statistical software (R Studio, 2012) leads to the following expressions of f'_t / f'_{co} and $\varepsilon_t / \varepsilon_{co}$, in which the coefficients were rounded for practical purposes:

$$\frac{f'_t}{f'_{co}} = 0.88 + 0.12 \left(\frac{h}{b}\right)^{0.3} \left(\frac{K_l}{f'_{co}}\right)^{0.38} \tag{IV-7}$$

$$\frac{\varepsilon_t}{\varepsilon_{co}} = 1.06 + 0.03 \left(\frac{h}{b}\right)^{0.86} \left(\frac{K_l}{f'_{co}}\right) \tag{IV-8}$$

Figure IV-2(a) and (b) show comparison between the experimental and predicted values of f'_t / f'_{co} and $\varepsilon_t / \varepsilon_{co}$ of the current experimental program and of the specimens tested at AUB and reported in Chapter II. The average ratio μ of predicted-to-test results for f'_t / f'_{co} is computed at 1.014 with a standard deviation $\sigma = 0.063$, while the average ratio μ of predicted-to-test results for $\varepsilon_t / \varepsilon_{co}$ is calculated at 0.989 with a standard deviation $\sigma = 0.152$, which is in support of the accuracy of Eqs. (IV-7) and (IV-8). Note that while the presence of holes in the anchored specimens reduces slightly the concrete cross-sectional area and hence decreases the unconfined concrete compressive strength as previously mentioned, the effect of holes in predicting f'_t / f'_{co} and $\varepsilon_t / \varepsilon_{co}$ has been neglected for practical purposes.

d)   Expressions of f'_{cu} and ε_{cu}

The expressions of f'_{cu} and ε_{cu} (Eqs. II-11 and II-12) are used to predict the

ultimate point coordinates for specimens confined with FRP sheets only or with a

combination of FRP sheets and anchors

2.   Cyclic Response

As was stated in Chapter II, a full cycle is divided into an unloading curve and a

reloading curve.

a)   Unloading Curve

Seeing that the intrinsic shape of the unloading curve is the same for anchored

and unanchored specimens, the same unloading curve expression Eq. (II-14) that was

developed for unanchored specimens, is adopted here in the following for both anchored

and unanchored specimens. The coefficient B_1 is expressed by Eq. (II-15).

b)   Plastic Strain

The results shown in Figure III-5, Figure III-6 and Figure III-7 show a slight

increase in the plastic strain due to repeated unloading-reloading cycles at a given strain

level. However, this increase is neglected while modeling the cyclic response, and a

constant plastic strain $\varepsilon_{pl,env}$ is assumed irrespective of the number of cycles. In

Chapter II the influence of different parameters on the plastic strain of unanchored

specimens was investigated. These parameters included the confinement level, the

geometry (circular, square, or rectangular) or aspect ratio of the section and the

unconfined concrete compressive strength. The envelope plastic strain was found independent of all these parameters and Eqs. (II-16, II-17 and II-18) were proposed to predict $\varepsilon_{pl,env}$ based on a regression analysis.

Similar to the results reported in Chapter II, Figure III-5, Figure III-6 and Figure III-7 show that for small values of unloading strain ($\varepsilon_{un,env} \leq 0.001$), the envelope plastic strain is almost zero. For $\varepsilon_{un,env} > 0.001$, Figure IV-3 shows a comparison between the experimental values of the envelope plastic strain $\varepsilon_{pl,env}$ of the specimens tested in this experimental program and the values predicted by applying Eqs. (II-17) and (II-18). The average ratio μ of predicted-to-test results for $\varepsilon_{pl,env}$ is computed at 1.011 with a standard deviation $\sigma = 0.136$, which is in support of the accuracy of Eqs. (II-17) and (II-18). Accordingly, these equations are used to predict the envelope plastic strain of anchored and unanchored specimens for $\varepsilon_{un,env} > 0.001$.

c)   Reloading Curve

As is the case of the unloading curve, the intrinsic shape of the reloading curve is the same for anchored and unanchored specimens (Figure III-8). The same expression of the reloading curve (Eq. II-20) proposed in Chapter II is used to describe the reloading curve for both anchored and unanchored specimens. In this equation, φ_N represents the ratio of stress degradation (Figure III-8) defined in Chapter II as $\varphi_N = \sigma_N / \sigma_{un,env}$ where N is the cycle number ($N = 0; 1; 2;$ and 3) (Figure III-8) and $\sigma_{N=0} = \sigma_{un,env}$. As seen in Figure III-8, for $\varepsilon_{un,env} \leq 0.001$, the loss of stress is negligible and $\varphi_N = 1$ irrespective of the cycle number. For $\varepsilon_{un,env} > 0.001$, the stress

degradation increases with increase in the number of cycles N. For specimens confined

with external FRP sheets only, Eq. (II-19) was proposed in Chapter II to compute the

stress degradation.

According to this equation, the strength degradation at the 1st, 2nd, and 3rd

reloading cycles is respectively equal to 6%, 10%, and 12%. For the current

experimental results, this amount is measured at about 8%, 12%, and 14% respectively

for the 1st, 2nd, and 3rd reloading cycles, close to what is predicted by Eq. (II-19).

Similar to what was suggested for unanchored specimens, for specimens confined with

FRP sheets and anchors, it is recommended to neglect the strength degradation beyond

the first reloading cycle and consider a constant value of $\varphi_N = 0.92$ for all the values of

N.

Similarly, for internal cycles, the same procedure adopted in Chapter II is also

adopted for anchored specimens.

C. Proposed Model versus Experimental Results

Figure IV-4 to Figure IV-9 show comparisons of the predictions of the

proposed model with the current test results and Figure IV-10 to Figure IV-13 show the

same comparison for the test results of the specimens tested at AUB reported in Chapter

II. For these latter specimens, the average lateral strain was measured at 60% ε_{fu}

while this average is 45% ε_{fu} for the specimens shown in (Table III-2). For the

purpose of the analytical modeling carried out in this study, a value of the rupture strain

50% ε_{fu} (average between the two sets of specimens) is used to predict the ultimate

stress and strain (Eqs. II-11 and II-12). Figure IV-14 compares the model prediction for

specimen $R1F2$ considering $\varepsilon_{h,rup} = 50\%\ \varepsilon_{fu}$ and $\varepsilon_{h,rup} = 60\%\ \varepsilon_{fu}$ and the difference between the two curves is not large. It can be seen from the comparisons shown in Figure IV-4 to Figure IV-9 and Figure IV-10 to Figure IV-13 that, despite some discrepancies, the model can reproduce the experimental results of specimens confined with external CFRP sheets or with a combination of CFRP sheets and anchors.

Table IV-1 – Values of A_e/A_c and ρ_f for tested specimens

Specimen	$\dfrac{A_e}{A_c}$	ρ_f
*S*000	-	-
*S*100	0.48072	0.00206
*S*300	0.48072	0.00618
*S*313	0.67226	0.00783
*S*400	0.48072	0.00824
*S*413	0.67226	0.01071
*M*000	-	-
*M*200	0.48323	0.00384
*M*213	0.67328	0.00450
*M*223	0.72348	0.00450
*M*300	0.48323	0.00576
*M*313	0.67328	0.00708
*M*323	0.72348	0.00708
*M*400	0.48323	0.00769
*M*413	0.67328	0.00966
*M*423	0.72348	0.00966
*L*000	-	-
*L*200	0.49485	0.00329
*L*224	0.72811	0.00370
*L*234	0.75807	0.00370
*L*300	0.49485	0.00493
*L*324	0.72811	0.00576
*L*334	0.75807	0.00576
*L*400	0.49485	0.00658
*L*424	0.72811	0.00822
*L*434	0.75807	0.00822
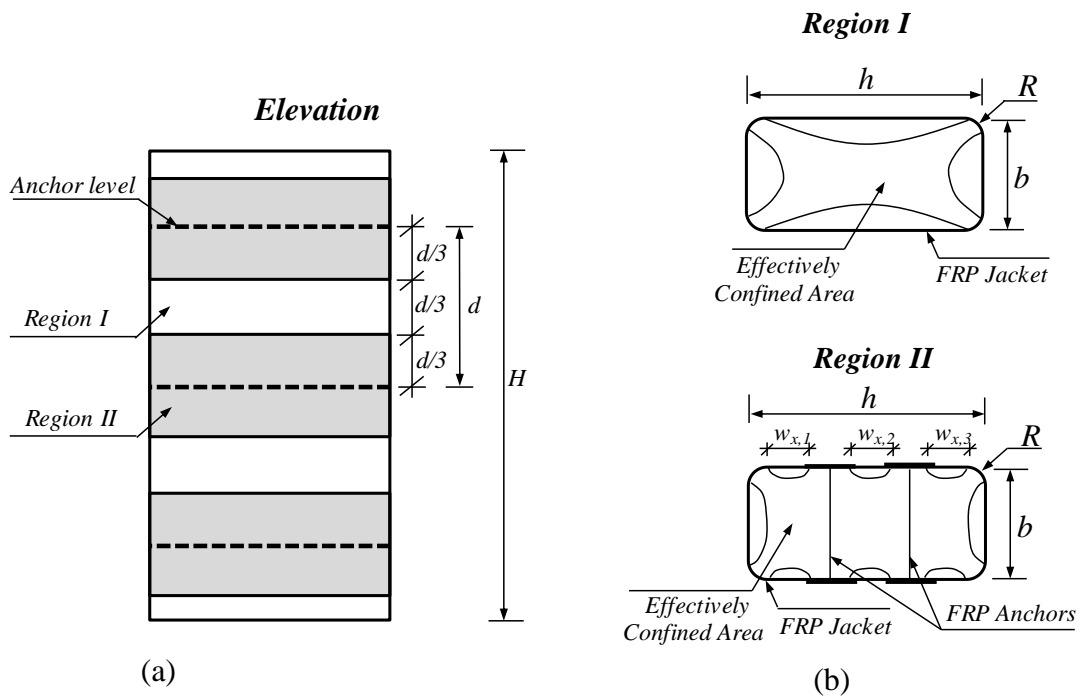
Figure IV-1 - The two confinement regions of anchored specimens: (a) specimen elevation, (b) specimen cross section
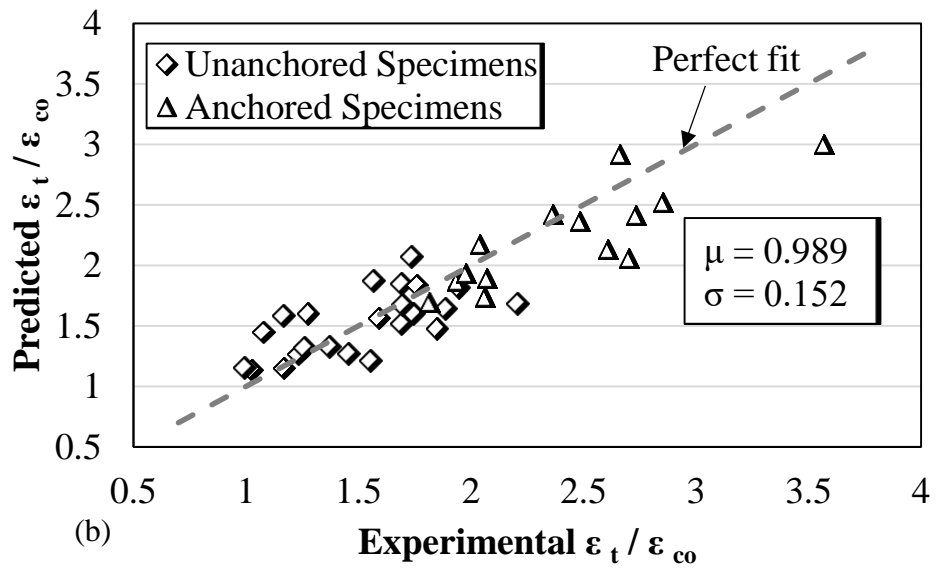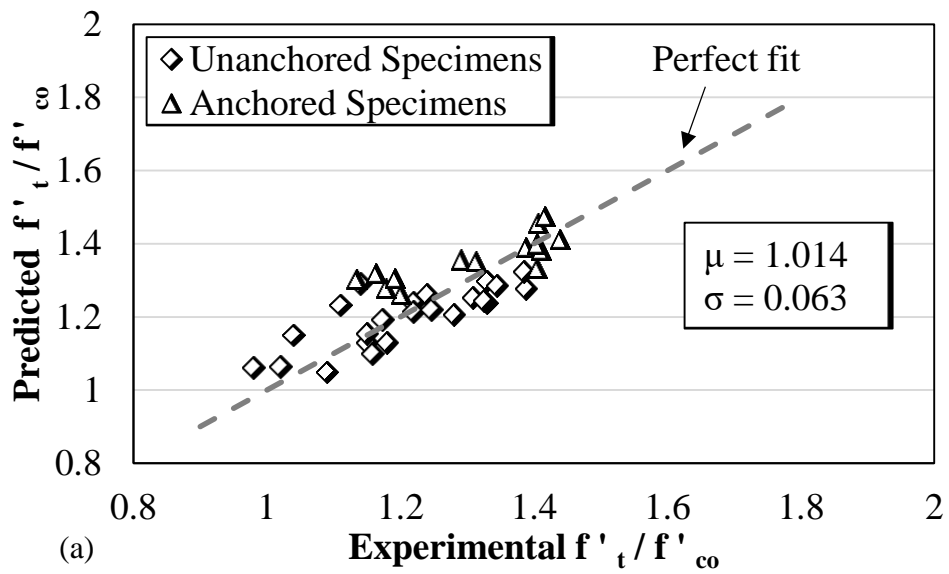
Figure IV-2 - Comparison between the experimental and predicted results for: (a) f'_t/f'_{co} , (b) $\varepsilon_t/\varepsilon_{co}$

111
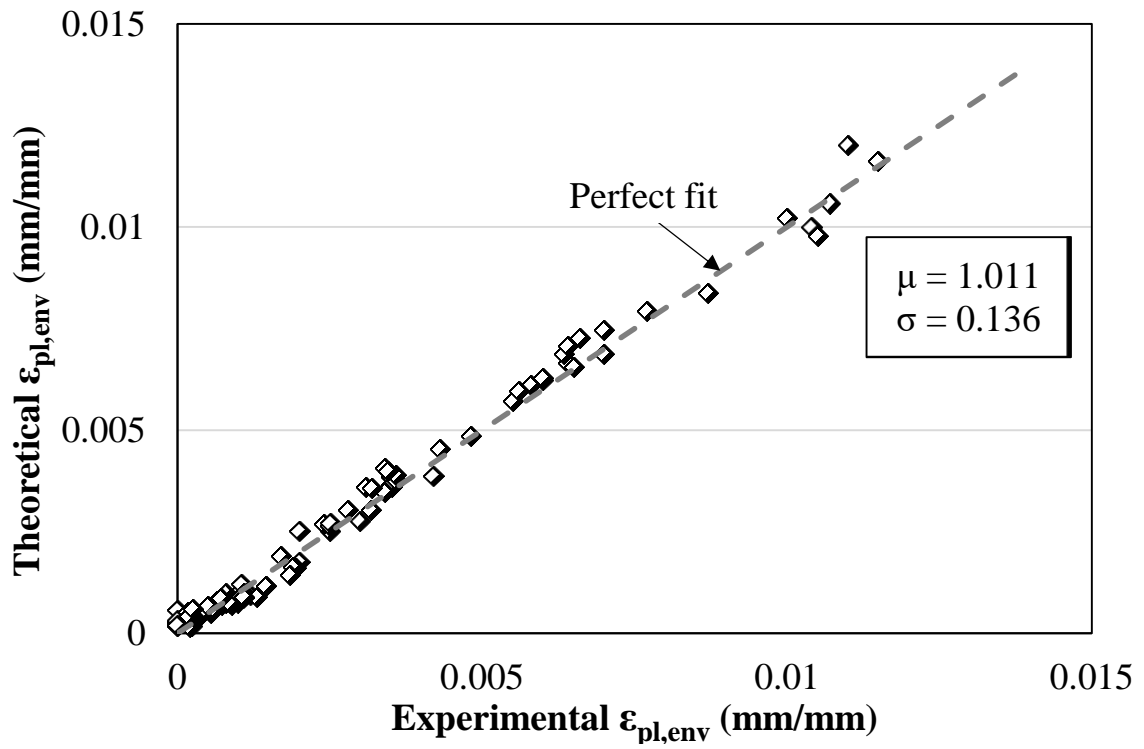
Figure IV-3 - Comparison of the proposed model of $\varepsilon_{pl,env}$ (Eqs. II-17 and II-18) with the current experimental results.

(a)

(b)
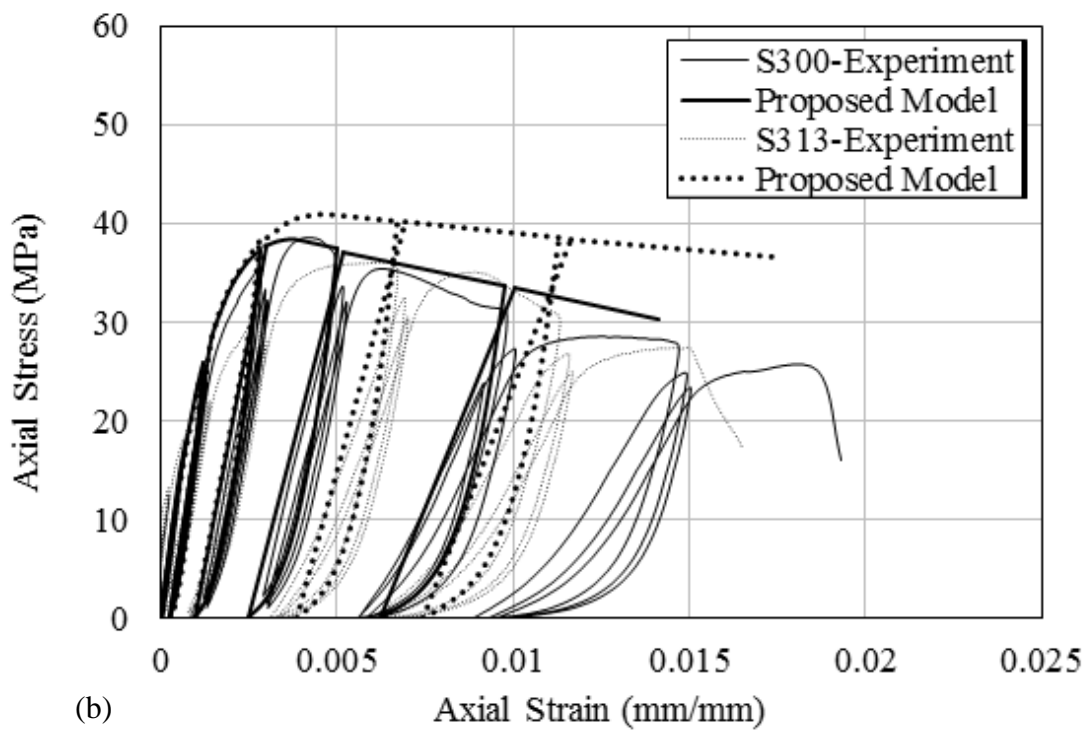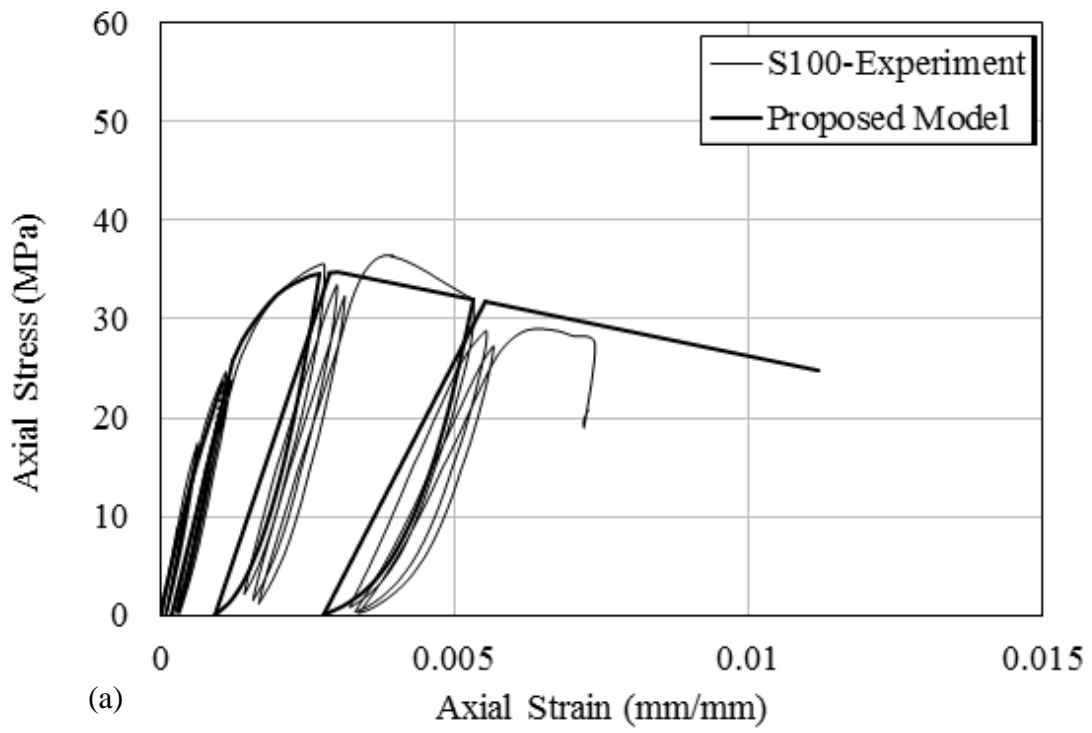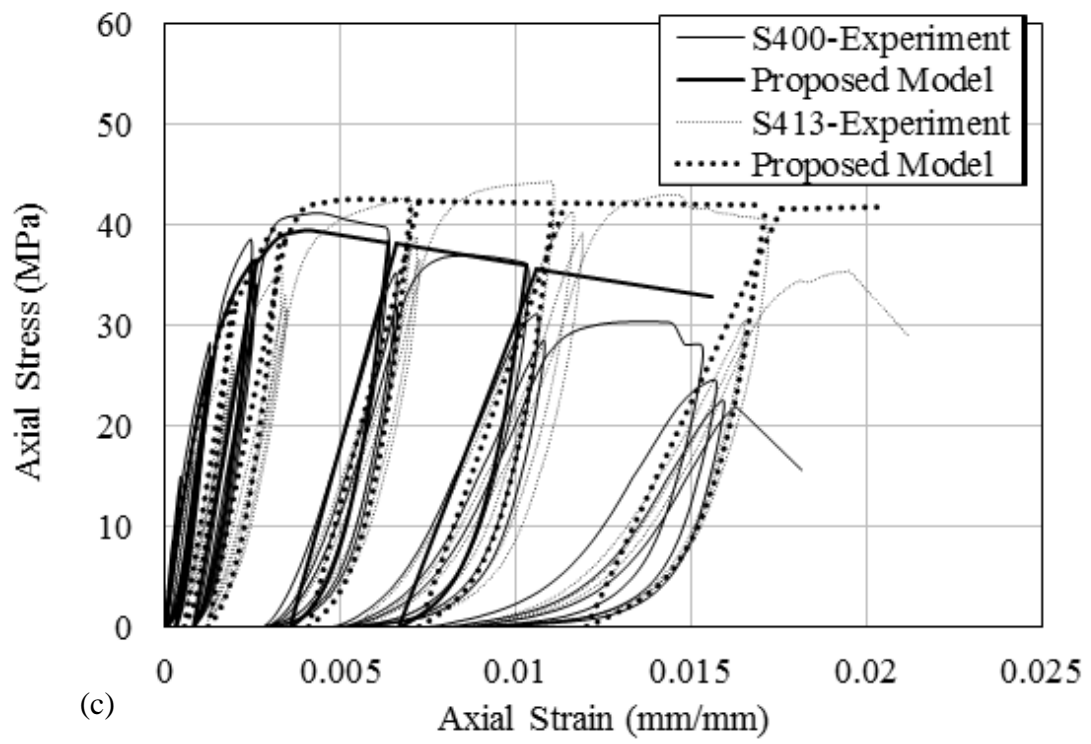
Figure IV-4 - Experimental and predicted axial stress-strain curves of all confined specimens of series *S*

(a)

(b)
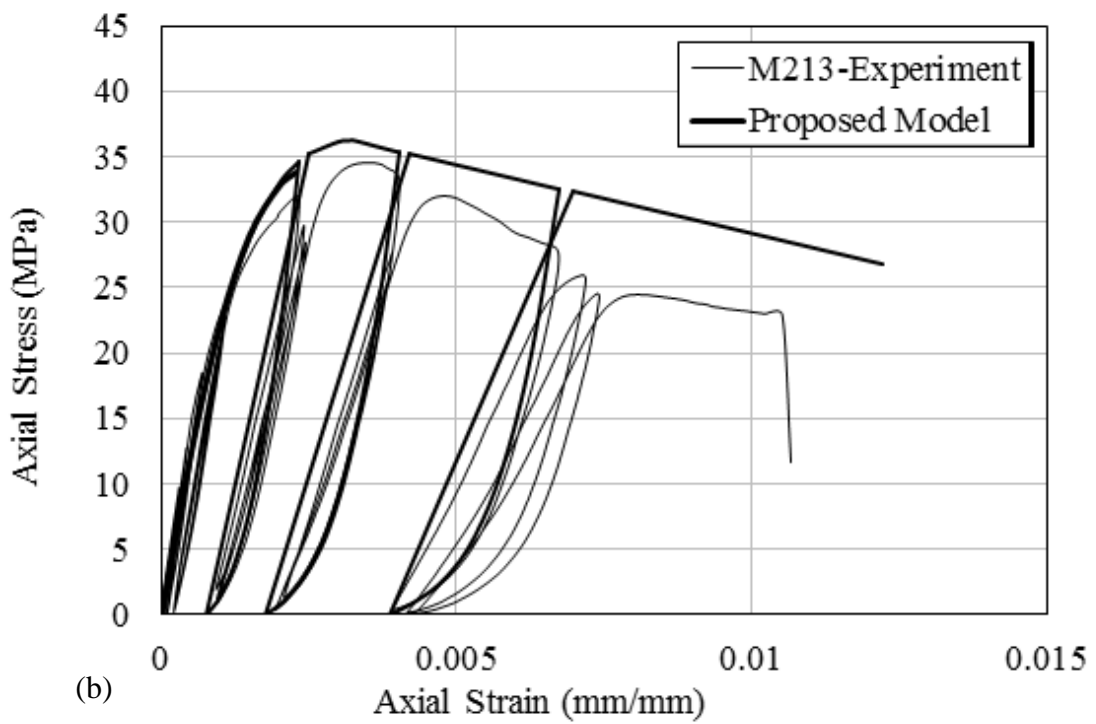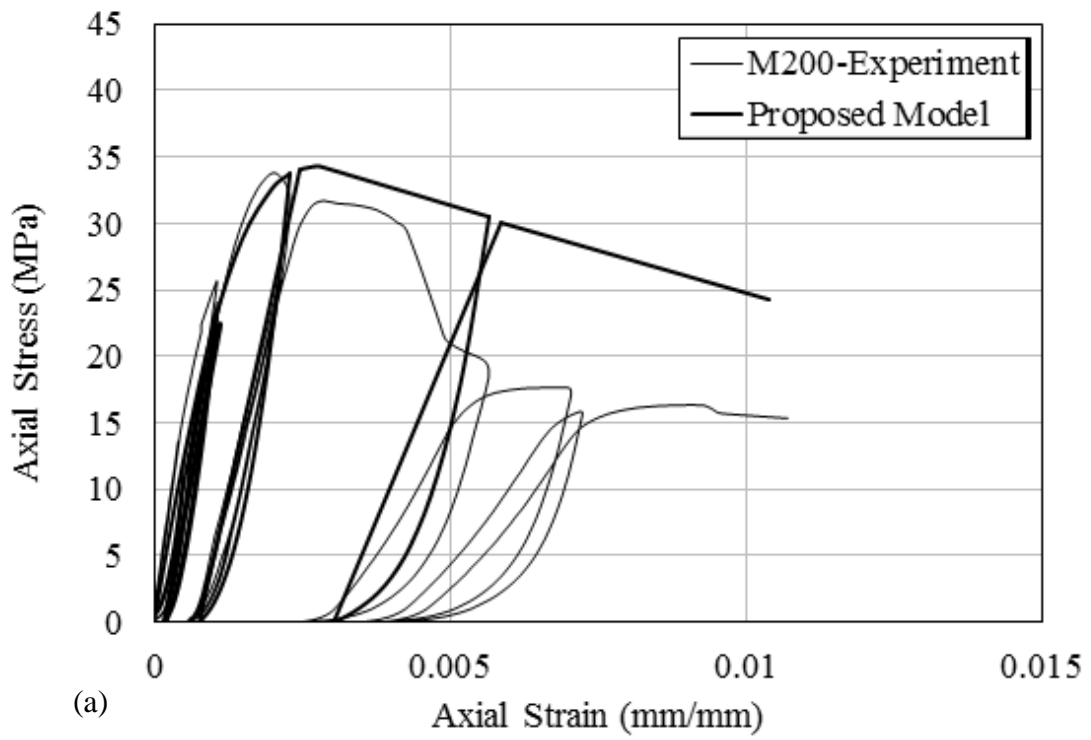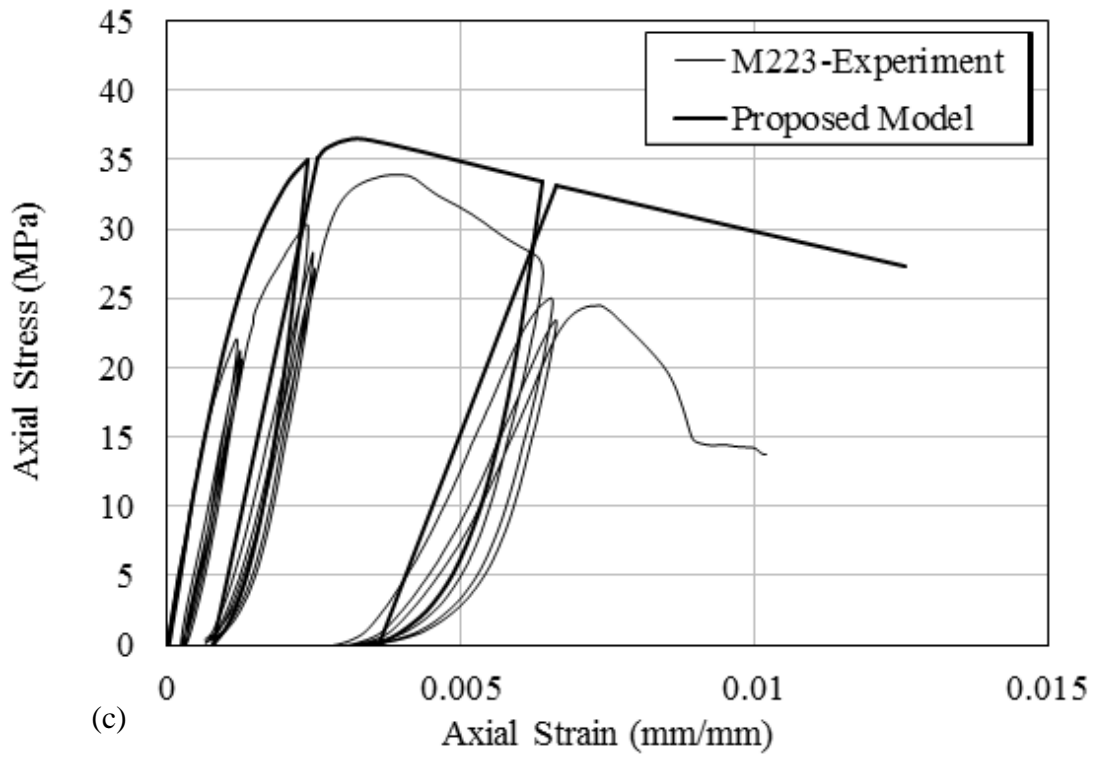
Figure IV-5 - Experimental and predicted axial stress-strain curves of all confined specimens of series *M* with *l* = 2

(a)

(b)

117
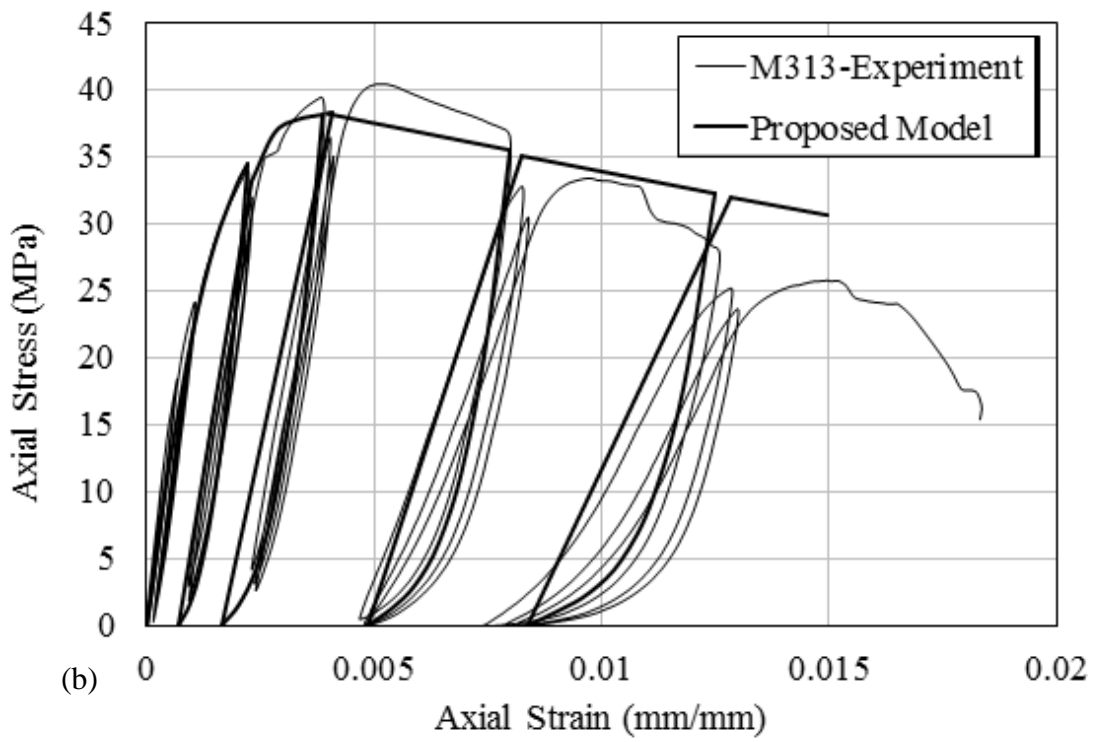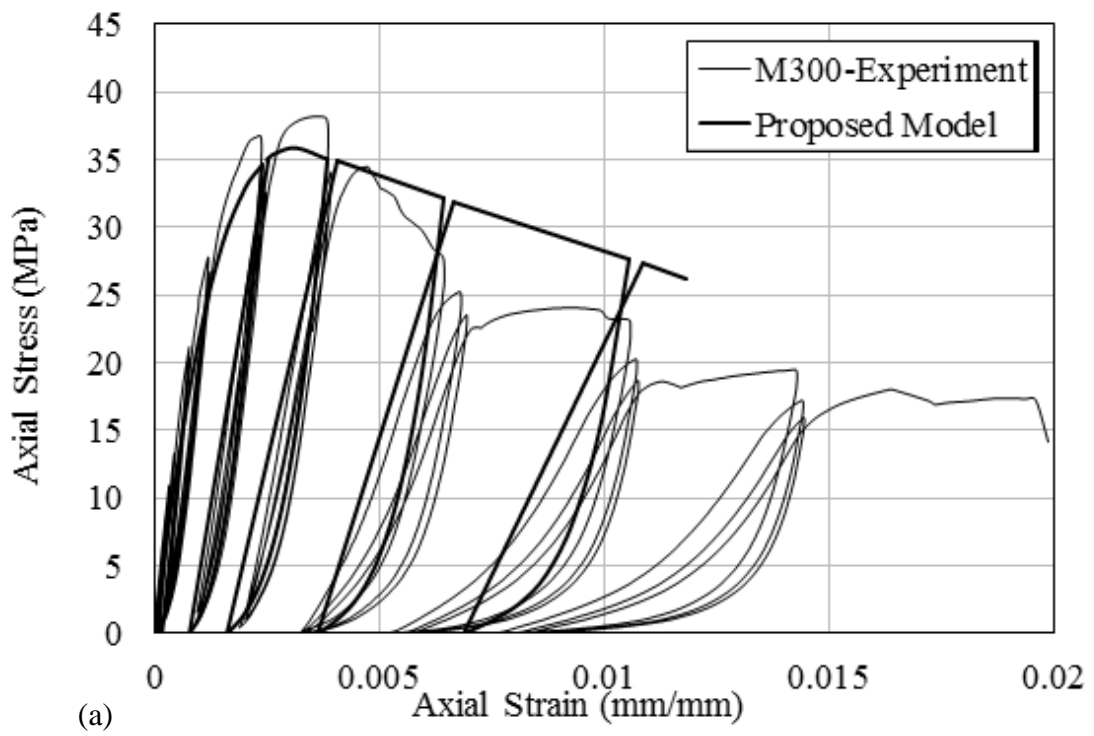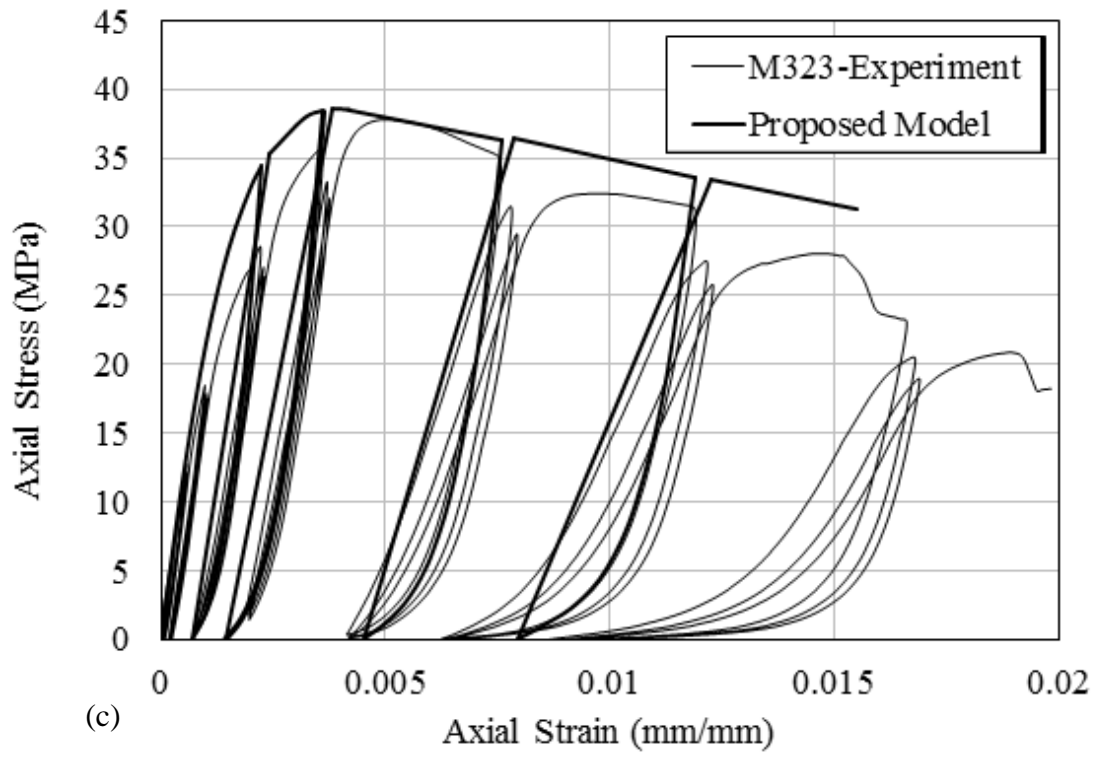
Figure IV-6 - Experimental and predicted axial stress-strain curves of all confined specimens of series *M* with *l* = 3

(a)

(b)

119
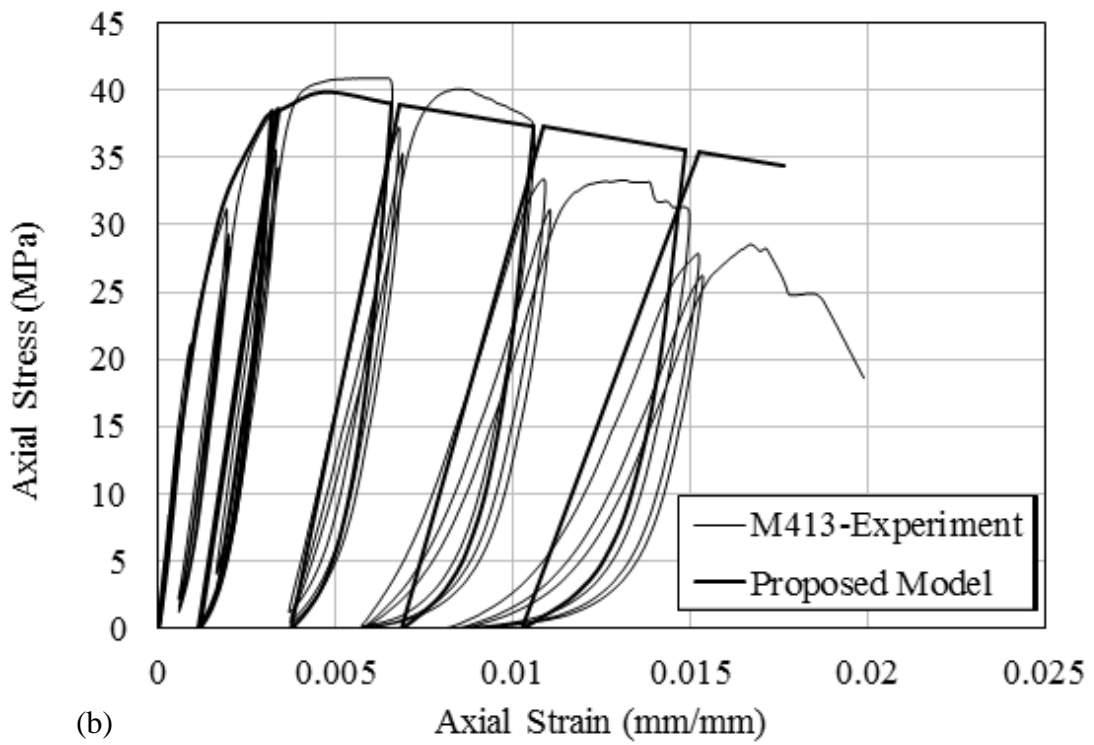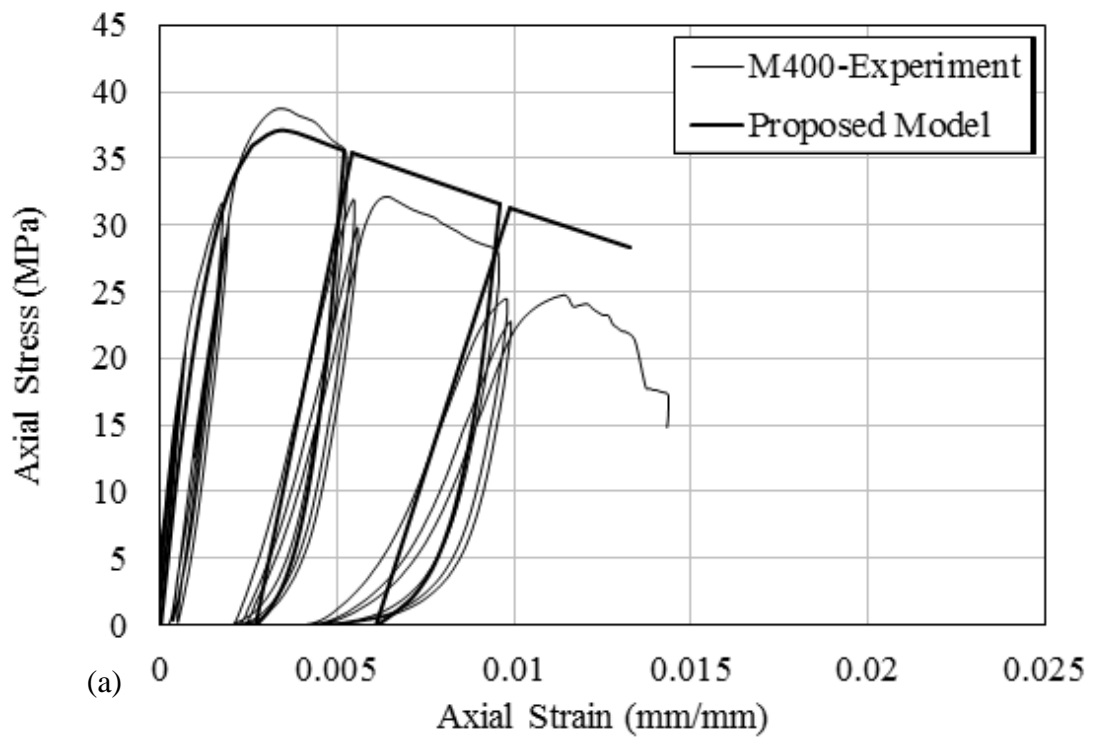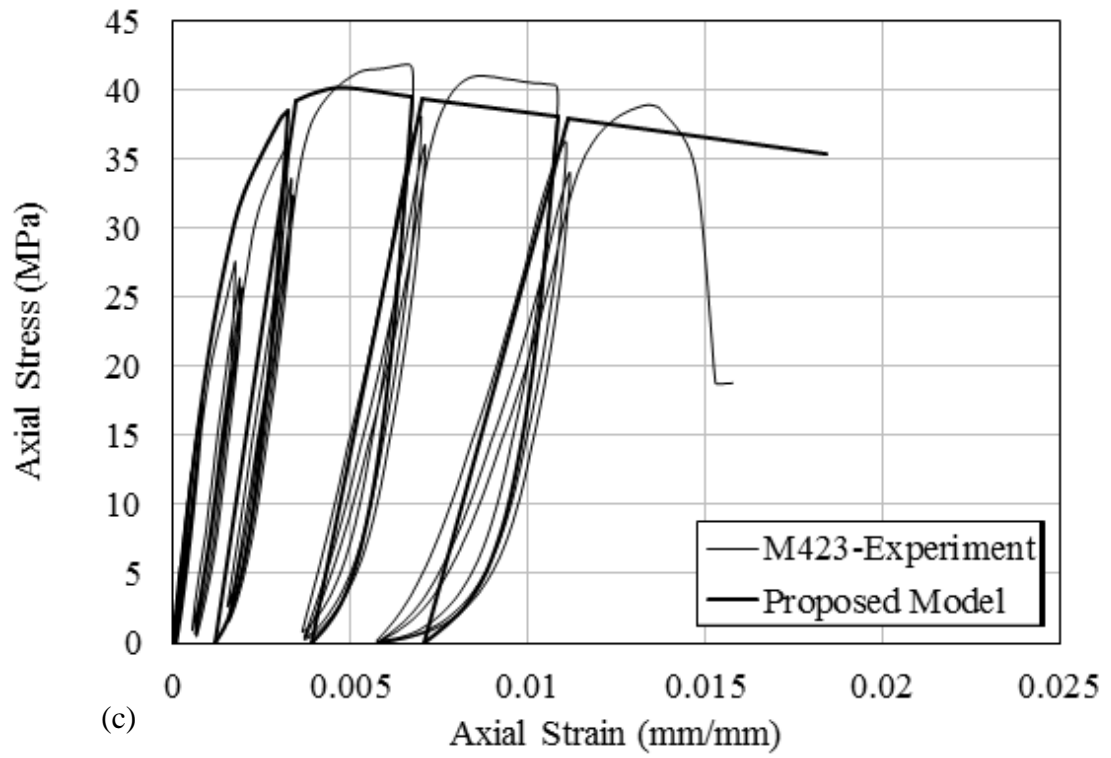
Figure IV-7 - Experimental and predicted axial stress-strain curves of all confined specimens of series M with $l = 4$

(a)

(b)
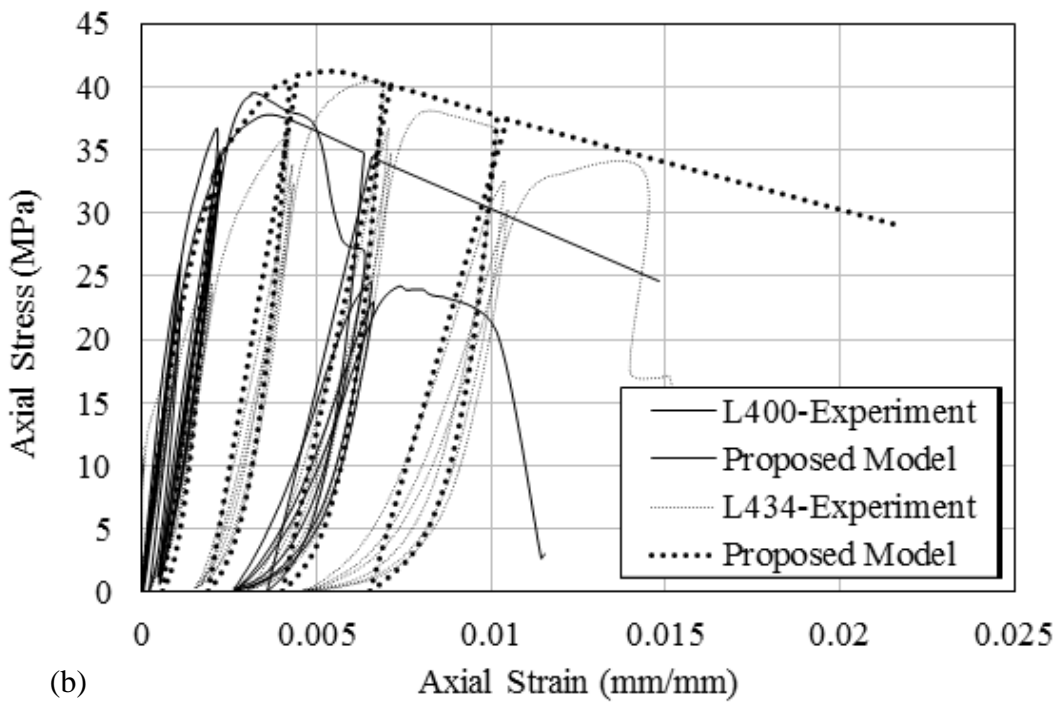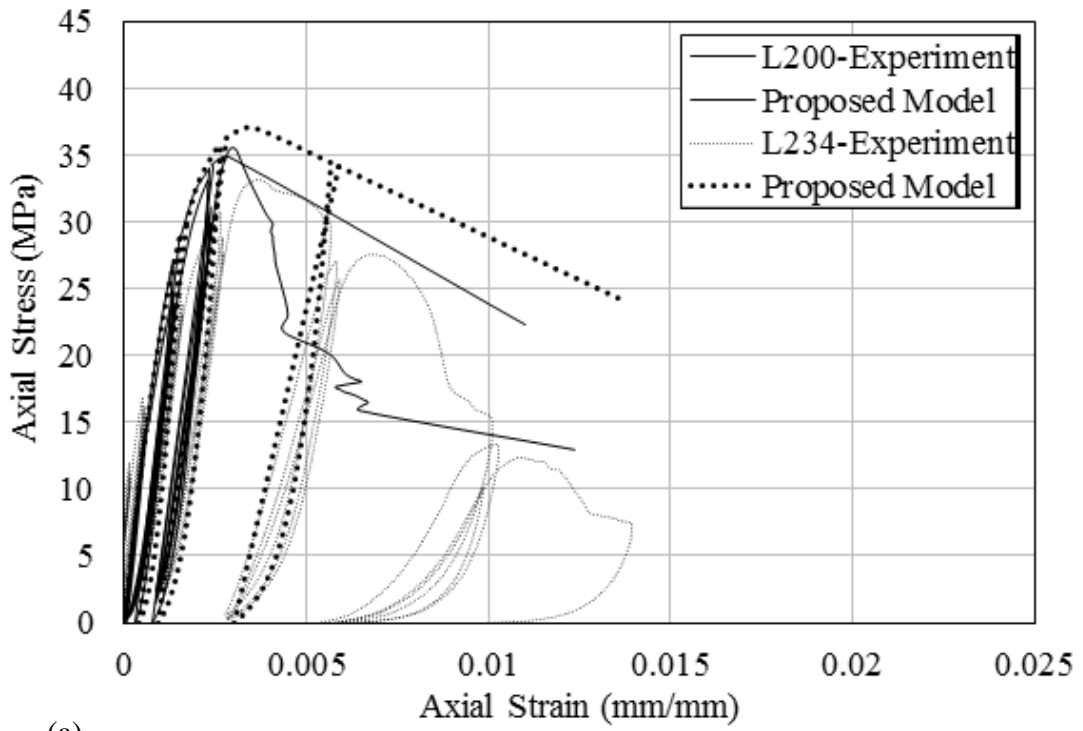
Figure IV-8 - Experimental and predicted axial stress-strain curves of the confined specimens of series *L* with *l* = 2 and *l* = 4

(a)

(b)
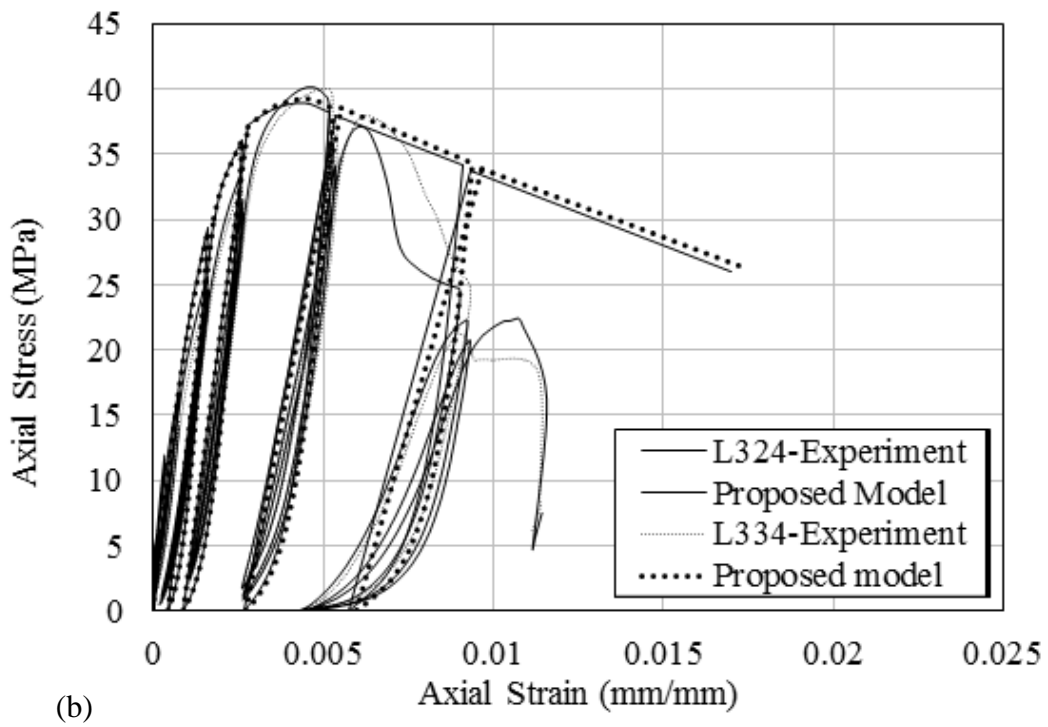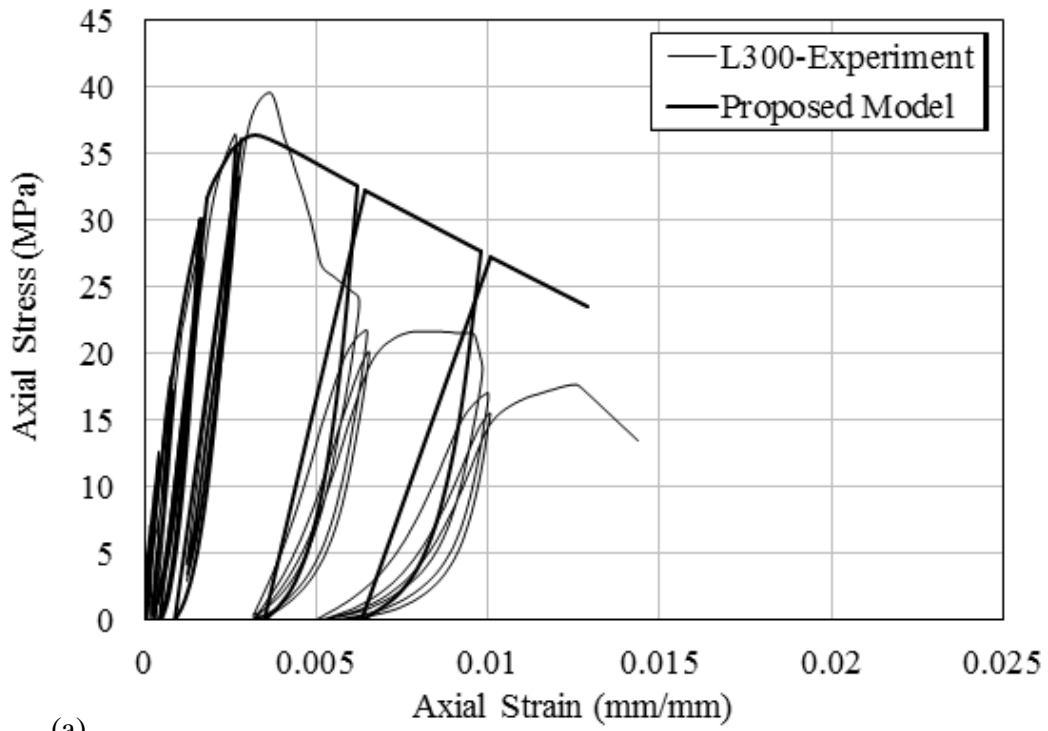
Figure IV-9 - Experimental and predicted axial stress-strain curves of the confined specimens of series *L* with *l* = 3
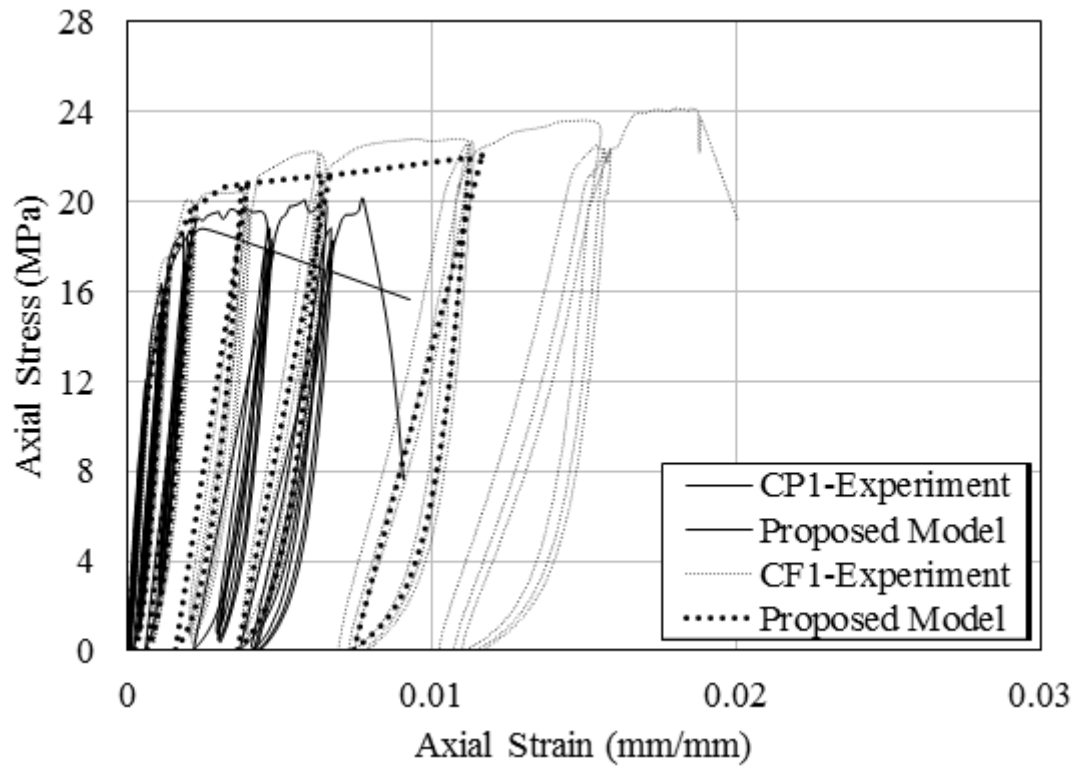
Figure IV-10 - Experimental and predicted axial stress-strain curves of specimens *CP1* and *CF1* (Chapter II)

(a)

(b)
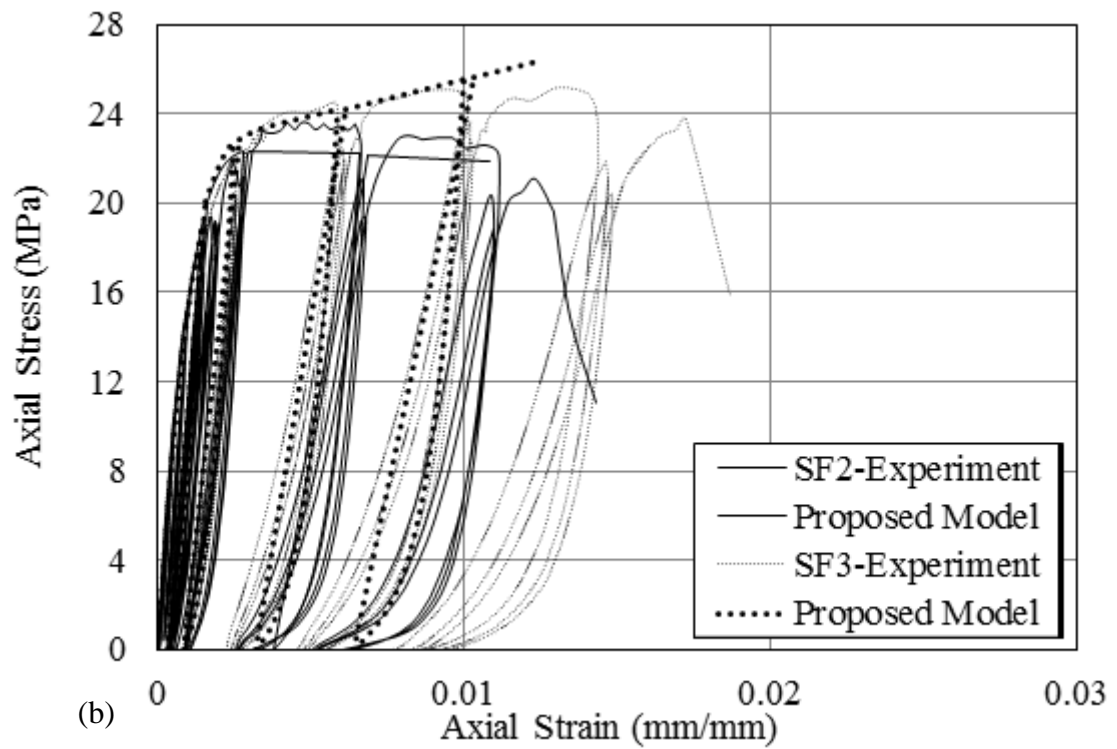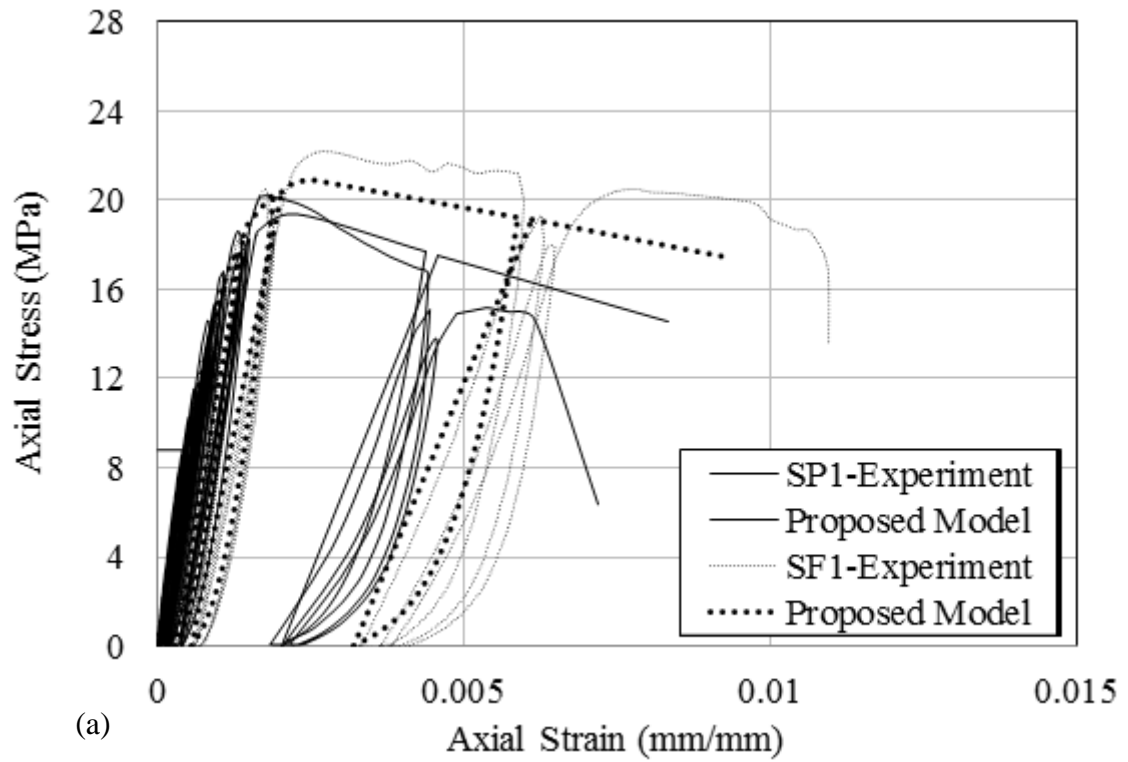
Figure IV-11- Experimental and predicted axial stress-strain curves of specimens $SP1$, $SF1$, $SF2$ and $SF3$ (Chapter II)

(a)

(b)
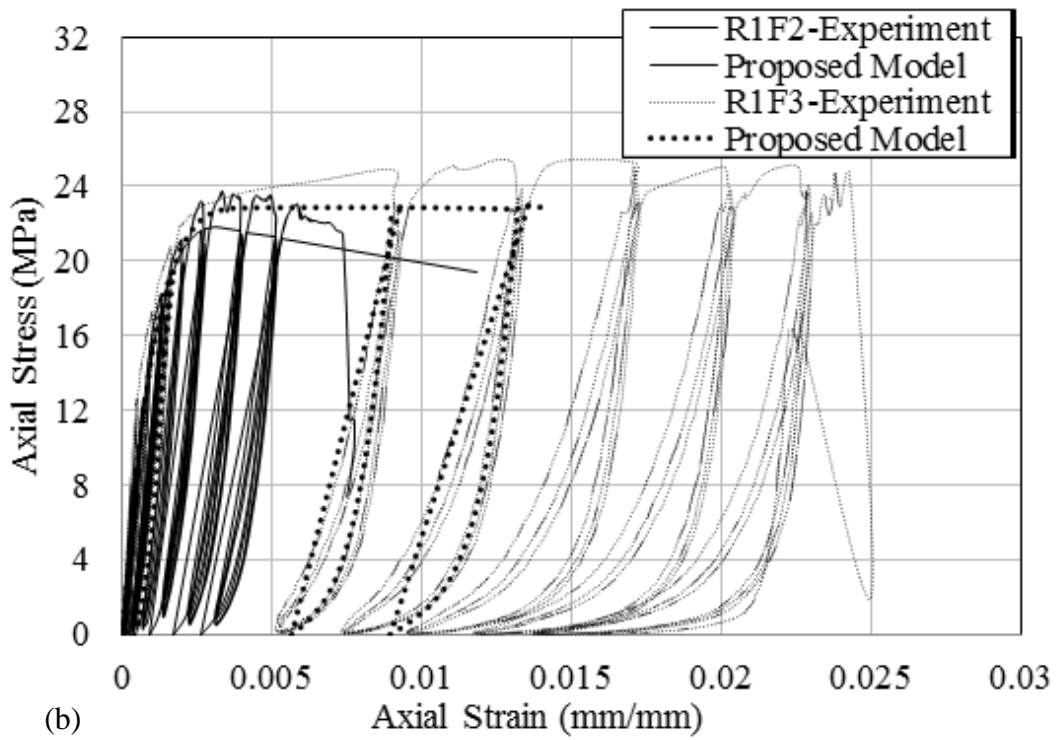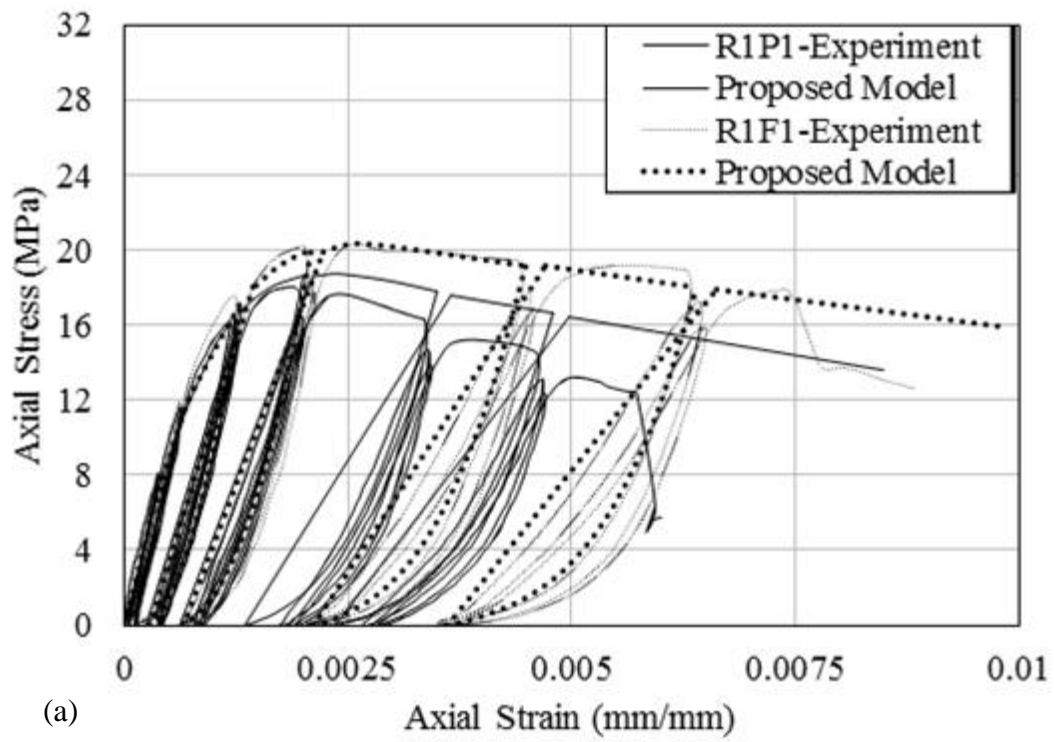
Figure IV-12 **-** Experimental and predicted axial stress-strain curves of specimens $R1P1$
$R1F1$, $R1F2$ and $R1F3$ (Chapter II)

125

(a)

(b)
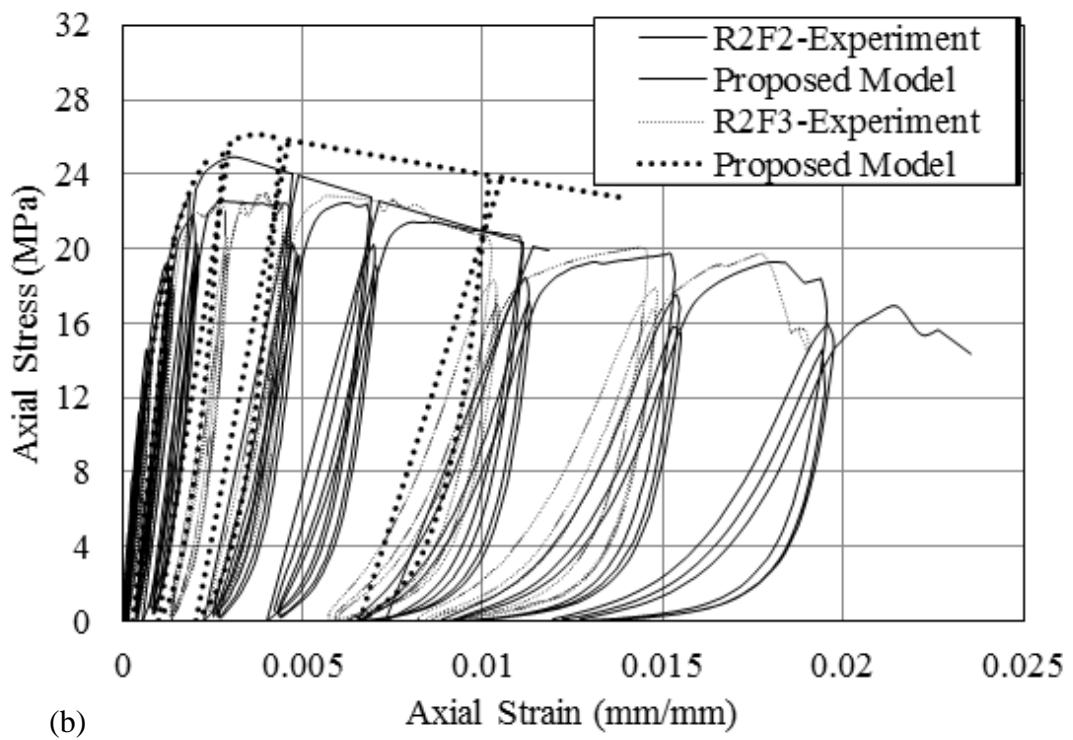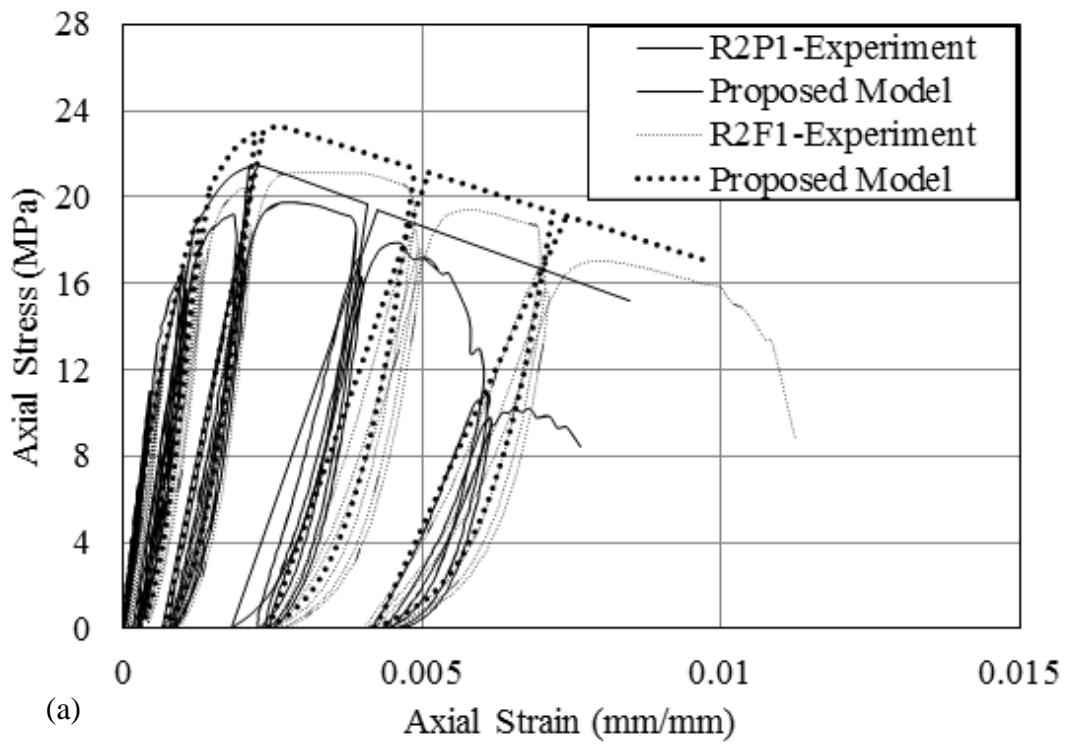
Figure IV-13 - Experimental and predicted axial stress-strain curves of specimens *R*2*P*1, *R*2*F*1, *R*2*F*2 and *R*2*F*3 (Chapter II)
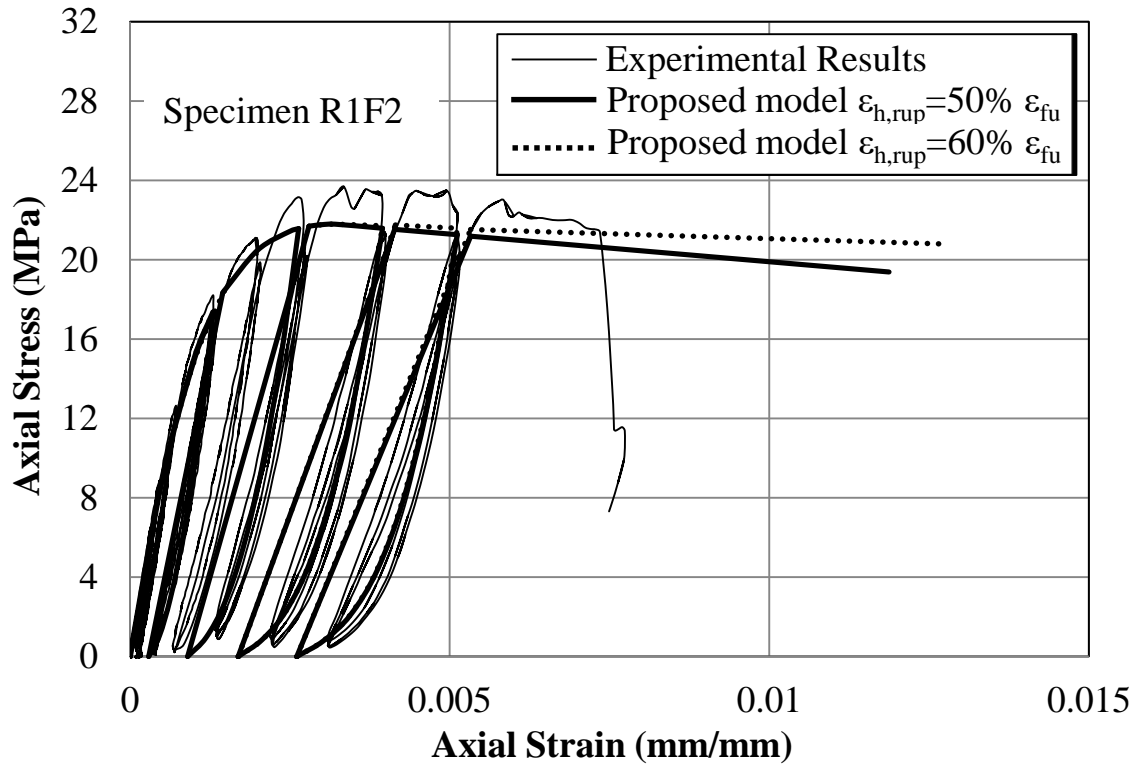
Figure IV-14 - Comparison of the model predictions considering $\varepsilon_{h,rup} = 50\% \, \varepsilon_{fu}$ and $\varepsilon_{h,rup} = 60\% \, \varepsilon_{fu}$ for specimen $R1F2$

CHAPTER V

FINITE ELEMENT MODELING OF FRP-CONFINED CONCRETE USING MODIFIED CONCRETE DAMAGED PLASTICITY

A.   Introduction

Concrete Damaged Plasticity Model (CDPM) available in the finite element software package (ABAQUS) has been widely used to model reinforced concrete columns under axial stress. However, the use of CDPM has limitations when applied to confined concrete. In this Chapter, we present a modified concrete damaged plasticity model to predict the behavior of unreinforced concrete columns of different cross-sections externally confined with FRP sheets. The model is validated against available experimental results.

B.   Concrete damaged plasticity model (CDPM)

In CDPM, the inelastic behavior of concrete is represented using the concepts of isotropic damaged elasticity together with isotropic tensile and compressive plasticity (ABAQUS, 2013). Within framework of damaged-plasticity, the effective stress tensor is defined as:

$$\overline{\sigma} = D : \sigma \tag{V-1}$$

Where σ is the stress tensor and D is the damage tensor defined as:

$$D = \frac{1}{1-d} I \tag{V-2}$$

I being the identity matrix, and d the scalar stiffness degradation variable.

$\overline{\sigma}$ is also expressed as:

$$\overline{\sigma} = D_O^{el} : \left(\varepsilon - \varepsilon^{pl} \right) \qquad \text{(V-3)}$$

Where D_o^{el} is the initial (undamaged) elasticity matrix, and ε and ε^{pl} are

respectively the total strain and the plastic strain tensors.

The effective stress deviator is defined as:

$$\overline{S} = \overline{\sigma} - \overline{p} \, I \qquad \text{(V-4)}$$

In which $\overline{p}$ the hydrostatic pressure defined as:

$$\overline{p} = \frac{\overline{\sigma}_1 + \overline{\sigma}_2 + \overline{\sigma}_3}{3} \qquad \text{(V-5)}$$

In which, $\overline{\sigma}_1$, $\overline{\sigma}_2$ and $\overline{\sigma}_3$ are the principal effective stresses.

The main plasticity functions in CDPM include the *yield criterion* and the *flow function*.

The *yield criterion* defines the yield condition under multiaxial stress state and is defined as follows in terms of effective stresses:

$$F = \frac{1}{1-\alpha} \left(\overline{q} - 3\alpha \overline{p} + \beta \left(\tilde{\varepsilon}^{pl} \right) \left\langle -\hat{\overline{\sigma}}_{min} \right\rangle - \gamma \left\langle \hat{\overline{\sigma}}_{min} \right\rangle \right) - \overline{\sigma}_c \left(\tilde{\varepsilon}_c^{pl} \right) = 0 \qquad \text{(V-6)}$$

Where $\alpha = \dfrac{f_{bo}/f'_{co}-1}{2f_{bo}/f'_{co}-1}$, $\beta = \dfrac{\overline{\sigma}_c \left(\tilde{\varepsilon}_c^{pl} \right)}{\overline{\sigma}_t \left(\tilde{\varepsilon}_t^{pl} \right)} (1-\alpha) - (1+\alpha)$, $\gamma = \dfrac{3(1-K_c)}{2K_c-1}$.

In these equations, $\hat{\overline{\sigma}}_{min}$ = minimum principal effective stress; $\langle \bullet \rangle$ is the Macauley

bracket defined as $\langle x \rangle = \dfrac{1}{2}(|x|+x)$; f_{bo}/f'_{co} = ratio of the compressive strength under

biaxial loading to uniaxial compressive strength, and $\bar{q}$ is the Mises equivalent effective stress expressed in terms of the principal effective stresses as follows:

$$\bar{q} = \sqrt{\frac{1}{2}\left[\left(\bar{\sigma}_1 - \bar{\sigma}_2\right)^2 + \left(\bar{\sigma}_2 - \bar{\sigma}_3\right)^2 + \left(\bar{\sigma}_3 - \bar{\sigma}_1\right)^2\right]} \qquad (V\text{-}7)$$

K_c is the ratio of the second stress invariant on the tensile meridian to that on the compressive meridian at initial yield for any given value of the pressure invariant such that the minimum effective principal stress is positive.

The tensile and compression meridians are straight lines in the deviatoric plane. In the ($\bar{\sigma}_1$, $\bar{\sigma}_2$, $\bar{\sigma}_3$) stress space, the deviatoric plane is a plane perpendicular to the hydrostatic axis of direction vector $\overrightarrow{ON}$ = (1, 1, 1). Figure V-1 shows the effective stress space, hydrostatic axis and deviatoric plane. All the points on the deviatoric plane have the same hydrostatic pressure ($\bar{\sigma}_1 + \bar{\sigma}_2 + \bar{\sigma}_3$ = constant).

The $\overline{\sigma}_t(\tilde{\varepsilon}_t^{pl})$ and $\overline{\sigma}_c(\tilde{\varepsilon}_c^{pl})$ are the effective tensile and compressive cohesion stresses respectively. $\overline{\sigma}_c(\tilde{\varepsilon}_c^{pl})$ is the compressive strain-hardening/softening function that determines the evolution of the yield surface with the plastic deformation.

$\tilde{\varepsilon}_t^{pl}$ and $\tilde{\varepsilon}_c^{pl}$ are respectively the tensile and compressive equivalent plastic strains. The compressive stresses and strains are considered positive and tensile stresses and strains are considered negative.

The *flow rule* determines the direction of plastic deformation and dictates the evolution of the plastic lateral to plastic axial strain increment. CDPM assumes a *non-associated potential plastic flow*:

$$\dot{\varepsilon}_{ij}^{p} = \eta \frac{\partial G}{\partial \overline{\sigma}_{ij}}, i, j = 1, 2, 3 \tag{V-8}$$

Where G is the *flow potential function* defined as:

$$G = \sqrt{\left(e\sigma_{to} \tan \psi\right) + \overline{q}^{2}} - \overline{p} \tan \psi \tag{V-9}$$

In this equation, e is the eccentricity, σ_{to} is the uniaxial tensile stress at failure, and ψ is the dilation angle.

The scalar stiffness degradation d is a function of a damage variable κ the evolution of which is controlled by the following equation (ABAQUS, 2013):

$$\dot{\kappa} = \eta H\left(\overline{\sigma}, \kappa\right) \tag{V-10}$$

The response is solution of Equations (V-3, V-6, V-8 and V-10) that requires an iterative procedure.

Accordingly, in ABAQUS, the non-linear behavior of concrete is defined by the following features: *damage variable*, *yield criterion*, *hardening/softening rule* and *flow rule*.

The current definition of the damage-plasticity aspects, incorporated in (ABAQUS), makes the *damage variable* and the *strain-hardening/softening rule* dependent on the plastic-deformation and the *flow rule* defined using constant parameters. The influence of each CDPM parameter on the behavior of FRP-confined concrete needs to be studied. The following section describes the FE modeling of an FRP-confined concrete specimen, i.e. the boundary conditions and interactions, element types and meshing, and material properties. The input parameters of CDPM, whose effect on FRP-confined concrete needs to be investigated through parametric study, are specified and the corresponding parametric studies are performed.

C.   FE modeling

The general-purpose finite element program (ABAQUS) is used to perform all the simulations.

1.   *Boundary conditions and interactions*

(Yu, Teng, Wong, & Dong, 2010b) reported that for FRP-confined columns with length equal to twice the diameter, the effect of the end constraints on the behavior in the mid-height region of the column is negligible. Accordingly, (Yu, Teng, Wong, & Dong, 2010b) suggested modeling only a vertical slice rather than the full-scale specimen and to use axisymmetric boundary conditions for modeling circular section. In the current study, the axial stress-axial strain curve of a full-scale specimen fully wrapped with FRP, simulated in (ABAQUS) assuming pinned ends, is compared to that of a slice with one end fixed against vertical translation and the second used to impose the applied load as a prescribed vertical displacement. Comparison between the two results shows minor difference and therefore, for computation efficiency, only a slice of the specimen will be modeled. Also, given the symmetry boundary conditions of the problem, only quarter the cross-section is modeled and symmetry boundary conditions are specified as shown in Figure V-2. For partially wrapped specimens with equally distributed FRP wraps, since the slice simplification cannot be used, and for computational efficiency, only half the height of the specimen was modeled with inclusion of symmetry boundary condition as shown in Figure V-2(b).

Tie constraint is used to model the interaction between FRP sheet and concrete, such that the nodes on both surfaces are constrained to displace similarly. This

assumption is in accordance with (Issa, Chami, & Saad, 2009) conclusion that the bond

between concrete and FRP does not affect significantly the confinement behavior.

2.   *Element type and meshing*

The FRP sheet is modeled as a shell element whereas the concrete core is

modeled as a solid element. Four-node shell elements with reduced integration (S4R),

and 8-node brick elements with three translation degrees of freedom at each node

(C3D8R) are used to discretize the FRP sheets and concrete core, respectively. The

mesh is refined to prevent any discontinuity in the stresses and strains distribution in the

concrete core and the FRP-sheet, and a mesh convergence study is conducted to

determine the optimal mesh size that provides accurate solution with reasonably short

analysis time.

3.   *Material properties*

a)   FRP sheets

Under tensile loading, the FRP sheets demonstrate linear elastic behavior

before brittle rupture at a stress equal to the ultimate rupture stress, f_{fu} . The FRP

sheets properties are specified using "LAMINA" material type in which the modulus of

elasticity E_1 in the hoop direction is defined in accordance with the value provided by

the manufacturer; while E_2, G_{12}, G_{13} and G_{23} are assigned small values, and the

Poisson's ratio v is set equal to zero.

b)   Concrete

The two parameters needed to describe the elastic behavior of concrete are the Poisson's ratio, ν_c, and the modulus of elasticity, E_c. When the modulus of elasticity is not measured experimentally, it is estimated according to (ACI-318-11/318R-11) as $E_c = 4,730\sqrt{f'_{co}}$ (f'_{co} in *MPa*). The Poisson's ratio ν_c of concrete under uniaxial compressive stress ranges from 0.15 to 0.22, with a representative value of 0.19 or 0.20 (ASCE, 1982). A value of ν_c equal to 0.18 is adopted to perform the numerical simulations of test results if no experimental value is reported.

Accurate modeling of the plastic behavior of concrete requires precise definition of the three features: tensile behavior, compressive behavior and plasticity parameters.

(1)   Tensile behavior

Using CDPM, *tension stiffening* and *tension damage* data allow describing the tensile behavior of concrete. Since plain concrete specimens are modeled, *tension stiffening* is specified using the *CONCRETE TENSION STIFFENING, TYPE=GFI* option with the uniaxial tensile strength set equal to 0.1 f'_{co}. Zero tensile damage is assumed since only monotonic loading is considered. It should be noted that the selection of the tensile properties of concrete does not have a significant effect on the behavior of FRP-confined concrete columns given that these columns are subjected to triaxial compression.

(2)   <u>Compressive behavior</u>

The non-linear compressive behavior of concrete is divided into *compression hardening* and *compression damage*.

It has been widely stated in the literature that the compression hardening/softening rule is one of the most important parameters controlling the behavior of confined concrete when modeled using finite element (Yu, Teng, Wong, & Dong, 2010a; 2010b; Karabinis, Rousakis, & Manolitsi, 2008; Tao, Wang, & Yu, 2013). The model proposed by (Popovics, 1973) and adopted later by (Mander, Priestley, & Park, 1988) to describe the uniaxial stress-strain curve of concrete is used in a first step to define the concrete compression hardening data and to perform parametric studies of specified CDPM parameters. However, it will be shown later that for confined specimens, a hardening/softening rule different from that used for unconfined specimens should be adopted. It is worth noting that (Tao, Wang, & Yu, 2013) who modeled concrete-filled steel stub columns under monotonic loading also performed a parametric study to evaluate the influence of the different input parameters of CDPM on the axial stress-strain response of the columns.

However, the influence of the input strain/hardening softening rule on the lateral strain of FRP-confined concrete in circular specimens needs to be evaluated prior to selecting the input hardening/softening rule for performing the sensitivity analysis. Therefore, two similar circular specimens provided by the same confinement level were modeled. For one of these specimens, the input hardening/softening rule defined previously is adopted and for the second, the model of (Popovics, 1973) adopted by (Mander, Priestley, & Park, 1988) is used to define the hardening/softening data before the peak stress while a perfectly plastic behavior is assumed after the peak stress.

Comparison of the lateral strain in the FRP between these two specimens shows that it is almost the same but it is slightly reduced (after the first peak stress has been reached) when a perfectly plastic behavior is assumed. Therefore, the hardening/softening rule previously described is suitable for performing the parametric study.

Damage variable defines the degradation of the elastic stiffness during cyclic loading; however, its effect on the monotonic behavior of FRP-confined concrete columns is not clear. This effect is investigated through a parametric study that evaluates the influence of the compressive damage parameter, d_c, on the monotonic lateral strain-axial strain and axial stress-axial strain curves. The parametric study is performed on a circular specimen of diameter $D = 200$ *mm*, unconfined compressive strength $f'_{co} = 18$ *MPa* and corresponding strain $\varepsilon_{co} = 0.002$, confined by a CFRP jacket of thickness $t_{wrap} = 0.13$ *mm* and tensile modulus of elasticity $E_{frp} = 230,000$ *MPa*. Figure V-3 shows the meshing of quarter of the concrete circular slice. Two extreme values of d_c are investigated: i) $d_c = 0$; and ii) $d_c = 0$ before concrete reaches the unconfined concrete peak stress f'_{co}, while $d_c = 1 - \sigma_c / f'_{co}$ for a point on the post-peak stress-strain curve at a stress σ_c. The concrete dilation angle is assigned a value $\psi = 30^{\circ}$ and the remaining plasticity parameters are assigned the values specified in the "*Plasticity Parameters*" section. As can be seen in Figure V-4, the compressive damage parameter, d_c, has a little effect on the stress-strain curve of FRP-confined concrete and more important effect on the lateral dilation. Given that the damage parameter affects slightly the stress-strain curve, and that only modeling of monotonic loading is considered, the effect of the compressive damage is neglected and $d_c = 0$ is adopted.

(3)   Plasticity parameters

The remaining parameters needed to model the concrete compressive behavior

are designated in the plasticity section of the CDPM, i.e. ψ, f_{bo}/f'_{co}, K_c, e, and the

viscosity parameter.

It has been reported in the literature that the flow potential eccentricity, e, and

the viscosity parameter have no important influence on the prediction accuracy (Tao,

Wang, & Yu, 2013). Default value of 0.1 is assigned to e, and a value of 10^{-7} (very

close to the default value of zero) is assigned to the viscosity parameter.

Experimental tests are available in the literature to quantify the ratio f_{bo}/f'_{co}

and the following empirical equation is proposed by (Papanikolaou & Kappos, 2007)

based on statistical analysis of a large set of test data:

$$\frac{f_{bo}}{f'_{co}} = 1.5\left(f'_{co}\right)^{-0.075} \tag{V-11}$$

where f'_{co} is in MPa.

The parameter K_c controls the shape of the yield surface in the deviatoric plane

when the minimum principal effective stress is positive. Consequently, K_c affects the

behavior of confined concrete in the case of non-uniform biaxial confinement.

However, K_c also defines the yield surface in the different meridian planes. In fact, for

positive values of $\overset{\wedge}{\sigma}_{\min}$, Eq. (V-6) reduces to:

$$F = \frac{1}{1-\alpha}\left(\overline{q} - 3\alpha\,\overline{p} - \gamma\,\overset{\wedge}{\sigma}_{\min}\right) - \overline{\sigma}_c\left(\tilde{\varepsilon}_c^{pl}\right) = 0 \tag{V-12}$$

Different values of γ corresponding to different values of K_c draw different

yield surfaces in the meridian planes. In the case of uniformly confined concrete, the

3D loading path is always on the compressive meridian of the failure surface. In this

case $\overset{\wedge}{\sigma}_{\min}$ is the uniform confining pressure $\overset{\wedge}{\sigma}_{\min} = \overline{\sigma}_1 = \overline{\sigma}_2$ and F is expressed as:

$$F = \frac{1}{1-\alpha}\left(\overline{q} - 3\alpha\,\overline{p} - \gamma\overline{\sigma}_1\right) - \overline{\sigma}_c\left(\tilde{\varepsilon}_c^{pl}\right) = 0 \tag{V-13}$$

which indicates that K_c modifies the yield surface of uniformly confined concrete.

K_c is directly related to f_{bo}/f'_{co}. According to (Yu, Teng, Wong, & Dong, 2010a), if the expression proposed by (Teng, Huang, Lam, & Ye, 2007) is used to compute the peak stress f'^{*}_{cc} of concrete confined by a constant confining pressure σ_l ($f'^{*}_{cc} = f'_{co} + 3.5\sigma_l$), K_c reduces to:

$$K_c = \frac{5.5 f_{bo}}{3 f'_{co} + 5 f_{bo}} \tag{V-14}$$

For the unconfined concrete compressive strength $f'_{co} = 18\,MPa$ used to perform all the parametric studies, $f_{bo}/f'_{co} = 1.208$, close to the default value of 1.16, and $K_c = 0.735$. It will be shown when modeling actively-confined concrete, that K_c is responsible for defining the peak stress value of actively-confined concrete.

Using CDPM, the effect of the dilation angle, ψ, is such that an increase in ψ results in an increase in the lateral dilation of concrete confined with FRP and accordingly in the concrete axial stress.

D.   Modified concrete damaged plasticity model for FRP-confined concrete

As a result of the parametric studies performed on FRP-confined concrete cylinder, it was found that the dilation angle, ψ, has a significant effect on both the stress-strain curve and lateral strain-axial strain curve. In addition, it is well known that

the definition of the compression hardening data dictates the stress-strain curve of FRP-confined concrete modeled using CDPM. Also as shows Figure V-4(a), using the unconfined concrete stress-strain curve to define compression hardening fails to predict the stress-strain curve of FRP-confined concrete. This conclusion was previously made by (Yu, Teng, Wong, & Dong, 2010a; 2010b; Rousakis T. C., Karabinis, Kiousis, & Tepfers, 2008; Karabinis & Rousakis, 2002), who proposed including the confining pressure as a parameter to define the concrete compression hardening. The dilation angle and the damage parameter were also included in the definition of the compression hardening rule in (Rousakis T. C., Karabinis, Kiousis, & Tepfers, 2008; Karabinis & Rousakis, 2002) where the damage parameter was defined as a function of the concrete strength.

In order to accurately predict the stress-strain curve and the lateral strain-axial strain curve of FRP-confined concrete modeled using CDPM, the compression hardening data and the dilation angle should be well defined.

1.   *Dilation angle*

As previously mentioned, the dilation angle is the only parameter that affects the lateral strain-axial strain curve. Defining a constant dilation angle in CDPM results in almost the same lateral strain-axial strain curve for different values of the FRP-jacket stiffness which is inconsistent with experimental observations where the increase in the FRP-jacket stiffness results in a reduction of the lateral dilation. Many plasticity models available in the literature that used a non-associated flow rule to model FRP-confined cylinders assumed a constant potential function parameter or a constant dilation angle (Mirmiran, Zagers, & Yuan, 2000; Issa, Chami, & Saad, 2009). (Eid & Paultre, 2007)

who proposed a Drucker-Prager type plasticity model for FRP-confined cylinders, expressed the dilatancy angle as a function of the lateral stiffness ratio. Also, (Rousakis T. C., Karabinis, Kiousis, & Tepfers, 2008), who analyzed FRP-confined cylinders using a non-associated flow rule in a Drucker-Prager type plasticity model, found that the plastic dilation is dependent on the concrete strength and the jacket confinement modulus. Increasing the confinement modulus or decreasing the concrete strength results in a restriction of the plastic dilation rate. Accordingly, (Rousakis T. C., Karabinis, Kiousis, & Tepfers, 2008) proposed closed-form expression of the plastic dilation parameter for low and high strength concrete function of the modulus of confinement and the concrete strength. (Yu, Teng, Wong, & Dong, 2010b), who used CDPM in (ABAQUS), related the dilation angle ψ to *the potential function parameter* β by the following expression:

$$\beta = (\sqrt{3}/9)\tan\psi \tag{V-15}$$

(Yu, Teng, Wong, & Dong, 2010b) proposed that β, in uniformly-confined sections, is dependent on the plastic deformation $\tilde{\varepsilon}_p$, the confining pressure σ_l, and the rate of confinement increment. Accordingly, defining the dilation angle ψ of FRP-confined concrete requires obtaining a series of lateral strain-axial strain (ε_l-ε_c) relationships for different $K_l = 2E_{frp}t_{frp}/D$, and computing β and ψ as a function of the equivalent plastic strain. The following equation, proposed by (Teng, Huang, Lam, & Ye, 2007), was used by (Yu, Teng, Wong, & Dong, 2010b) to generate the lateral strain-axial strain curves:

$$\phi\left(\frac{-\varepsilon_l}{\varepsilon_{co}}\right) = \frac{\varepsilon_c}{\varepsilon_{co}} \Bigg/ \left(1 + 8\frac{\sigma_l}{f'_{co}}\right)$$

$$= 0.85\left\{\left[1 + 0.75\left(\frac{-\varepsilon_l}{\varepsilon_{co}}\right)\right]^{0.7} - \exp\left[-7\left(\frac{-\varepsilon_l}{\varepsilon_{co}}\right)\right]\right\}$$

(V-16)

where $\sigma_l = -K_l\varepsilon_l$.

It should be noted that (Lim & Ozbakkaloglu, Lateral Strain-to-Axial Strain Relationship of Confined Concrete, 2014) found that Eq. (V-16) represented one of the best performing models in predicting the lateral strain-axial strain curves of concrete specimens of circular cross-section of normal and high strength confined with FRP. Accordingly, this expression is adopted to derive the dilation angle model explained hereafter.

In the following, calibration of the dilation angle to predict the theoretical lateral strain-axial strain curve of FRP-confined concrete is performed. For FRP-confined circular specimens, the lateral strain-axial strain curve depends on the ratio of the stiffness of the FRP jacket, K_l, to the unconfined concrete compressive strength, f'_{co}, K_l/f'_{co}. To calibrate the dilation angle of FRP-confined circular specimens, theoretical curves proposed by (Teng, Huang, Lam, & Ye, 2007) (Eq. V-16) are first generated for different values of K_l/f'_{co} ranging from 0 to 40 as shown in Figure V-5. As can be seen in these figures, beyond an axial strain close to 0.002 the lateral strain-axial strain curve becomes almost linear, and therefore, in FE modeling, a constant dilation angle is proposed for each value of K_l/f'_{co}. Finite Element simulations are then performed on the same circular specimen used in the parametric evaluation, and the FRP-jacket thickness, t_{wrap} is varied to achieve the values of K_l/f'_{co} shown in Table V-1. For each value of the FRP-jacket thickness, t_{wrap}, i.e. for each value of K_l/f'_{co},

a value of the dilation angle ψ is specified in (ABAQUS) such that the lateral strain-axial strain curve obtained in FE simulation matches approximately the theoretical lateral strain-axial strain curve given by Eq. (V-16) as can be seen in Figure V-5. Table V-1 shows, for each K_l/f'_{co} the dilation angle ψ specified in (ABAQUS) to predict the corresponding theoretical axial strain-lateral strain curve. As can be seen in Table V-1, to the value $K_l/f'_{co} = 40$ corresponds the minimum dilation angle allowed in (ABAQUS) ($\psi = 0.1°$, very close to zero) and beyond this value the theoretical lateral dilation cannot be predicted accurately using CDPM. The plot in Figure V-6 shows that a linear relationship exists between ψ and K_l/f'_{co} (presented in Table V-1), which can be expressed as follows:

$$\psi = -1.4587 \frac{K_l}{f'_{co}} + 57.296 \qquad \text{for } 0 \le \frac{K_l}{f'_{co}} \le 40 \qquad \text{(V-17)}$$

As stated previously, the lateral dilation of FRP-confined circular specimens cannot be predicted in (ABAQUS) for $K_l/f'_{co} > 40$, and therefore the proposed dilation angle expression (Eq. V-17) is limited for values of K_l/f'_{co} ranging between zero and 40. According to Eq. (V-17), for K_l/f'_{co} close to zero and 40 respectively, ψ is slightly greater than 56 and lower than 0.1, in which case ψ values greater than 56 or lower than 0.1 will be substituted by 56 and 0.1, respectively. Equation (V-17) does not consider the variation of the dilation angle as a function of the equivalent plastic strain as (Yu, Teng, Wong, & Dong, 2010b) proposed. However, as shown in Figure V-5, assuming the dilation angle to be dependent only on K_l/f'_{co} leads to close predictions of the theoretical curves while adopting a simple procedure.

For specimens of square or rectangular cross-section or for partially wrapped specimens, the definition of the dilation angle is complex due to the non-uniformity of the lateral dilation. Two methods are proposed to define the dilation angle in this case:

a)   Method I

Define a constant dilation angle for the whole concrete volume using Eq. (V-17) with K_l defined using Eq. (II-10).

b)   Method II

This method utilizes the fact that for a concrete column of circular section fully confined by FRP, $K_l = -\sigma_l/\varepsilon_l$. The expression given in Eq. (V-17) can be used to define the dilation angle of each element of the concrete as a function of the equivalent confining pressure σ_l acting on the element, and its lateral dilation ε_l. The equivalent confining pressure is defined according to (Yu, Teng, Wong, & Dong, 2010b) as:

$$\sigma_l = \frac{2(\sigma_2 + 0.039 f'_{co})(\sigma_3 + 0.039 f'_{co})}{\sigma_2 + \sigma_3 + 0.078 f'_{co}} - 0.039 f'_{co} \tag{V-18}$$

where σ_2 and σ_3 are the two principal lateral stresses respectively, and ε_l is the average lateral strain defined as:

$$\varepsilon_l = \frac{\varepsilon_2 + \varepsilon_3}{2} \tag{V-19}$$

where ε_2 and ε_3 are the two principal lateral strains.

For non-circular cross-sections, (Yu, Teng, Wong, & Dong, 2010b) used this same procedure to define the rate of confinement increment needed as a parameter to

evaluate ψ in their model along with the equivalent plastic strain and the confining pressure.

According to *Method II*, the dilation angle ψ of each element is defined as a function of the effective confining pressure σ_l and the lateral strain ε_l that vary during the analysis. (ABAQUS) allows the material properties (dilation angle and compression hardening) to be modified progressively with variation in the field variables during the solution process. The field variable associated with the dilation angle is defined in the user subroutine *USDFLD* coded in FORTRAN as the ratio of the effective confining pressure σ_l (Eq. V-18) to the negative of the average lateral strain ε_l (Eq. V-19) ($-\sigma_l / \varepsilon_l$). Calling this subroutine requires including the *USER DEFINED FIELD* option in the definition of the concrete material. Results of both methods (*Methods I and II*) are shown when comparing the proposed model versus experimental results discussed in a subsequent section of this dissertation.

2. *Hardening/softening rule*

It is well known that, for FRP-confined concrete columns, the confining pressure provided to the concrete core is not constant during loading but increases as concrete dilation increases. It has been widely stated in the literature that the stress-strain curve of FRP-confined concrete can be constructed as a set of points on a series of curves of actively-confined concrete, as shown in Figure V-7. Accordingly, many analysis-oriented models were proposed based on this principle (Teng, Huang, Lam, & Ye, 2007; Mirmiran & Shahawy, 1996; Spoelstra & Monti, 1999; Fam & Rizkalla, 2001). At the intersection points between the FRP-confined concrete stress-strain curve and the series of stress-strain curves of actively-confined concrete, i.e. for a given axial

strain, both the FRP-confined concrete and the actively-confined concrete have the same confining pressure and lateral strain.

A recent experimental investigation performed by (Lim & Ozbakkaloglu, 2014) assessed the assumption of stress path independency for normal strength concrete (NSC), and high strength concrete (HSC). This examination showed that for NSC, at a given axial and lateral strain and confining pressure, a slightly lower stress is exhibited by FRP-confined concrete as compared to actively-confined concrete. The difference between the two curves is more important for HSC and it grows larger as the concrete strength increases. In return, the assumption of path independency was approved for the lateral strain-axial strain relationship (Lim & Ozbakkaloglu, 2014) given that this relationship was found only dependent on the instantaneous confining pressure and not on the application path for both NSC and HSC. Based on their findings, (Lim & Ozbakkaloglu, 2014) proposed a unified stress-strain model for FRP and actively confined concrete of both normal and high strength. With the aim of assessing the difference in the axial stresses ($\Delta\sigma_c$) previously described, (Lim & Ozbakkaloglu, 2014) computed experimentally the difference in the confining pressures $\Delta\sigma_l$ between the two companion specimens at a given axial strain ε_c and stress σ_c. Using regression analysis, the following expression of $\Delta\sigma_l$ was proposed by (Lim & Ozbakkaloglu, 2014):

$$\Delta\sigma_l = 0.13 f'_{co}{}^{0.24} K_l{}^{0.95} \varepsilon_l \qquad\qquad (V\text{-}20)$$

where $\Delta\sigma_l$, f'_{co} and K_l are expressed in *MPa*.

Accordingly, (Lim & Ozbakkaloglu, 2014) proposed a model to generate the axial stress-strain and lateral strain-axial strain curves that follows an incremental

procedure similar to that suggested by (Teng, Huang, Lam, & Ye, 2007) (presented later in this dissertation) yet considering different constitutive expressions. The major difference between the two models is that according to (Teng, Huang, Lam, & Ye, 2007), at a given lateral strain, the lateral confining pressure σ_l that is computed depending on the stiffness of the FRP jacket, is used to define the axial strain and stress. As for (Lim & Ozbakkaloglu, 2014), σ_l is used to compute the axial strain at a given lateral strain, whereas, whereas $\sigma_l^* = \sigma_l - \Delta\sigma_l$ is considered when determining the axial stress; $\Delta\sigma_l$ is defined according to Eq. (V-20).

(Yu, Teng, Wong, & Dong, 2010b) used the assumption of path independency of both the stress and the lateral strain - axial strain relationship to define the *compression hardening data*, the *damage parameter* and the *dilation angle* of FRP-confined concrete. The dilation angle definition of (Yu, Teng, Wong, & Dong, 2010b) was previously explained. According to (Yu, Teng, Wong, & Dong, 2010b), at a given confining pressure and plastic strain, the compression hardening data and the damage data correspond to the data of actively-confined concrete at the same confining pressure and plastic strain. Therefore, the hardening/softening rule of FRP-confined concrete was made dependent on the confining pressure defined as a field variable. For each confining pressure, the compression hardening data was found using the theoretical stress-strain curve proposed by (Teng, Huang, Lam, & Ye, 2007) for actively confined concrete.

In this study, as mentioned earlier, a zero damage variable is considered to model FRP-confined concrete subject to monotonic loading.

As for the compression hardening data of FRP-confined concrete, the current study adopts (Yu, Teng, Wong, & Dong, 2010b) concept with modification of the

146

definition of the hardening/softening rule for actively-confined concrete and with incorporation of the new findings of (Lim & Ozbakkaloglu, 2014) related to the path independency and described previously. The new hardening/softening rule will be presented in the following. In order to account for the findings of (Lim & Ozbakkaloglu, 2014), the confining pressure (used as the first field variable) is defined as $\sigma_l^* = \sigma_l - \Delta\sigma_l$ where σ_l is the confining pressure computed based on the actual lateral stresses (Eq. V-18) and $\Delta\sigma_l$ (Eq. V-20) defines the reduction of lateral stress in FRP-confined concrete relative to actively-confined concrete. For circular specimens, the terms K_l and ε_l in Eq. (V-20) are defined respectively as $2E_{frp}\,t_{wrap}/D$ and $(\varepsilon_2 + \varepsilon_3)/2$ (Eq. V-19). For square and rectangular specimens, ε_l is also defined according to Eq. V-19 whereas two methods are used to define K_l similar to *Methods I and II* used to define the dilation angle and described previously. It should be noted that σ_l used to compute K_l according to *Method II* ($K_l = -\sigma_l/\varepsilon_l$), is defined as by Eq. (V-18) without subtracting $\Delta\sigma_l$ given that the assumption of path independency was found valid for defining of the lateral strain.

A new strain hardening/softening rule is proposed to predict the stress-strain curve of actively-confined concrete for different confining pressures. A parametric study is performed on actively-confined concrete to investigate the sensitivity of the stress-strain response to variations in the input material parameters and for calibrating the input compression hardening data.

a)   <u>Parametric Study for Actively-Confined Concrete</u>

For actively confined concrete, the parametric study is performed on the same circular specimen of diameter $D = 200$ *mm*, compressive strength $f'_{co} = 18$ *MPa* and corresponding axial strain $\varepsilon_{co} = 0.002$ with an applied constant confining pressure, $\sigma_l = 5$ *MPa*. The first loading step defined in (ABAQUS) corresponds to the application of the confining pressure and in the second step a prescribed displacement is applied to simulate the vertical loading. The two parameters whose effect on the stress-strain curve is evaluated through parametric study are K_c and ψ. To perform the parametric studies, (Popovics, 1973) is used to generate the compression hardening data.

For an unconfined concrete compressive strength $f'_{co} = 18$ *MPa*, K_c was previously found equal to 0.735. (Seow & Swaddiwudhipong, 2005) reported that experimental values of K_c range between 0.5 and 1. An investigation on the effect of K_c on the stress-strain curve is shown in Figure V-8 where values of 0.6, 2/3 (default value in ABAQUS), 0.735 (Eq. V-14) and the upper limit 1 are considered. Values of K_c lower than 0.6 are not considered in the study since the definition of the yield surface in (ABAQUS) includes $\gamma = 3(1 - K_c)(2K_c - 1)$ and therefore values close to 0.5 make the denominator close to zero. To perform the parametric study, the dilation angle of concrete is assigned a value $\psi = 30°$ and the remaining plasticity parameters are assigned the values as explained previously in the "*Plasticity Parameters*" section. As can be seen in Figure V-8, K_c controls the magnitude of peak stress of confined concrete where higher values of K_c lead to smaller peak stress. Figure V-8 plots also the analysis oriented model, initially proposed by (Mander, Priestley, & Park, 1988), with

modifications of the peak compressive strength expression proposed by (Teng, Huang, Lam, & Ye, 2007) and expressed as follows:

$$\frac{\sigma_c}{f'_{cc}{}^*} = \frac{(\varepsilon_c / \varepsilon_{cc}{}^*) r}{r - 1 + (\varepsilon_c / \varepsilon_{cc}{}^*)^r} \tag{V-21}$$

where $(\varepsilon_c, \sigma_c)$ are the coordinates of a point on the stress-strain curve of actively confined concrete, $(\varepsilon_{cc}{}^*, f'_{cc}{}^*)$ are the coordinates of the peak point of the same curve and r is defined as:

$$r = \frac{E_c}{E_c - \dfrac{f'_{cc}{}^*}{\varepsilon_{cc}{}^*}} \tag{V-22}$$

$f'_{cc}{}^*$ and $\varepsilon_{cc}{}^*$ are defined respectively as:

$$\frac{f'_{cc}{}^*}{f'_{co}} = 1 + 3.5 \frac{\sigma_l}{f'_{co}} \tag{V-23}$$

$$\frac{\varepsilon_{cc}{}^*}{\varepsilon_{co}} = 1 + 17.5 \frac{\sigma_l}{f'_{co}} \tag{V-24}$$

It should be noted that many analysis oriented stress-strain models have been proposed in the literature and many expressions have been developed to quantify $(\varepsilon_{cc}{}^*, f'_{cc}{}^*)$. (Lim & Ozbakkaloglu, 2014) assessed the performance of all available models of $(\varepsilon_{cc}{}^*, f'_{cc}{}^*)$ and found that the expressions of (Teng, Huang, Lam, & Ye, 2007) (Eqs. V-23 and V-24) performed well in predicting the experimental results. Accordingly, these expressions are adopted in the current study.

It can be seen in Figure V-8 that for $K_c = 0.735$ the peak stress of concrete obtained from FE analysis corresponds to the analytical peak stress obtained from (Teng, Huang, Lam, & Ye, 2007).

The sensitivity analysis shows also that the dilation angle ψ has no noticeable effect on the stress-strain curve of actively-confined concrete.

Figure V-9 plots the stress-strain response of circular concrete slices confined with different constant confining pressures with (Popovics, 1973) used to define compression hardening data and the other parameters defined as previously described. As can be seen in Figure V-9, although these curves predict correctly the peak stress of confined concrete, they do not predict accurately the increase of the axial strain at peak stress and the reduction of the steepness of the post-peak branch due to the confining pressure. Therefore, the input compression hardening data must be modified for more accurate prediction of the behavior of actively-confined concrete. Note that using the hardening/softening rule proposed by (Yu, Teng, Wong, & Dong, 2010b) led to axial stress-strain curves that overestimate the corresponding experimental curves for some of the specimens presented in this dissertation especially specimens exhibiting a post-peak descending behavior.

b)   Modified Strain Hardening/Softening Rule for Actively-Confined Concrete

For each confining stress, the input compression hardening data in (ABAQUS) is calibrated such that the FE stress-strain curve matches the theoretical stress-strain curve generated by (Teng, Huang, Lam, & Ye, 2007) (Eqs. V-21 to V-24). The following procedure is adopted, for each value of the confining pressure σ_l:

- The theoretical stress-strain curve is generated using Eqs. V-21 to V-24.
- The first branch of the unconfined concrete stress-strain curve proposed by (Popovics, 1973) is modified to make the unconfined concrete peak stress occur at a

strain ε_{cc}^* instead of ε_{co}. This is achieved by computing ε_{cc}^* and adding the difference

$\varepsilon_{cc}^* - \varepsilon_{co}$ linearly to the strain values between 0 and ε_{co} as shown in Figure V-10.

- The post-peak branch of unconfined concrete stress-strain curve

(Popovics, 1973) is substituted by the theoretical post-peak branch obtained using

(Teng, Huang, Lam, & Ye, 2007) in which all the stresses values are reduced by

$f'_{cc}^* - f'_{co}$ as shown in Figure V-10.

This modified stress-strain curve is used to generate the input compression

hardening data. It should be noted that (Tao, Wang, & Yu, 2013) also proposed

modifying the input stress-strain curve of unconfined concrete to capture the behavior of

concrete filled steel stubs, however the method proposed to modify the curve is slightly

different than that used in this study. Figure V-11(a-c) show that the stress-strain curves

obtained from FE analysis using the new compression hardening data compare well

with the theoretical model proposed by (Teng, Huang, Lam, & Ye, 2007) obtained for

σ_l varying from 1 to 9 MPa, i.e. for $\sigma_l / f'_{co} \leq 0.5$. To assess the accuracy of the

proposed method for $\sigma_l / f'_{co} > 0.5$, comparison is made in Figure V-12 between the

theoretical stress-strain curves of (Teng, Huang, Lam, & Ye, 2007) for $\sigma_l = 10\ MPa$

and the FE analysis results. The results of FE analysis in Figure V-12 were obtained

using two approaches: "FE-Results-*i*" in which the new proposed hardening/softening

rule is adopted, and "FE-Results-*ii*" in which (Popovics, 1973) is used to generate the

compression hardening data before the peak stress while a perfectly plastic behavior is

assumed after the peak stress. It can be seen in Figure V-12 that the results obtained

using the two methods are reasonably close. Consequently, for the purpose of

simplification, for high confining pressures ($\sigma_l / f'_{co} > 0.5$) the hardening/softening rule

is modeled using (Popovics, 1973) before the peak stress and a perfectly-plastic behavior after the peak stress.

E.   Proposed model versus experimental results

The performance of the proposed model using the modified CDPM for the FRP-confined concrete specimens having different cross-section shapes is validated against experimental results available in the literature. For circular specimens, since *Method I* and *Method II* for defining the dilation angle produce almost similar results for both the stress-strain and the axial strain-lateral strain curves, the results of only *Method I* are reported. For square or rectangular specimens and for partially wrapped specimens, the results of both methods (*Methods I and II*) are reported. It is worth noting that using the concept of field variable to define the input material properties might generate numerical errors. As the confining pressure increases, the hardening/softening curve is modified. In the case where the slope of the new curve is higher than the slope of the previous curve, the lateral strain generated at this step may be lower as well as the new computed confining pressure. This may create numerical errors. To address this problem, an additional condition is imposed on the first field variable in the user subroutine to prevent it from decreasing which is in accordance with the real behavior.

Figure V-13 through Figure V-16 show comparisons of the FE predictions with the test results of (Yu, Teng, Wong, & Dong, 2010b; Lam & Teng, 2004; Valdmanis, De Lorenzis, Rousakis, & Tepfers, 2007; Wong, Yu, Teng, & Dong, 2008). Comparisons are shown for both the stress-strain response and the lateral strain-axial strain response, respectively. The FE results are also compared in

Figure V-17, Figure V-18 and Figure V-19 with the test data of FRP confined

specimens reported recently by (Vincent & Ozbakkaloglu, 2013) (Ozbakkaloglu T. ,

2012; Ozbakkaloglu T. , 2013), in addition to the specimens tested at AUB and reported

in Chapter II. The details of all the specimens are provided in Table V-2 and Table V-3.

The experimental curves of *H-W*2, *A*20*R*15*L*5 and *A*10*R*30*L*5 are obtained as the

average of many identical specimens tested. All the specimens are fully wrapped over

their entire height except specimens *CP*1, *SP*1, *R*1*P*1 and *R*2*P*1 that are wrapped with

discontinuous FRP strips of width $W = 50$ *mm* and spaced at $s' = 50$ *mm* (Figure II-1b).

All the specimens are wrapped with CFRP sheets except the specimens of

(Ozbakkaloglu T. , 2012; Ozbakkaloglu T. , 2013; Wong, Yu, Teng, & Dong, 2008) that

are confined with an FRP tube. For the specimens tested by (Lam & Teng, 2004), a

value of $\varepsilon_{co} = 0.002$ is assumed given that the exact value was not reported. (Lam &

Teng, 2004) reported an initial modulus of elasticity of concrete $E_c = 27,981$ *MPa* for

the specimens wrapped with one and two layers of CFRP and a modulus of $E_c = 29,828$

MPa for the specimen wrapped with three layers. (Valdmanis, De Lorenzis, Rousakis,

& Tepfers, 2007) reported $E_c = 24,400$ *MPa* for all the three specimens. For the

remaining specimens, E_c is computed as $E_c = 4,730\sqrt{f'_{co}}$. Note that in Figure V-13 to

Figure V-18, the curves are terminated at a lateral strain corresponding to the

experimental hoop rupture strain. For the specimens tested at AUB (Table II-1), since

the experimental lateral strains were not reported due to the large scatter in the

measured values, the analytically predicted stress-strain curves were terminated at the

axial strains corresponding to a sudden drop in the experimental stress-strain response.

It can be seen from Figure V-13 to Figure V-19 that the FE results obtained

using the proposed modified CDPM model are in close agreement with test results

reported in the technical literature. It can also be seen for the two square specimens in Figure V-16(a), and for the square, rectangular and partially wrapped specimens in Figure V-19 that both methods (*Methods I and II*) lead to good predictions of the experimental stress-strain curves. However, as can be seen in Figure V-16(b), for the average corner hoop strain-axial strain curves, at the same axial strain, lower corner hoop strain is obtained using *Method II* when compared to *Method I*. This is attributed to the fact that using Method II, the dilation angle in the corner region where the confining pressures are high is lower than the constant value specified using Method I. For the HSC circular specimen, *H-W2* (

Figure V-17), and the UHSC square specimen *A*10*R*30*L*5 (Figure V-18b) close agreement is observed between the experimental and FE results. The discrepancy between the experimental and FE results increases for circular specimens of higher concrete strengths (*Specimen UH-W6*-1 in Figure V-18). As for specimen *A*20*R*15*L*5*, it can be seen that using *Method I* allows a good representation of the experimental results. However, *Method II* overestimates the stress in the specimen and the high dilation angle in the region close to the flat sides causes the lateral strain to reach the experimental rupture value early.

Table V-1 - Variation of the dilation angle, ψ , with respect to the ratio of the stiffness of the FRP-jacket to the unconfined concrete compressive strength, K_l / f'_{co} .

K_l / f'_{co}	0	5	10	15	20	25	30	35	40
ψ	56	50	45	35	28	22	12	5	0.1

Table V-2 – Geometry of modeled specimens

Paper	Specimen	Cross-section	D (mm)	b (mm)	h (mm)	R (mm)	H (mm)
(Lam & Teng, Ultimate Condition of Fiber Reinforced Polymer-Confined	CFRP one layer	Circle	152	-	-	-	305
	CFRP two layers						
	CFRP three layers						
(Valdmanis, De Lorenzis, Rousakis, & Tepfers, 2007)	CFRP one layer	Circle	150	-	-	-	300
	CFRP two layers						
	CFRP three layers						
(Wong, Yu, Teng, & Dong, 2008)	-	Circle	152	-	-	-	305
(Yu, Teng, Wong, & Dong, Finite element modeling of	Specimen I	Square	-	150	150	24.0	-
	Specimen II					25.0	
(Vincent & Ozbakkaloglu, 2013)	H-W2	Circle	152	-	-	-	305
	UH-W6-1	Circle	152	-	-	-	305
(Ozbakkaloglu T. , Axial	A20R15L5	Rectangle	-	112.5	225	15.0	300
(Ozbakkaloglu T. , 2013)	A10R30L5	Square	-	150	150	30.0	300

Table V-3 – Material properties of modeled specimens

| Paper	Specimen	f'_{co} (MPa)	ε_{cu} (mm/mm)	E_{frp} (MPa)	t_{wrap} (mm)
(Lam & Teng, 2004)	CFRP one layer	35.9	0.0020	230,000	0.165
	CFRP two layers				0.330
	CFRP three layers	34.3			0.495
(Valdmanis, De Lorenzis, Rousakis, & Tepfers, 2007)	CFRP one layer	23.3	0.0020	234,000	0.170
	CFRP two layers				0.340
	CFRP three layers				0.510
(Wong, Yu, Teng, & Dong, 2008)	-	39.6	0.0026	80,100	0.340
(Yu, Teng, Wong, & Dong, 2010b)	Specimen I	46.0	0.0026	250,000	0.330
	Specimen II	37.5	0.0031	80,100	0.510
(Vincent & Ozbakkaloglu, 2013)	H-W2	64.5	0.0027	240,000	0.234
	UH-W6-1	110.0	0.0035	240,000	0.702
(Ozbakkaloglu T. , Axial	A20R15L5	78.2	0.0030	240,000	1.170
(Ozbakkaloglu T. , 2013)	A10R30L5	107.3	0.0035	240,000	1.170
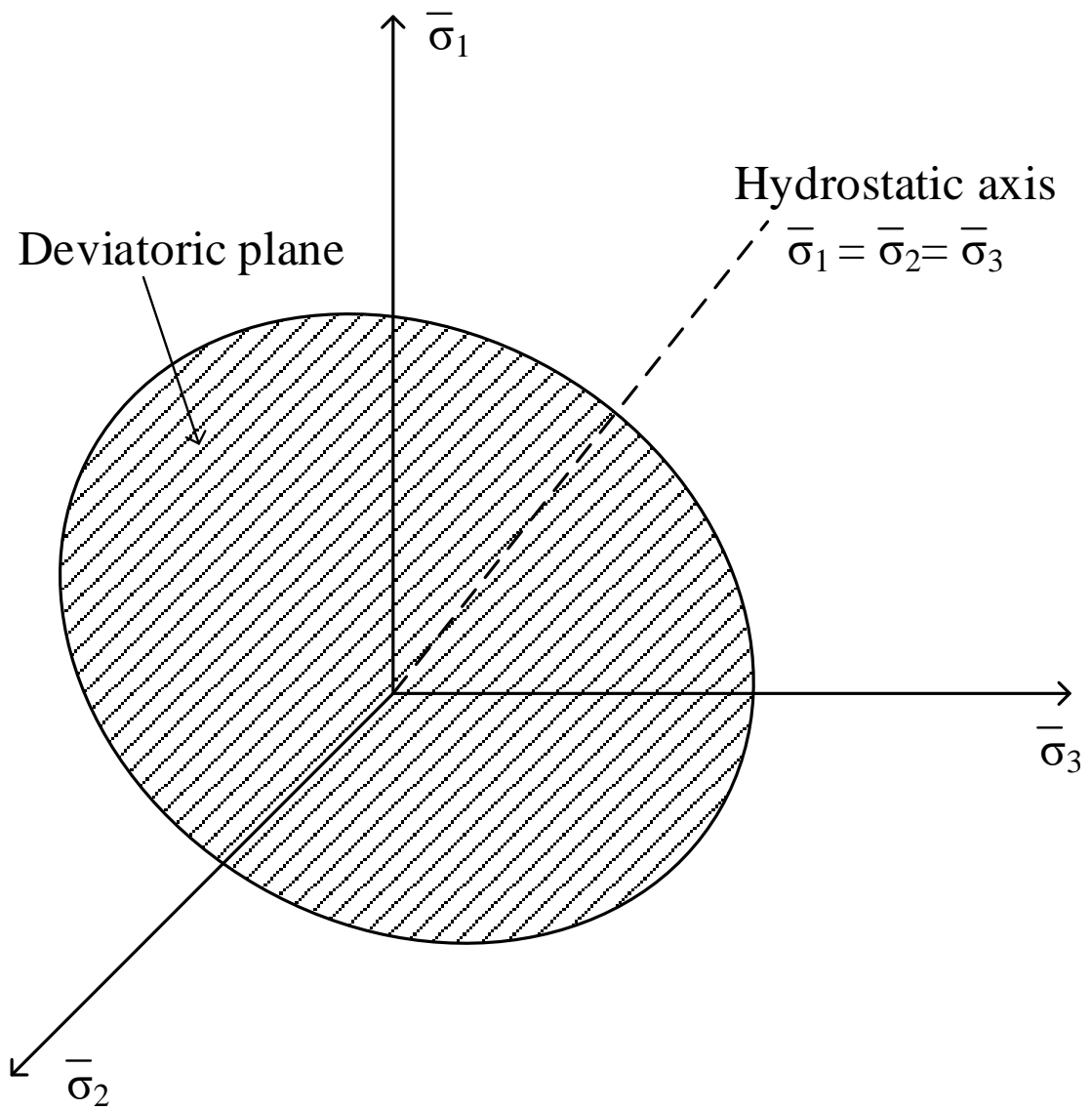
Figure V-1 – Hydrostatic axis and deviatoric plane in the effective stress space
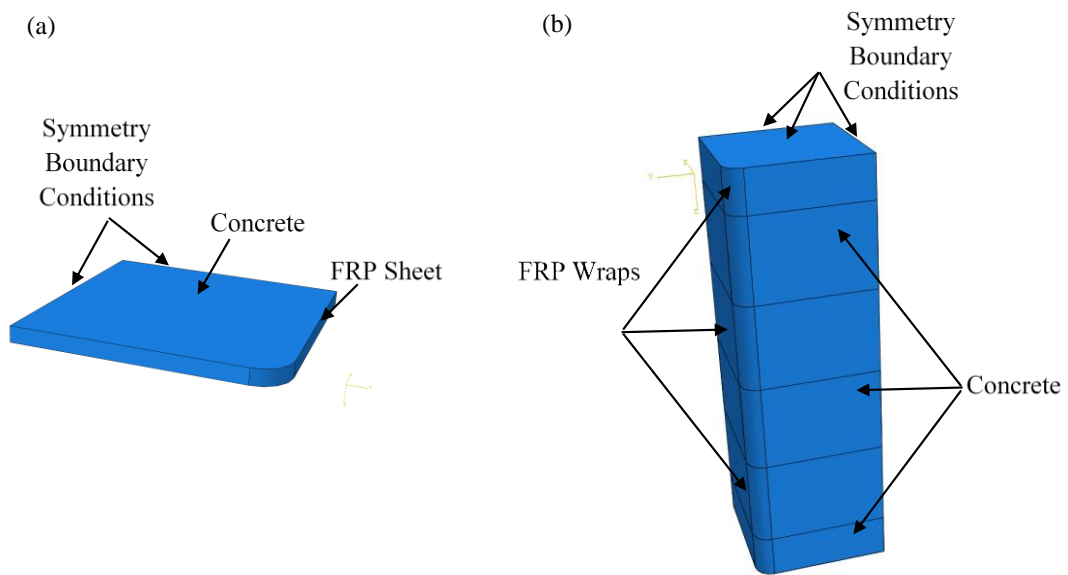
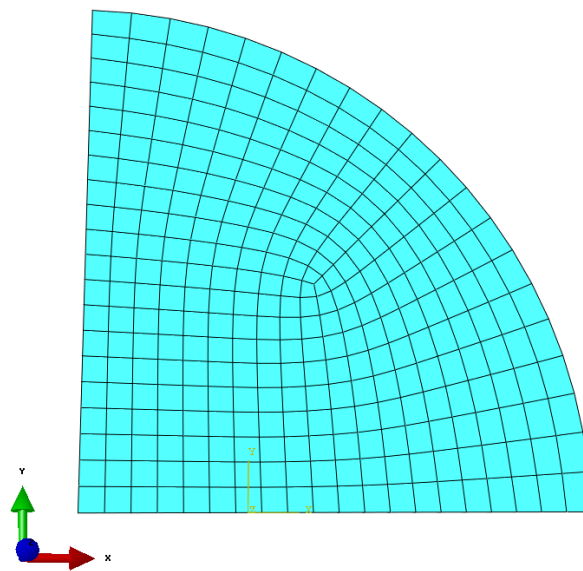Figure V-2 - Symmetry boundary conditions for square or rectangular specimens (a) fully wrapped, (b) partially wrapped.

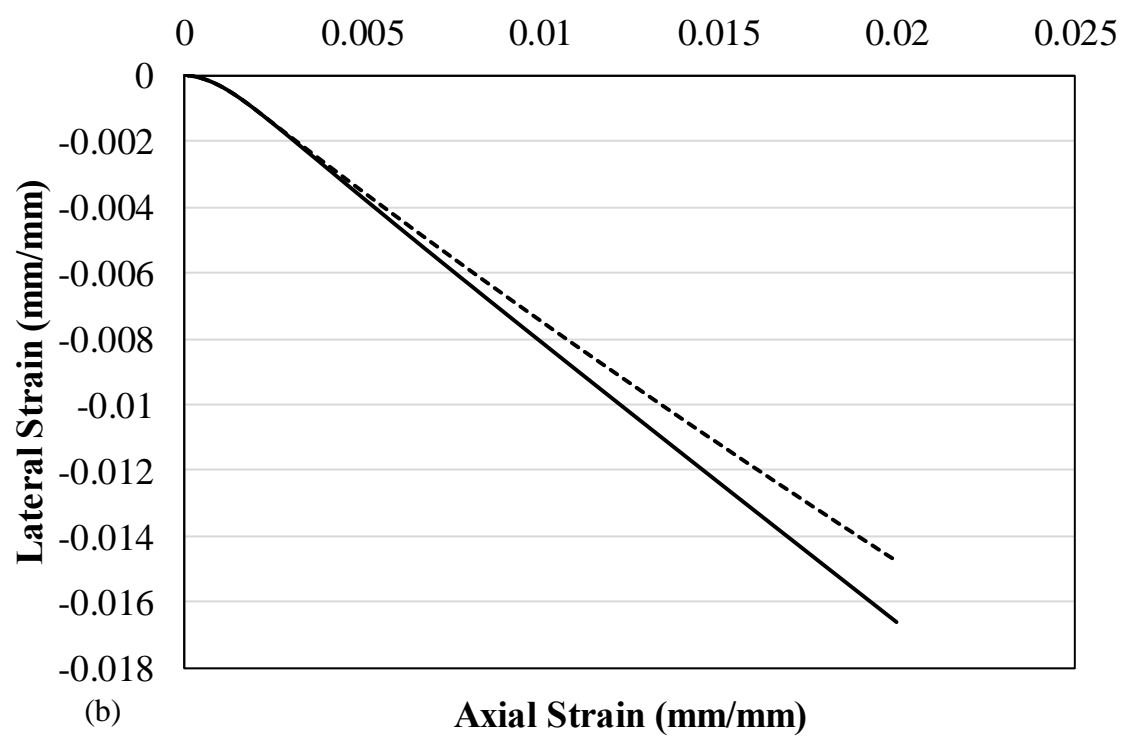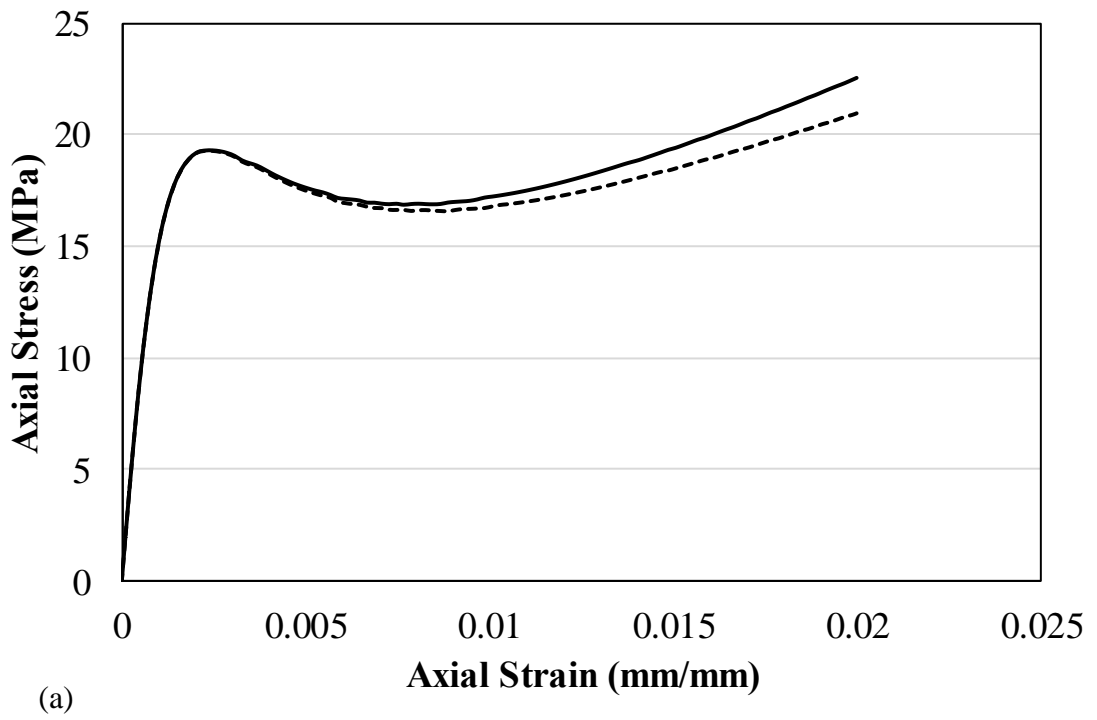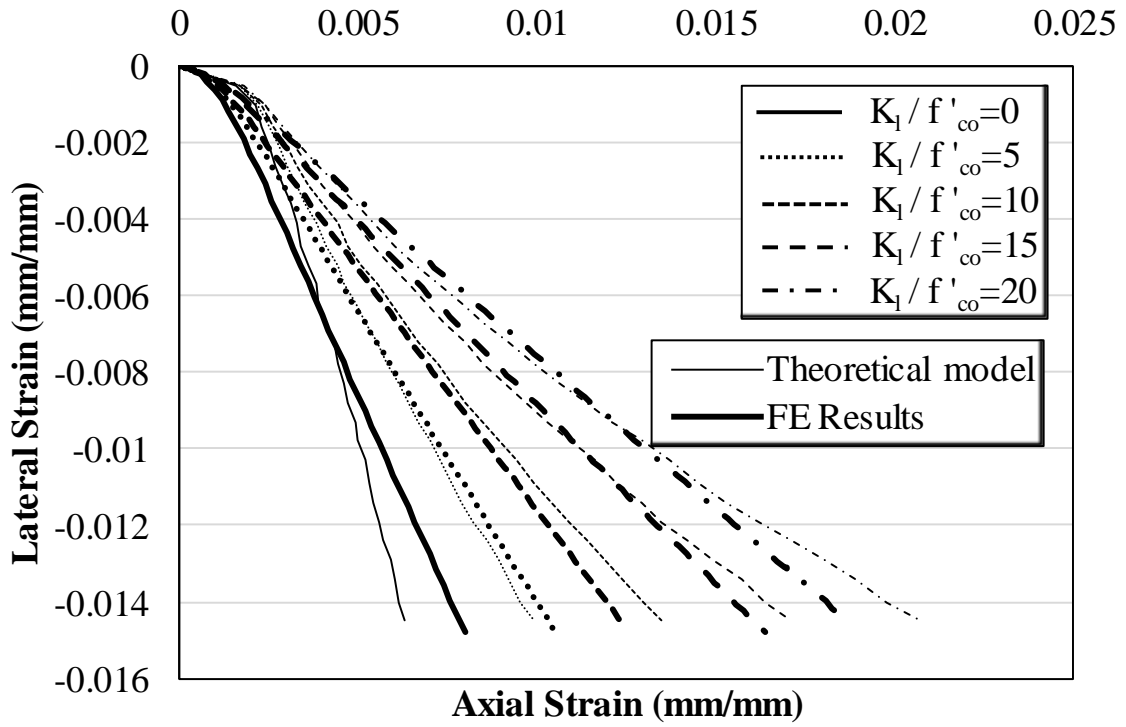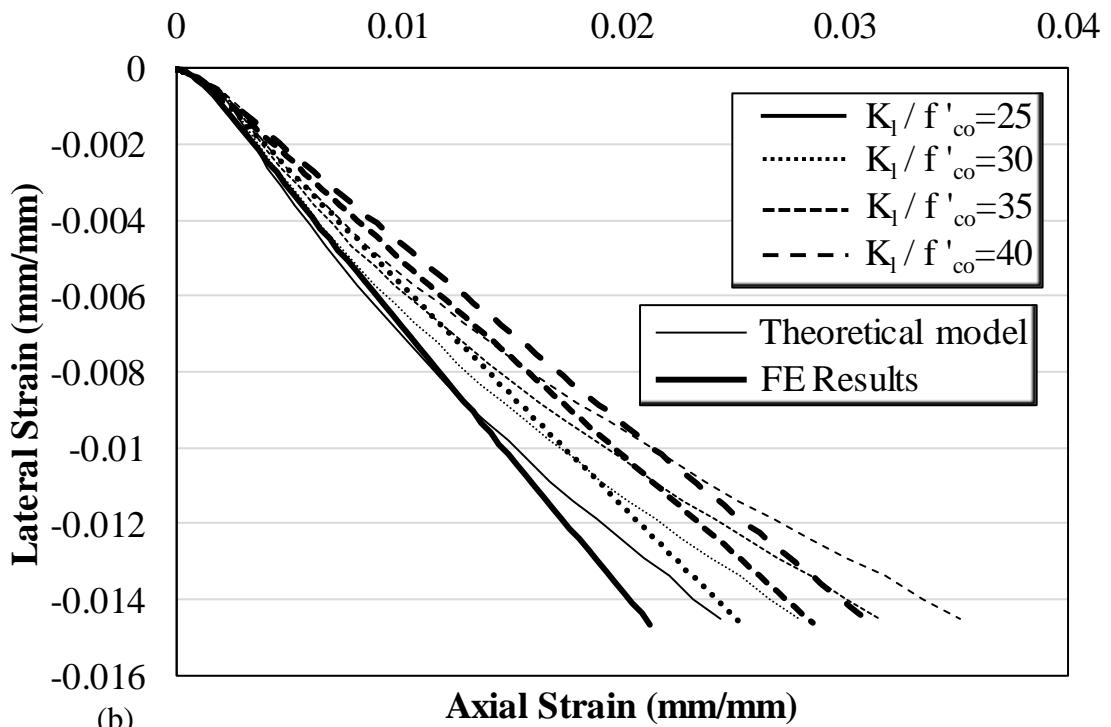Figure V-3 - Meshing of quarter the circular slice

(a)

(b)

Figure V-4 - Influence of d_c on: (a) the stress-strain curve, (b) the lateral strain - axial strain curve of FRP-confined concrete

Figure V-5 - Theoretical versus FE lateral strain-axial strain curves for:
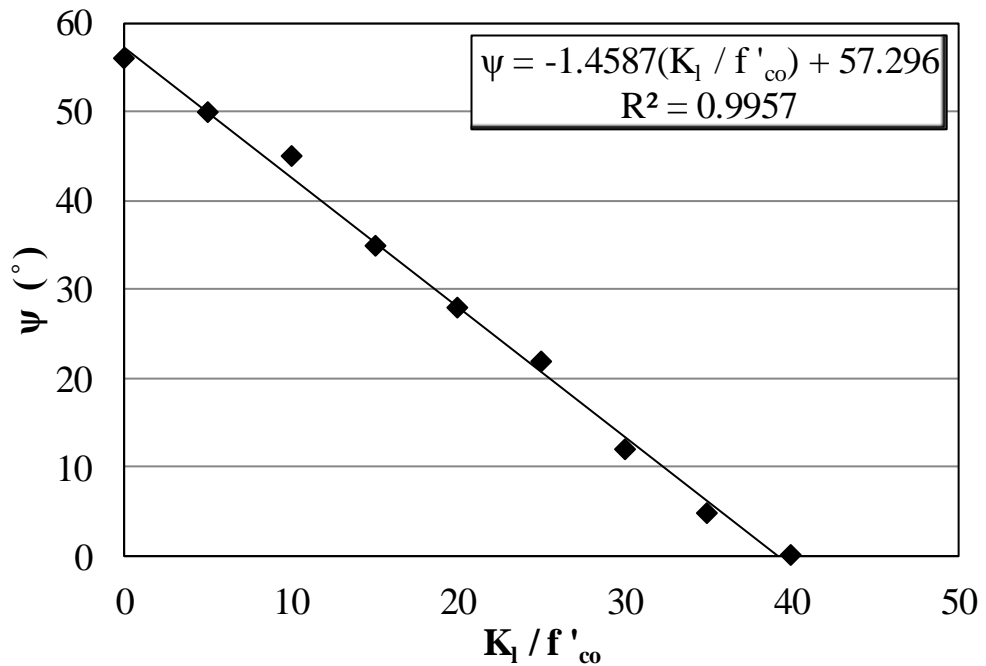(a) $0 \le K_l/f'_{co} \le 20$, (b) $25 \le K_l/f'_{co} \le 40$

Figure V-6 - Regression analysis of the dilation angle, ψ , with respect to the ratio of the stiffness of the FRP-jacket to the unconfined concrete compressive strength, K_l/f'_{co}

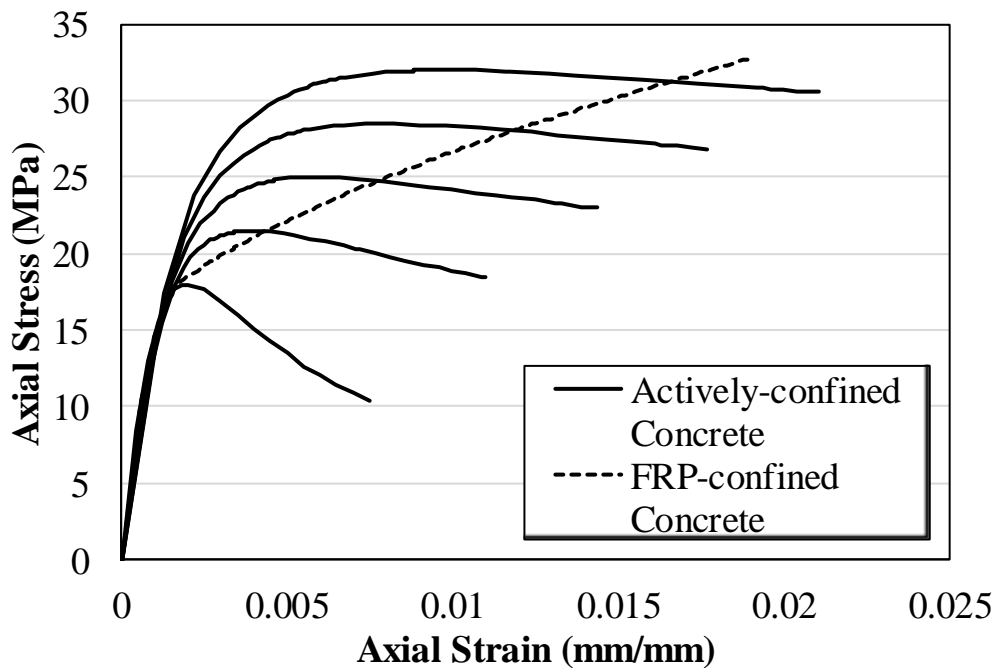Figure V-7 - Typical stress-strain curves of actively-confined concrete and FRP-confined concrete.
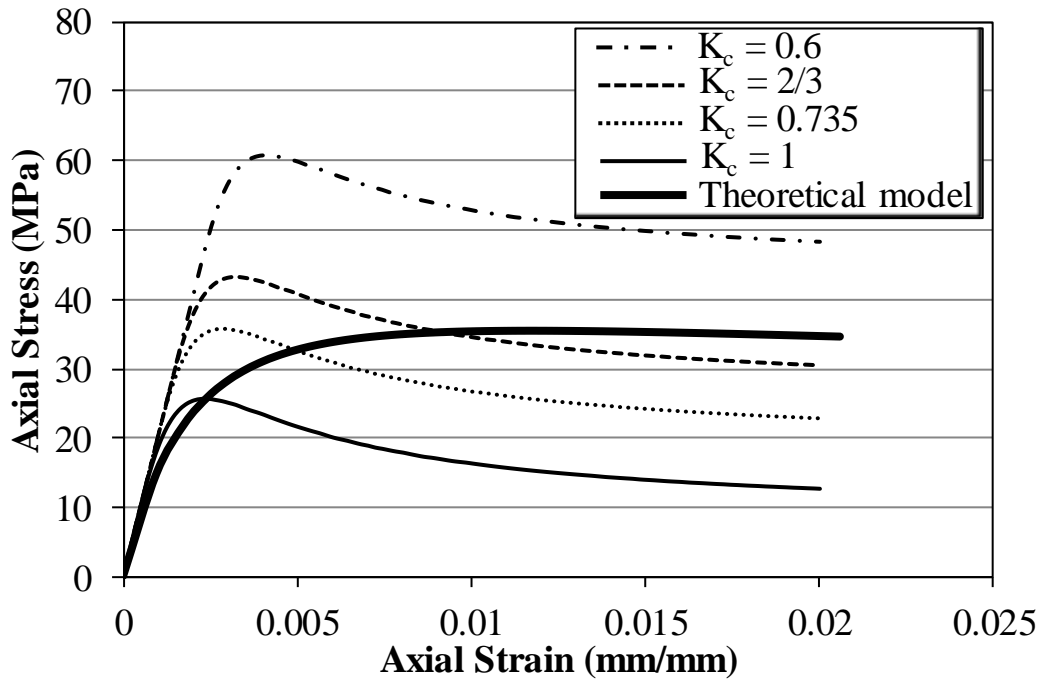
Figure V-8 - Influence of K_c on the stress-strain curve of actively-confined concrete
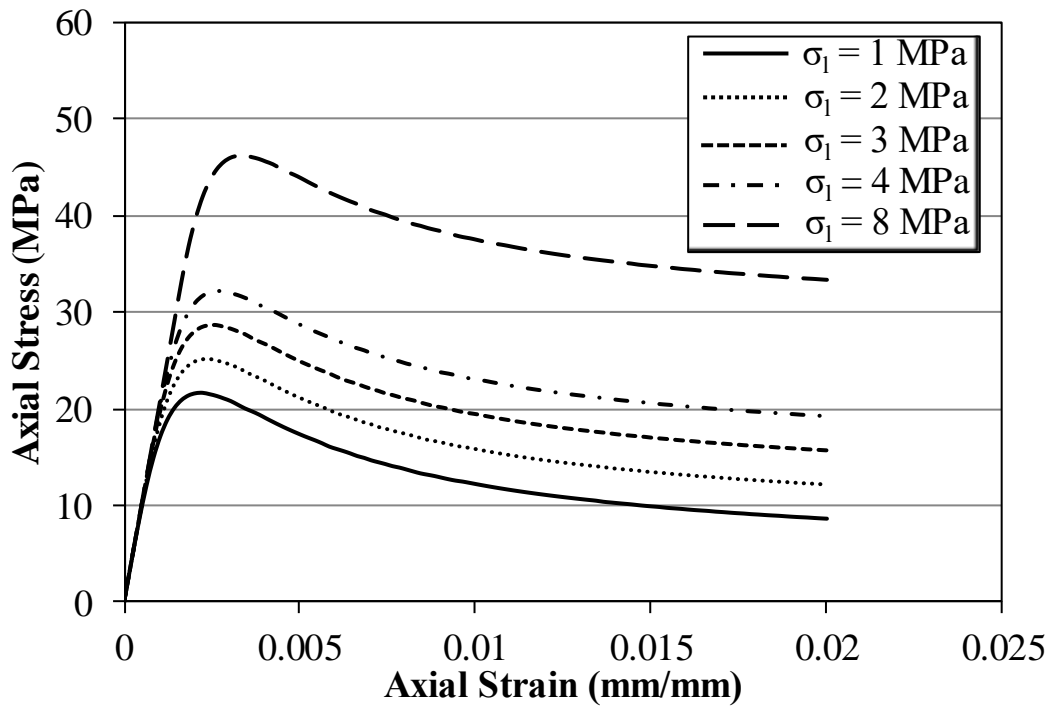
Figure V-9 - Stress-strain curves of actively-confined concrete with compression hardening data according to (Popovics, 1973)
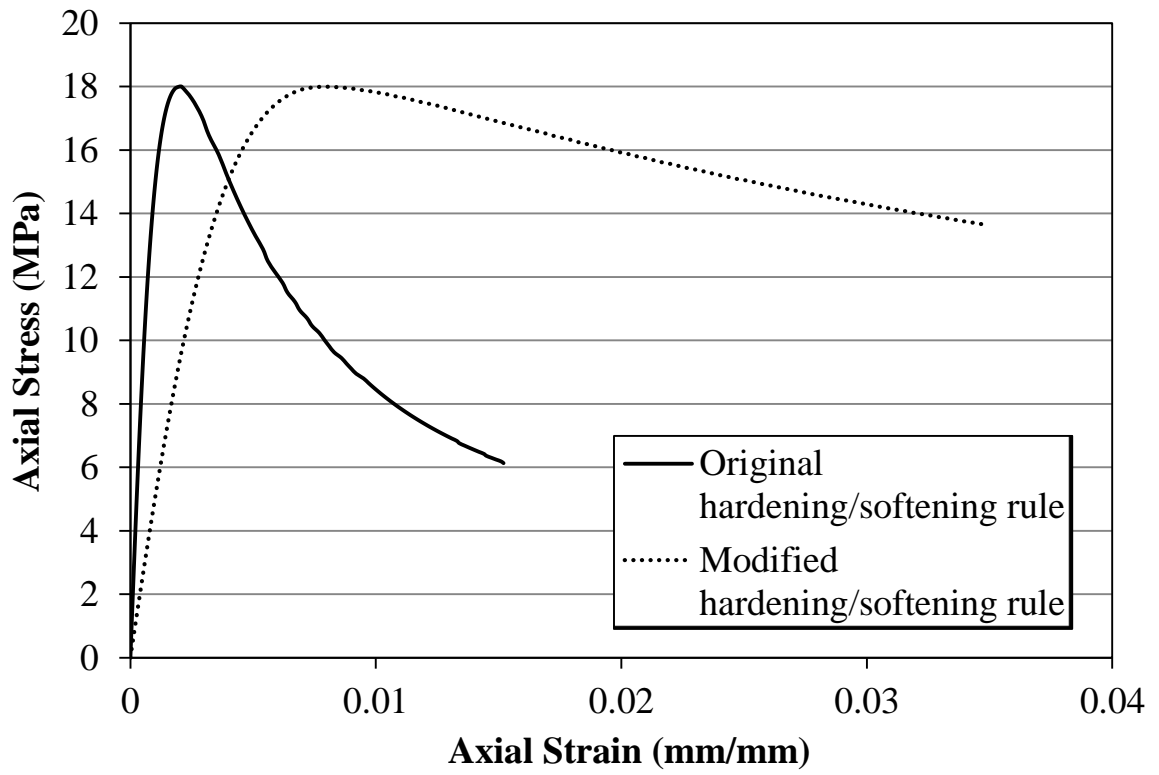
Figure V-10 - Original and modified strain/hardening softening rule
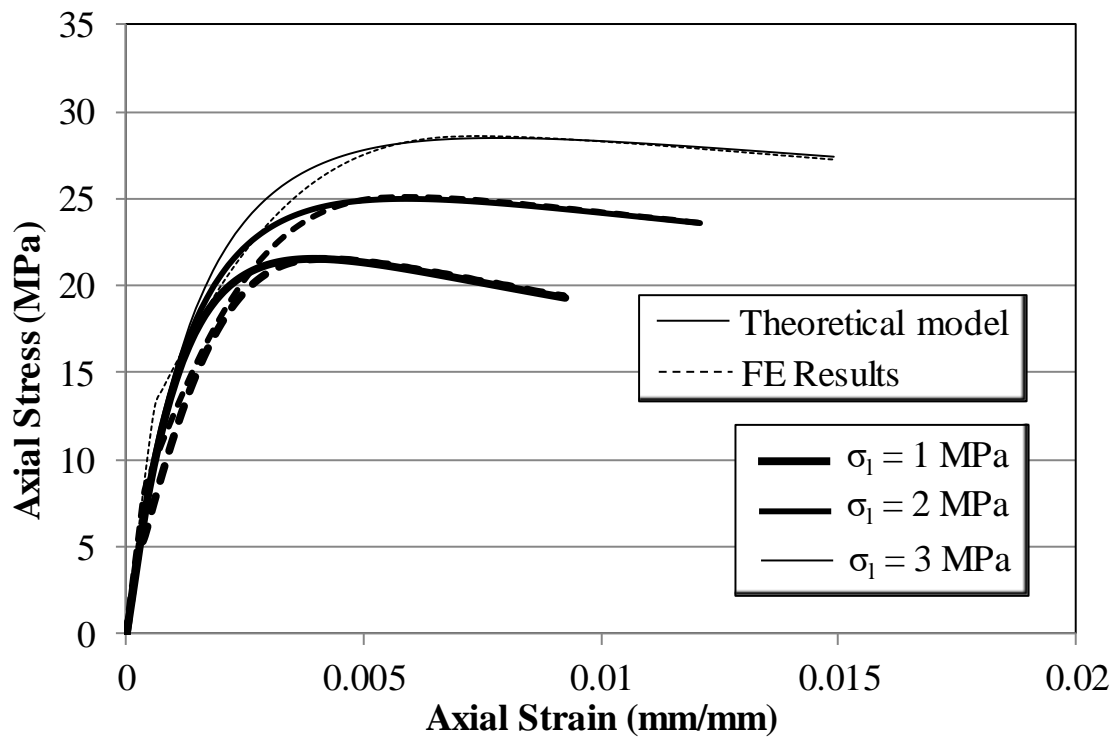
(a)
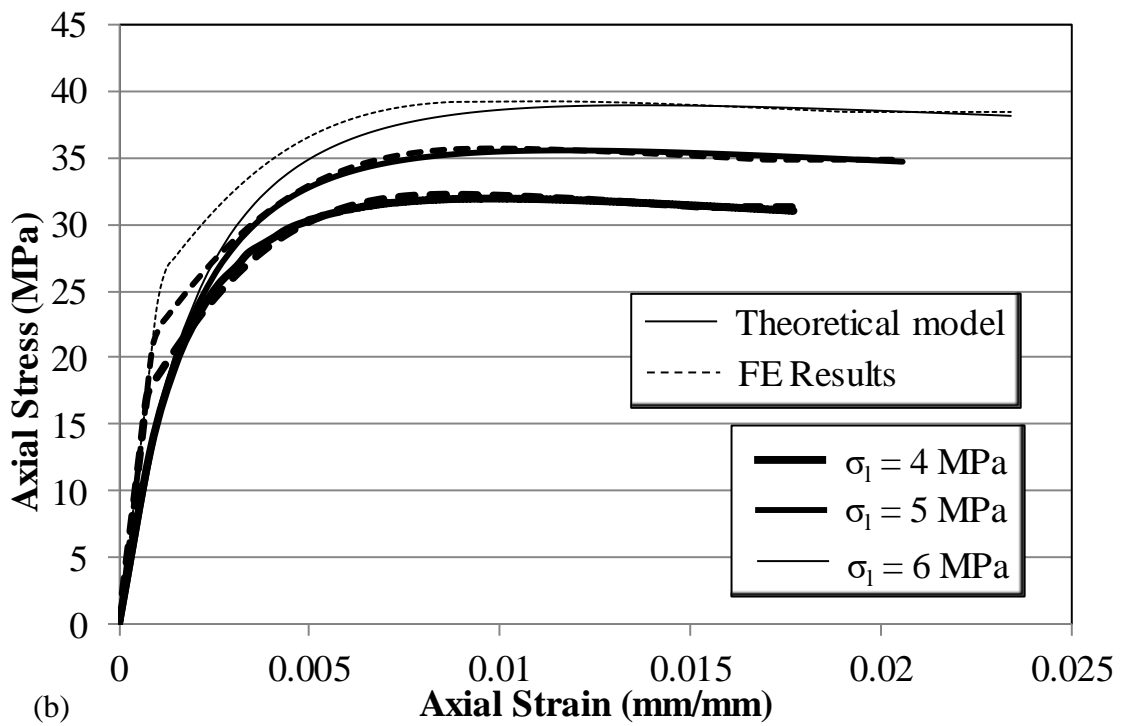
(b)
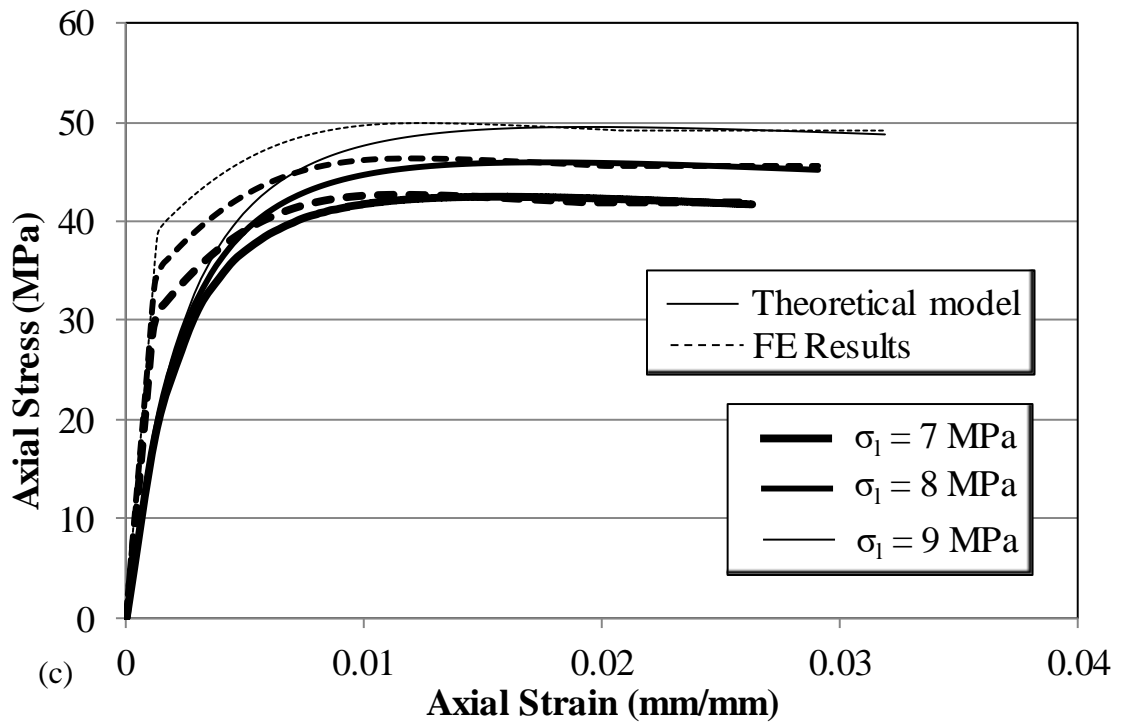
Figure V-11 - FE results of actively-confined concrete using modified strain hardening/softening rule versus theoretical results for $\sigma_l / f'_{co} \leq 0.5$
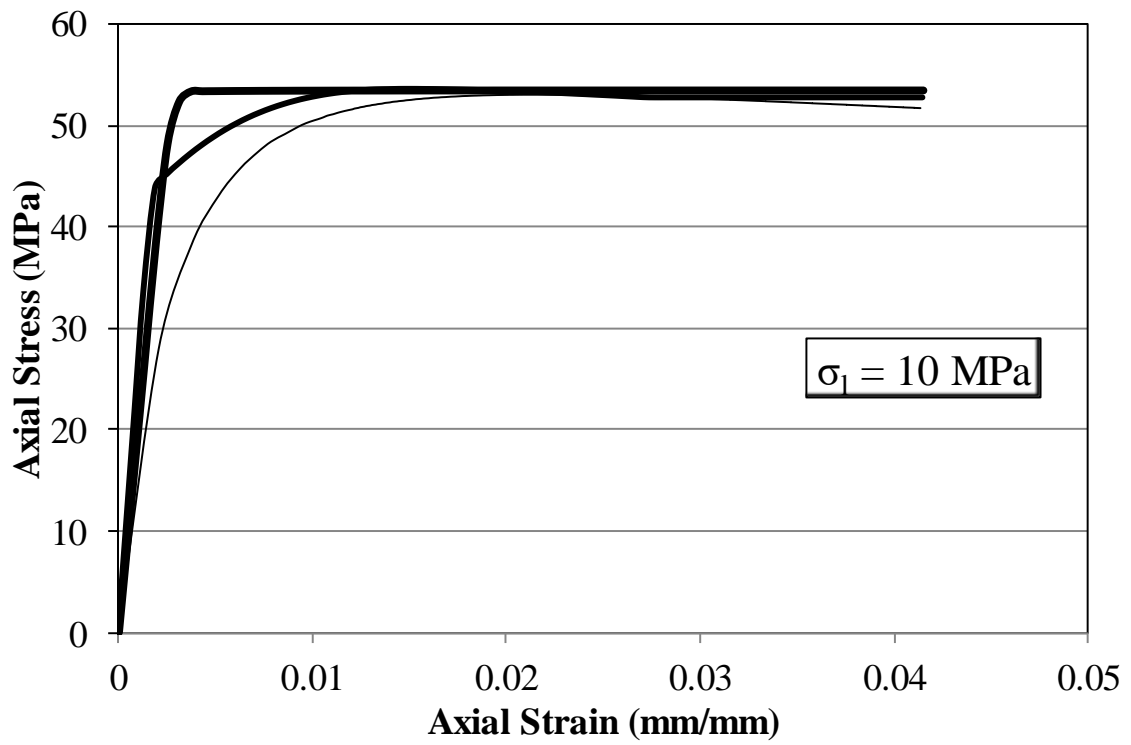
Figure V-12 - Comparison between (Teng, Huang, Lam, & Ye, 2007) theoretical stress-strain curve for actively-confined concrete with $\sigma_l = 10$ *MPa* and the FE results using methods *i* and *ii*
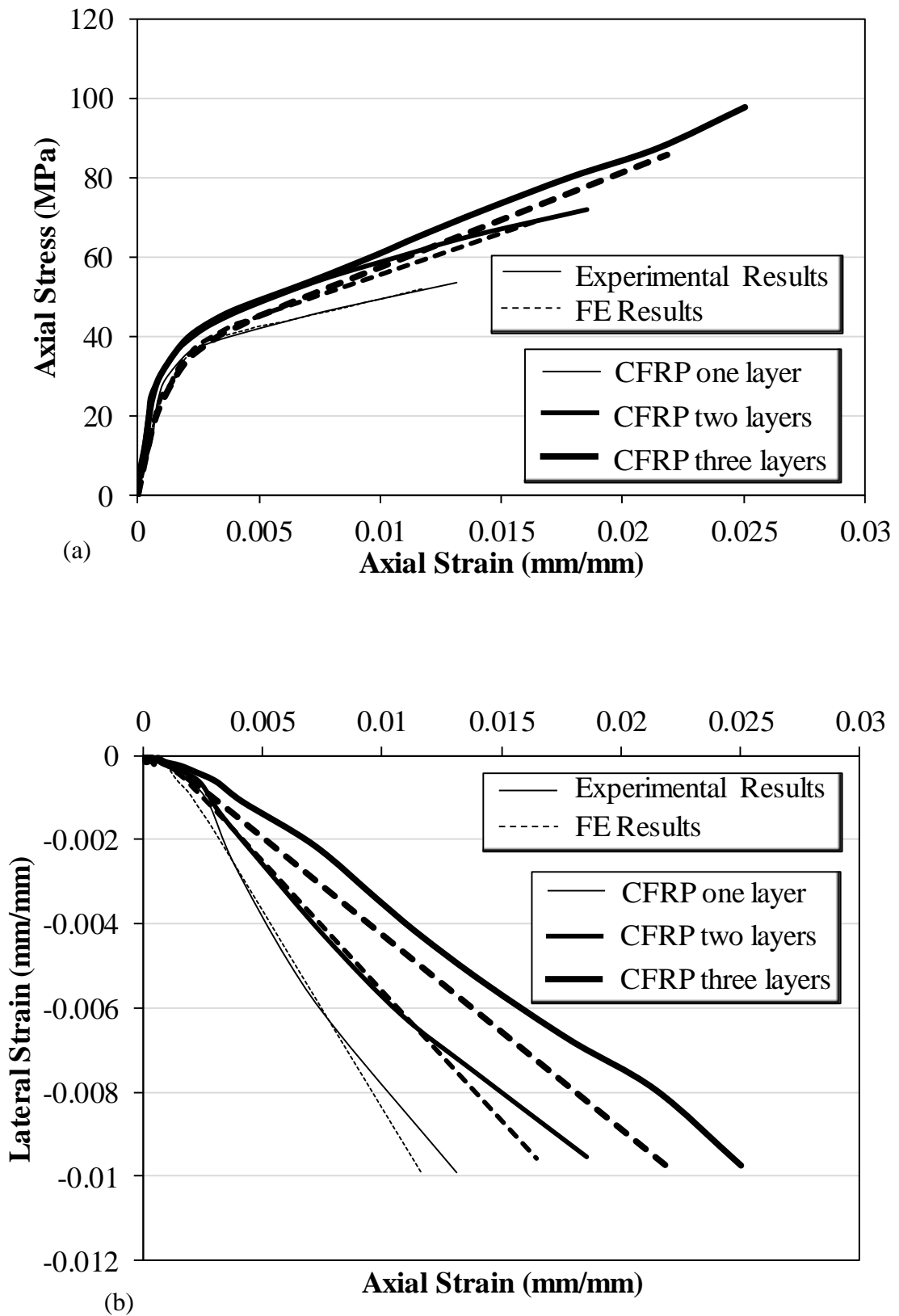
Figure V-13 - FE Results versus experimental results of: (a) stress-strain curves and (b) lateral strain-axial strain curves of specimens tested by (Lam & Teng, 2004)
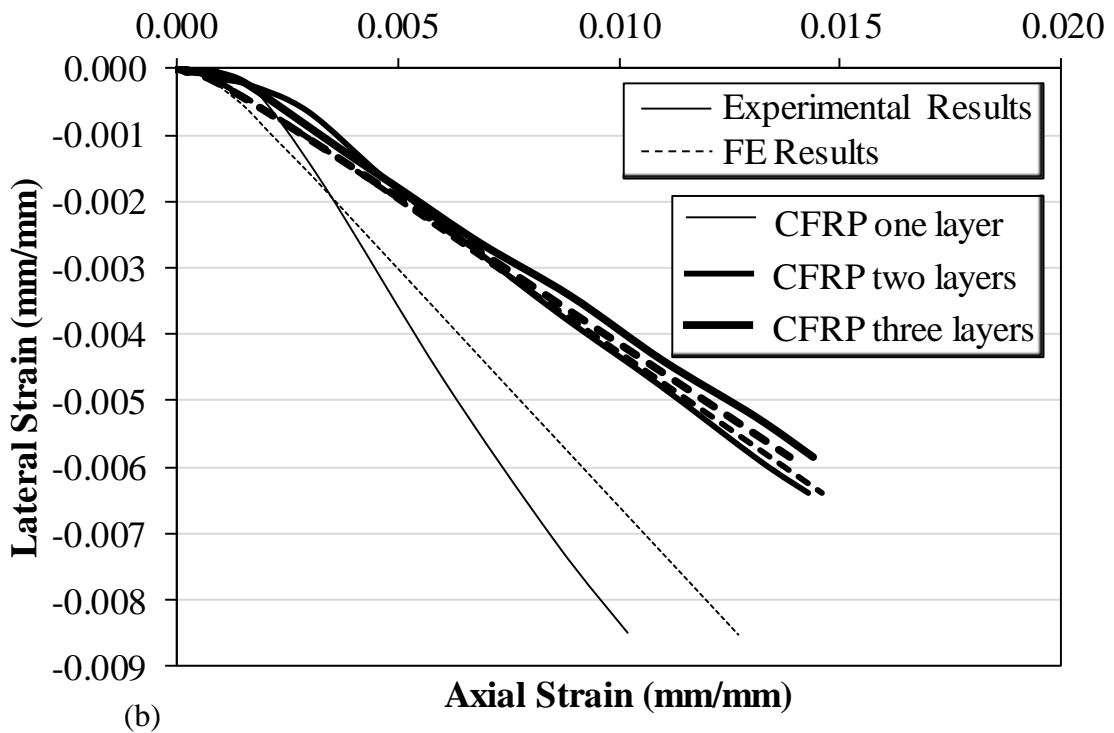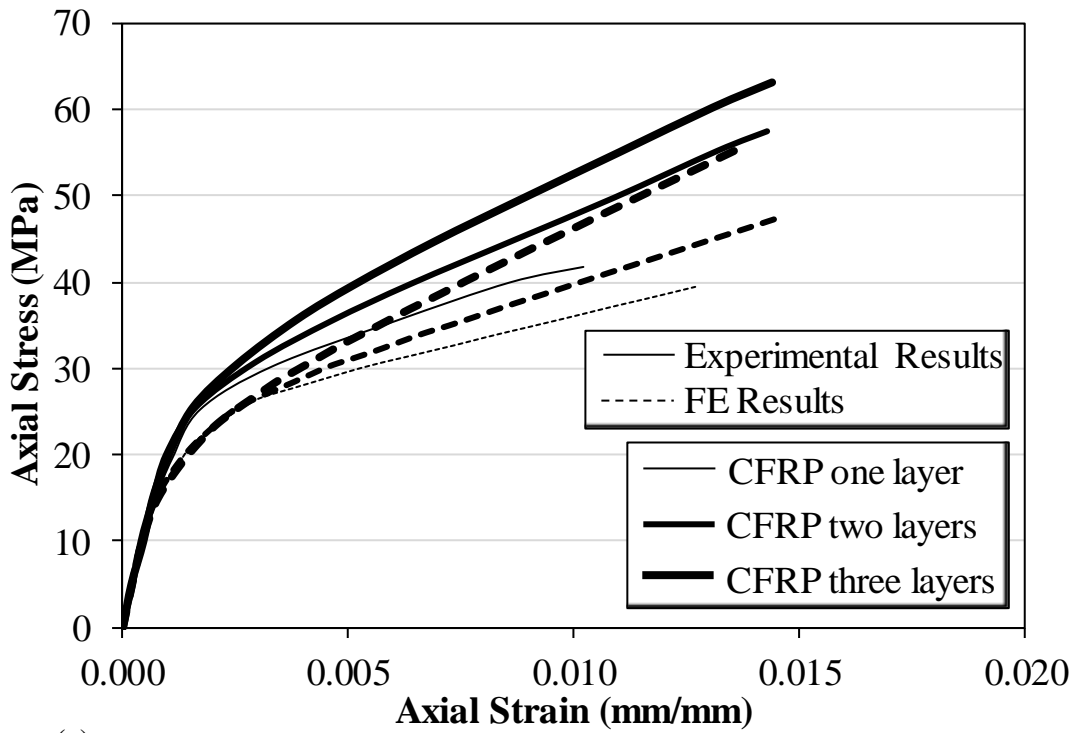
Figure V-14 - FE Results versus experimental results of: (a) stress-strain curves and (b) lateral strain-axial strain curves of specimens tested by (Valdmanis, De Lorenzis, Rousakis, & Tepfers, 2007)
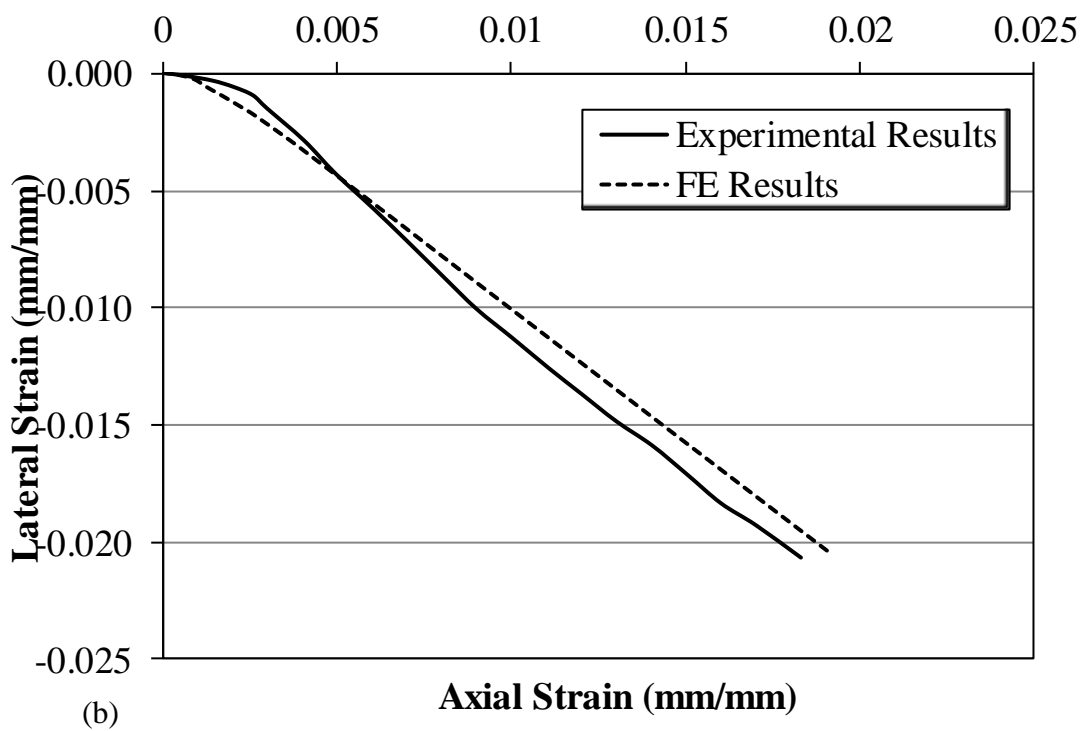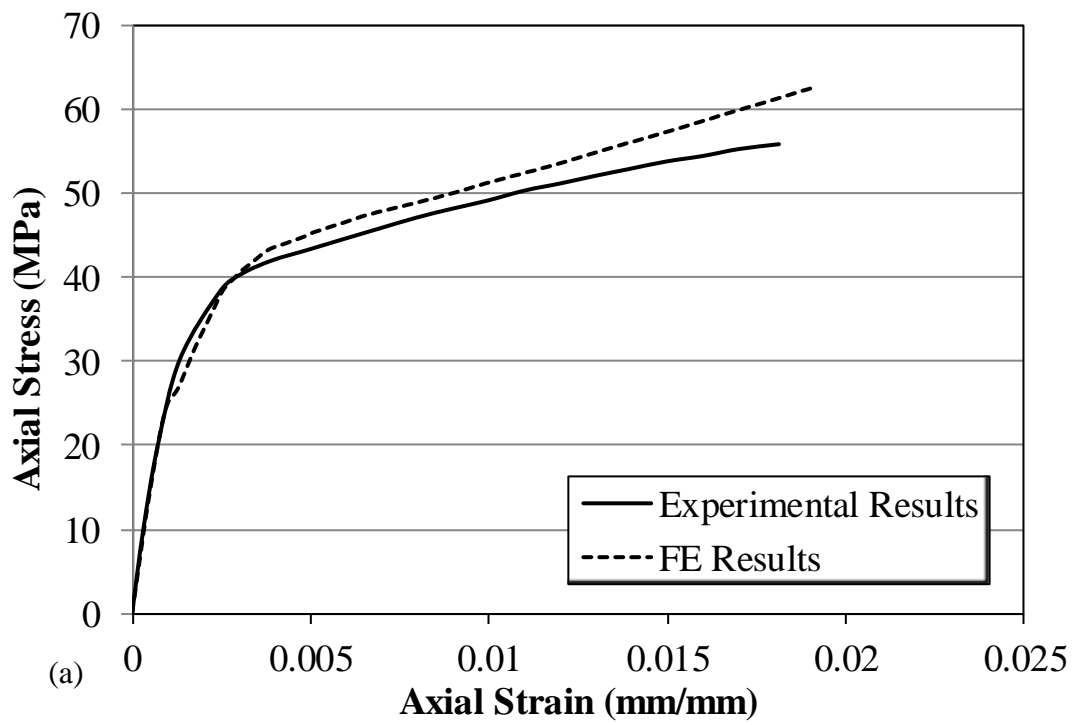
Figure V-15 - FE Results versus experimental results of: (a) stress-strain curves and (b) lateral strain-axial strain curves of specimens tested by (Wong, Yu, Teng, & Dong, 2008)
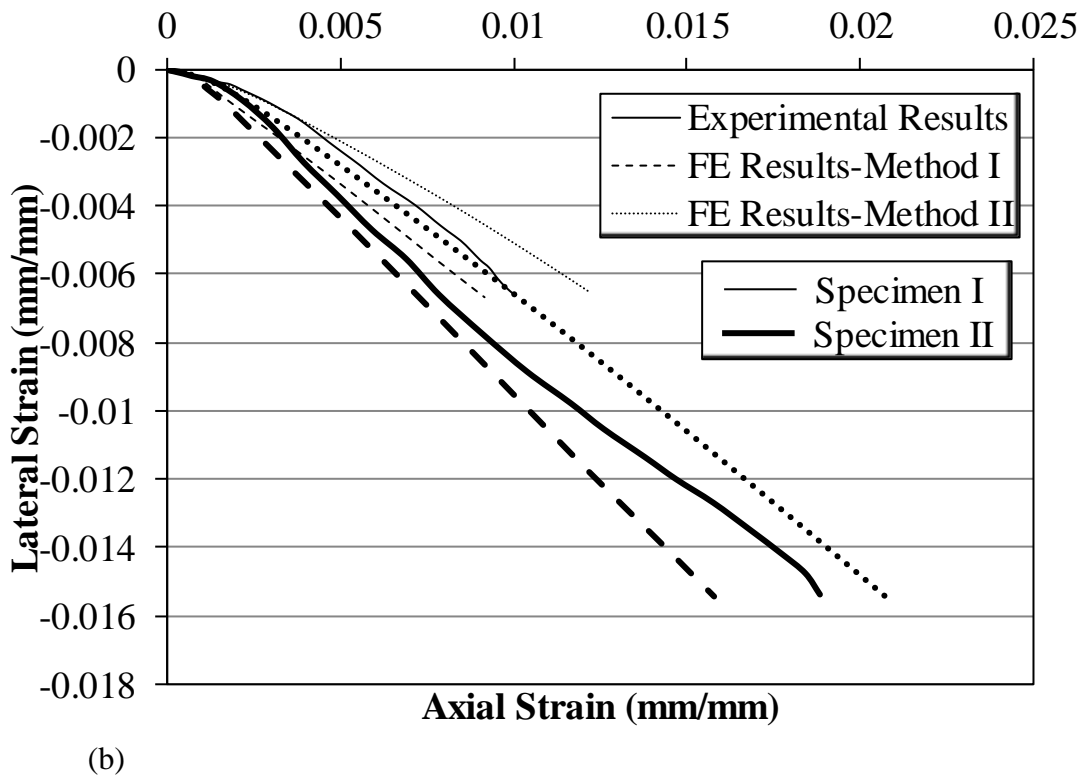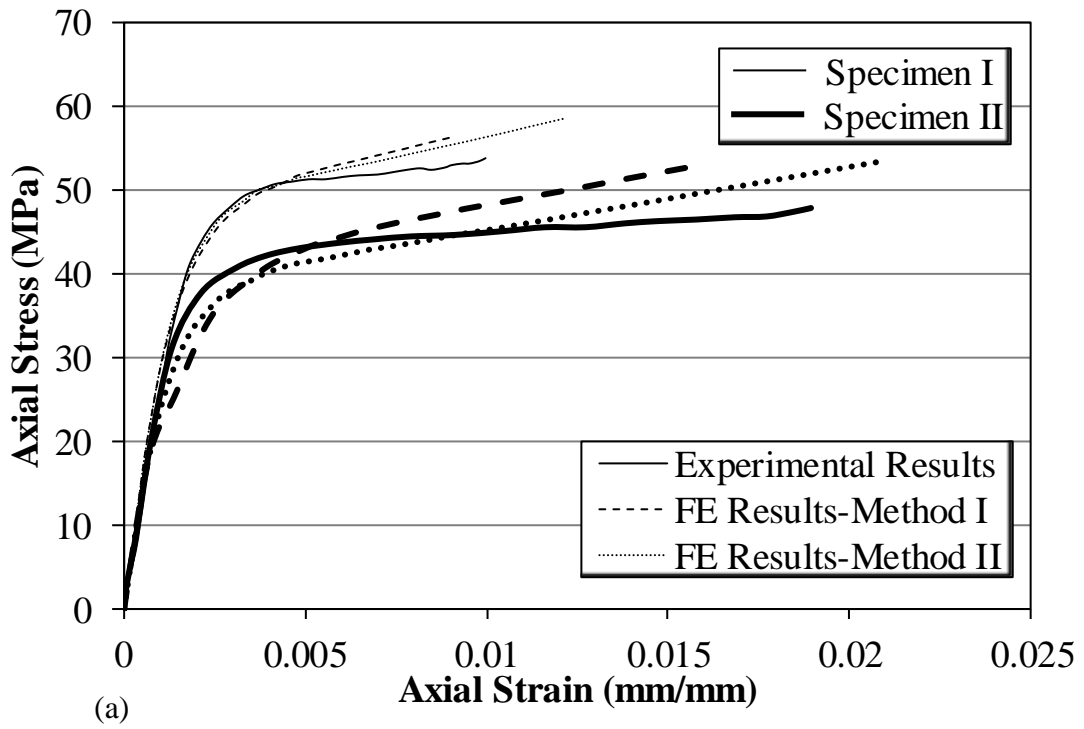
Figure V-16- FE Results versus experimental results of: (a) stress-strain curves and (b) average corner hoop strain-axial strain curves of specimens reported by (Yu, Teng, Wong, & Dong, 2010b)
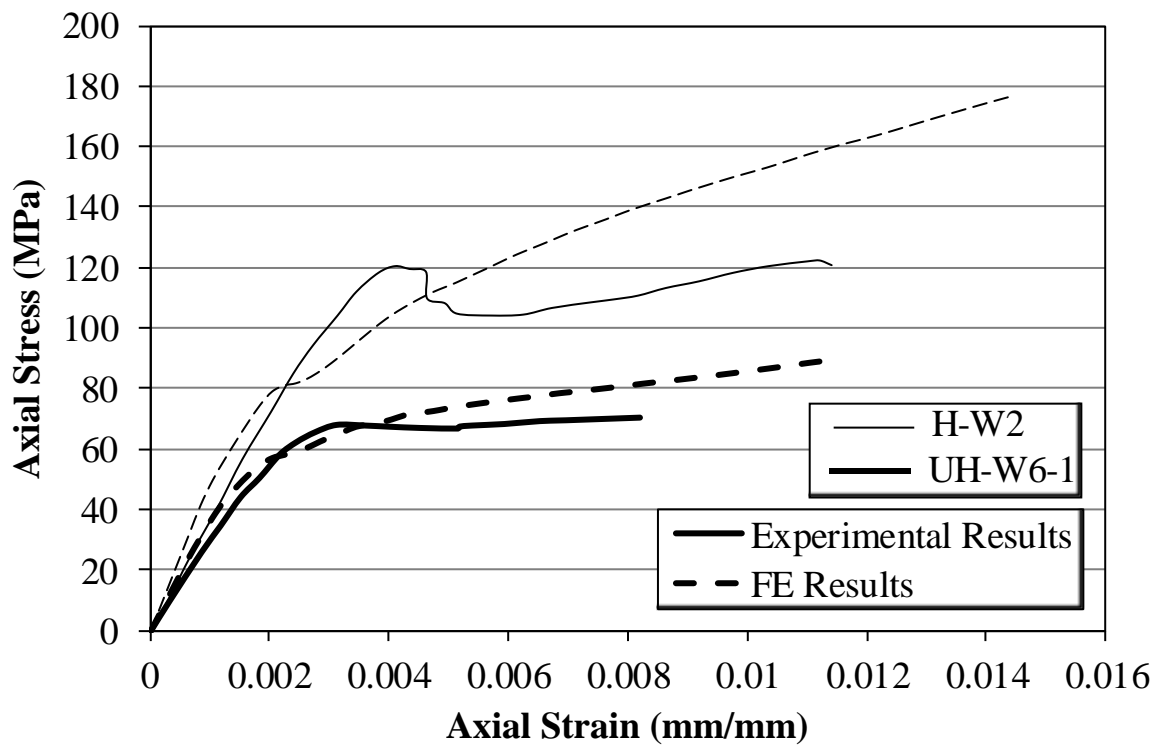
Figure V-17 - Comparison between the experimental and FE stress-strain curves of specimens *UH-W*6-1 and *H-W*2 tested by (Vincent & Ozbakkaloglu, 2013).

(a)

(b)
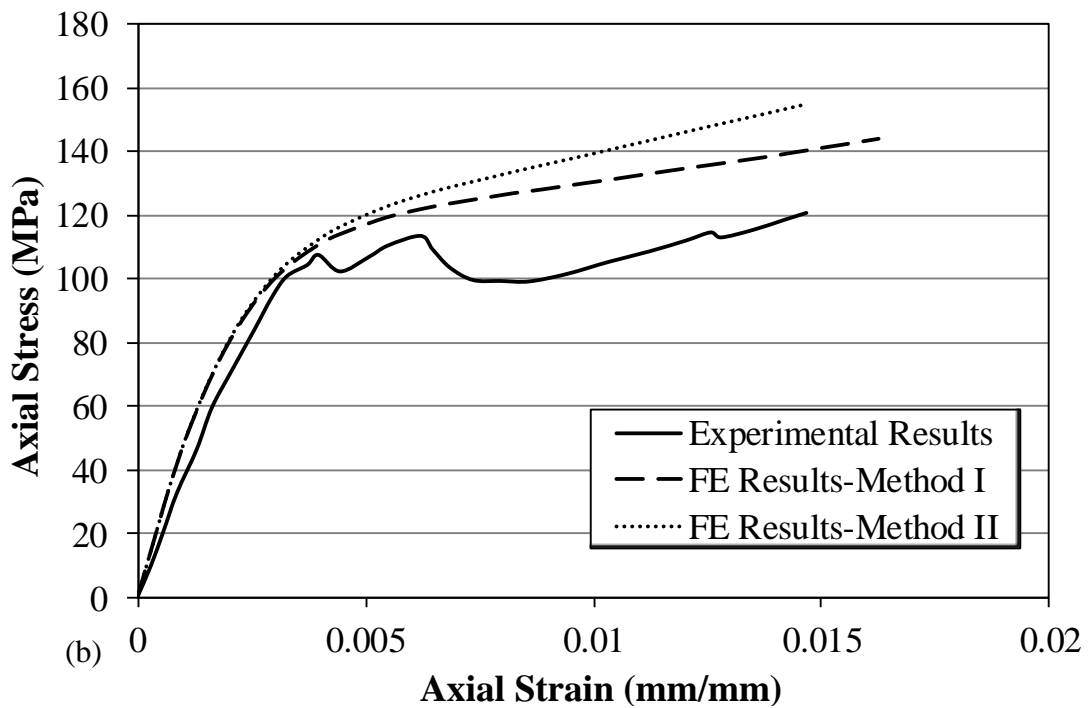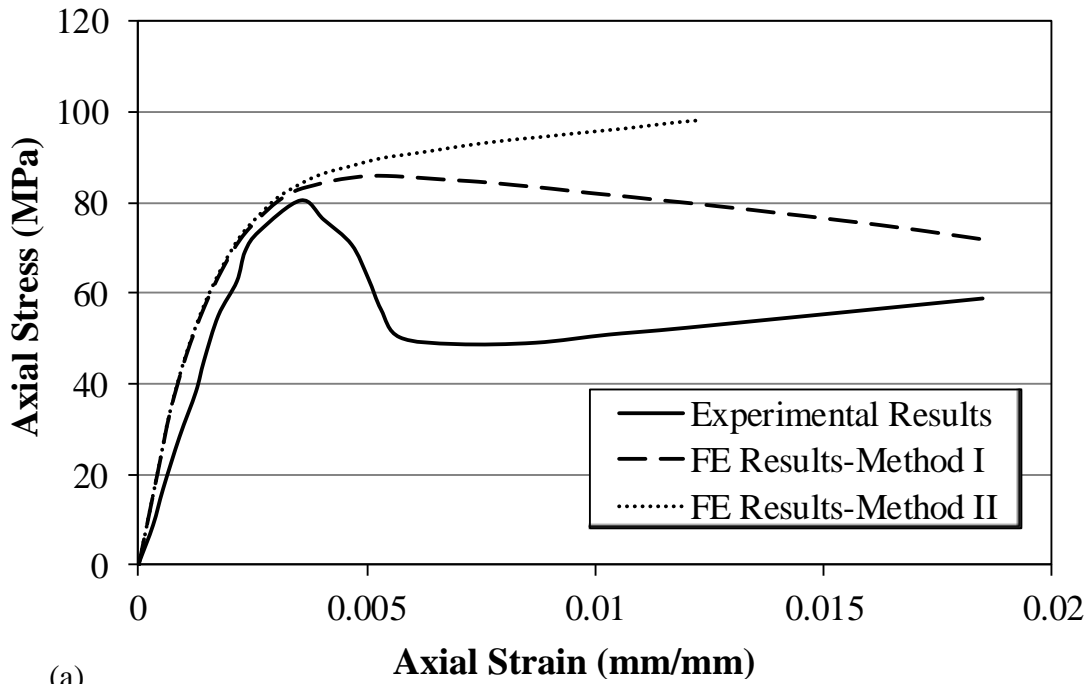
Figure V-18 - Comparison between the experimental and FE stress-strain curves of specimens (a) *A*20*R*15*L*5 (Ozbakkaloglu T. , 2012) and (b) *A*10*R*30*L*5 (Ozbakkaloglu T. , 2013).
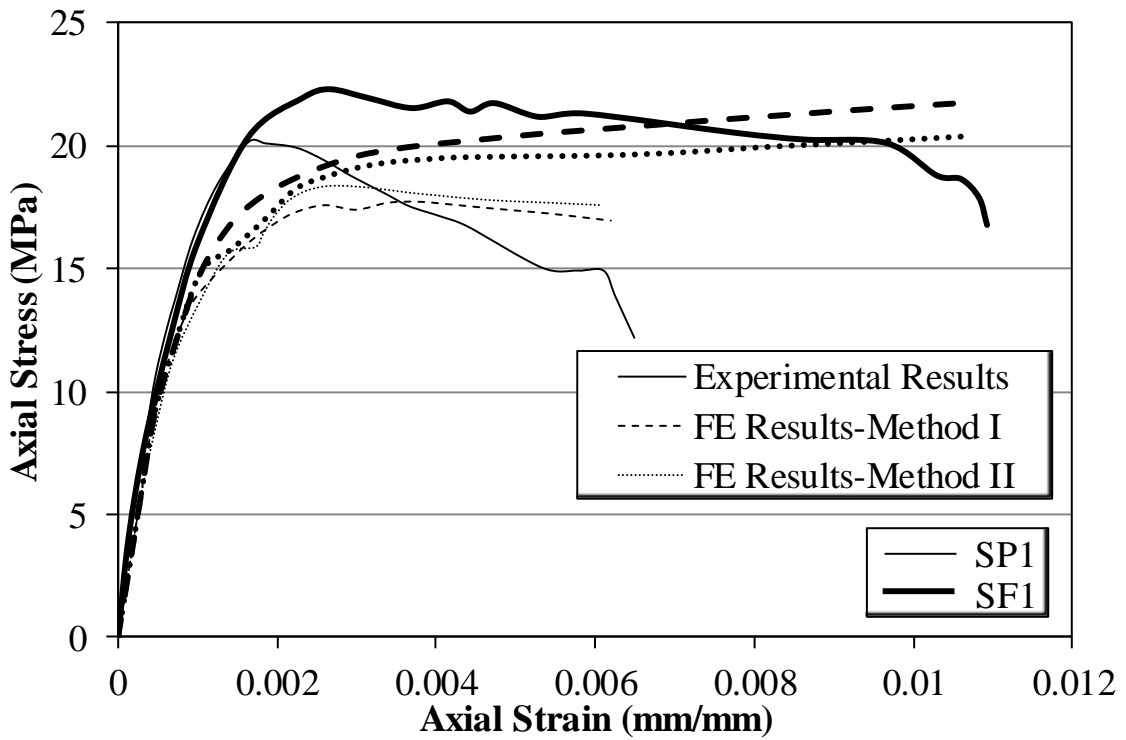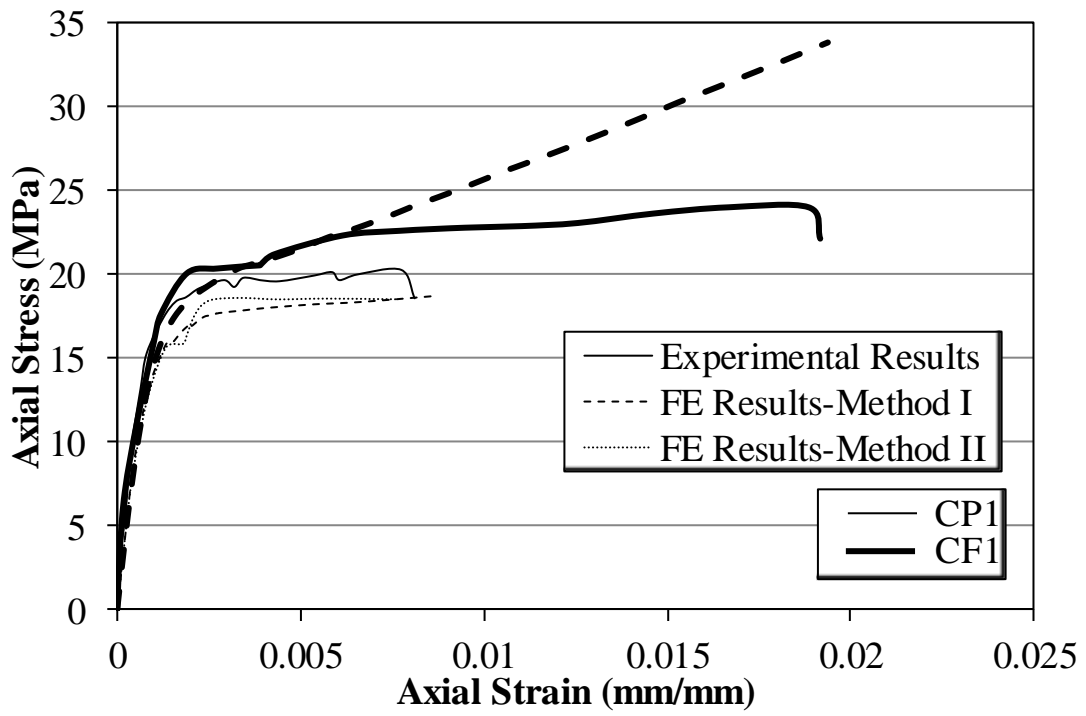
Figure V-19 - FE stress-strain curves versus the envelope of the experimental curves of specimens tested at AUB (Chapter II)

Figure V-19 - Continued

175
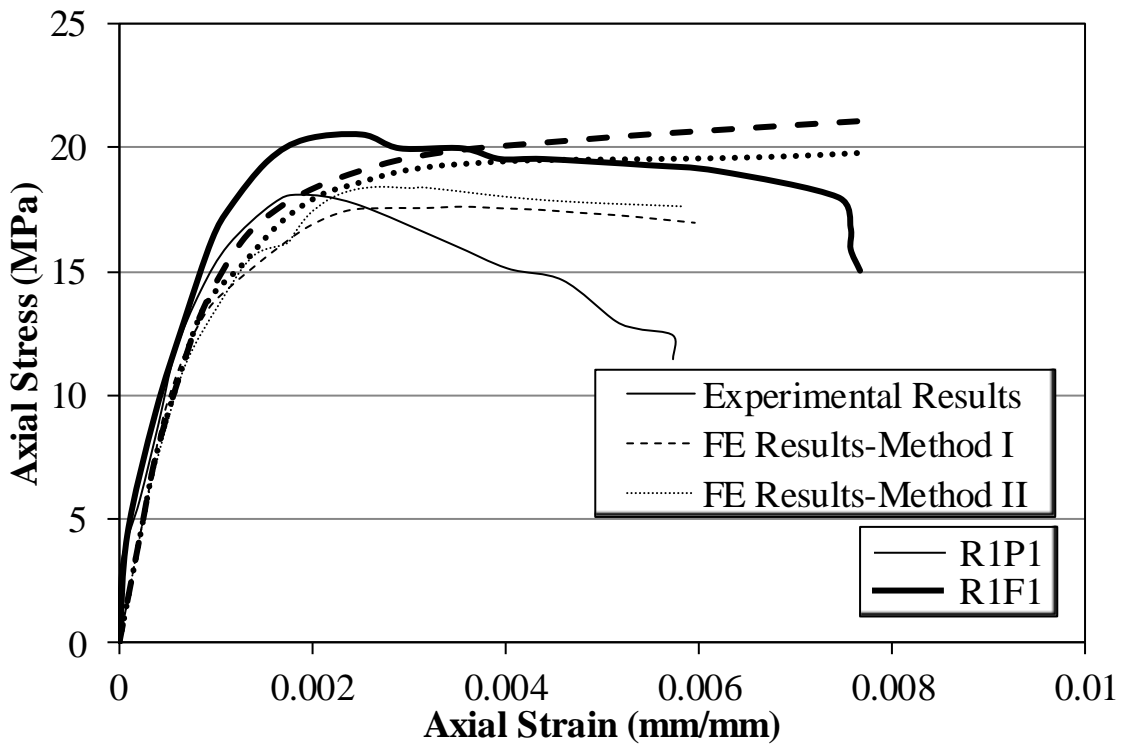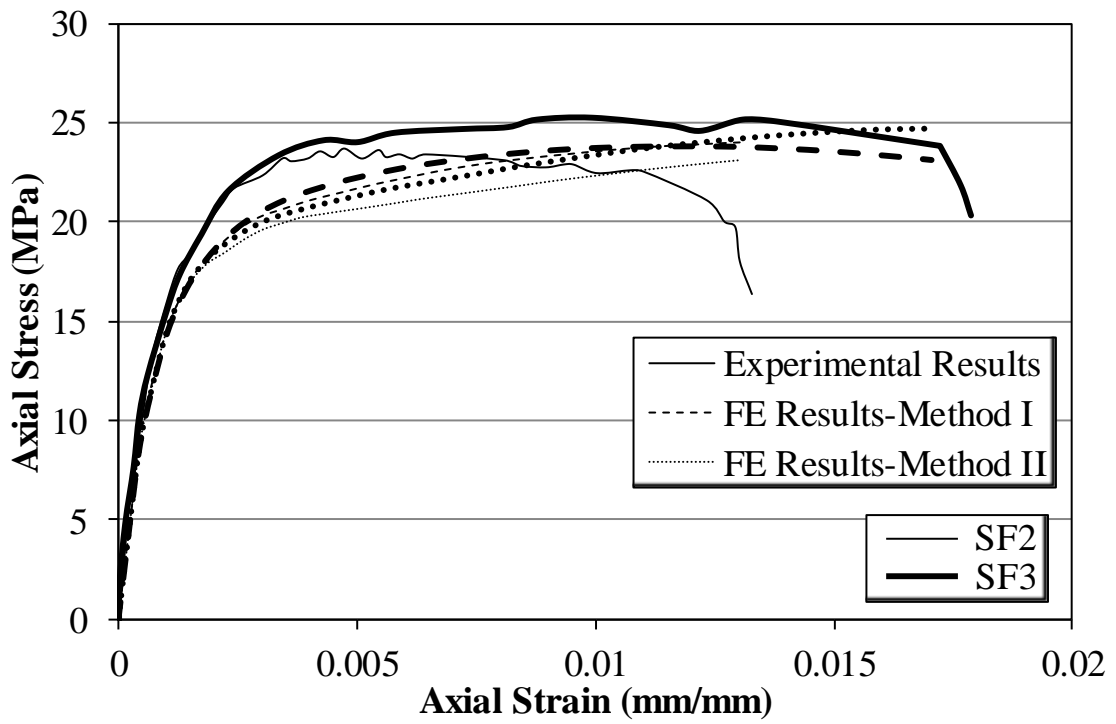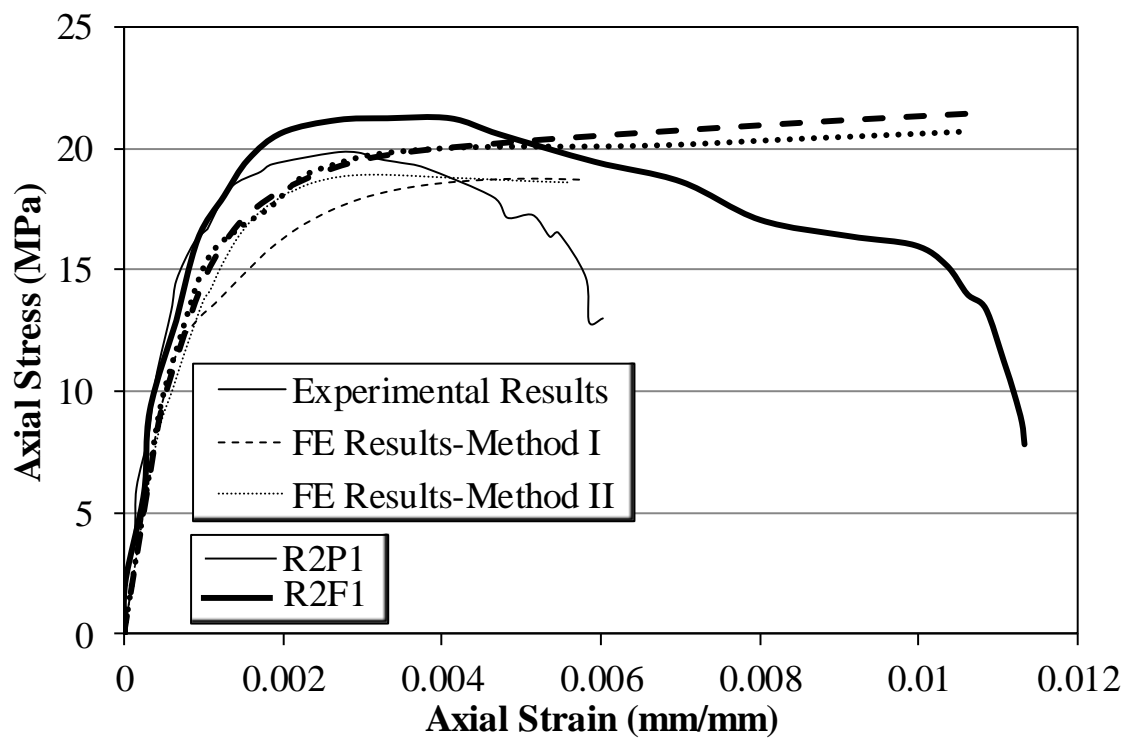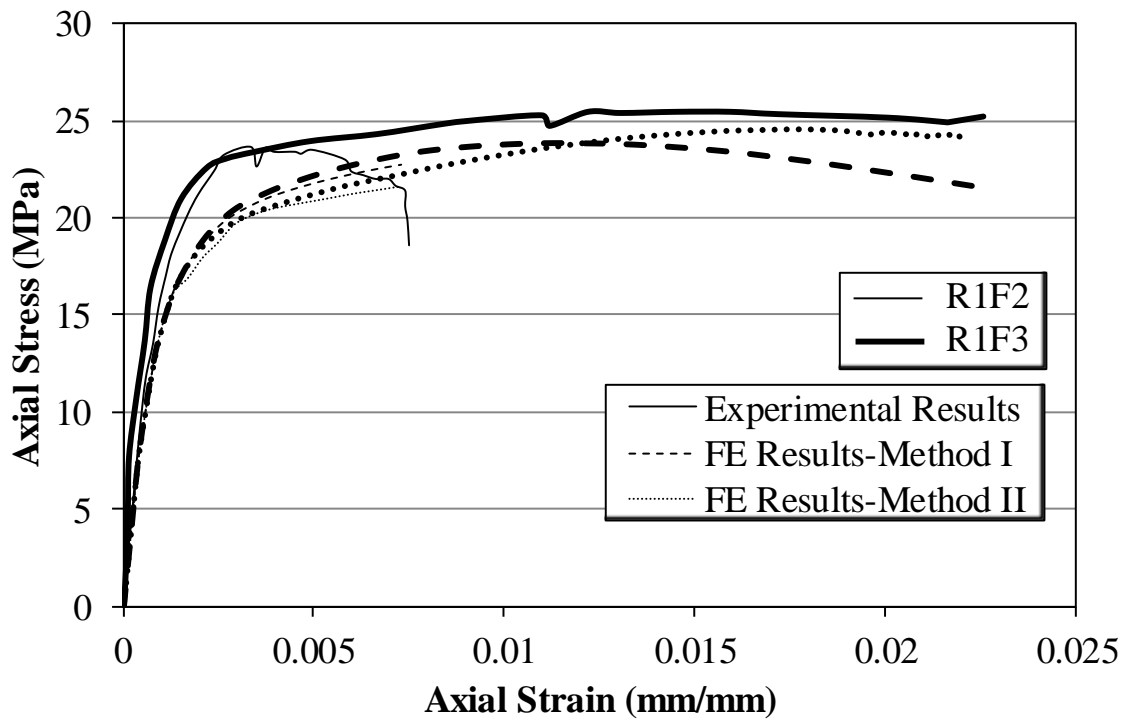
Figure V-19 - Continued
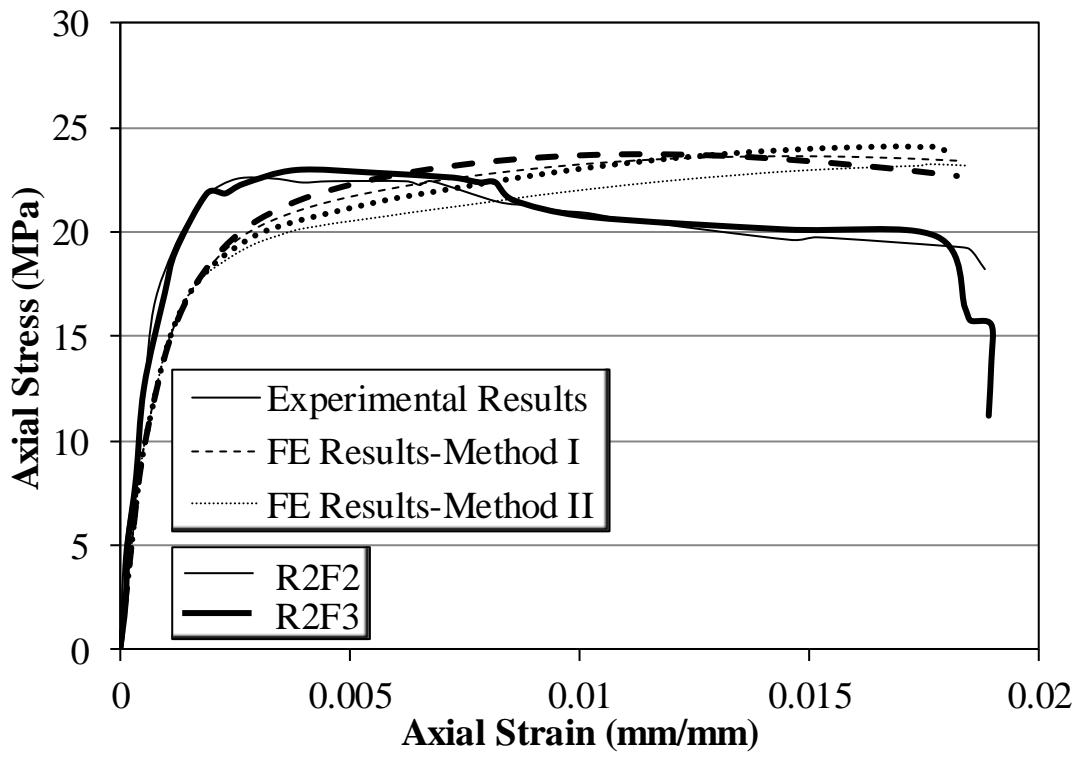
Figure V-19 - Continued

CHAPTER VI

FLEXURAL DEFORMATION CAPACITY OF FRP-CONFINED CONCRETE COLUMNS

A.   Introduction

As previously stated, many experimental and analytical investigations have been performed to evaluate the axial stress-strain response of concrete columns wrapped with FRP sheets. On the other hand, studies have been conducted to evaluate the response of full-scale columns strengthened with FRP sheets in their support region and subjected simulated seismic loading. These studies clearly demonstrated an improvement in the lateral load capacity and ductility of the columns under seismic loading due to the confinement effect.

In this chapter, we present the results of a parametric study performed to investigate the influence of different design parameters of unconfined and FRP-confined RC columns on the moment-curvature ($M - \phi$) response of the column section. The $M - \phi$ curve is an indication of the moment and rotation capacity of a section and it can be used to generate the lateral load-drift response of the column.

B.   Nonlinear Flexural Analysis

Nonlinear flexural analysis is carried out in this study for predicting the moment-curvature ($M - \phi$) response of unconfined and FRP-confined concrete sections. The aim of this analysis is to investigate the effect of different design parameters on the $M - \phi$ response. These parameters include: the section

dimensions, the confinement level, the presence or absence of FRP anchors, the axial load level and the ratio of longitudinal steel reinforcement.

Two RC rectangular cross-sections of close areas are studied: the first of dimensions 1000 *mm* x 300 *mm* and the second of dimensions 850 *mm* x 350 *mm*. For each section, three cases of confinement are considered: unconfined concrete, concrete confined with external FRP sheets, and concrete confined with a combination of FRP sheets and anchors. The axial stress-strain properties of concrete confined with external FRP sheets are those of a concrete column of same cross-section wrapped with an FRP sheet of a known thickness over its entire height. As for concrete confined with a combination of FRP sheets and anchors, the properties are those of a column wrapped with FRP sheets over its entire height and provided with additional FRP anchors. Details of anchor preparation are provided in Figure I-2. All the anchors are of same cross-sectional area, placed at the middle of the longer side of the cross-section and regularly spaced in the vertical direction. Similar to what was suggested in Chapter IV, the anchor fans are considered wrapped with one additional FRP layer. The total cross-sectional area of the anchors over the column height is equal to the total cross-sectional area of the FRP jacket crossing the vertical plane of the specimen. A $150-mm$ anchor spacing is selected with an anchor fan of $60-mm$, similarly to the specimens tested and reported in Chapter III. Typical section and elevation of anchored specimens are provided in Figure III-1. A corner radius of $30-mm$ is assumed for all confined specimens.

Table VI-1 shows the values of the different parameters investigated. In this table, $\rho = A_s / A_c$ is the reinforcement ratio where A_s is the area of longitudinal

reinforcement and A_c is the column cross-section area (gross area); $\eta = P/P_o$ is the load ratio, where P is the applied axial load and $P_o = f'_{co} A_c$.

As can be seen in Table VI-1, the sections are either unconfined ($t_{wrap} = 0$) or confined ($t_{wrap} \neq 0$). For confined specimens, three different thicknesses are considered: $t_{wrap} = 0.78, 1.17,$ and 1.56 *mm*. In order to compare the effect of the presence of FRP anchors on the $M - \phi$ response, for each thickness of the FRP sheet, two companion sections are considered: one confined with external FRP sheets only and the other confined with a combination of FRP sheets and anchors the details of which are explained previously. For each of the sections described above, three reinforcement ratios are considered: $\rho = 1.0, 1.5,$ and 2.3 %. Figure VI-1 shows the distribution of longitudinal reinforcement in sections 1000 *mm* x 300 *mm* and 850 *mm* x 350 *mm*. Details of the lateral reinforcement are not shown. Reinforcement ratios of 1.0, 1.5, and 2.3 % are ensured using steel re-bars of respective diameter 16 *mm*, 20 *mm*, and 25 *mm*. The last parameter investigated is the axial load level with four different values (η = 0.00, 0.10, 0.15, 0.20) taken into consideration.

The details of all the specimens of section 1000 *mm* x 300 *mm* are summarized in Table VI-2 to Table VI-5. In these tables,

- the unconfined specimens are designated as $XH - \rho$

- the specimens confined with external FRP sheet only are designated as

$XuHv - \rho$ where u = 1, 2 and 3 respectively for t_{wrap} = 0.78, 1.17, and 1.56 *mm* and v = 1, 2 and 3 respectively for η = 0.1, 0.15, and 0.2.

- the specimens confined with external FRP sheet and anchors are designated as $XuaHv - \rho$ where u and v are defined previously and a is a letter indicating an anchored specimen.

For instance, specimen $XH - 1.5$ represents an unconfined section of dimensions 1000 mm x 300 mm with no applied axial load and having a reinforcement ratio of 1.5%.

The specimens of section 850 mm x 350 mm are designated identically to specimens of section 1000 mm x 300 mm with the X letter substituted by Y. For brevity, the details of these sections are not presented in a separate table. For instance, specimen $Y2aH2 - 2.3$ represents a section of dimensions 850 mm x 350 mm, having a reinforcement ratio of 2.3% and subject to an axial load equal to $0.15f'_{co} A_c$, wrapped with an external FRP sheet of thickness $t_{wrap} = 1.17$ mm and provided with additional anchors.

1.   *Material models*

A615Gr60 steel is considered. The constitutive stress-strain ($f_s - \varepsilon_s$) relationship of steel reinforcement is shown in Figure VI-2 and is expressed in Eqs. (VI-1) to (VI-3). In this figure, ε_{sy} = Yield strain of steel = 2.07E-03, f_{sy} = Yield stress of steel = 413.7 MPa, ε_{sh} = Strain in steel at onset of strain hardening = 0.01, ε_{su} = Ultimate strain capacity of steel = 0.09, and f_{su} = Ultimate stress capacity of steel = 620.5 MPa.

$$f_s = E_s \varepsilon_s \qquad \text{for} \qquad \varepsilon_s \leq \varepsilon_{sy} \tag{VI-1}$$

$$f_s = f_{sy} \qquad \text{for} \qquad \varepsilon_{sy} < \varepsilon_s \le \varepsilon_{sh} \tag{VI-2}$$

$$f_s = f_{sy} + \left(f_{su} - f_{sy}\right)\sqrt{\frac{\varepsilon_s - \varepsilon_{sh}}{\varepsilon_{su} - \varepsilon_{sh}}} \qquad \text{for} \qquad \varepsilon_{sh} < \varepsilon_s \le \varepsilon_{su} \tag{VI-3}$$

For unconfined concrete, the compressive properties are defined according to the stress-strain (ε_c, σ_c) model proposed initially by (Popovics, 1973) and adopted later by (Mander, Priestley, & Park, 1988):

$$\frac{\sigma_c}{f'_{co}} = \frac{\left(\varepsilon_c/\varepsilon_{co}\right)r}{r - 1 + \left(\varepsilon_c/\varepsilon_{co}\right)^r} \tag{VI-4}$$

r is defined as:

$$r = \frac{E_c}{E_c - \dfrac{f'_{co}}{\varepsilon_{co}}} \tag{VI-5}$$

The curve is assumed to terminate at $\varepsilon_c = 2\varepsilon_{co}$. Confined concrete properties are defined as per the stress-strain model proposed in Chapter IV. It should be noted that the model neglects the contribution of internal steel ties to confinement.

2. *Results and discussion*

The specimens are modeled using (SAP-2000, Version 18). The output results show the variation of the moment capacity *M* of the section as a function of the curvature ϕ. The variation of many different parameters with respect to the curvature ϕ can be observed. These parameters include: the maximum strain in concrete and steel, the neutral axis position, the compression force in concrete and the compression and tensile forces in steel. A close examination of the results show that the majority of the specimens failed when the maximum strain in concrete reached its ultimate value specified in the input concrete material model. For few specimens with low

reinforcement ratio and high confinement levels, failure occurs by rupture of the

longitudinal steel reinforcement before concrete failure. The $M - \phi$ curves of these

specimens are characterized by a brittle drop at the ultimate point (Figure VI-3 to Figure

VI-10).

Figure VI-3 to Figure VI-6 show the $M - \phi$ curves of all the specimens of

section 1000 mm x 300 mm while Figure VI-7 to Figure VI-10 show the same for the

specimens of section 850 *mm* x 350 *mm*. The value of "t_{wrap}" mentioned on each

graph is the thickness of the FRP layer of the confined specimens presented on the same

graph.

Figure VI-11 shows the details of a typical moment-curvature response of a

confined or unconfined RC section. The point of coordinates (ϕ_y, M_y) is the point

where first yield of longitudinal reinforcement occurs while the point (ϕ_u, M_u) is the

point where the section is considered failed.

a) Yield point

An examination of the results shows that ϕ_y is only affected by the section

dimensions and the axial load level, while the confinement level has no noticeable

effect. As expected, ϕ_y increases with increase in the axial load level or with decrease

in the section depth. As for M_y, the results demonstrate a higher M_y in confined

specimens compared to unconfined specimens for all axial load levels. As a result, for

confined specimens, the point of first yield (ϕ_y, M_y) is closer to the peak point of the

first branch of the curve than it is for unconfined specimens. However, when

comparing the value of M_y among confined specimens having the same cross-section,

it can be noticed that varying the confinement level, within the range studied, has no

important effect on M_y.

b) <u>Moment capacity and ultimate curvature</u>

In each of the graphs shown in Figure VI-3 to Figure VI-10, nine $M - \phi$

curves are presented all corresponding to specimens of same cross-section and subject

to the same load level η. Three of these curves are those of all the three unconfined

specimens of this section and subject to this load level η. The six remaining curves are

those of all the six specimens, of the same section and subject to the same axial load,

and confined with an FRP sheet of thickness specified on the graph. Among these six

specimens, three are confined with an external FRP sheet only and three are confined

with FRP sheet and anchors.

(1) <u>Effect of the reinforcement ratio</u>

As can be noticed from Figure VI-3 to Figure VI-10, for all axial load ratios

and confinement levels, increasing the reinforcement ratio from 1% to 1.5% and 2.3%,

causes an increase in the moment capacity and a decrease in the rotation capacity of the

section. However, as previously noticed, some of the confined specimens having a low

reinforcement ratio failed by steel rupture. For some of these specimens, the ultimate

curvature is lower than that of the same specimens reinforced with a higher

reinforcement ratio. For instance, the ultimate curvature of specimen $X2aH - 1.0$ that

failed by steel rupture is smaller than that of specimen $X2aH - 1.5$ despite the fact that

the latter specimen has a higher reinforcement ratio.

(2) Effect of the confinement level

Figure VI-3 to Figure VI-10 also show that the ductility increases with increase in the confinement level, all the other parameters being the same. This can be observed in Figure VI-4(b) where the specimens have dimensions of 1000 *mm* x 300 *mm* and an axial load level $\eta = 0.1$. For $\rho = 1.0\%$, the ultimate ductility of the unconfined specimen $XH1-1.0$ is $\phi_u = 2.1E-05/mm$. When the same specimen is confined with an external FRP sheet of thickness $t_{wrap} = 0.78$ *mm* ($X1H1-1.0$), the ultimate ductility increases to reach $\phi_u = 5.6E-05/mm$. Due to the additional confinement provided by the anchors, and specially the improvement in ductility in the stress-strain curves of anchored specimens compared to their companion unanchored specimens, the ultimate curvature of specimen $X1aH1-1.0$ is $\phi_u = 7.5E-05/mm$ greater than that of specimen $X1H1-1.0$.

The positive effect of the higher confinement level on the ductility can also be observed by comparing the ductility of specimens $X1H1-1.0$ (Figure VI-4a), $X2H1-1.0$ (Figure VI-4b) and $X3H1-1.0$ (Figure VI-4c) that are externally confined specimens differing only by the thickness of the FRP layer. This thickness is 0.78 *mm*, 1.17 *mm* and 1.56 *mm* respectively for specimens $X1H1-1.0$, $X2H1-1.0$ and $X3H1-1.0$. The respective ultimate curvature is: $5.6E-05/mm$, $7.0E-05/mm$ and $8.1E-05/mm$ which proofs the increase in ductility with increase in confinement.

(3) Effect of the axial load level

Figure VI-12 shows the effect of the axial load level on the $M-\phi$ response. The specimens shown are identical specimens externally confined with FRP that differ in

185

the axial load level where $X1H - 2.3$, $X1H1 - 2.3$, $X1H2 - 2.3$ and $X1H3 - 2.3$ are subjected to respective axial load ratios $\eta = 0, 0.1, 0.15$ and 0.2. Figure VI-12 shows that increasing the axial load ratio from $\eta = 0$ to $\eta = 0.2$ causes an increase in the moment capacity of the section and a decrease in its rotation capacity.

(4) Ductility ratio

To better illustrate the effect of different design parameters on the sections response, the ductility ratio ϕ_u/ϕ_y is quantified for all the specimens. Results of selected specimens are shown in Figure VI-13 and Figure VI-14. Figure VI-13(a) illustrates the variation of ϕ_u/ϕ_y in function of the reinforcement ratio ρ for all the unconfined specimens of series X. Figure VI-13(b) shows the same for all the specimens of series X confined with an external FRP sheet of thickness $t_{wrap} = 0.78$ *mm*. The results are in support of the conclusion stated previously, that for both confined and unconfined specimens, the ductility decreases with increase in load ratio and reinforcement ratio. Figure VI-14(a) and (b) show the effect of the confinement level on the ductility for both anchored and unanchored specimens for sections of series X having $\rho = 1.5\%$. The value of ϕ_u/ϕ_y for the anchored specimen $X3aH - 1.5$ having $\rho = 1.5\%$, $t_{wrap} = 1.56$ *mm* and $\eta = 0$ is not shown in this figure given that this section failed by tensile steel rupture. Figure VI-14 clearly shows that, for both anchored and unanchored specimens, the ductility increases with increase in the confinement level at all load ratios.

C. Lateral load-drift ($V - \delta$) curves

In this section, the $M - \phi$ curves presented previously are used to generate the $V - \delta$ curves of a cantilever column of length $L = 2,000 \ mm$. The column is subjected to a constant concentric axial load P and an increasing lateral load V applied at the column free end (Figure VI-15) producing an increasing lateral displacement δ. The $V - \delta$ curves are observed as the envelope curves of the lateral load-drift response of columns subject to a constant axial load and cyclic lateral loading that simulate a seismic loading.

Similar to what was done in the section "Nonlinear Flexural Analysis", different column section dimensions, axial load level, reinforcement ratio and confinement properties are studied. The column under consideration is either unconfined or confined in its plastic hinge region (Figure VI-16). It should be noted that the plastic hinge region is the zone of the column that is mostly damaged during an earthquake. Previous experimental and numerical investigations have shown that, with increase in the applied lateral load, inelastic deformations develop in the region of the column near the support called the plastic hinge region. In this study, the confinement of this zone is either ensured by external FRP sheets only or by a combination of FRP sheets and anchors. The height of the confined region at the column end is selected such that it exceeds the plastic hinge length of the column. As will be shown in section "*D*" of this chapter, expressions of the plastic hinge length are available in the literature. However, to the best of the author's knowledge, no expression has been proposed for FRP-confined specimens of rectangular cross-section. A conservative estimate of the value of the plastic hinge length is *0.75 H*. Two different columns sections are considered: 1000 *mm* x 300 *mm* and 850 *mm* x 350 *mm* corresponding to a maximum

plastic hinge length of 750 *mm*. Accordingly, the length of the confinement region is set to 850 *mm* (Figure VI-16). The columns reinforcement details, axial load levels and confined region properties are those considered in the section "Nonlinear Flexural Analysis".

The model proposed by (Harajli, 2008) is used to generate these curves. The model idealizes the curvature distribution as shown in Figure VI-17. Before first yield of longitudinal steel ($M \leq M_y$), the curvature distribution is linear along the column height. When M exceeds M_y, a plastic hinge region of length L_p forms; the curvature in this region is assumed constant. The lateral drift δ is computed using the following two equations:

$$\delta = \frac{\phi L^2}{3} \text{ for } M \leq M_y \tag{VI-6}$$

$$\delta = \phi L_p \left(L - \frac{L_p}{2} \right) + \frac{\phi_y \left(L - L_p \right)^2}{3} \quad \text{for} \quad M \geq M_y \tag{VI-7}$$

In these equations, ϕ is the total curvature at the column basis and L_p is expressed as:

$$L_p = L \left(1 - \frac{M_y}{M} \right) \tag{VI-8}$$

After getting the $M - \phi$ curve for the section at the column basis, δ is obtained from Eqs. (VI-6) and (VI-7). Neglecting the $P - \delta$ effect, the moment M at the column basis is assumed to be solely produced by the lateral load V such that

$$M = V \times L \tag{VI-9}$$

Using the $M - \phi$ curves generated in the section "Nonlinear Flexural Analysis" and Eqs. (VI-6) to (V-9), the $V - \delta$ curves can be generated. Figure VI-18(a)

and (b) plots the lateral load versus the drift ratio of selected columns where the drift ratio is equal to δ/L. The specimens are of cross-section 850 *mm* x 350 *mm* and subjected to an axial load level $\eta = 0.2$. The curves shown in Figure VI-18(a) are for the unconfined specimens and the specimens confined with external FRP sheets only while Figure VI-18(b) show the same for the unconfined specimens and the specimens confined with a combination of FRP sheets and anchors. It can be observed from both graphs, that higher confinement levels lead to higher ductility levels, similar to what was observed when studying the $M - \phi$ curves. However, in the lateral load - drift ratio curves, the ductility level does not seem to be affected by the reinforcement ratio as was the case for $M - \phi$ curves. This is mainly attributed to the fact that, as the reinforcement ratio increases, the moment increases in the first and second branch of the curve increase. However, the increase is more important in the second branch of the curve. Accordingly, for a given curvature value, M_y/M gets smaller as the reinforcement ratio increases, resulting in an increase in L_p and accordingly in the lateral drift δ.

D. Existing Plastic Hinge Model

The approach adopted previously to draw the $V - \delta$ curves considers that the plastic hinge length increases with increase in the applied moment up to a maximum value. Studies available in the literature have proposed expressions to predict a unique value of the plastic hinge length (the maximum value) which was mainly used to get the ultimate drift δ_u. Most of these expressions are for unconfined RC columns and fewer are for confined columns.

For columns confined with FRP sheets in the plastic hinge region, early studies (Seible, Priestley, Hegemier, & Innamorato, 1997; Monti, Nisticò, & Santini, 2001) adopted the expression proposed by (Paulay & Priestley, 1992) for unconfined RC columns. (Binici B. , 2008) and (Binici & Mosalam, 2007) also used an expression for unconfined RC columns that was proposed by (Lu, Gu, & Guan, 2005) modified from that proposed by (Priestley & Park, Strength and Ductility of Concrete Bridge Columns under Seismic Loading, 1987). (Zou, Teng, De Lorenzis, & Xia, 2007; Eslami & Ronagh, 2013) and (Ghatte, Comert, Demir, & Ilki, 2016) considered a plastic hinge length equal to half the section depth. All these expressions do not account explicitly for the confinement provided by the FRP sheets.

(Elsanadedy & Haroun, 2005) and (Juntanalikit, Jirawattanasomkul, & Pimanmas, 2016) used the following expression proposed by (Priestley, Seible, & Calvi, 1996) for confined specimens:

$$L_p = g + 0.044 f_{sy} d_b \qquad (f_{sy} \text{ in } MPa) \qquad\qquad \text{(VI-10)}$$

Recent studies investigated the effect of external confinement with FRP sheets on the length of the plastic hinge region and proposed expressions of L_p that take into account the confinement level.

(Gu, Wu, Wu, & Wu, 2012) used the results of experimental studies and analytical investigations to develop an expression of the plastic hinge length in FRP-confined circular columns. They found that for low confinement levels ($\lambda_l < 0.1$) the plastic hinge length increases with increase in confinement, while after a confinement level of 0.1, the effect of confinement on the plastic hinge length becomes negative. λ_l is the confinement ratio defined in circular sections as:

$$\lambda_l = \frac{f_l}{f'_{co}} = \frac{2 E_{frp} t_{wrap} \varepsilon_{fu}}{D f'_{co}} \tag{VI-11}$$

In this equation, f_l is the confinement pressure. This f_l differs from that defined in

Eq. (II-9) by the fact that $\varepsilon_{h,rup}$ in Eq. (II-9) is the experimental hoop rupture strain

while ε_{fu} in Eq. (VI-11) is the rupture strain obtained from coupon test. Their study

lead to the following expression of L_p

$$L_p = 0.022 f_{sy} d_b + (0.59 - 2.30\lambda_l + 2.28\lambda_l^2) L \quad \text{for } 0.1 \le \lambda_l < 0.5 \tag{VI-12}$$

In which L is the column shear span, d_b is the diameter of the longitudinal reinforcement

and f_{sy} in MPa.

For $\lambda_l < 0.1$, the study suggested that L_p increases linearly with respect to λ_l

starting from $L_p = 0.08L + 0.022 f_{sy} d_b$ at $\lambda_l = 0$ (Priestley, Seible, & Calvi, 1996) and

joining the curve drawn from Eq. (VI-12) at $\lambda_l = 0.1$. This increase can be expressed as:

$$L_p = 0.022 f_{sy} d_b + (0.08 + 3.028\lambda_l) L \quad \text{for } 0 \le \lambda_l < 0.1 \tag{VI-13}$$

(Mortezaei & Ronagh, 2012) used the nonlinear finite element method to

perform parametric studies on FRP strengthened reinforced concrete (RC) columns of

square cross-section subjected to far-fault and near-fault earthquakes. Based on their

investigation, they proposed two different equations for near-fault and far-fault

earthquakes which represent modifications of the expressions proposed by (Bae &

Bayrak, 2008) for unconfined RC columns. Their expressions accounted for the effect

of axial load, height to depth ratio, and reinforcement ratio.

(Youssf, ElGawady, & Mills, 2015) performed a parametric study using the

Finite Element (FE) software (LS-DYNA) to investigate the effect of FRP-confinement

on the plastic hinge length L_p of columns of circular cross-sections. The study concluded that increasing the confinement ratio increases the plastic hinge length at a more important rate for low confinement levels, $\lambda_l < 0.4$. λ_l is defined as per Eq. (VI-11). The following equation, incorporating the effect of the confinement level was proposed to compute the plastic hinge length:

$$L_p = 0.8\,\lambda_l\,L + 0.022\,f_{sy}\,d_b \tag{VI-14}$$

This expression was later adopted by (Parghi & Alam, 2016).

(Jiang, Wu, & Wu, 2014) focused on the plastic hinge length of FRP-confined square RC columns. The study suggested modifying the expression proposed by (Gu, Wu, Wu, & Wu, 2012) to account for the reduction of the confinement effect in square cross-sections using the shape factor $k_s = (2r/b)^{0.72}$. The proposed expression is defined as:

$$L_p = L_{po} + \left(\frac{2r}{b}\right)^{0.72} L_{pc} \tag{VI-15}$$

Where

$$L_{po} = 0.08L + 0.022 f_{sy}\, d_b \tag{VI-16}$$

and

$$L_{pc} = \begin{cases} 3.028\lambda_l\,L & for\ 0 \le \lambda_l < 0.1 \\ (0.51 - 2.30\lambda_l + 2.28\lambda_l^{\,2}) & for\ 0.1 \le \lambda_l < 0.5 \end{cases} \tag{VI-17}$$

For square sections, λ_l is defined as per Eq. (VI-11) by substituting D by b. For circular sections, $2r/b = 1$ and Eq. (VI-15) reduces to Eqs. (VI-12) and (VI-14).

In a manner similar to (Gu, Wu, Wu, & Wu, 2012) and (Jiang, Wu, & Wu, 2014), (Yuan, Wu, & Li, 2016) suggested that the plastic hinge length is the sum of two components with one of them reflecting the contribution of the FRP confinement.

$$L_p = L_{po} + L'_{pc} \tag{VI-18}$$

Where L_{po} is defined according to Eq. (VI-16) and L'_{pc}, takes into account the confinement effect.

Two different expressions are adopted to define L'_{pc} with the following expression being more accurate when compared to experimental results

$$L'_{pc} = 0.11 \left(\frac{2r}{b} + 0.2 \right)^{0.14} \left(e^{-1.2\lambda_l} - e^{-30\lambda_l} \right) L \tag{VI-19}$$

This equation is applicable to both circular and square cross-sections.

To the best of the author's knowledge, no expression was previously proposed to compute the plastic hinge length of FRP-confined specimens of rectangular cross-section.

Table VI-1 - Values of the design parameters investigated

$h \times b$ (*mm* x *mm*)	1000 x 300, 850 x 350
t_{wrap} (*mm*)	0, 0.78, 1.17, 1.56
$\rho\,(\%)$	1.0, 1.5, 2.3
η	0, 0.1, 0.15, 0.2
Anchors	Presence or absence

Table VI-2 - Summary of sections details for section 1000 *mm* x 300 *mm*, $\eta = 0$

Specimen	h x b $(mm \times mm)$	η	t_{wrap} (mm)	Anchors	ρ (%)
$XH-1.0$					1.0
$XH-1.5$			0	0	1.5
$XH-2.3$					2.3
$X1H-1.0$					1.0
$X1H-1.5$				0	1.5
$X1H-2.3$			0.78		2.3
$X1aH-1.0$					1.0
$X1aH-1.5$				1	1.5
$X1aH-2.3$					2.3
$X2H-1.0$					1.0
$X2H-1.5$	1000 x 300	0		0	1.5
$X2H-2.3$			1.17		2.3
$X2aH-1.0$					1.0
$X2aH-1.5$				1	1.5
$X2aH-2.3$					2.3
$X3H-1.0$					1.0
$X3H-1.5$				0	1.5
$X3H-2.3$			1.56		2.3
$X3aH-1.0$					1.0
$X3aH-1.5$				1	1.5
$X3aH-2.3$					2.3

Table VI-3 - Summary of sections details for section 1000 *mm* x 300 *mm*, $\eta = 0.1$

Specimen	h x b $(mm \times mm)$	η	t_{wrap} (mm)	Anchors	ρ (%)
$XH1-1.0$	1000 x 300	0.1	0	0	1.0
$XH1-1.5$					1.5
$XH1-2.3$					2.3
$X1H1-1.0$			0.78	0	1.0
$X1H1-1.5$					1.5
$X1H1-2.3$					2.3
$X1aH1-1.0$				1	1.0
$X1aH1-1.5$					1.5
$X1aH1-2.3$					2.3
$X2H1-1.0$			1.17	0	1.0
$X2H1-1.5$					1.5
$X2H1-2.3$					2.3
$X2aH1-1.0$				1	1.0
$X2aH1-1.5$					1.5
$X2aH1-2.3$					2.3
$X3H1-1.0$			1.56	0	1.0
$X3H1-1.5$					1.5
$X3H1-2.3$					2.3
$X3aH1-1.0$				1	1.0
$X3aH1-1.5$					1.5
$X3aH1-2.3$					2.3

Table VI-4 - Summary of sections details for section 1000 mm x 300 mm, $\eta = 0.15$

Specimen	$h \times b$ $(mm \times mm)$	η	t_{wrap} (mm)	Anchors	ρ (%)
$XH2-1.0$					1.0
$XH2-1.5$			0	0	1.5
$XH2-2.3$					2.3
$X1H2-1.0$					1.0
$X1H2-1.5$				0	1.5
$X1H2-2.3$			0.78		2.3
$X1aH2-1.0$					1.0
$X1aH2-1.5$				1	1.5
$X1aH2-2.3$					2.3
$X2H2-1.0$					1.0
$X2H2-1.5$	1000 x 300	0.15		0	1.5
$X2H2-2.3$					2.3
$X2aH2-1.0$			1.17		1.0
$X2aH2-1.5$				1	1.5
$X2aH2-2.3$					2.3
$X3H2-1.0$					1.0
$X3H2-1.5$				0	1.5
$X3H2-2.3$					2.3
$X3aH2-1.0$			1.56		1.0
$X3aH2-1.5$				1	1.5
$X3aH2-2.3$					2.3

Table VI-5 - Summary of sections details for section 1000 mm x 300 mm, $\eta = 0.2$

Specimen	$h \times b$ $(mm \times mm)$	η	t_{wrap} (mm)	Anchors	ρ (%)
$XH3-1.0$					1.0
$XH3-1.5$			0	0	1.5
$XH3-2.3$					2.3
$X1H3-1.0$					1.0
$X1H3-1.5$				0	1.5
$X1H3-2.3$			0.78		2.3
$X1aH3-1.0$					1.0
$X1aH3-1.5$				1	1.5
$X1aH3-2.3$					2.3
$X2H3-1.0$					1.0
$X2H3-1.5$	1000 x 300	0.2		0	1.5
$X2H3-2.3$					2.3
$X2aH3-1.0$			1.17		1.0
$X2aH3-1.5$				1	1.5
$X2aH3-2.3$					2.3
$X3H3-1.0$					1.0
$X3H3-1.5$				0	1.5
$X3H3-2.3$					2.3
$X3aH3-1.0$			1.56		1.0
$X3aH3-1.5$				1	1.5
$X3aH3-2.3$					2.3

Figure VI-1 - Distribution of the longitudinal reinforcement in the two sections
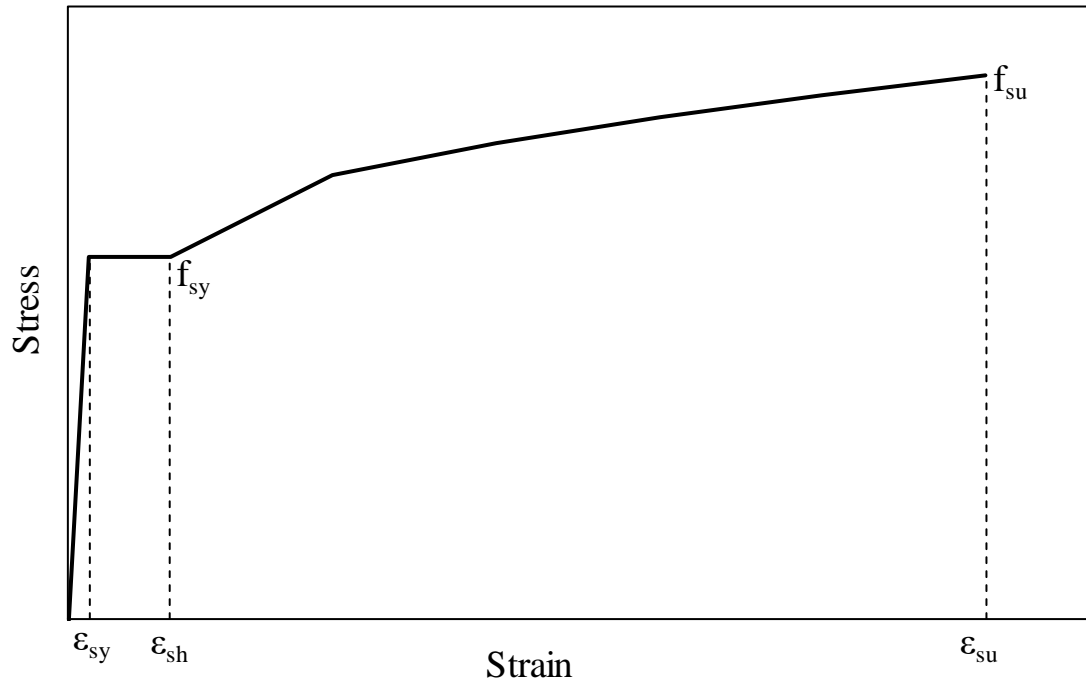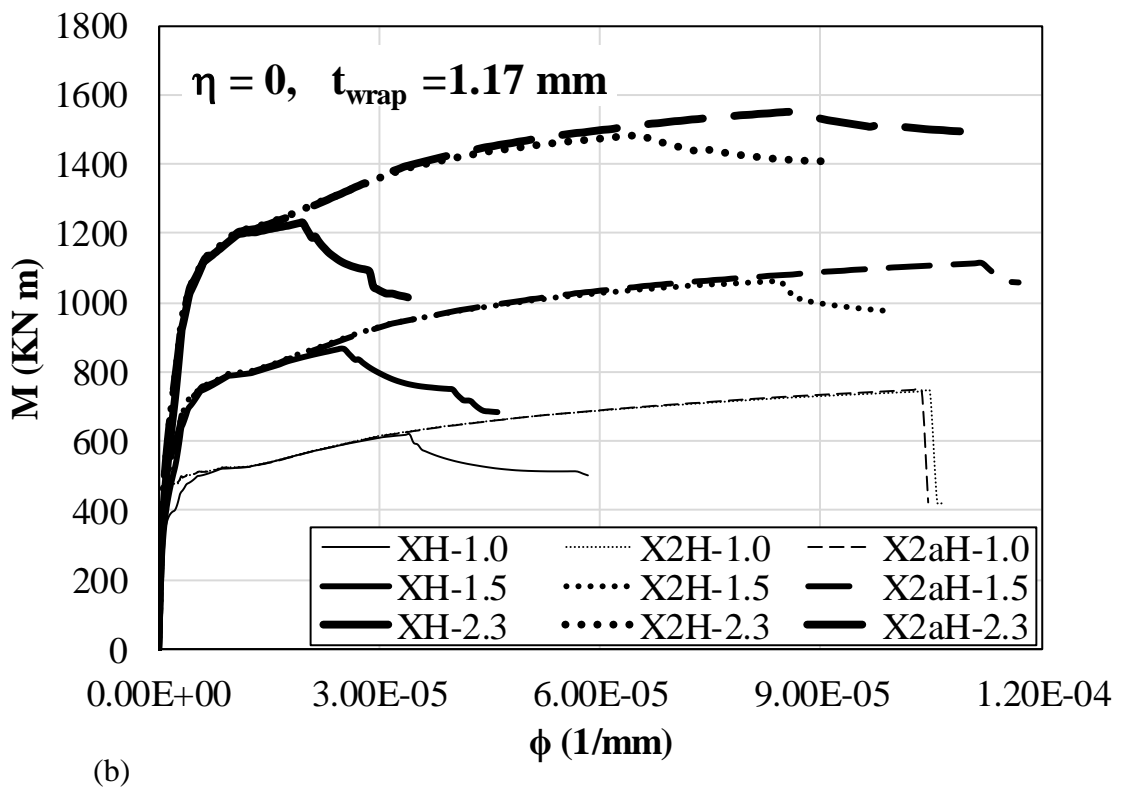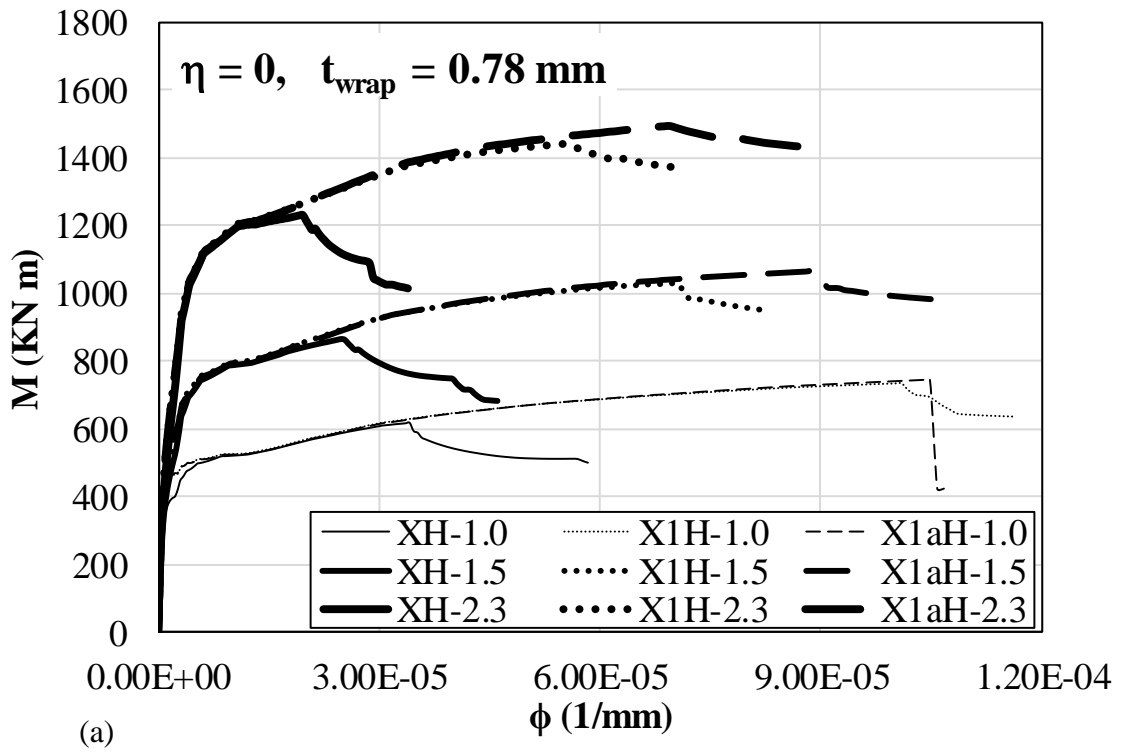(1000 *mm* x 300 *mm* and 850 *mm* x 350 *mm*)
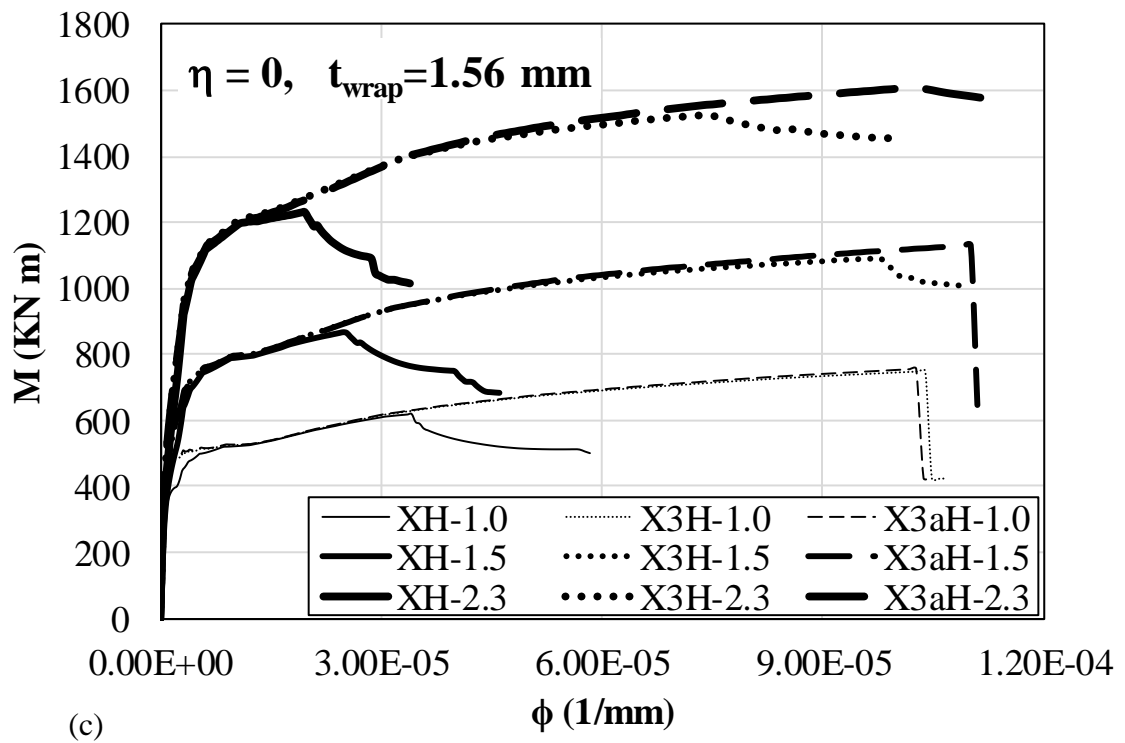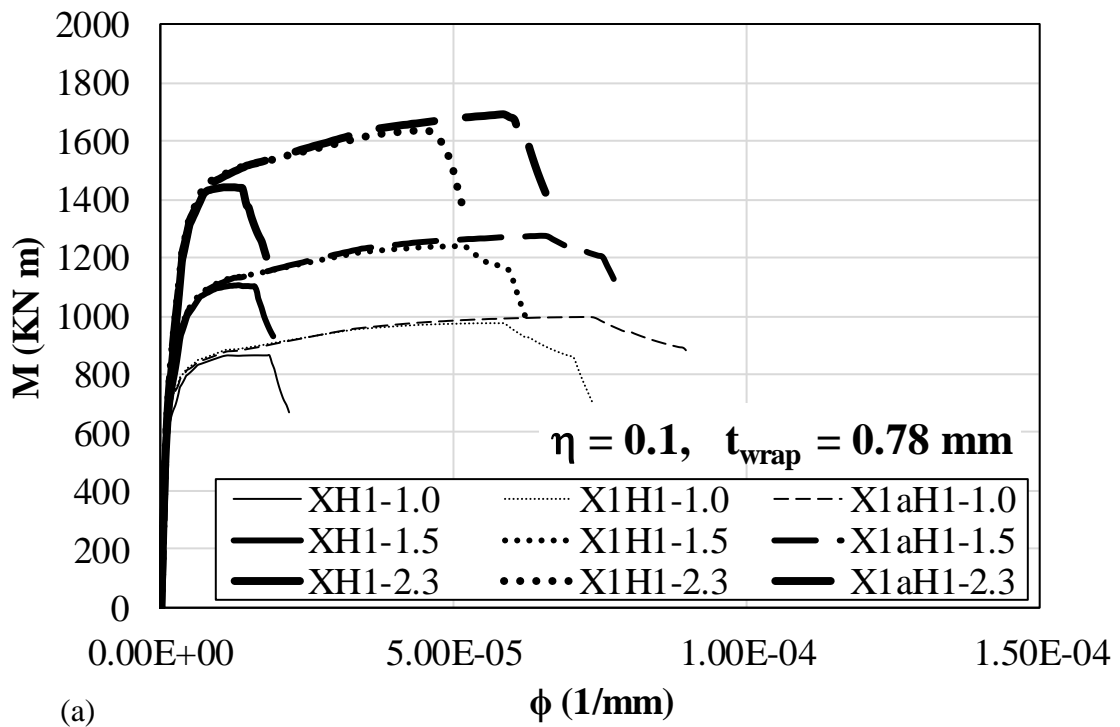
Figure VI-2 - Constitutive stress-strain model of steel

(a)
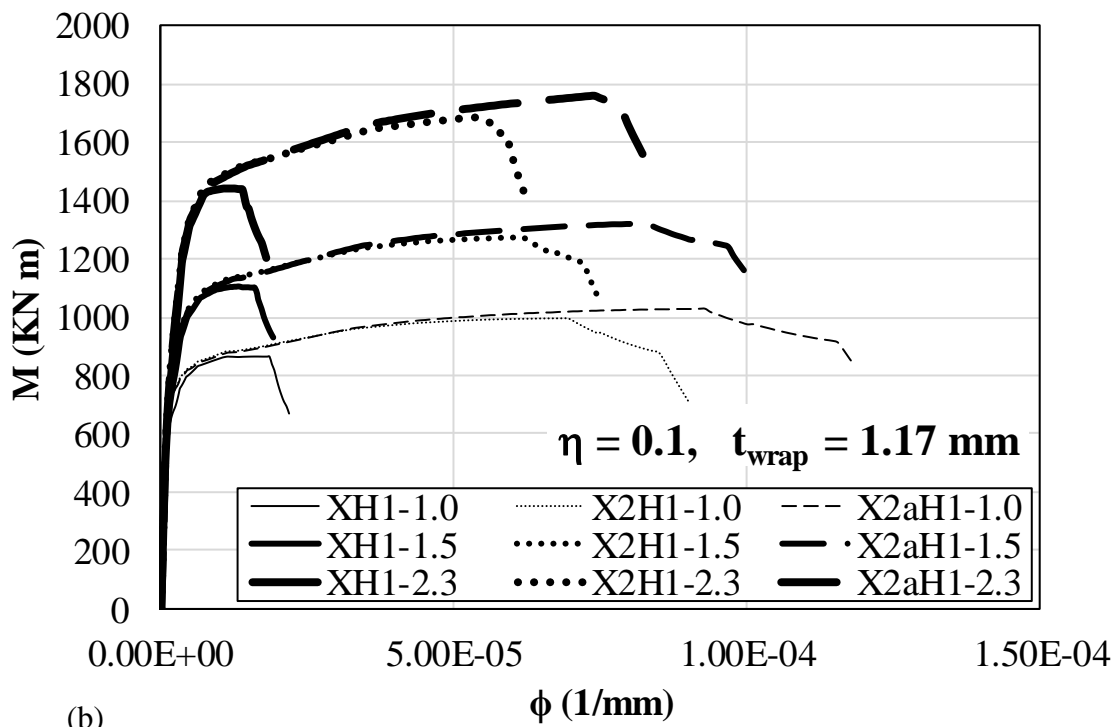

(b)

201

Figure VI-3 - $M - \phi$ curves for the specimens of dimensions 1000 *mm* x 300 *mm* and $\eta = 0$

(a)

(b)

Figure VI-4 - $M - \phi$ curves for the specimens of dimensions 1000 *mm* x 300 *mm* and $\eta = 0.1$

(a)

(b)
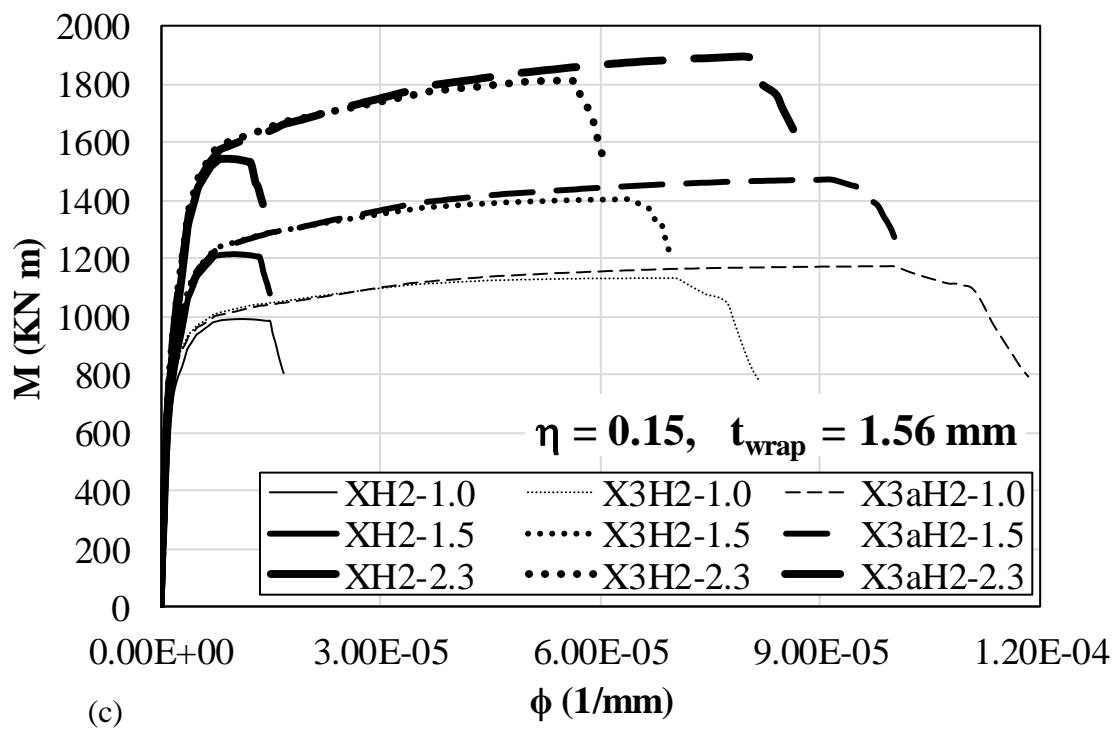
Figure VI-5 - $M - \phi$ curves for the specimens of dimensions 1000 *mm* x 300 *mm* and $\eta = 0.15$
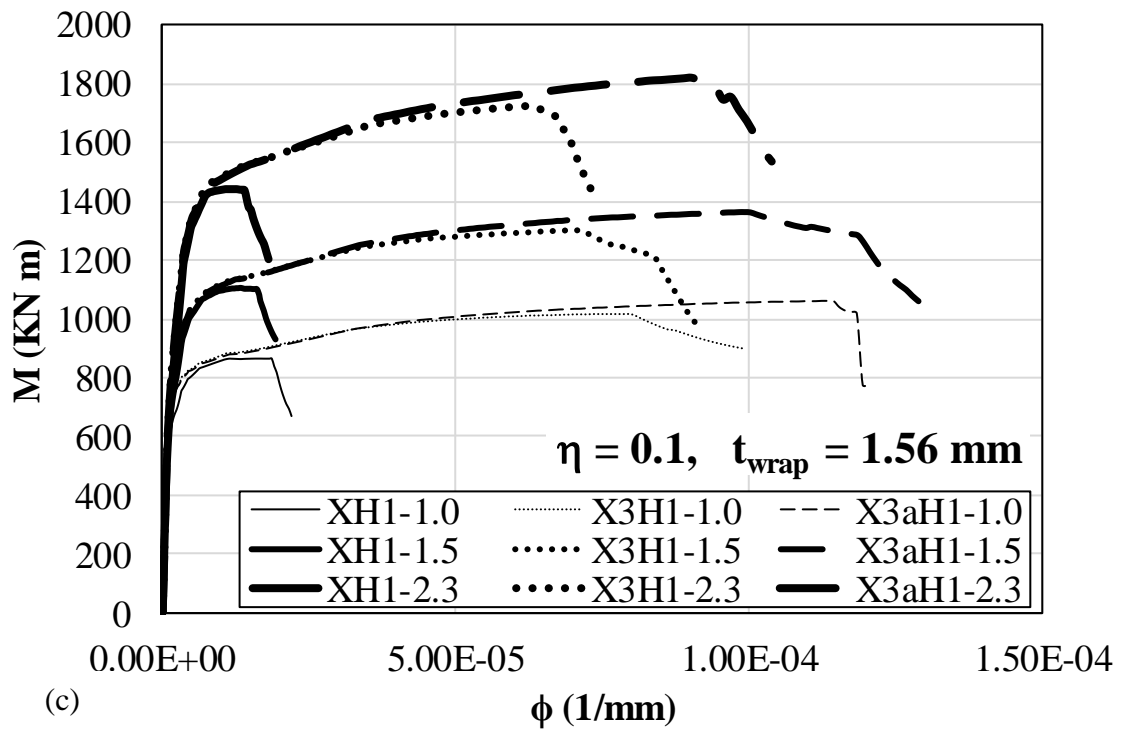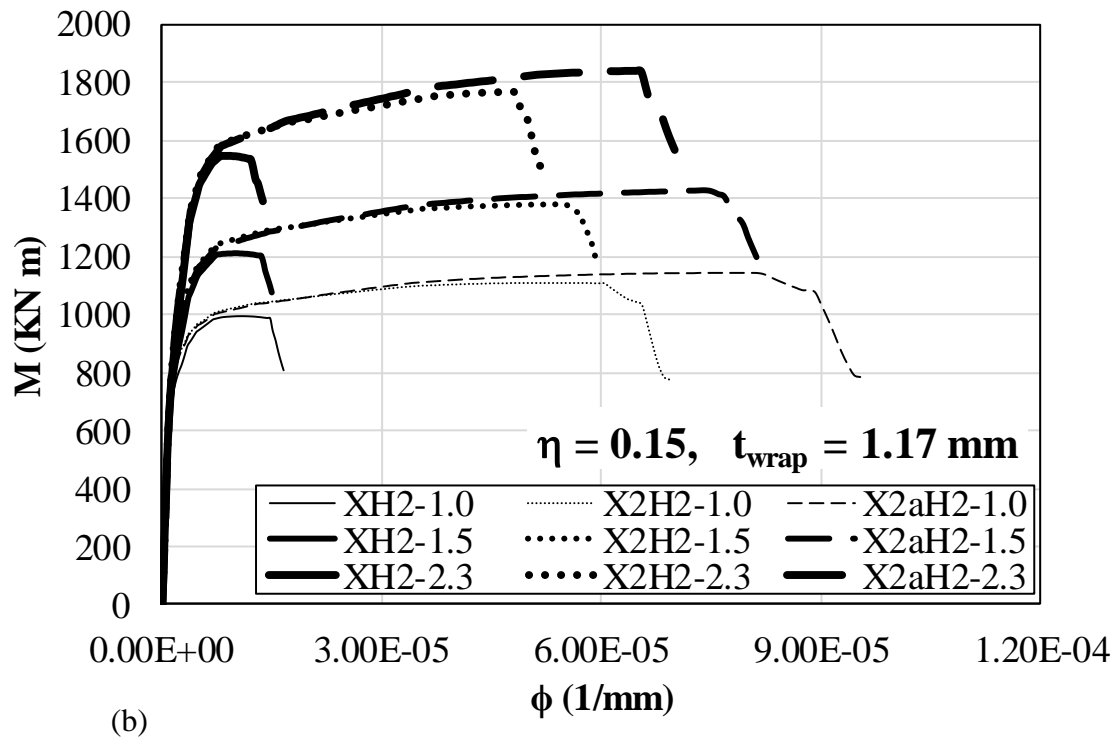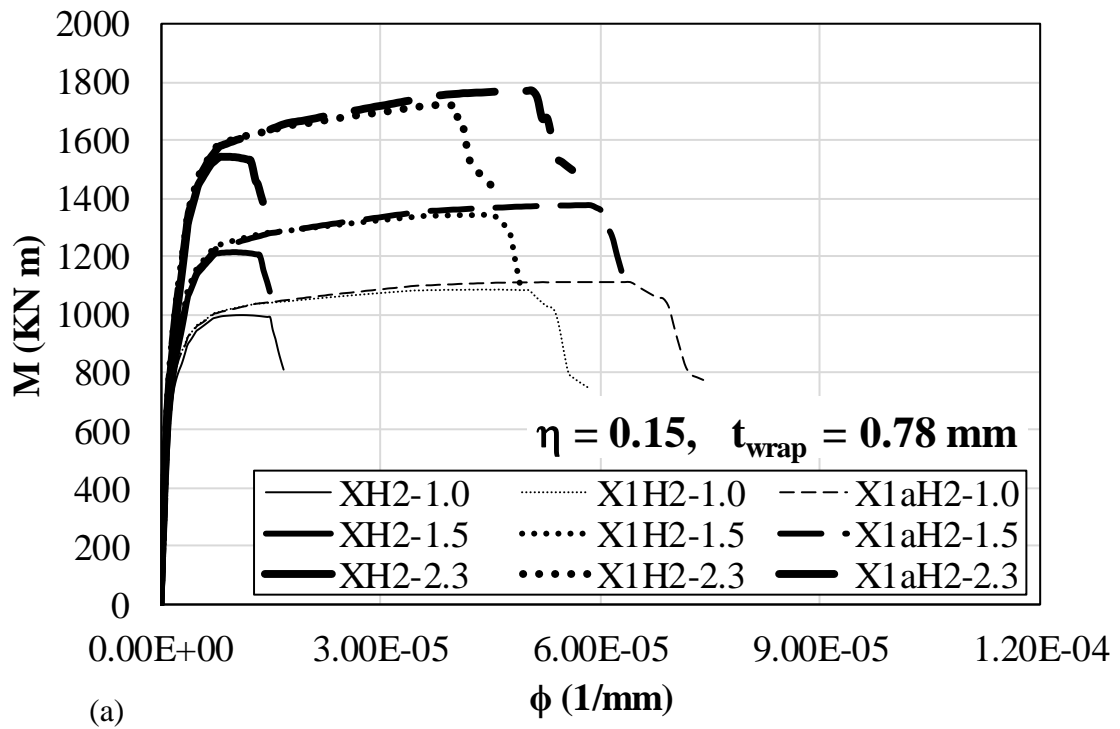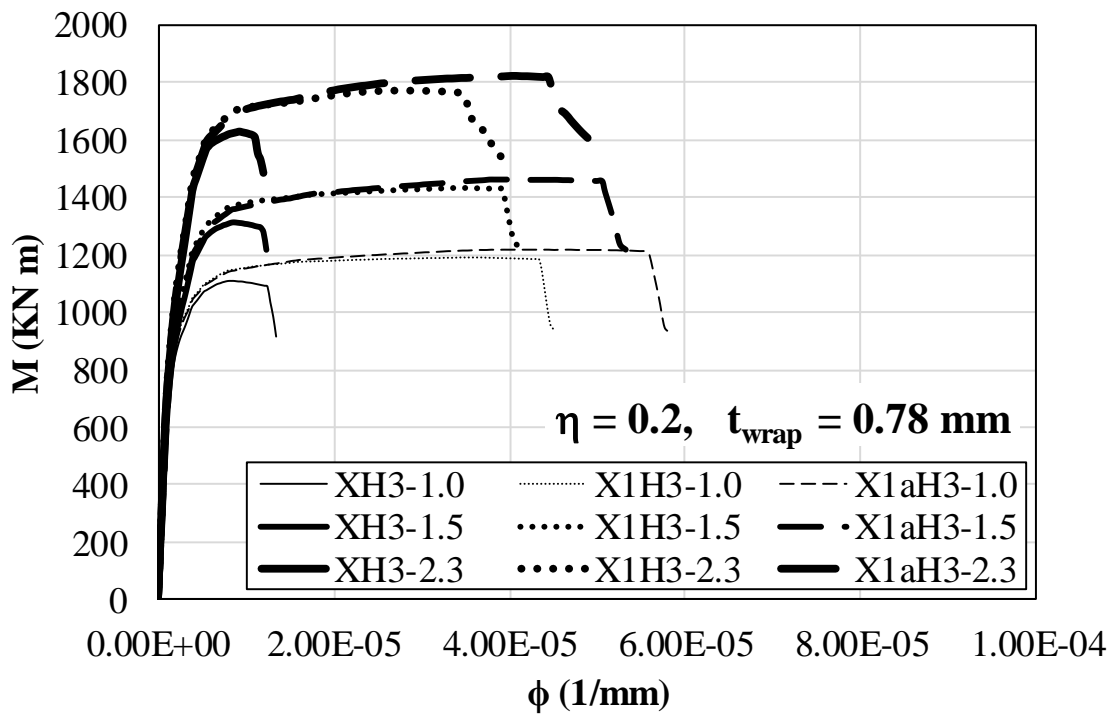
(a)
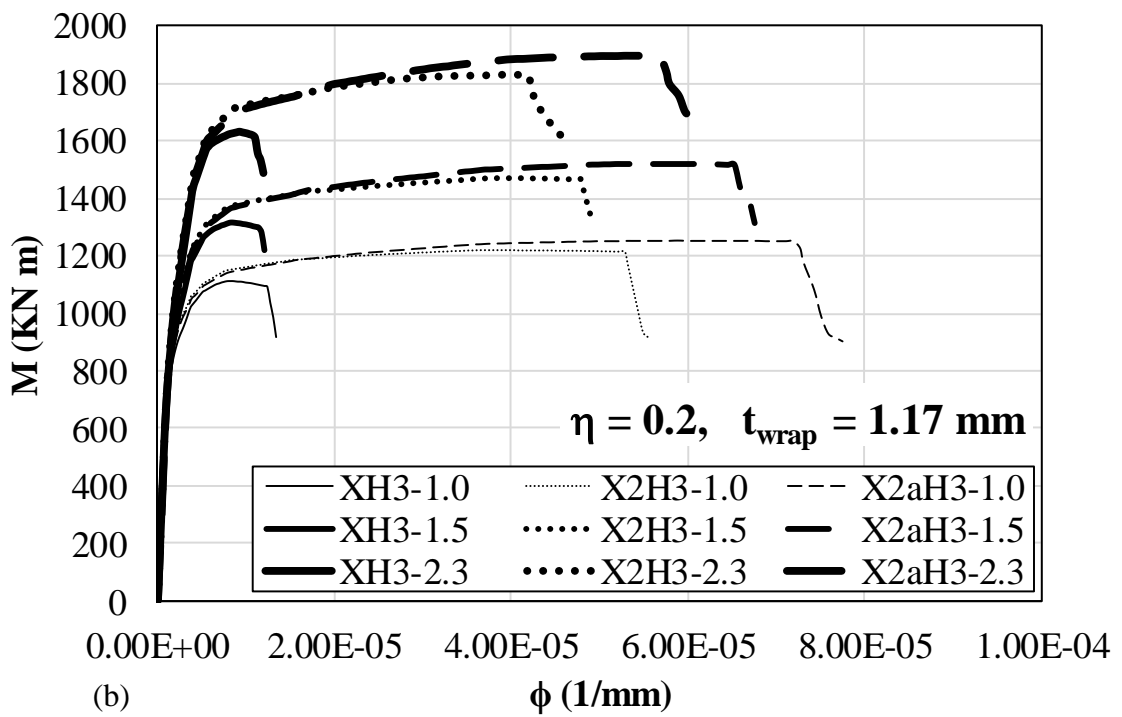
(b)
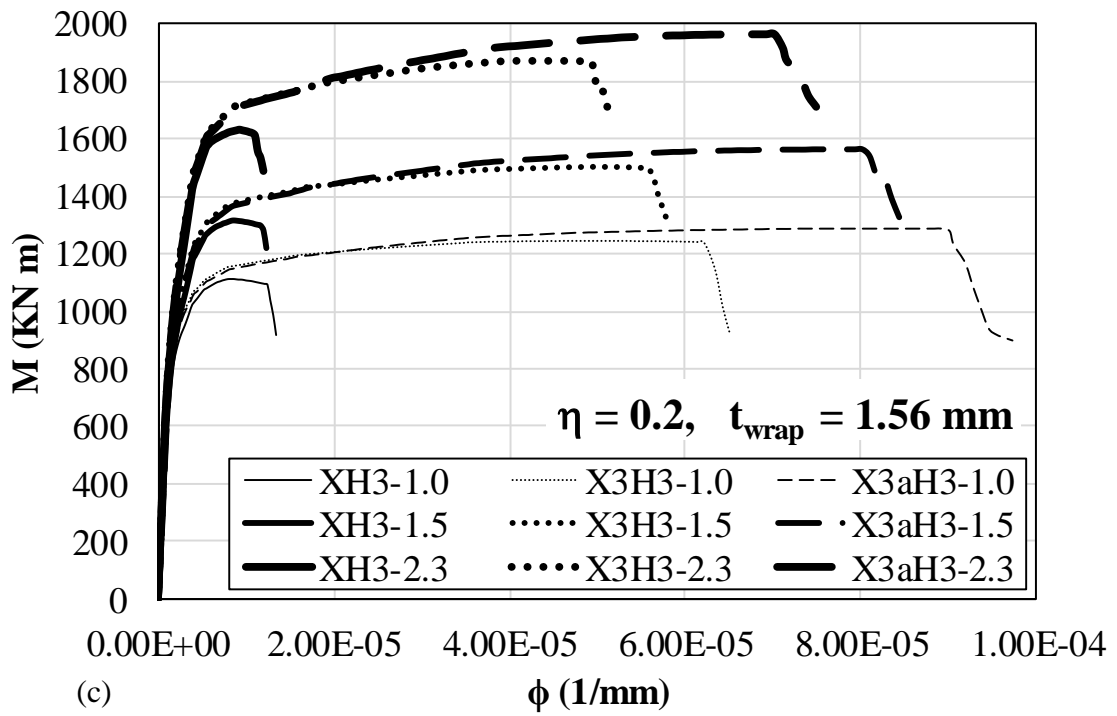
Figure VI-6 - $M - \phi$ curves for the specimens of dimensions 1000 *mm* x 300 *mm* and $\eta = 0.2$

(a)

(b)
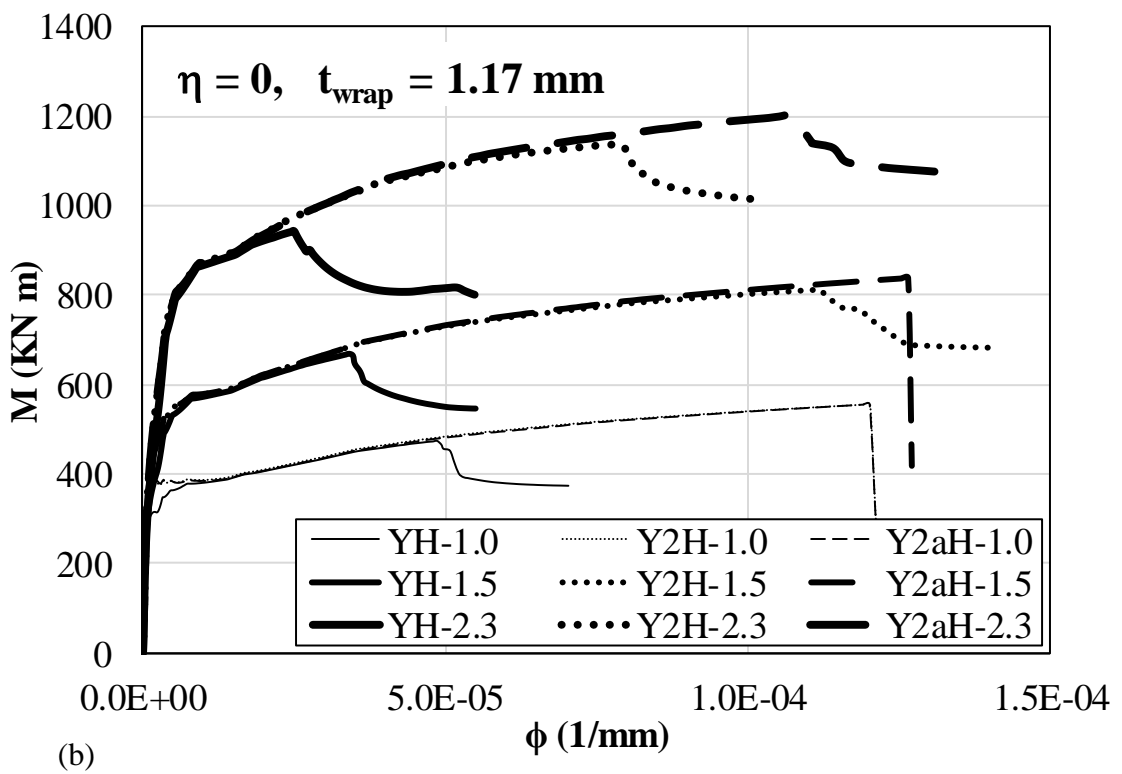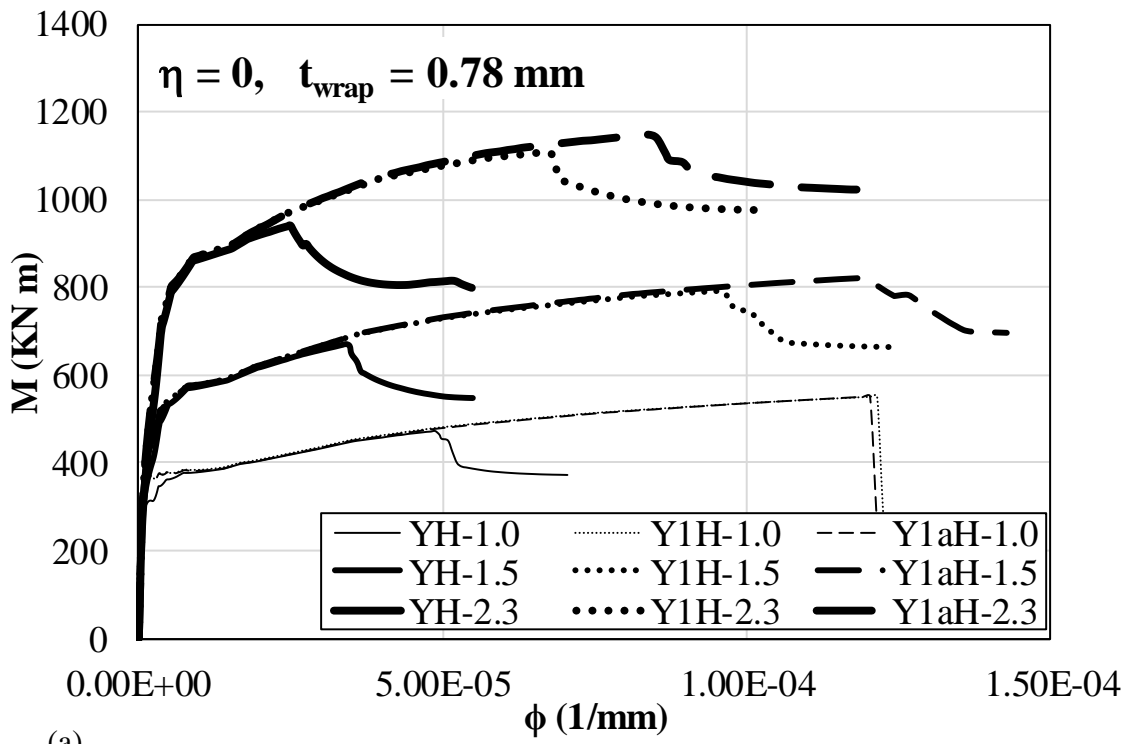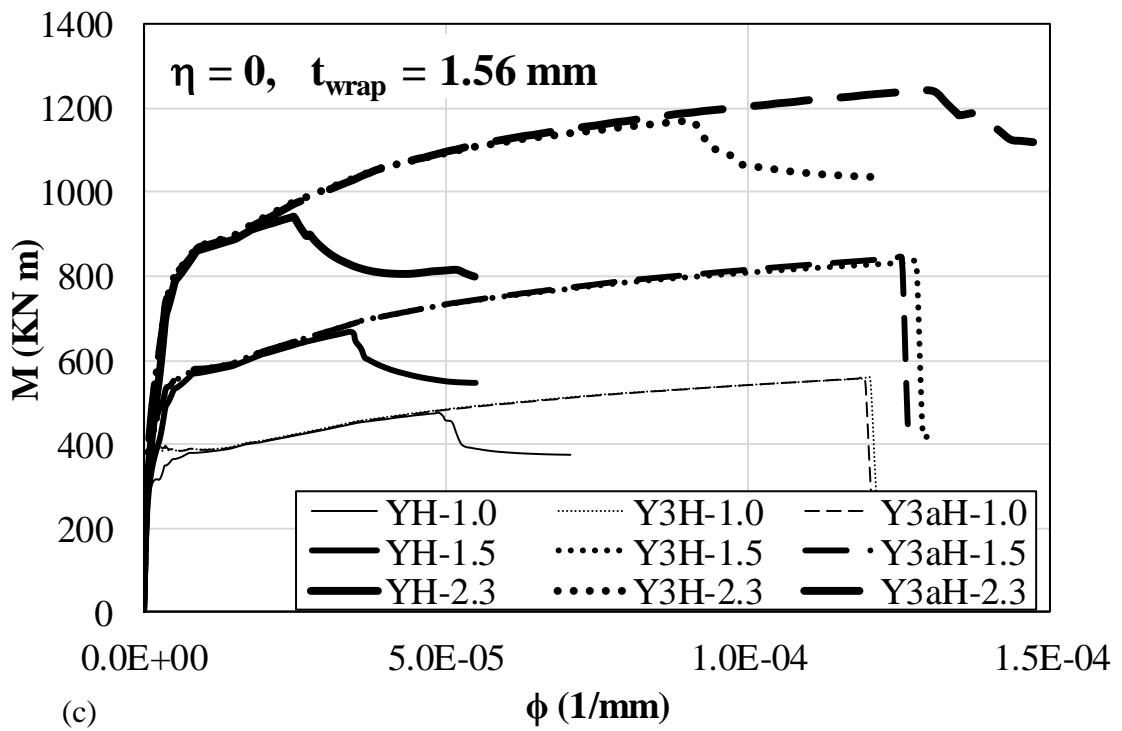
Figure VI-7 - $M - \phi$ curves for the specimens of dimensions 850 *mm* x 350 *mm* and $\eta = 0$

(a)

(b)

$\eta = 0.1, \quad t_{wrap} = 1.56 \ mm$

—— YH1-1.0	·········· Y3H1-1.0	- - - - Y3aH1-1.0
—— YH1-1.5	•••••• Y3H1-1.5	— • Y3aH1-1.5
—— YH1-2.3	••••• Y3H1-2.3	—— Y3aH1-2.3

(c)
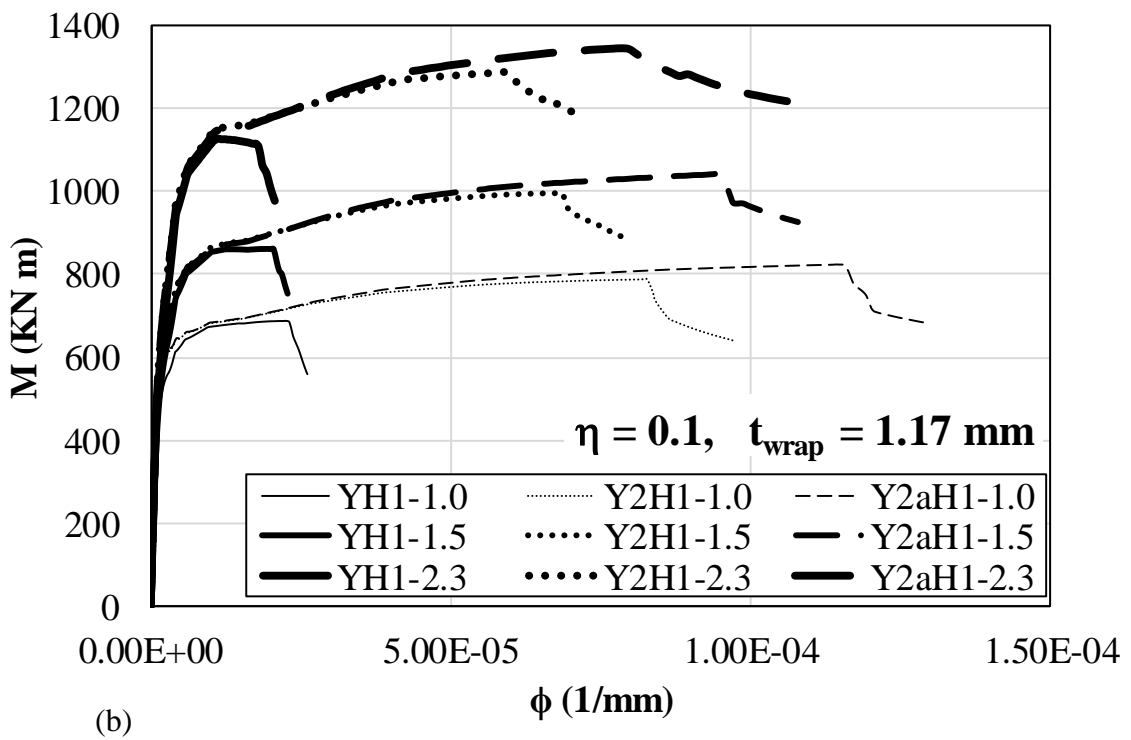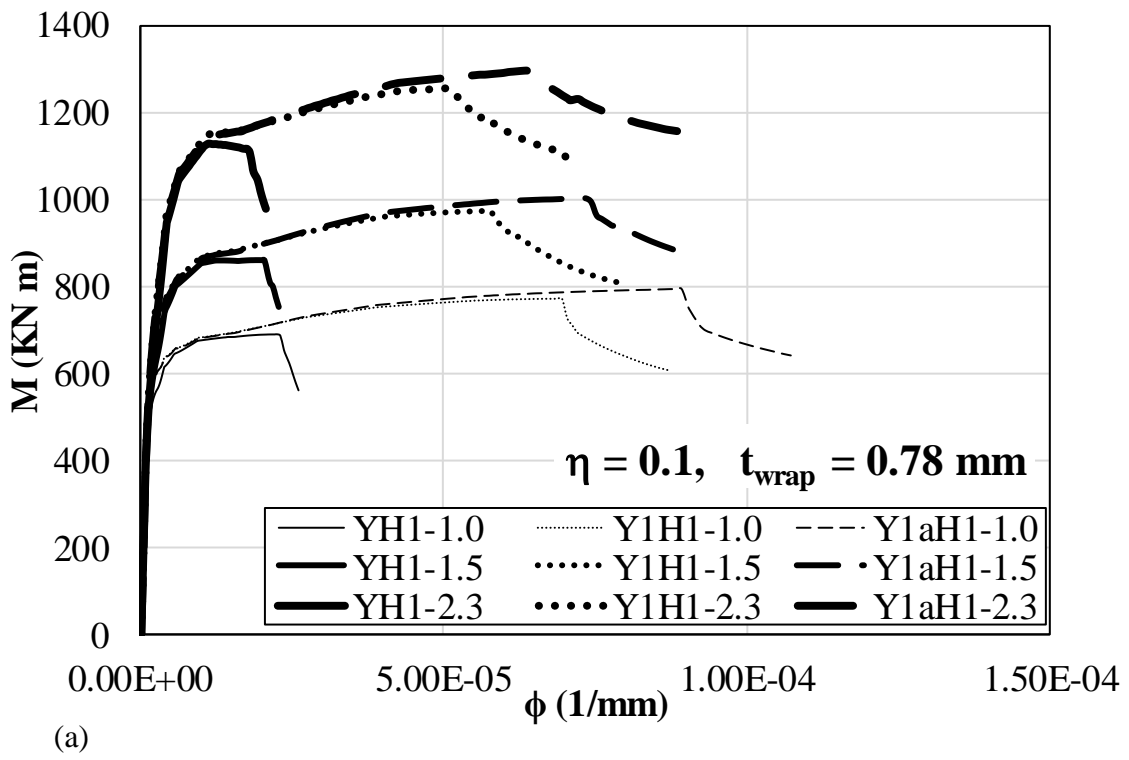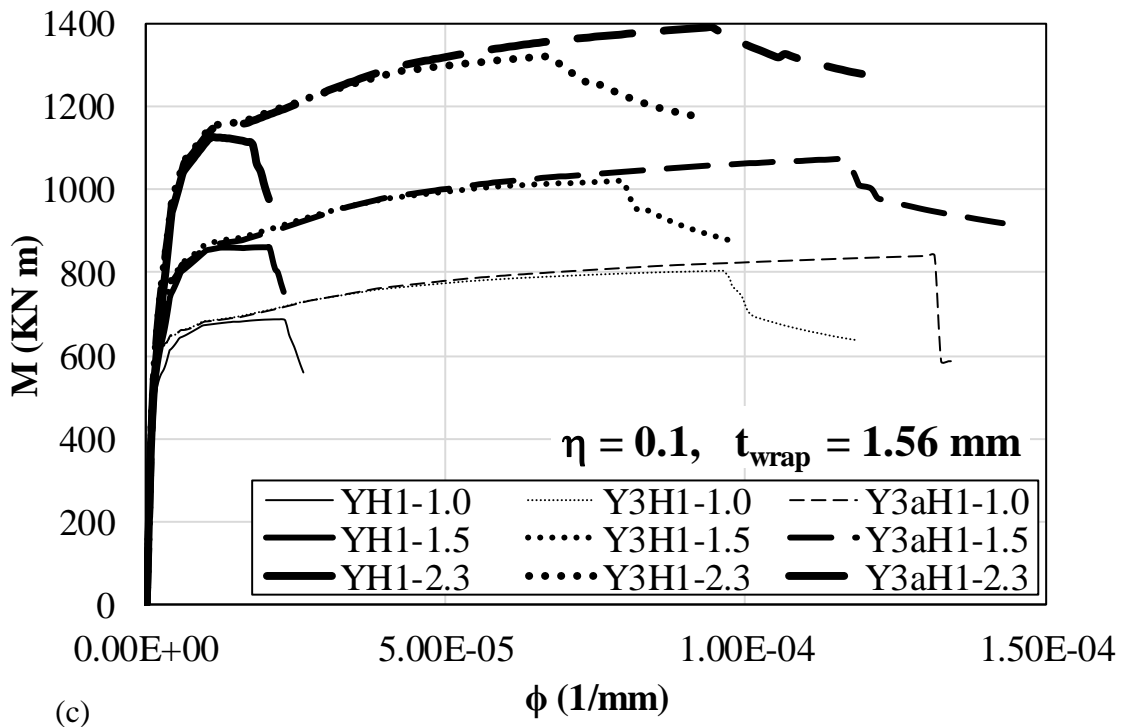
Figure VI-8 - $M - \phi$ curves for the specimens of dimensions 850 *mm* x 350 *mm* and $\eta = 0.1$

$\eta = 0.15$, $t_{wrap} = 0.78$ mm

(a)

$\eta = 0.15$, $t_{wrap} = 1.17$ mm

(b)

213
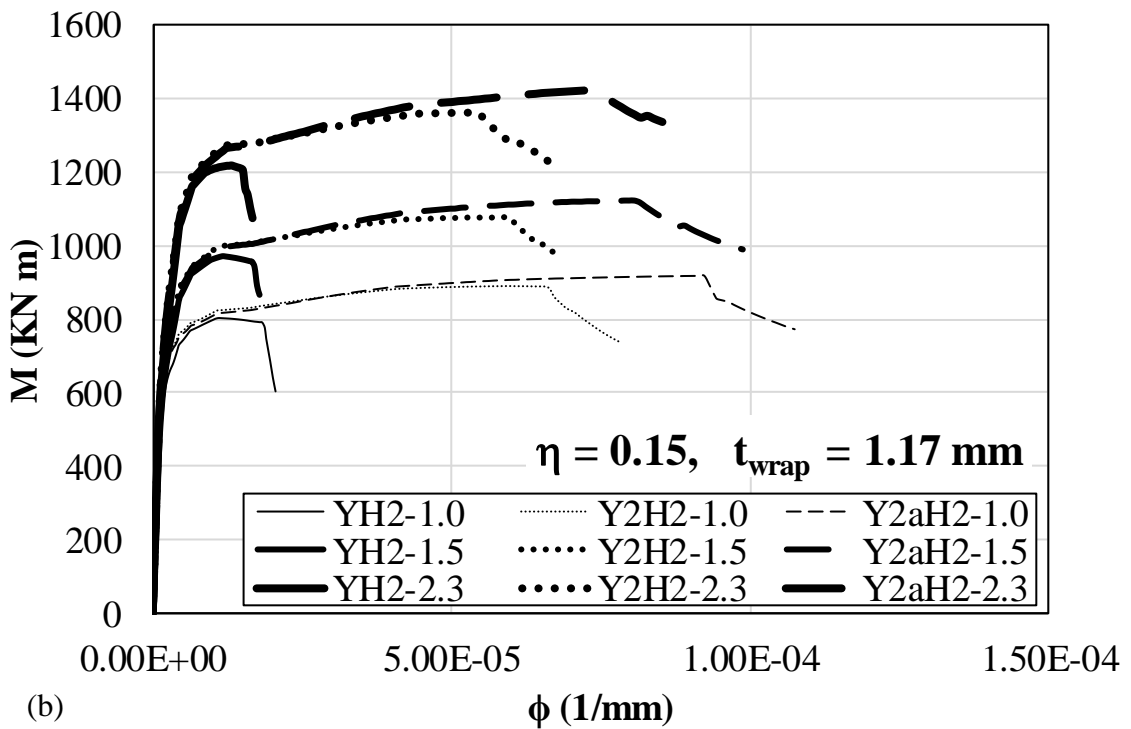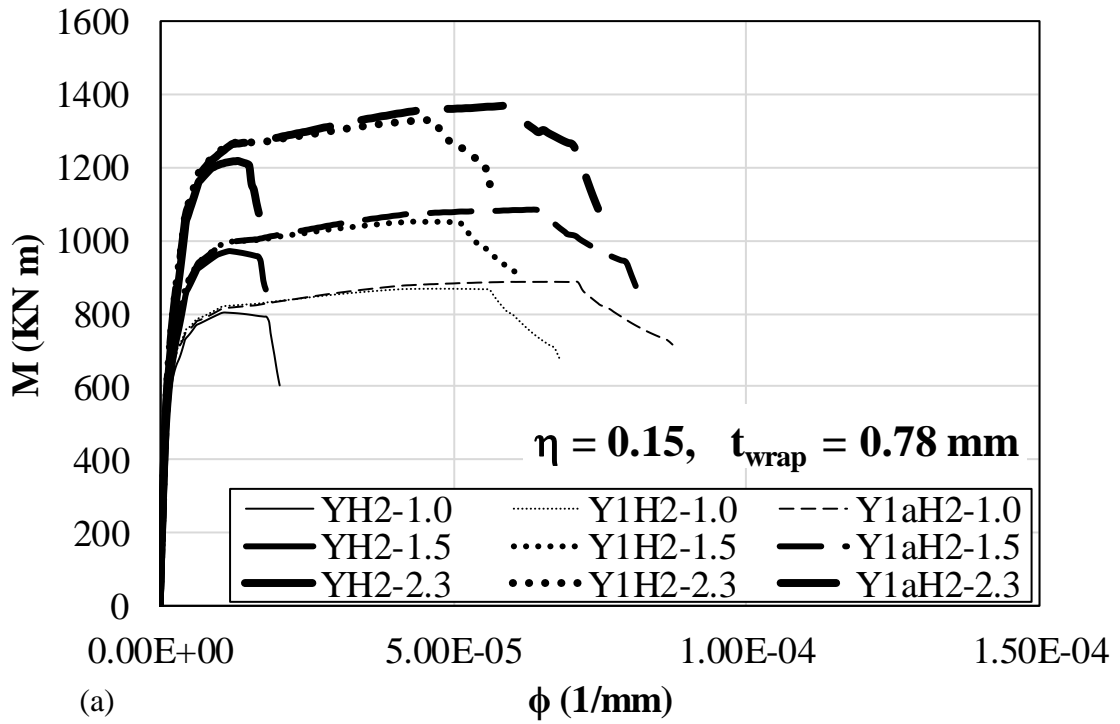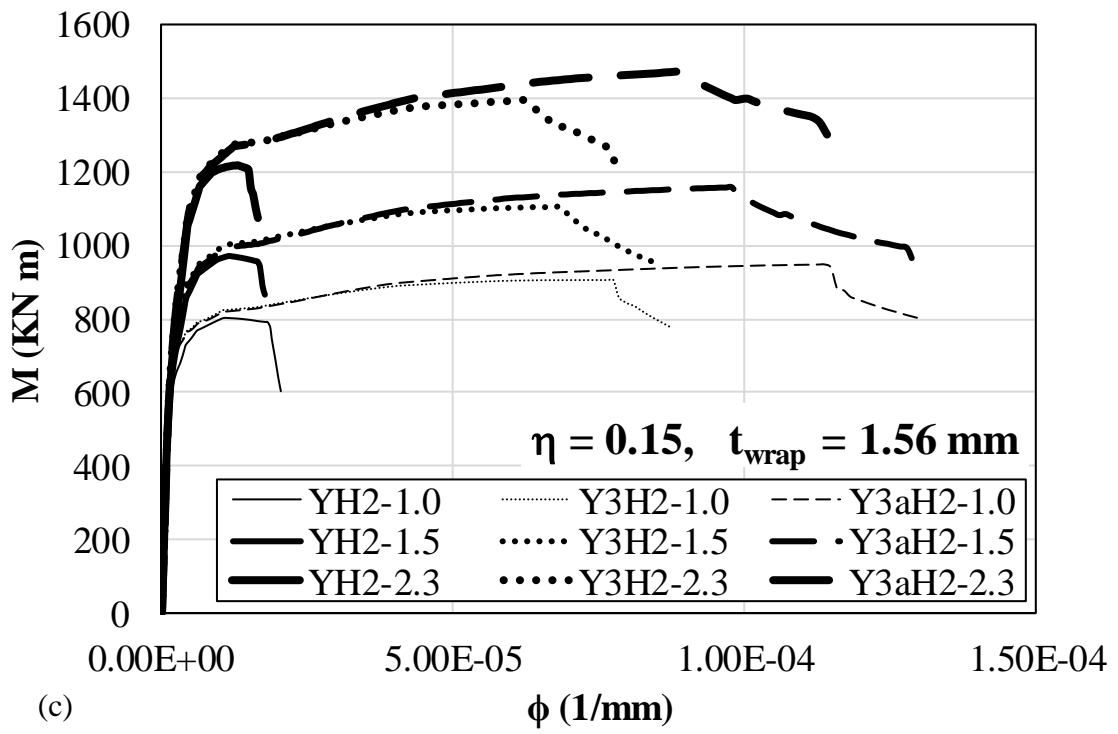
Figure VI-9 - $M - \phi$ curves for the specimens of dimensions 850 *mm* x 350 *mm* and $\eta = 0.15$

(a)

(b)
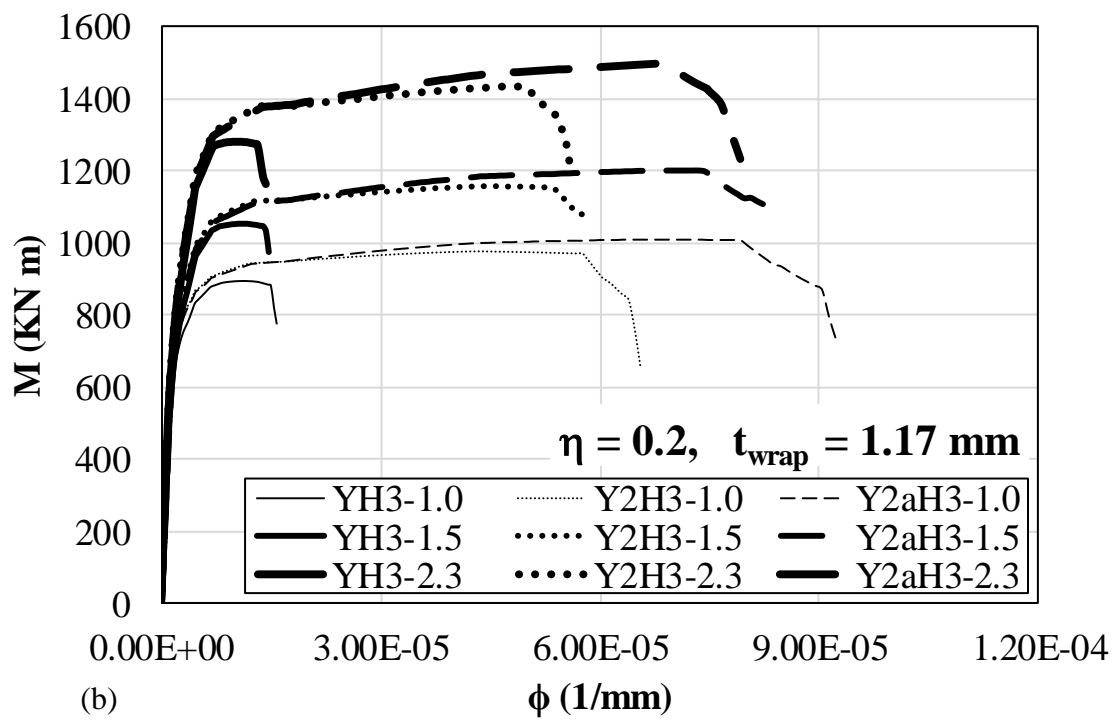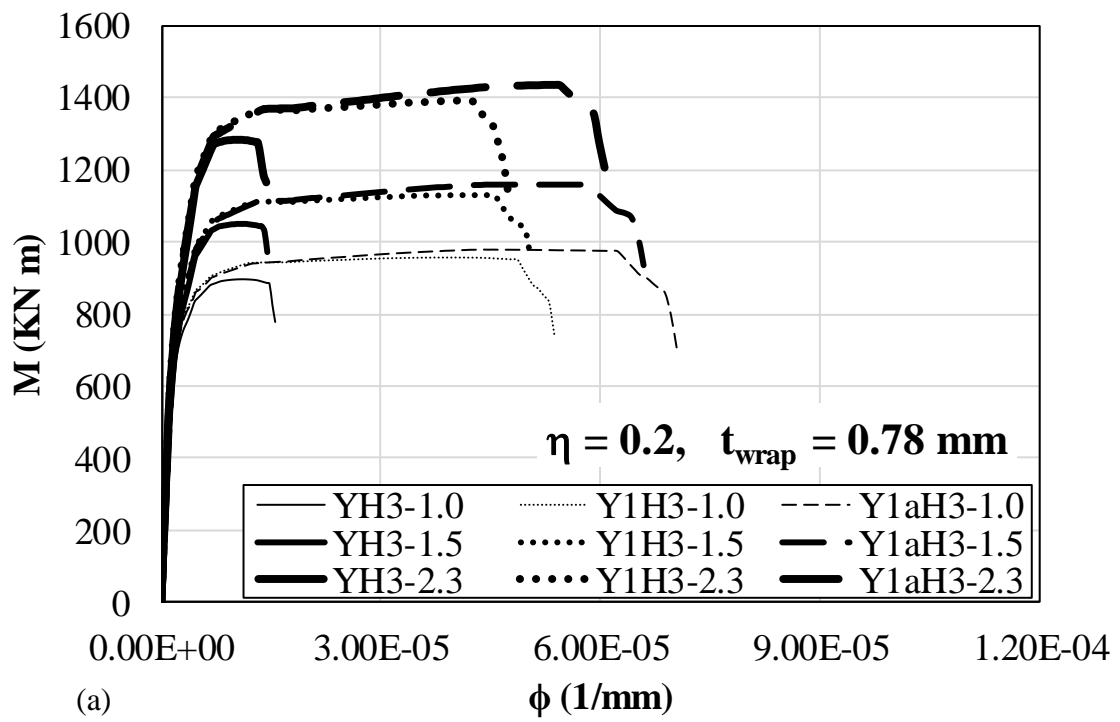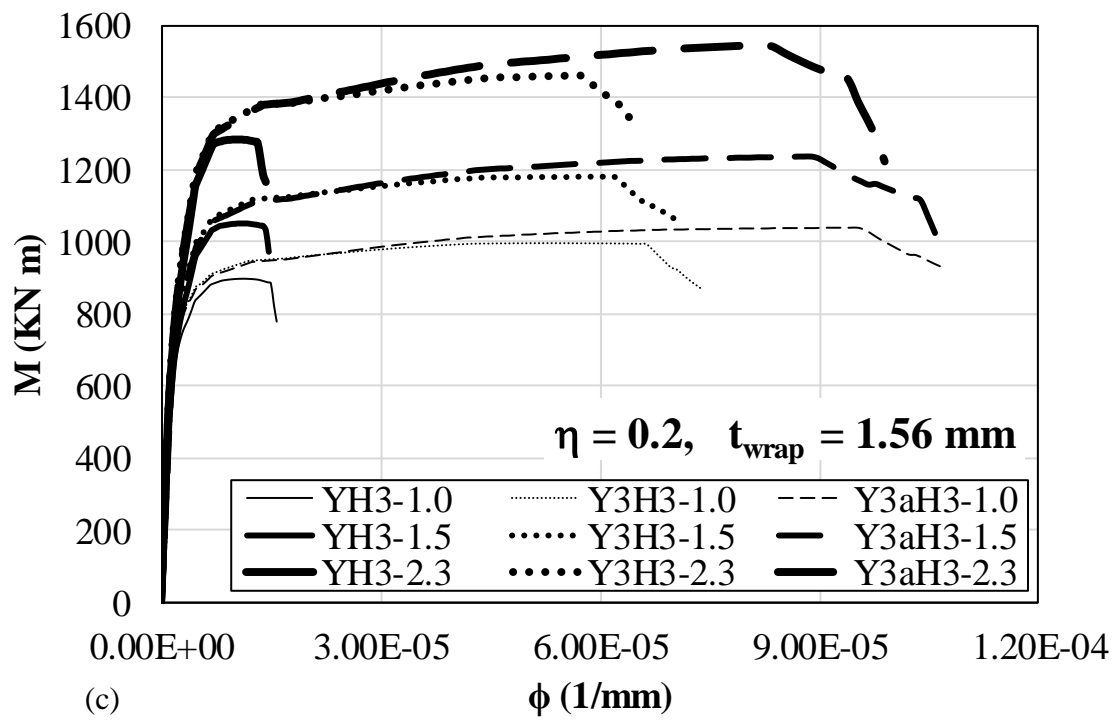
Figure VI-10 - $M - \phi$ curves for the specimens of dimensions 850 *mm* x 350 *mm* and $\eta = 0.2$
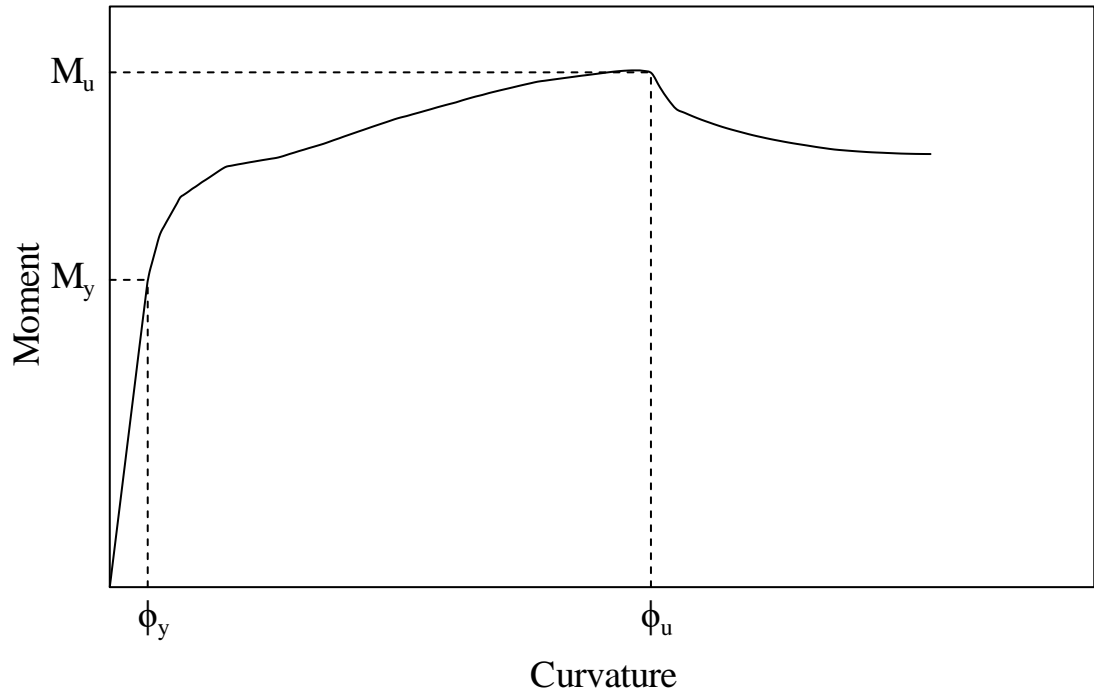
Figure VI-11 - Typical moment-curvature response
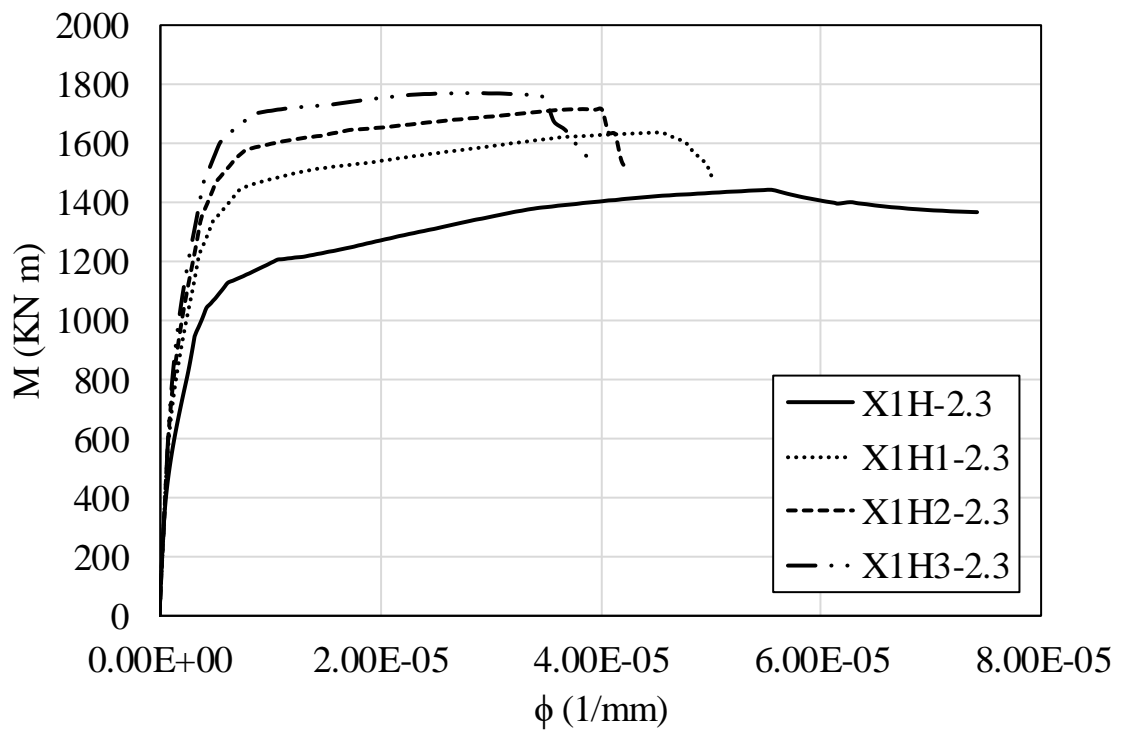
Figure VI-12 - Effect of the axial load level on the $M - \phi$ response

(a)

(b)
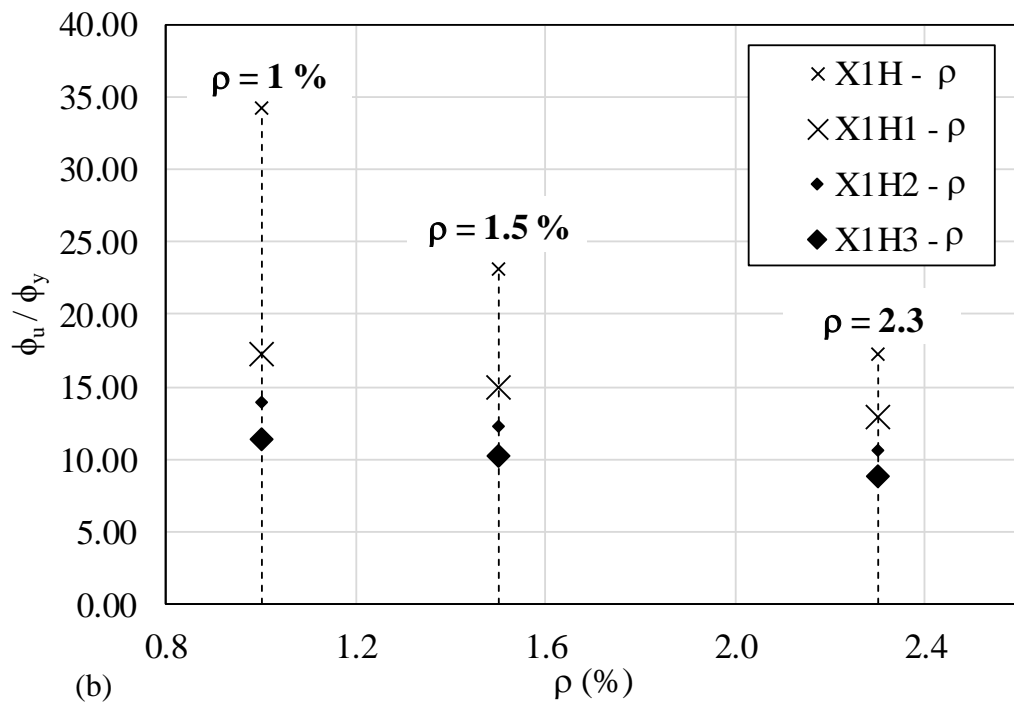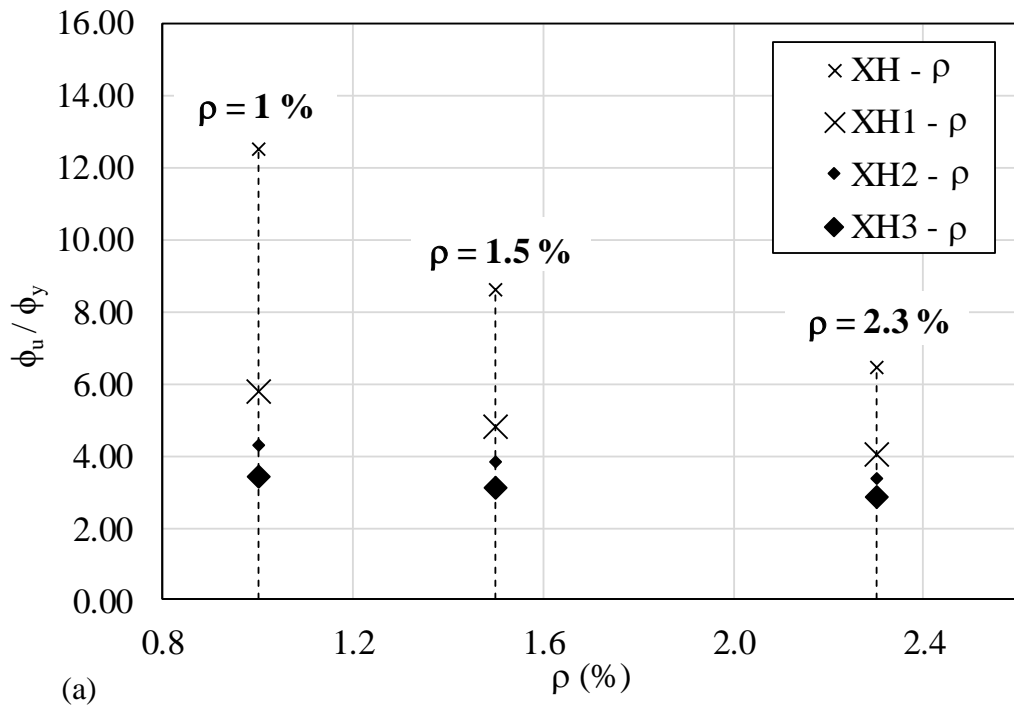
Figure VI-13 - Variation of ϕ_u / ϕ_y in function of the reinforcement ratio ρ for selected specimens

(a)

(b)
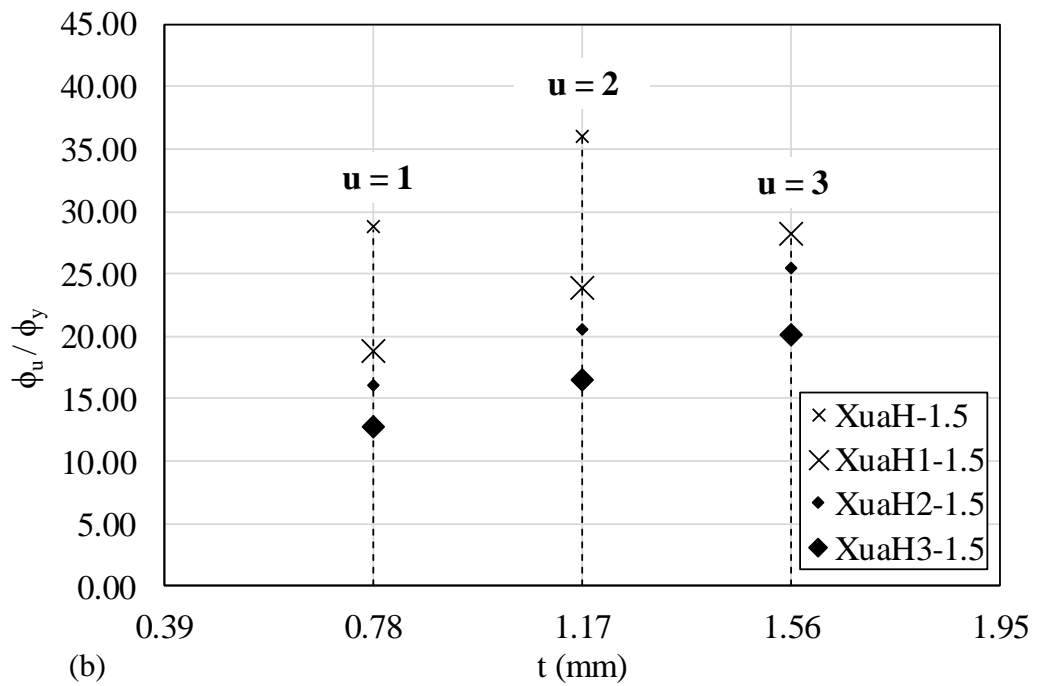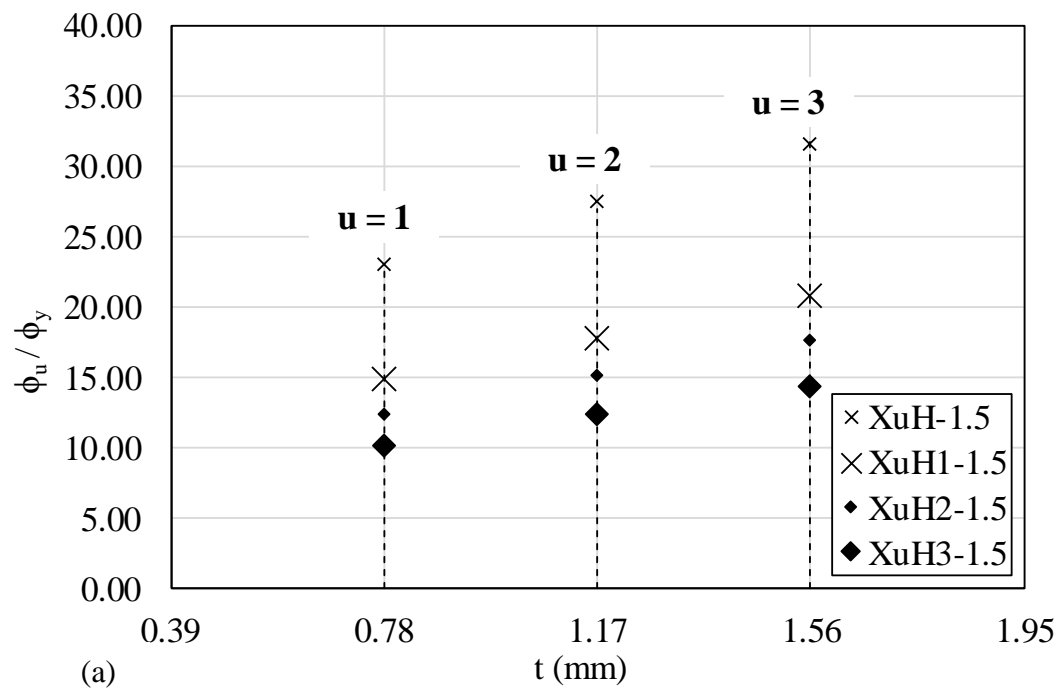
Figure VI-14 - Variation of ϕ_u/ϕ_y in function of the thickness of external FRP layer
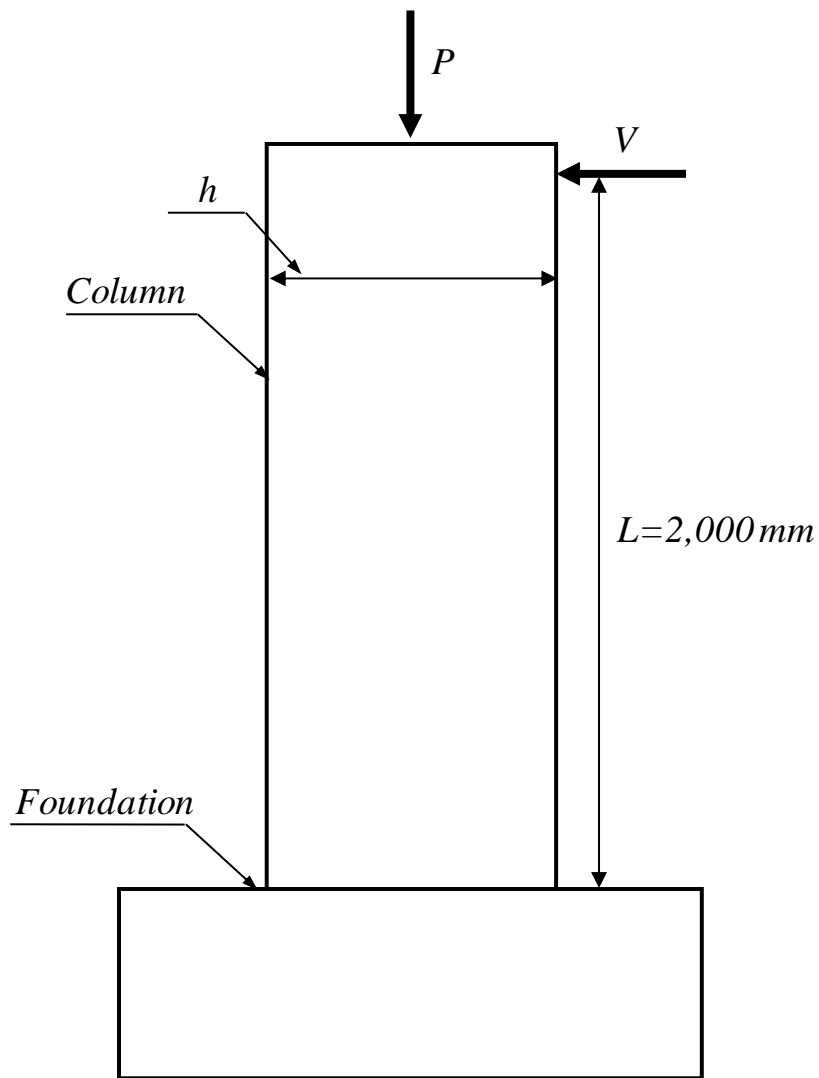
Figure VI-15 - Axial and lateral loading applied to the column
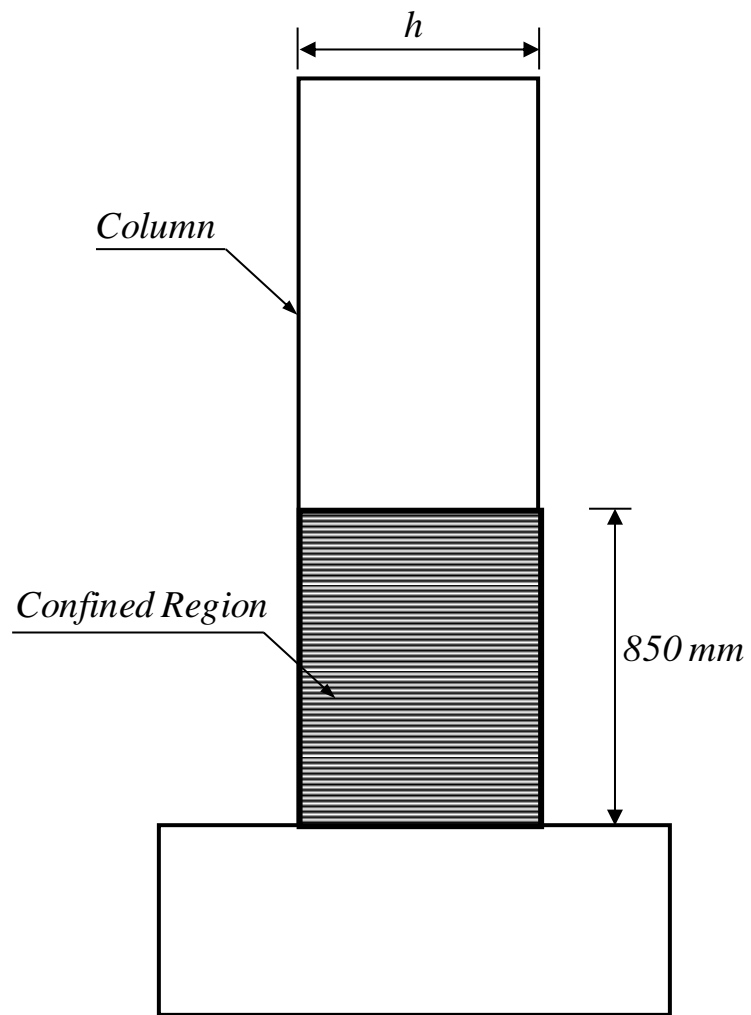
Figure VI-16 - Confined region of the column
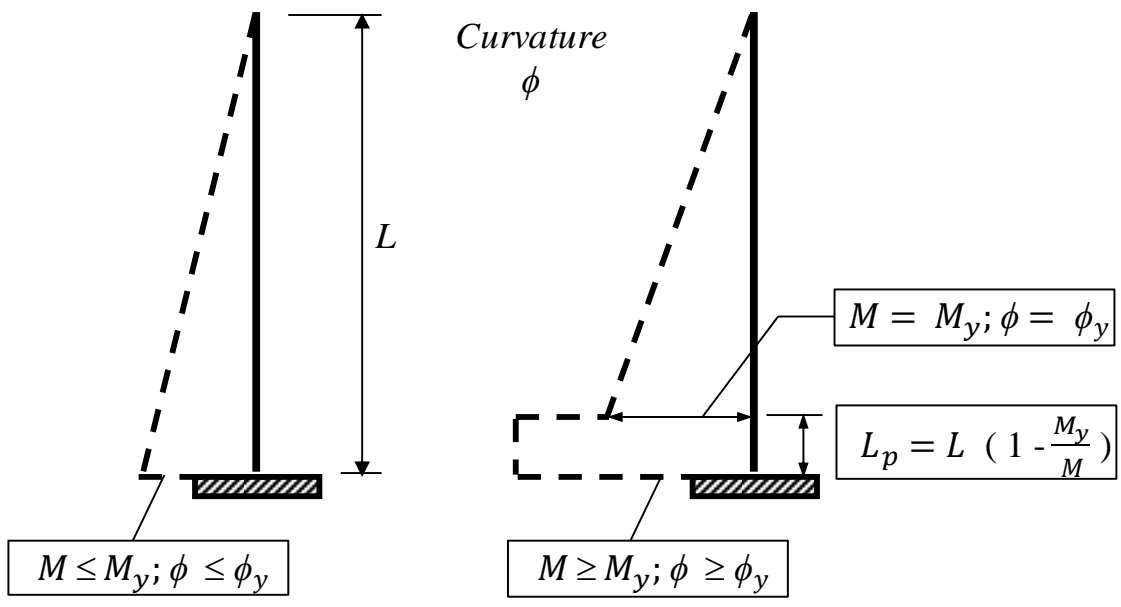
Figure VI-17 - Idealized curvature diagram for drift computation (Harajli 2008)

(a)

(b)
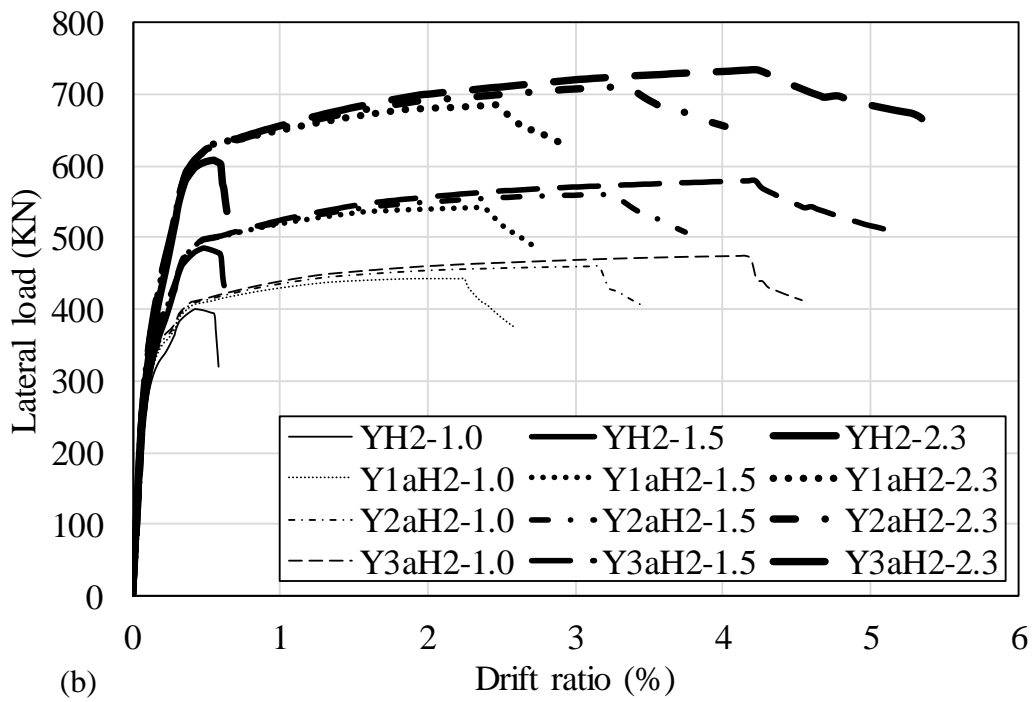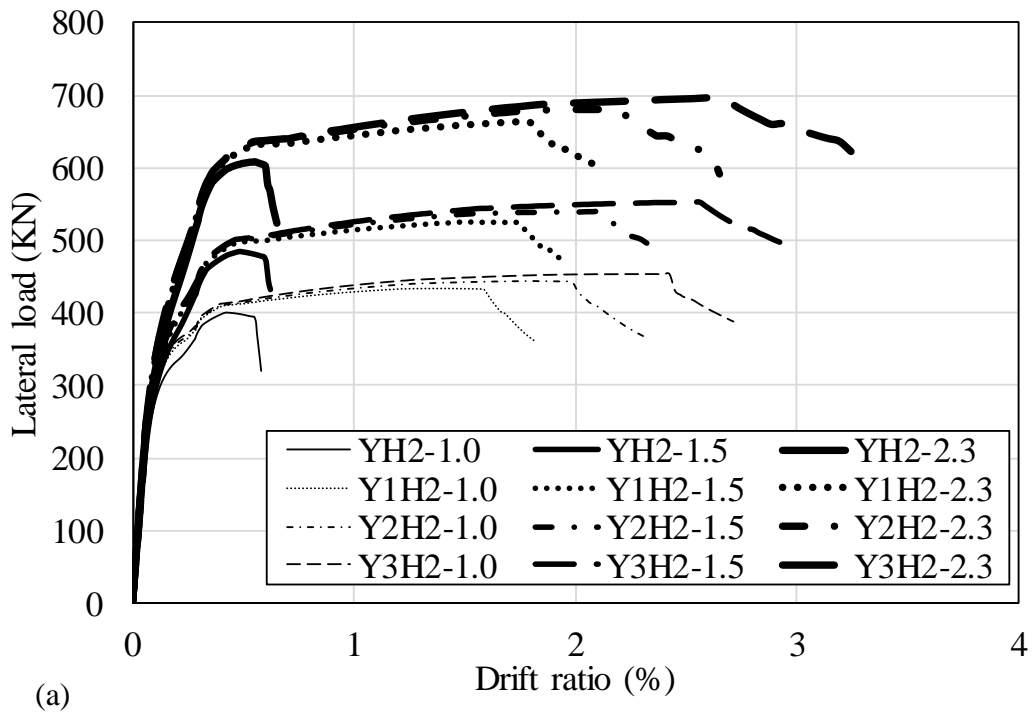
Figure VI-18 - Lateral load versus drift ratio response of selected columns

CHAPTER VII

SUMMARY, CONCLUSIONS AND RECOMMENDATIONS

A.   Summary

The research presented in this study is concerned with studying the cyclic axial compressive behavior of concrete columns confined with external FRP sheets only and columns confined with external FRP sheets and anchors. This behavior is studied experimentally and analytically and a stress-strain model is proposed to better describe it. Making use of the proposed stress-strain model, a parametric study is performed to investigate the influence of different design parameters on the flexural deformation of unconfined and FRP-confined RC columns. The finite element method is also used to simulate the axial response of specimens confined with external FRP sheets only and subjected to monotonic loading.

In the first part of the investigation, the results of eighteen CFRP-confined concrete column specimens, tested at an earlier stage, under axial cyclic compressive loading are presented and discussed. The parameters investigated included the shape of the cross section (circular, square, and rectangular), and area of the CFRP reinforcement. These test results generated are combined with other test results reported in the technical literature for developing a generalized constitutive axial stress-strain model of CFRP-confined concrete.

In the second part of this investigation, an experimental study is carried out for evaluating the stress-strain response of rectangular concrete columns confined with a combination of CFRP jacket and CFRP anchors under cyclic axial compression. A total of 27 small scale specimens are tested. The test parameters included cross section

aspect ratio, area of the CFRP wraps, and area and configuration of the CFRP anchors. A constitutive design oriented model, presenting slight modifications of the model proposed in the first part, is suggested to describe the monotonic and cyclic envelope response of specimens confined with FRP sheets only or with a combination of FRP sheets and anchors.

Concrete damaged plasticity model available in ABAQUS software is used to simulate concrete columns confined with FRP jackets when subjected to monotonic axial compressive loading. A parametric study was carried out to evaluate the sensitivity of the stress-strain and lateral strain-axial strain responses to different input materials parameters. Based on the results of this study, modifications were introduced to the concrete damaged plasticity model (CDPM) used in ABAQUS for FE modeling of FRP-confined concrete columns under monotonically applied axial compression.

Finally, a parametric study is performed to investigate the influence of different design parameters on the moment-curvature ($M - \phi$) response of unconfined and FRP-confined RC columns. The parameters investigated include: the cross-section dimensions (850 mm x 350 mm or 1000 mm x 300 mm), the reinforcement level, the presence or absence of anchors, the thickness of the external FRP layer for confined specimens, and the axial load-level. The $M - \phi$ curves are then used to generate the lateral load-drift curves of a cantilever column of lengths $L = 2,000$ mm, subjected to a constant concentric axial load P and an increasing lateral load V applied at the column free end. Different design parameters are also considered in this section.

B.   Conclusions

Based on the results of this experimental and analytical investigations, the following conclusions and observations are drawn:

1. Confining concrete columns with external FRP sheets causes an enhanced envelope stress-strain response and more-ductile axial stress-strain behavior. The enhancement in the behavior is more noticeable for specimens of circular cross-sections than in square or rectangular cross-sections.

2. The characteristic parts of the cyclic response: unloading and reloading branches, and the values of plastic strains and stress degradation with number of cycles, are not significantly affected by the shape of the section, the confinement level and the concrete compressive strength.

3. The model proposed in the first part of this investigation makes use of earlier models developed in the technical literature in which the characteristic parameters are simplified and modified to account for a wider range of test data. It is composed of a monotonic envelope response and cyclic response and accounts for most parameters that are known to influence the stress-strain response of FRP-confined concrete in a unified approach. It considers ascending and descending post-peak stress-strain responses; it is simpler than earlier models developed in the technical literature, especially in describing the cyclic response.

4. Comparisons of the model predictions with the reported test results and other test data reported in the technical literature show a good accuracy of the model.

5. Adding CFRP anchors to CFRP jacketed rectangular concrete columns improves the confinement effectiveness of the CFRP jacket, leading to substantially enhanced stress-strain response and more-ductile axial stress-strain behavior.

6. The absolute value of the percent improvement in the slope of the post-peak branch of the stress-strain response due to the CFRP anchors was independent of the aspect ratio of the cross section. However, this percent improvement increased with increase in the cross-sectional area of the anchors.

7. For the range of anchor configurations used in this study, changing the anchor configuration while maintaining the total anchors' cross-sectional area did not produce a noticeable effect on the envelope stress-strain response.

8. The intrinsic shape of the cyclic response of specimens confined with a combination of CFRP wraps and CFRP anchors was similar to that of CFRP confined specimens without anchors. That is, the same cyclic response characteristics of CFRP jacketed columns developed in the technical literature can be extended to columns having a combination of CFRP jackets and CFRP anchors.

9. The expressions proposed for the envelope response represent a slight modification of those proposed in the first part. Realizing that the cyclic response is not affected by the presence of anchors, the same expressions proposed in the first part to describe the cyclic response of specimens confined with external FRP sheets only are used to predict the response of anchored specimens.

10. Comparisons of the model predictions with the reported test results show a good accuracy of the model.

11. As part of the modifications introduced to the concrete damaged plasticity model (CDPM), a new hardening/softening rule is proposed to predict the stress-strain behavior of concrete with different active (or constant) confining pressures and a new expression of the dilation angle is generated for FRP-confined concrete. The path dependency of the concrete stress is also taken into account. A user subroutine USDFLD available in ABAQUS is used to define the variation of concrete properties during the loading process.

12. For FRP-confined specimens of non-circular cross-section (i.e. square or rectangular) or specimens wrapped with discontinuous strips, the definition of the compression hardening/softening rule is similar to circular specimens. However, in this case, two methods are proposed to define the dilation angle and lead to close predictions for normal strength concrete and larger difference for higher concrete strengths.

13. The results of the proposed modified CDPM are compared with experimental results of FRP-confined circular and rectangular concrete specimens reported in Chapter II and other results reported in the literature. FE results generated using the proposed model were in very good agreement with the test data.

14. The parametric study performed to investigate the lateral deformation capacity of confined columns demonstrates the positive effect of confinement on the section ductility. It also shows that the increase in the reinforcement ratio or the load ratio causes an improvement in the moment capacity and a reduction in the ductility. As expected, the presence of anchors causes an improvement in the ultimate rotation capacity given that the anchors provide additional confinement to the section. The results clearly show that confining the plastic hinge region

with FRP sheets or with a combination of FRP sheets and anchors results in an improved performance of the columns especially in terms of maximum lateral displacement sustained before failure. Finally, a summary of the expressions available in the technical literature proposed to quantify the plastic hinge length in confined columns is presented.

C.   Recommendations for future studies

Further experimental and analytical work is still needed to complement this work:

- The proposed model is applicable to the range of parameters (section sizes, FRP confinement ratios, rectangular section aspect ratios, etc.) used in this study. Further experimental investigations in support of the proposed model should consider the effect of larger concrete section sizes. Also, additional experimental work for expanding the application of the model may consider the effect of combined external FRP confinement and internal confinement by transverse steel ties.

- The efficiency of FRP-confinement in increasing lateral deformation capacity was studied analytically using non-linear flexural analysis. Further experimental work is needed to experimentally evaluate this efficiency.

- In addition, using the FE method to study the response of concrete columns confined with FRP sheets and anchors or internal steel ties, constitute an important topic that needs further investigation.

APPENDIX I

PREPARATION AND TESTING OF THE SPECIMENS REPORTED IN Chapter III

Figure AI-1 - Molds of anchored specimens provided with PVC pipes

Figure AI-2 – Casting concrete in pre-pared molds

Figure AI- 3 – Cured concrete specimens after removal of PVC pipes

Figure AI- 4 – Wrapping and adding anchors to cured concrete specimens

Figure AI- 5 – Typical failure of anchored specimens

BIBLIOGRAPHY

ABAQUS. (2013). *ABAQUS Theory and User Manuals, version 6.13-1.*

Abbasnia, R., & Holakoo, A. (2012). An investigation of stress-strain behavior of FRP-confined concrete under cyclic compressive loading. *International Journal of Civil Engineering, 10*(3), 201-209.

Abbasnia, R., & Ziaadiny, H. (2013). Experimental Investigation and Strength Modeling of CFRP-Confined Concrete Rectangular Prisms under Axial Monotonic Compression. *Material Structures*, 1-16.

Abbasnia, R., Ahmadi, R., & Ziaadiny, H. (2012). Effect of confinement level, aspect ratio and concrete strength on the cyclic stress-strain behavior of FRP-confined concrete prisms. *Composites Part B: Engineering, 43*(2), 825-831.

Abbasnia, R., Hosseinpour, F., Rostamian, M., & Ziaadiny, H. (2012). Effect of corner radius on stress-strain behavior of FRP confined prisms under axial cyclic compression. *Engineering Structures, 40*, 529-535.

Abbasnia, R., Hosseinpour, F., Rostamian, M., & Ziaadiny, H. (2013). Cyclic and monotonic behavior of FRP confined concrete rectangular prisms with different aspect ratios. *Construction and Building Materials, 40*, 118-125.

ACI-318-11/318R-11. (2011). *Building Code Requirements for Reinforced Concrete and Commentary.* Farmington Hills (MI): American Concrete Institute.

ACI-440.2R-08. (2008). *Guide for the design and construction of externally bonded FRP systems for strengthening concrete structures.* Farmington Hills, MI: American Concrete Institute (ACI).

ASCE. (1982). *State of the Art Report on Finite Element Analysis of Reinforced Concrete.* ASCE Task committee on concrete and masonry.

Bae, S., & Bayrak, O. (2008). Plastic Hinge Length of Reinforced Concrete Columns. *ACI Structural Journal*, 290-300.

Binici, B. (2008). Design of FRPs in Circular Bridge Column Retrofits for Ductility Enhancement. *Engineering Structures, 30*, 766-776.

Binici, B., & Mosalam, K. (2007). Analysis of Reinforced Concrete Columns Retrofitted with Fiber Reinforced Polymer Lamina. *Composites: Part B: Engineering, 38*, 265–276.

Black, S. (2014, November). *High-Performance Composites.* Retrieved from CompositesWorld (CW).

Chaallal, O., Shahawy, M., & Hassan, M. (2003). Performance of axially loaded short rectangular columns strengthened with carbon fiber-reinforced polymer wrapping. *ASCE-Journal of Composites for Construction, 7*(3), 200-208.

Csuka, B., & Kollar, L. (2010). FRP-confined circular concrete columns subjected to concentric loading. *Journal of Reinforced Plastics and Composites, 29*(23), 3504-3520.

Doran, B., Koksal, H. O., & Turgay, T. (2009). Nonlinear finite element modeling of rectangular square concrete columns confined with FRP. *Materials & Design, 30*(8), 3066-3075.

Eid, R., & Paultre, P. (2007). Plasticity-based model for circular concrete columns confined with fibre-composite sheets. *Engineering Structures, 29*(12), 3301-3311.

Elsanadedy, H. M., & Haroun, M. A. (2005). Seismic Design Guidelines for Squat

    Composite-Jacketed Circular and Rectangular Reinforced Concrete Bridge

    Columns. *ACI Structural Journal, 102*(4), 505-514.

Eslami, A., & Ronagh, H. (2013). Effect of FRP wrapping in seismic performance of

    RC buildings with and without special detailing–A case study. *Composites Part*

    B: Engineering, 45(1), 1265-1274.

Fam, A., & Rizkalla, S. (2001). Confinement Model for Axially Loaded Concrete

    Confined by Circular Fiber-Reinforced Polymer Tubes. *ACI Structural Journal,*

    98(4), 451-461.

Galal, K., Arafa, A., & Ghobarah, A. (2005). Retrofit of RC square short columns.

    Engineering Structures, 27(5), 801-813.

Ghatte, H. F., Comert, M., Demir, C., & Ilki, A. (2016). Evaluation of FRP

    Confinement Models for Substandard Rectangular RC Columns Based on Full-

    Scale Reversed Cyclic Lateral Loading Tests in Strong and Weak Directions.

    Polymers, 8(9), 323.

Ghobarah, A., & Galal, K. E. (2004). Seismic rehabilitation of short rectangular RC

    columns. *Journal of Earthquake Engineering, 8*(1), 45-68.

Gu, D. S., Wu, Y. F., Wu, G., & Wu, Z. S. (2012). Plastic hinge analysis of FRP

    confined circular concrete columns. *Construction and Building Materials, 27*,

    223-233.

Hajsadeghi, M., Alaee, F. J., & Shahmohammadi, A. (2011). Investigation on behaviour

    of square/rectangular reinforced concrete columns retrofitted with FRP Jacket.

    Journal of Civil Engineering and Management, 17(3), 400-408.

Hany, N., & Tarabay, R. (2015). the experimenety. *nnmmmmm, 5*(3), 155-156.

Harajli, M. (2008). Seismic Behavior of RC Columns with Bond-Critical Regions: Criteria for Bond Strengthening Using External FRP Jackets. *ASCE-Journal of Composites for Construction, 12*(1), 69-79.

Harajli, M., & Hantouche, E. (2014). Effect of active versus passive confinement on seismic response of wide RC columns with lap splices. *Journal of Structural Engineering*, 04014221. doi:10.1061/(ASCE)ST.1943-541X.0001196

Harajli, M., Hantouche, E., & Soudki, K. (2006). Stress-strain model for fiber-reinforced polymer jacketed concrete columns. *ACI Structural Journal, 103*(5), 672-682.

Ilki, A., Peker, O., Karamuk, E., Demir, C., & Kumbasar, N. (2008). FRP retrofit of low and medium strength circular and rectangular reinforced concrete columns. *Journal of Materials in Civil Engineering, 20*(2), 169-188.

Issa, C., Chami, P., & Saad, G. (2009). Compressive strength of concrete cylinders with variable widths CFRP wraps: Experimental study and numerical modeling. *Construction and Building Materials, 23*(6), 2306-2318.

Jiang, C., Wu, Y. F., & Wu, G. (2014). Plastic Hinge Length of FRP-Confined Square RC Columns. *ASCE-Journal of Composites for Construction, 18*(4), 04014003.

Jiang, J. F., & Wu, Y. F. (2012). Identification of material parameters for Drucker-Prager plasticity model for FRP confined circular concrete columns. *International Journal of Solids and Structures, 49*(3-4), 445-456.

Jiang, J. F., & Wu, Y. F. (2014). Characterization of yield surfaces for FRP-confined concrete. *Journal of Engineering Mechanics, 140*(12), 04014096.

Juntanalikit, P., Jirawattanasomkul, T., & Pimanmas, A. (2016). Experimental and numerical study of strengthening non-ductile RC columns with and without lap

splice by Carbon Fiber Reinforced Polymer (CFRP) jacketing. *Engineering Structures, 125*, 400-418.

Kabir, M. Z., & Shafei, E. (2012). Plasticity modeling of FRP-confined circular reinforced concrete columns subjected to eccentric axial loading. *Composites Part B: Engineering, 43*(8), 3497-3506.

Karabinis, A. I., Rousakis, T. C., & Manolitsi, G. E. (2008). 3D finite-element analysis of substandard RC columns strengthened by fiber-reinforced polymer sheets. *ASCE-Journal of Composites for Construction, 12*(5), 531-540.

Karabinis, A., & Rousakis, T. (2002). Concrete Confined by FRP Material: a Plasticity Approach. *Engineering Structures, 24*(7), 923-932.

Karantzikis, M., Papanicolaou, C. G., Antonopoulos, C. P., & Triantafillou, T. C. (2005). Experimental investigation of nonconventional confinement for concrete using FRP. *ASCE-Journal of Composites for Construction, 9*(6), 480-487.

Kim, I., Jirsa, J. O., & Bayrak, O. (2011). Use of carbon fiber-reinforced polymer anchors to repair and strengthen lap splices of reinforced concrete columns. *ACI Structural Journal, 108*(5), 630-640.

Kim, Y., Quinn, K., Ghannoum, W., & Jirsa, J. O. (2014). Strengthening of reinforced concrete T-beams using anchored CFRP materials. *ACI Structural Journal, 111*(5), 1027-1036.

Koksal, H. O., Doran, B., & Turgay, T. (2009). A practical approach for modeling FRP wrapped concrete columns. *Construction and Building Materials, 23*(3), 1429-1437.

Lam, L., & Teng, J. (2004). Ultimate Condition of Fiber Reinforced Polymer-Confined Concrete. *ASCE-Journal of Composites for Construction, 8*(6), 539–548.

Lam, L., & Teng, J. G. (2001). Strength of RC cantilever slabs bonded with GFRP strips. *ASCE-Journal of Composites for Construction, 5*(4), 221-227.

Lam, L., & Teng, J. G. (2003a). Design-oriented stress-strain model for FRP-confined concrete. *Construction and Building Materials, 17*(6-7), 471-489.

Lam, L., & Teng, J. G. (2003b). Design-oriented stress-strain model for FRP-confined concrete in rectangular columns. *Journal of Reinforced Plastics and Composites, 22*(13), 1149-1186.

Lam, L., & Teng, J. G. (2009). Stress-strain model for FRP-confined concrete under cyclic axial compression. *Engineering Structures, 31*(2), 308-321.

Lam, L., Teng, J. G., Cheung, C. H., & Xiao, Y. (2006). FRP-confined concrete under axial cyclic compression. *Cement and Concrete composites, 28*(10), 949-958.

Li, X., Lv, H., Zhang, G. C., Sha, S., & Zhou, S. (2013). Seismic retrofitting of rectangular reinforced concrete columns using fiber composites for enhanced flexural strength. *Journal of Reinforced Plastics and Composites*. doi:10.1177/0731684413477222

Lim, J. C., & Ozbakkaloglu, T. (2014a). Design Model for FRP-Confined Normal-and High-Strength Concrete Square and Rectangular Columns. *Magazine of Concrete Research, 66*(20), 1020-1035.

Lim, J., & Ozbakkaloglu, T. (2014). Investigation of the Influence of the Application Path of Confining Pressure: Tests on Actively Confined and FRP-Confined Concretes. *ASCE-Journal of Struct Engineering, 141*(8), 04014203.

Lim, J., & Ozbakkaloglu, T. (2014). Lateral Strain-to-Axial Strain Relationship of Confined Concrete. *ASCE-Journal of Structural Engineering, 141*(5), 04014141.

Lim, J., & Ozbakkaloglu, T. (2014). Stress-Strain Model for Normal- and Light-Weight Concretes under Uniaxial and Triaxial Compression. *Construction and Building Materials, 71*, 492-509.

Lim, J., & Ozbakkaloglu, T. (2014). Unified Stress-Strain Model for FRP and Actively Confined Normal-Strength and High-Strength Concrete. *ASCE-Journal of Composites for Construction, 19*(4), 04014072.

Lim, J., & Ozbakkaloglu, T. (2014b). Confinement Model for FRP-Confined High-Strength Concrete. *ASCE-Journal of Composites for Construction*, 04013058.

LS-DYNA. (2007). *LS-DYNA keyword user's manual.* Livermore Software Technology Corporation 970.

Lu, Y., Gu, X., & Guan, J. (2005). Probabilistic Drift Limits and Performance Evaluation of Reinforced Concrete Columns. *ASCE-Journal of Structural Engineering, 131*(6), 966-978.

Mander, J. B., Priestley, M. J., & Park, R. (1988). Theoretical stress-strain model for confined concrete. *ASCE-Journal of Structural Engineering, 114*(8), 1804-1826.

Mirmiran, A., & Shahawy, M. (1996). A New Concrete-Filled Hollow FRP Composite Column. *Composites Part B, 27*(3-4), 263-268.

Mirmiran, A., & Shahawy, M. (1997). Behavior of concrete columns confined by fiber composites. *ASCE-Journal of Structural Engineering, 123*(5), 583-590.

Mirmiran, A., Zagers, K., & Yuan, W. Q. (2000). Nonlinear finite element modeling of concrete confined by fiber composites. *Finite Elements in Analysis and Design, 35*(1), 79-96.

Monti, G., Nisticò, N., & Santini, S. (2001). Design of FRP jackets for upgrade of circular bridge piers. *ASCE-Journal of Composites for Construction, 5*(2), 94-101.

Mortezaei, A., & Ronagh, H. R. (2012). Plastic hinge length of FRP strengthened reinforced concrete columns. *Scientia Iranica, 19*(6), 1365–1378.

Orton, S. L., Jirsa, J. O., & Bayrak, O. (2008). Design considerations of carbon fiber anchors. *ASCE-Journal of Composites for Construction, 12*(6), 608-616.

Ozbakkaloglu, T. (2012). Axial Compressive Behavior of Square and Rectangular High Strength Concrete-Filled FRP Tubes. *ASCE-Journal of Composites for Construction, 17*(1), 151-161.

Ozbakkaloglu, T. (2013). Behavior of Square and Rectangular Ultra High-Strength Concrete Filled FRP Tubes under Axial Compression. *Composites part B, 54*, 97-111.

Ozbakkaloglu, T., & Akin, E. (2012). Behavior of FRP-confined normal- and high-strength concrete under cyclic axial compression. *ASCE-Journal of Composites for Construction, 16*(4), 451-463.

Ozbakkaloglu, T., Gholampour, A., & Lim, J. (2016). Damage-plasticity model for FRP-confined normal-strength and high-strength concrete. *ASCE-Journal of Composites for Construction, ASCE.* doi:http://dx.doi.org/10.1061/(ASCE)CC.1943-5614.0000712, 04016053.

Ozbakkaloglu, T., Lim, J. C., & Vincent, T. (2013). FRP-confined concrete in circular sections: Review and assessment of stress–strain models. *Engineering Structures, 49*, 1068-1088.

Papanikolaou, V., & Kappos, A. (2007). Confinement-Sensitive Plasticity Constitutive Model for Concrete in Triaxial Compression. *International Journal of Solid Structures, 44*(21), 7021-7048.

Parghi, A., & Alam, M. (2016). Seismic behavior of deficient reinforced concrete bridge piers confined with FRP – A fractional factorial analysis. *Engineering Structures, 126*, 531-546.

Paulay, T., & Priestley, M. J. (1992). *Seismic Design of Reinforced Concrete and Masonry Buildings.* New York (NY): John Wiley & Sons.

Pessiki, S., Harries, K., Kestner, J., Sause, R., & Ricles, J. (2001). Axial Behavior of Reinforced Concrete Confined with FRP Jackets. *ASCE-Journal of Composites for Construction, 4*(237), 237-245.

Popovics, S. (1973). A numerical approach to the complete stress-strain curve of concrete. *Cement and Concrete Research, 3*(5), 583–599.

Priestley, M. J., & Park, R. (1987). Strength and Ductility of Concrete Bridge Columns under Seismic Loading. *ACI Structural Journal, 84*(1), 61–76.

Priestley, M. J., Seible, F., & Calvi, G. M. (1996). *Seismic Design and Retrofit of Bridges.* John Wiley & Sons.

R Studio. (2012). *R 0.97.551 [Computer software]*. Boston.

Rochette, P., & Labossière, P. (2000). Axial Testing of Rectangular Column Model Confined with Composites. *Journal of Composites for Construction*, 129–136.

Rousakis, T. C., Karabinis, A. I., Kiousis, P. D., & Tepfers, R. (2008). Analytical modelling of plastic behavior of uniformly FRP confined concrete members. *Composites, Part B: Engineering, 39*(7-8), 1104-1113.

Rousakis, T., Karabinis, A., & Kiousis, P. (2007). FRP-confined concrete members: Axial compression experiment and plasticity modelling. *Engineering Structures, 29*(7), 1343-1353.

Samaan, M., Mirmiran, A., & Shahawy, M. (1998). Model of concrete confined by fiber composites. *ASCE-Journal of Structural Engineering, 124*(9), 1025-1031.

SAP-2000. (Version 18). *Integrated software for structural analysis and design.*

Seible, F., Priestley, M. J., Hegemier, G., & Innamorato, D. (1997). Seismic Retrofit of RC Columns with Continuous Carbon Fiber Jackets. *ASCE-Journal of Composites for Construction, 1*(2), 52-62.

Seow, P., & Swaddiwudhipong, S. (2005). Failure Surface for Concrete under Multiaxial Load – a Unified Approach. *ASCE-Journal of Materials in Civil Engineering, 17*(2), 219-228.

Shehata, I., Carneinro, L., & Shehata, L. (2002). Strength of Short Concrete Columns Confined with CFRP Sheet. *Materials Structures, 35*(1), 50-58.

Spoelstra, M. R., & Monti, G. (1999). FRP-confined concrete model. *ASCE-Journal of composites for construction, 3*(3), 143-150.

Tan, K. H. (2002). Strength enhancement of rectangular reinforced concrete columns using fiber-reinforced polymer. *ASCE-Journal of Composites for Construction, 6*(3), 175-183.

Tao, Z., Wang, Z., & Yu, Q. (2013). Finite Element Modelling of Concrete-Filled Steel Stub Columns under Axial Compression. *Journal of Constructional Steel Research, 89*, 121-131.

Teng, J. G., Xiao, Q. G., Yu, T., & Lam, L. (2015). Three-dimensional finite element analysis of reinforced concrete columns with FRP and/or steel confinement. *Engineering Structures, 97*(15-28).

Teng, J., Huang, Y., Lam, L., & Ye, L. (2007). Theoretical Model for Fiber-Reinforced Polymer-Confined Concrete. *ASCE-Journal of Composites for Construction, 11*(2), 201-210.

Teng, J., Jiang, T., Lam, L., & Luo, Y. (2009). Refinement of a Design-Oriented Stress-Strain Model for FRP-Confined Concrete. *Journal of Composites for Construction, 13*(4), 269-278.

Valdmanis, V., De Lorenzis, L., Rousakis, T., & Tepfers, R. (2007). Behaviour and Capacity of CFRP-Confined Concrete Cylinders Subjected to Monotonic and Cyclic Axial Compressive Load. *Structural Concrete-London-Thomas Telford Limited, 8*(4), 187-200.

Vincent, T., & Ozbakkaloglu, T. (2013). Influence of Concrete Strength and Confinement Method on Axial Compressive Behavior of FRP Confined High- and Ultra High Strength Concrete. *Composites part B, 50*, 413-428.

Wang, Z., Wang, D., Smith, S., & Lu, D. (2012a). CFRP-confined square RC columns. I: Experimental investigation. *ASCE-Journal of Composites for Construction, 16*(2), 150-160.

Wang, Z., Wang, D., Smith, S., & Lu, D. (2012b). CFRP-confined square RC columns. II: Cyclic axial compression stress-strain model. *ASCE-Journal of Composites for Construction, 16*(2), 161-170.

Wang, Z., Wang, D., Smith, S., & Lu, D. (2012c). Experimental testing and analytical modeling of CFRP-confined large circular RC columns subjected to cyclic axial compression. *Engineering Structures, 40*, 64-74.

Wong, Y., Yu, T., Teng, J., & Dong, S. (2008). Behavior of FRP-Confined Concrete in Annular Section Columns. *Composites part B, 39*(3), 451-466.

Wu, H. L., Wang, Y. F., Yu, L., & Li, X. R. (2009). Experimental and computational studies on high-strength concrete circular columns confined by aramid fiber-reinforced polymer sheets. *ASCE-Journal of Composites for Construction, 13*(2), 125-134.

Wu, Y., & Jiang, J. (2013). Effective Strain of FRP for Confined Circular Concrete Columns. *Composites Structures, 95*, 479–491.

Xiao, Y., & Wu, H. (2000). Compressive behavior of concrete confined by carbon fiber composite jackets. *Journal of Materials in Civil Engineering, 12*(2), 139-146.

Youssef, M. N., Feng, M. Q., & Mosallam, A. S. (2007). Stress–strain model for concrete confined by FRP composites. *Composites Part B: Engineering, 38*(5), 614-628.

Youssf, O., ElGawady, M., & Mills, J. (2015). Displacement and Plastic Hinge Length of FRP-Confined Circular Reinforced Concrete Columns. *Engineering Structures, 101*, 465–476.

Youssf, O., ElGawady, M., Mills, J., & Ma, X. (2014). Finite element modelling and dilation of FRP-confined concrete columns. *Engineering Structures, 79*, 70-85.

Yu, T., Teng, J. G., Wong, Y. L., & Dong, S. L. (2010a). Finite element modeling of confined concrete-I: Drucker-Prager type plasticity model. *Engineering Structures, 32*(3), 665-679.

Yu, T., Teng, J. G., Wong, Y. L., & Dong, S. L. (2010b). Finite element modeling of confined concrete-II: Plastic-damage model. *Engineering Structures, 32*(3), 680-691.

Yuan, F., Wu, Y., & Li, C. (2016). Modelling plastic hinge of FRP-confined RC columns. *Engineering Structures*.

Zou, X. K., Teng, J. G., De Lorenzis, L., & Xia, S. H. (2007). Optimal Performance-Based Design of FRP Jackets for Seismic Retrofit of Reinforced Concrete Frames. *Composites: Part B: Engineering, 38*, 584–597.